

Aus dem Institut für Tierpathologie
Lehrstuhl für Allgemeine Pathologie und Pathologische Anatomie
(Vorstand: Prof. Dr. W Hermanns)

und dem

Lehrstuhl für Molekulare Tierzucht und Biotechnologie
(Vorstand: Prof. Dr. E. Wolf)
der Tierärztlichen Fakultät der Ludwig-Maximilians-Universität München

Arbeit angefertigt unter der Leitung von
Dr. N. Herbach,
Prof. Dr. B. Aigner und Prof. Dr. R. Wanke

**Clinical and pathomorphological characterisation of
two diabetic mouse models derived from the Munich
ENU mouse mutagenesis project**

Inaugural-Dissertation
zur Erlangung der tiermedizinischen Doktorwürde
der Tierärztlichen Fakultät der Ludwig-Maximilians-Universität München

von
Lelia Muriel van Bürck
aus Dachau

München, 2010

Gedruckt mit Genehmigung der Tierärztlichen Fakultät
der Ludwig-Maximilians-Universität München

Dekan:	Univ.-Prof. Dr. Braun
Berichterstatter:	Univ.-Prof. Dr. Wanke
Korreferent/en:	Univ.-Prof. Dr. Wolf Univ.-Prof. Dr. Förster Univ.-Prof. Dr. Hartmann Univ.-Prof. Dr. Gehlen

Tag der Promotion: 13. Februar 2010

Meinen Eltern

Parts of the work have been published in March 2010.

Original article:

van Bürck L, Blutke A, Kautz S, Rathkolb B, Klafßen M, Wagner S, Kemter E, Hrabé de Angelis M, Wolf E, Aigner B, Wanke R, and Herbach N (2010) Phenotypic and pathomorphological characteristics of a novel mutant mouse model for maturity-onset diabetes of the young type 2 (MODY 2). *Am J Physiol Endocrinol Metab* 298, E512-523.

Table of content

1.	Introduction	1
2.	Literature review	2
2.1	Genetically modified mice in biomedical research	2
2.1.1	The murine model system	2
2.1.1.1	Biological parameters	2
2.1.1.2	Genetic features	3
2.1.2	Random mutagenesis in mice	3
2.2	<i>N</i>-ethyl-<i>N</i>-nitrosourea (ENU)-induced mutagenesis	4
2.2.1	Biochemical features of ENU	4
2.2.2	Contribution of ENU mutagenesis to biomedical research	6
2.2.3	ENU mutagenesis project strategies	7
2.3	The Munich ENU mouse mutagenesis project	7
2.3.1	Research focus	7
2.3.2	Mutagenesis and screening protocol	8
2.3.3	Linkage analysis of dominant mutations	9
2.3.4	Phenotype screening for diabetic mouse models	10
2.3.5	Initial characterisation of the ENU strains GLS001 and GLS006	11
2.4	Diabetes mellitus in human beings	12
2.4.1	Definition and description of diabetes mellitus	12
2.4.2	Diagnostic criteria for diabetes mellitus	13
2.4.3	Classification of diabetes mellitus	15
2.4.4	Global burden of diabetes mellitus	16
2.5	Maturity-onset diabetes of the young (MODY)	17
2.5.1	Characteristics of MODY	17
2.5.2	MODY subtypes	19
2.6	The catalytic enzyme glucokinase	22
2.6.1	Physiological and biochemical function of the glucokinase enzyme	22
2.6.2	Regulation of glucokinase expression	23
2.6.3	Structure-function relationship in human glucokinase	25
2.6.4	Glucokinase-associated diseases in human subjects	27

2.6.5	Clinical screening criteria for MODY 2	31
3.	Research design and methods	32
3.1	Animals	32
3.1.1	Breeding, husbandry, and analyses	32
3.1.2	Breeding strategy for linkage analysis	35
3.2	Identification of the causative mutation	36
3.2.1	Fine mapping in GLS001 mice	36
3.2.1.1	DNA isolation	36
3.2.1.2	PCR amplification of the polymorphic sequences	37
3.2.1.3	Gel electrophoresis	38
3.2.2	Candidate gene sequencing	40
3.2.2.1	Sample preparation for RNA and DNA isolation	40
3.2.2.2	RNA isolation	41
3.2.2.3	cDNA synthesis by reverse transcription of total hepatic RNA	42
3.2.2.4	PCR amplification of the candidate gene	43
3.2.2.5	Purification of PCR products	45
3.2.2.6	Sequence analysis	46
3.3	Genotyping of the identified mutations	46
3.3.1	Restriction fragment length polymorphism (RFLP) analysis in GLS001 mice	46
3.3.2	Amplification refractory mutation system PCR (ARMS PCR) in GLS006 mice	47
3.4	Ex vivo studies of functional consequences of the causative mutations	49
3.4.1	Quantification of glucokinase enzyme activity	49
3.4.1.1	Tissue sample preparation	51
3.4.1.2	Work flow of glucokinase activity determination	51
3.4.1.3	Determination of protein contents	54
3.4.2	Determination of glucokinase transcript abundances by quantitative real-time PCR	54
3.4.2.1	Tissue sample preparation, RNA isolation and cDNA synthesis	55
3.4.2.2	Quantitative real-time PCR performance	55

3.4.3	Western blot analysis	56
3.4.3.1	Isolation and preparation of pancreatic islets	56
3.4.3.2	Sodium dodecyl sulphate polyacrylamide gel electrophoresis (SDS-PAGE)	59
3.4.3.3	Blotting	60
3.4.3.4	Western blot analysis	61
3.5	Clinical analyses and tests	62
3.5.1	Body weights	62
3.5.2	Blood glucose determination	63
3.5.3	Oral glucose tolerance tests (OGTT)	63
3.5.4	Serum insulin determination by Enzyme-Linked Immunosorbent Assay (ELISA)	64
3.5.5	Intraperitoneal insulin tolerance tests (ipITT)	65
3.6	Necropsy and organ preparation	65
3.6.1	Gravimetric organ analyses	65
3.6.2	Liver preparation	65
3.6.3	Pancreas preparation	66
3.7	Immunohistochemical procedures	67
3.7.1	Insulin immunostaining of pancreas sections	67
3.8	Quantitative stereological investigations of the pancreas	68
3.8.1	Quantification of the pancreas volume according to Cavalieri's principle	68
3.8.1.1	Determination of the individual tissue shrinkage	69
3.8.2	Specific morphometric parameters in mice of different age groups	70
3.8.2.1	Neonatal mice	70
3.8.2.2	Adult mice	70
3.9	Statistical analysis and data presentation	71
4.	Results	72
4.1	Identification of the causative mutation	72
4.1.1	GLS001 mice: Munich <i>Gck</i> ^{M210R} mutants	72
4.1.1.1	Fine mapping	72
4.1.1.2	Candidate gene sequencing of the glucokinase (<i>Gck</i>) gene	72

4.1.2	GLS006 mice: Munich <i>Gck</i> ^{D217V} mutants	74
4.1.3	Candidate gene sequencing of the glucokinase (<i>Gck</i>) gene	74
4.2	Allelic differentiation of mutant mice	75
4.2.1	Genotyping of Munich <i>Gck</i> ^{M210R} mutants	75
4.2.2	Genotyping of Munich <i>Gck</i> ^{D217V} mutants	75
4.3	Functional consequences of the mutations	76
4.3.1	Quantification of glucokinase activity	76
4.3.2	Determination of glucokinase RNA expression in Munich <i>Gck</i> ^{M210R} mutants	80
4.3.3	Western blot analysis in Munich <i>Gck</i> ^{M210R} mutants	82
4.3.3.1	Quantification of glucokinase protein levels	82
4.3.3.2	Determination of apoptosis	82
4.4	Clinical findings in Munich <i>Gck</i>^{M210R} and <i>Gck</i>^{D217V} mutants	83
4.4.1	Basic clinical features	83
4.4.1.1	Body weight	84
4.4.1.2	Blood glucose levels	87
4.4.2	Specific clinical findings	90
4.4.2.1	Course of blood glucose levels after oral glucose application	91
4.4.2.2	Serum insulin	93
4.4.2.3	Beta cell function indices	95
4.4.2.4	Intraperitoneal insulin tolerance test (ipITT)	97
4.4.3	Comparison of clinical parameters of both strains	98
4.4.3.1	Body weight of neonatal and 3-day-old mutants	99
4.4.3.2	Blood glucose levels of neonatal and 1-day-old mutants	99
4.4.3.3	Glucose tolerance in heterozygous mutants	100
4.4.3.4	Serum insulin levels in heterozygous mutants	101
4.4.3.5	Homeostasis model assessment of baseline insulin secretion (HOMA B)	102
4.5	Survival studies in Munich <i>Gck</i>^{M210R} and <i>Gck</i>^{D217V} mutants	102
4.6	Organ weights	104
4.7	Analysis of specific organ alterations in Munich <i>Gck</i>^{M210R} mutants	106

4.8	Qualitative histological evaluation of the endocrine pancreas	107
4.8.1	Munich <i>Gck</i> ^{M210R} mutants	107
4.8.1.1	Pancreata from neonatal mice	107
4.8.1.2	Pancreata from 210-day-old mice	109
4.8.2	Munich <i>Gck</i> ^{D217V} mutants	110
4.8.2.1	Pancreata from 550-day-old mice	110
4.9	Quantitative stereological analysis of the endocrine pancreas	111
4.9.1	Munich <i>Gck</i> ^{M210R} mutants	111
4.9.1.1	Stereological findings in pancreata from neonatal male mice	111
4.9.1.2	Quantitative stereological parameters of pancreata from 210-day-old mutants	112
4.9.2	Munich <i>Gck</i> ^{D217V} mutants	113
4.9.2.1	Stereological findings in pancreata from 550-day-old male mice	113
5.	Discussion	116
5.1	Genetic aspects	116
5.2	Functional consequences of the mutations	118
5.2.1	Glucokinase activity	118
5.2.2	Glucokinase RNA expression	120
5.2.3	Glucokinase protein levels	121
5.3	Phenotypic characteristics	121
5.3.1	Heterozygous mutants	121
5.3.2	Homozygous mutants	124
5.4	Specific organ alterations	126
5.4.1	Liver	126
5.4.2	Endocrine pancreas	127
5.5	Conclusion and further prospects	132
6.	Summary	135
7.	Zusammenfassung	137
8.	References	140
9.	Attachment	168

9.1	Basic glucokinase enzyme kinetics and their extrapolation to studies	168
9.2	Low resolution mapping results	170
9.2.1	GLS001 mice	170
9.2.2	GLS006 mice	173
9.3	Abbreviations of chemical compounds and solutions	177
9.4	Evaluation of DNA concentrations via gel electrophoresis	178
9.5	Principle of evaluation of real-time PCR primer efficiencies	179
9.6	Evaluation of real-time PCR results, using the $2^{-\Delta CT}$ method	181
9.7	Histological staining methods	182
9.7.1	Haematoxylin and eosin (HE) staining	182
9.7.2	Periodic acid-Schiff (PAS) staining	182
9.7.3	Masson's trichrome staining (modified according to Goldner and Weigert)	183
9.7.4	Fat red staining	185
	Acknowledgements	186

1. Introduction

The release of the human genome sequence with high accuracy and nearly complete coverage in 2004 (Human Genome Sequencing 2004) represented a milestone in genome research and launched the entry into the “post-genome era” (Davies and Wynshaw-Boris 2009). Nevertheless, the transfer of the genomic sequence into any information about the function of the corresponding genes, their allelic variations and the metabolic pathways involved, requires functional genome research using animal models. Applying forward and reverse genetics, a plenitude of murine disease models has already been generated and examined, providing the opportunity to elucidate the structure and function of genomes and the transformation of genome-based knowledge into clinical research application (Collins *et al.* 2003a; Desaintes 2008) (<http://www.informatics.jax.org/>).

Major research efforts focussed on the investigation of important human diseases like diabetes mellitus (Collins *et al.* 2003b). The alarming dimensions of worldwide diabetes prevalence, the estimated increment of diabetic patients within the next 20 years (Wild *et al.* 2004), the accompanying public health and economic burden, and the absence of translational strategies to combat this “epidemic disease” have triggered the interest in diabetes research (Garfield *et al.* 2003; Gary and Brancati 2004). Since the pathogenesis of diabetes mellitus is not completely understood, experimental animal models represent a suitable tool to elucidate the genetic and pathogenic aspects of this disease. The power of ENU- (*N*-ethyl-*N*-nitrosourea) based random mutagenesis to generate mutant mouse models that recapitulate human disease phenotypes like diabetes mellitus has already been reported (Aigner *et al.* 2008). Integrated into the framework of the superordinated cluster “diabetes models” of the research training group “Functional Genome Research in Veterinary Medicine” supported by the DFG (Deutsche Forschungsgemeinschaft), the aim of the present study was the genetic, clinical and pathomorphological investigation of two novel diabetic mouse strains derived from the Munich ENU mouse mutagenesis project.

2. Literature review

2.1 Genetically modified mice in biomedical research

Due to ethical and technical limitations in human experimental research, animal models represent essential tools in biomedical research (Macchiarini *et al.* 2005; Moore 1999). Genetic predisposition and familiar heritability enact an important part in the pathogenesis of the most common human diseases, including e.g. obesity, cardiovascular diseases as well as diabetes mellitus. Therefore, genetically modified model systems have taken on great significance to contribute to basic biological research and its application in human medicine (Moore 1999; Spradling *et al.* 2006). However, in the majority of cases, the mouse, for a plethora of reasons, is still considered as the model organism of choice for the investigation of developmental and disease processes in the mammalian organism (Cox and Brown 2003; Rosenthal and Brown 2007).

2.1.1 The murine model system

2.1.1.1 Biological parameters

From practical and biological viewpoints, the laboratory mouse represents a powerful model. Mice are small mammals and many metabolic pathways are analogues to those in human beings. Therefore, mutant mouse phenotypes often recapitulate human disease phenotypes (Bedell *et al.* 1997; Woychik *et al.* 1998). The short generation time of about 10 weeks, the high number of offspring, and the possibility to maintain mice under standardised conditions represent key features that emphasise the potential of the mouse as an ideal model system (Silver 1995). Additionally, with the advanced breeding technologies, including assisted reproductive technologies like intracytoplasmic sperm injection (ICSI) or *in vitro* fertilisation (IVF), the successful establishment of protocols for surgical manipulations, and the adaption and *de novo* development of clinical assay technologies, the laboratory mouse became a favoured disease model (Nagy *et al.* 2003; Rossant and McKerlie 2001).

2.1.1.2 Genetic features

During the last 100 years, a high number of genetically defined inbred mouse strains, relevant for human biology and disease have been established (Beck *et al.* 2000; Paigen 2003). With the recent release of the nearly complete mouse genome sequence, comparative analysis of the human and the murine genome revealed remarkable similarities between both species. Ninety-nine percent of the murine genes possess homologues in the human genome and 96% of them are located within a similar conserved syntenic interval. Additionally, 40% of the mouse genome can be aligned confidentially to the human genome and 80% of the proteins, identified in the mouse have strict orthologues in human beings (Mouse Genome Sequencing 2009). Functional genome analysis of aberrant phenotypes comprises two complementary approaches: forward and reverse genetics (Brown *et al.* 2006; Nguyen and Xu 2008; Rosenthal and Brown 2007). The gene-driven approach involves the direct genetic manipulation of specific genes to control gene activity temporally, spatially, and reversibly by using reverse genetics techniques. The most common genetic manipulations in reverse genetics imply additive gene transfer, gene targeting by homologous recombination, and gene trapping. The phenotype-driven approach, based on forward genetics techniques starts with the observation of an abnormal phenotype as a result of spontaneous or induced genetic alterations and aims to proceed towards the identification and molecular understanding of the underlying genetic aberrations (Argmann *et al.* 2006; Russ *et al.* 2002).

2.1.2 Random mutagenesis in mice

Different approaches have been established for random mutagenesis in mice:

Table 2.1: Comparison of random mutagenesis strategies (adapted from Hrabé de Angelis *et al.* 2007 and Stanford *et al.* 2001).

Mutagenesis strategy	Mutation frequency	Type of mutation induced
Spontaneous	5×10^{-6} per locus	Point mutations, small deletions, chromosomal rearrangements
X-rays	$13-50 \times 10^{-5}$ per locus	Chromosomal rearrangements
Chemical mutagens	$11-150 \times 10^{-5}$ per locus ^a	Chromosomal rearrangements, point mutations, translocations, small deletions ^a
Insertional mutagenesis	5-100 % of all transgenic animals ^a	Insertions, deletions, disruption of endogenous gene expression or coding sequence ^a

^a Depending on the respective agent/strategy that is applied

With the description of the alkylating effect of some chemical mutagens and the discovery of the high mutagenic potential of nitroso-compounds (a category of alkylating agents), this group of chemical mutagens has reached predominant importance until today (van Harten 1998). According to the sensitivity of the targeted germ cell stage, alkylating agents can be divided into agents that affect:

- stem cell spermatogenesis and induce predominantly intragenic lesions (small deletions, base pair substitutions) like Procarbazine, Triethylenemelamine, *N*-ethyl-*N*-nitrosourea, and Methylnitrosourea, agents that affect
- early spermatids, like Chlorambucil and Melphalan, and agents that affect
- late spermatids or spermatozoa and predominantly cause large lesions (chromosome aberrations, deletions) such as Ethylmethanesulfate, Methylethanesulfate, Cyclophosphamide, and Diethylsulfate (Hrabé de Angelis *et al.* 2007).

2.2 *N*-ethyl-*N*-nitrosourea (ENU)-induced mutagenesis

Alkylating agents can also be differentiated into mono- (including *N*-ethyl-*N*-nitrosourea), bi-, or poly-functional alkylating agents. Monofunctional agents are most suitable because they act at a higher concentration level than polyfunctional agents before cell death arises and are therefore less cytotoxic. Furthermore, monofunctional agents induce higher mutation rates and are reported to induce a higher proportion of point mutations than polyfunctional alkylating agents (Sanderson and Shield 1996; van Harten 1998). In 1979, *N*-ethyl-*N*-nitrosourea (ENU) was discovered to be the most potent chemical mutagen in the mouse that has been investigated so far (Russell *et al.* 1979). Since that time, ENU has emerged as the most favourable alkylating agent for application in chemical mutagenesis and has been used in many different laboratories and mutagenesis experiments as an *in vivo* germline mutagen (Balling *et al.* 1998; O'Brien and Frankel 2004; Smits *et al.* 2008).

2.2.1 Biochemical features of ENU

ENU is a monofunctional alkylating agent (Fig. 2.1A) that needs no metabolic processing for its activation. ENU acts by transferring its ethyl group to oxygen or nitrogen residues at various reactive nucleophilic sites of the DNA. Mispairing of the DNA double strand and, finally base pair substitution, or base-pair loss represent the consequences from ENU-mediated DNA alkylation (Guenet 2004; Hrabé de Angelis

et al. 2004; Shibuya and Morimoto 1993) (Fig. 2.1B, C). Further, a dose-dependent linear relationship between the administered ENU dose and the resulting mutation rate has been reported (Favor *et al.* 1997; Favor *et al.* 1990).

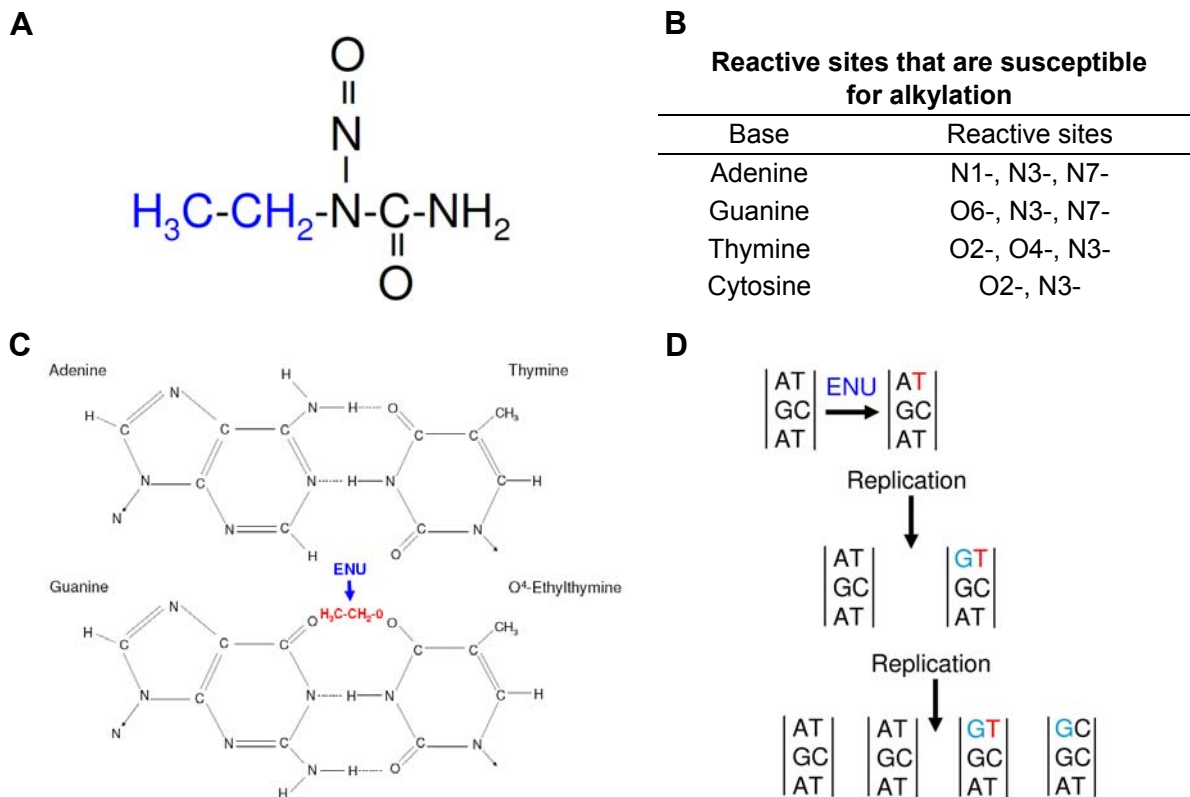


Figure 2.1: Biochemical structure of ENU (A), reactive sites that are susceptible for ENU induced alkylation (B), and example of ENU-induced base pair substitutions (C, D). Alkylation of thymine results in formation of O⁴-Ethylthymine (C) which is, by mistake, recognised as cytosine, leading to the corresponding base exchange during replication Modified according to Hrabé de Angelis *et al.* 2004 and Noveroske *et al.* 2000.

ENU predominantly induces point mutations, thereby leading to allelic series for functional gene analysis (Schimenti and Bucan 1998; Stanford *et al.* 2001). A/T→T/A transversions (27-30%) and A/T→G/C transitions (30-37%) represent the most common ENU-induced modifications. If a coding sequence is affected, missense mutations are reported to represent the most frequent consequences. Most of the mutations sequenced yet, bear these types of mutations (Noveroske *et al.* 2000; Papathanasiou and Goodnow 2005), whereas nonsense, splice-site, and frameshift mutations as well as in-frame deletions occur less frequently (Barbaric *et al.* 2007). The respective point mutation can lead to complete loss-of-function (null mutation),

partial loss-of-function (hypomorphs), gain-of-function (hypermorphs) or altered function (neomorphs) of the affected proteins (O'Brien and Frankel 2004). The predominance of A/T→T/A transversions limits the spectrum of ENU-induced mutations. Evaluation of data from both phenotype- and genotype-driven screens showed that genes with a long coding sequence length (>1000 bases), high numbers of exons (>10 exons), and high G and C contents (>58%), are more susceptible for ENU-induced mutations. Additionally, many mutations are often neighbored by G and C nucleotides. Consequentially, about 50% of the mouse genes are supposed to be underrepresented in ENU mutagenesis projects (Barbaric *et al.* 2007). However, the mutation efficacy of ENU and the possibility to produce a large number of mutant offspring from one treated mouse (Balling *et al.* 1998) represent appreciable advantages of ENU-driven mutagenesis. Mutation frequency of ENU-induced mutations varies, depending on the applied dose and the administration protocol (Coghill *et al.* 2002; Favor *et al.* 1990; Hitotsumachi *et al.* 1985). In current ENU-driven screens, mutation rates of 1 mutation in 0.1-2.5 Mb were observable (Beier 2000; Concepcion *et al.* 2004; Sakuraba *et al.* 2005). Assuming a mutation frequency of 1 in every 1 Mb together with total length of the haploid mouse genome of 2.5×10^9 bp and 20,200 coding sequences with an average length of 1000 bp (Barbaric *et al.* 2007; Mouse Genome Sequencing 2009), ENU mutagenesis would result in about 2500 mutations per genome (including mutations in non-coding regions) and in 20 mutated coding nucleotides per genome. Due the redundancy within the genetic code, many of the base exchanges within coding regions are predicted to be silent mutations (i.e. change in a base pair without altering the protein coding amino acid). Additionally, the mean distance of 1-2.5 Mb between two mutations allows segregation of most silent and non-causative mutations by phenotype-selective breeding strategies (Griffiths *et al.* 1999; Russ *et al.* 2002).

2.2.2 Contribution of ENU mutagenesis to biomedical research

Disease-associated alleles in human beings are usually characterised by subtle genetic modifications (Korf 1995). ENU induces preferably point mutations that involve a broad range of mutant phenotypes (Justice *et al.* 1999).

Screening for mutations in ENU mutagenesis projects imply two complementary strategies, e.g. phenotype- (forward genetics) and genotype-driven screens (reverse genetics). In phenotype-driven screens mutant models are selected according to

defined phenotypes of interest, observable in human diseases. This strategy aims to identify the causative mutation and subsequently, the disease-associated gene of the selected phenotypes. In genotype-driven strategies, mutations in specific genes of interest are identified by DNA analysis from sperm archives, embryonic stem cells or ENU-mutagenised mice without previous phenotypic screening (Acevedo-Arozena *et al.* 2008; Kennedy and O'Bryan 2006). The aim in both approaches is the identification of disease-associated genes/alleles and the dissection of the structure-to-function relationships of the affected protein. This attempt is not limited to monogenic Mendelian traits but can also focus on the investigation of diseases, resulting from interactions of multiple loci. Since ENU-generated models usually are monogenic, a practical approach towards multigenic alterations is the application of sensitised/modifier screens (Acevedo-Arozena *et al.* 2008; Nolan *et al.* 2002). An additional important aspect is the potential of ENU to induce various types of alleles (allelic series).

2.2.3 ENU mutagenesis project strategies

ENU-driven projects can be classified into genome-wide and region-specific screens. The choice of the project type depends on the aim of the study. Genome-wide screens provide the opportunity to investigate the genetic regulation of a specific biological process, whereas region-specific screens are usually applied to obtain allelic series, or are performed for functional analysis of a particular genomic interval (Kile and Hilton 2005). Up to now, several genome-wide and region-specific ENU screens have been accomplished, with emphasis on different research focuses. The Munich ENU mouse mutagenesis project was one of the first established large-scale ENU programs (Cordes 2005; Kennedy and O'Bryan 2006).

2.3 The Munich ENU mouse mutagenesis project

In the phenotype-driven large-scale Munich ENU mouse mutagenesis project, a high number of mutant mice has been generated and tested for a multitude of phenotypic abnormalities by high-throughput screening (Hrabé de Angelis *et al.* 2000).

2.3.1 Research focus

In order to extend the quantity and quality of mouse mutant resources, the Munich ENU project aimed to produce a plethora of mouse mutants, recapitulating

phenotypes of relevant inherited human diseases. The large-scale screening strategy allows addressing the “phenotype gap” between the available spectrum of mutant mice and human disease phenotypes. For this purpose, the production of a broad range of various phenotypes was expected (Brown and Balling 2001; Brown and Peters 1996; Hrabé de Angelis and Balling 1998). Representing a prerequisite for the practicability of the phenotype–driven strategy, standardised feasible procedures to evaluate phenotypes of interest were established. The screening and phenotyping protocol was mainly focused on the identification of postnatal aberrant phenotypes with major screens for dysmorphology, behaviour, immunology, clinical chemistry, and additional associated screens (DNA repair, deafness, nociceptive and mitochondrial disease) (Balling 2001; Soewarto *et al.* 2000). Screening strategies were primarily established to discover aberrant phenotypes that result from dominant or recessive mutations (Hrabé de Angelis *et al.* 2000).

2.3.2 Mutagenesis and screening protocol

The Munich ENU mouse mutagenesis project was carried out on the inbred C3HeB/FeJ (C3H) genetic background. At an age of 10-14 weeks, male mice were injected intraperitoneally with weekly doses of 90 mg/kg ENU for a period of three weeks. After a time period of transient sterility (10-15 days, depending on the dosage and application protocol) (Hitotsumachi *et al.* 1985; Russell *et al.* 1979), mutagenised G0 males were mated with C3H females to produce G1 offspring, which were subsequently screened for abnormal phenotypes (screen for dominant mutations). Inheritance of the abnormal phenotype on the C3H genetic background was tested in G2 progenies, derived from mating G1 animals, exhibiting an aberrant phenotypic trait, with healthy C3H mice. Screening for recessive mutations was carried out on G3 animals, generated by mating G1 males, which did not show an abnormal phenotype in the screen for dominant mutations, with female C3H mice to produce G2 female mice which were then again mated with their fathers. Inheritance of the abnormal phenotype was tested in G4 intercross mice or in progenies resulting from G4xG3 backcrosses (Aigner *et al.* 2008; Hrabé de Angelis *et al.* 2000) (Fig. 2.2). In the clinical chemical screen, blood samples from fasted mice were analysed for more than 20 parameters, including basic haematology, plasma enzyme activities, electrolyte concentrations, and substrates like glucose concentrations, serum cholesterol, and urea (Rathkolb *et al.* 2000). Established mutant strains were bred on

the C3H inbred genetic background to allow phenotypic studies without interfering influences of variations in the genetic background (Hrabé de Angelis *et al.* 2000). More than 15,000 G1 offspring and 500 G3 pedigrees were screened for clinically relevant parameters, resulting in more than 100 phenotypic mutant strains. Further, a large number of phenotypic mutant mice, which were not yet tested for inheritance of the abnormal phenotype, were conserved by sperm freezing (Aigner *et al.* 2008; Hrabé de Angelis *et al.* 2000).

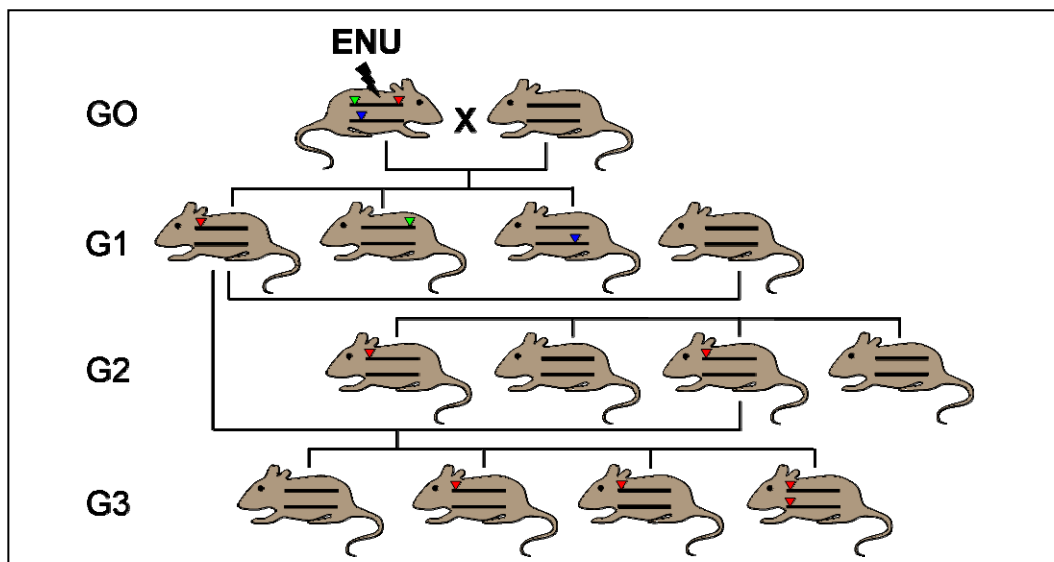


Figure 2.2: Generation of ENU-induced mutant mouse models. After intraperitoneal ENU administration, male G0 mice were mated to female wild-type mice to produce G1 mice. The screen for dominant mutations was carried out in the G1 offspring. The inheritance of the abnormal phenotype for dominant mutations was tested in the G2 offspring, and the screen for recessive mutations was accomplished with G3 progeny. Modified according to Aigner *et al.* 2008.

2.3.3 Linkage analysis of dominant mutations

The identification of the causative mutation starts with the determination of the affected chromosomal region. Genetic linkage is the logical consequence of physical linkage, and is appropriate for linkage analysis of loci that are polymorphic (with two or more distinguishable alleles) (Silver 1995). In the Munich ENU mouse mutagenesis project, linkage analysis was performed using an outcross-backcross breeding panel. Heterozygous phenotypic mutants on the C3H inbred genetic background were mated to wild-type mice of a second inbred strain (C57BL/6J). Male G1 hybrid offspring, displaying the abnormal phenotype, were again backcrossed to wild-type females of the second inbred strain. The resulting G2 progenies were

classified into phenotypic mutants and phenotypic wild-type mice. Using a panel of genome-wide DNA markers (single-nucleotide polymorphisms (SNPs) or microsatellites¹ (Lindblad-Toh *et al.* 2000; Xing *et al.* 2005)), which are polymorphic for the two inbred strains used, DNA analysis of phenotypic mutant G2 mice and phenotypic wild-type littermates was carried out. High throughput genotyping of the outcross-backcross panel was performed by matrix-assisted laser desorption ionisation time-of-flight mass spectrometry (Buetow *et al.* 2001; Hrabé de Angelis *et al.* 2000). Genotypic discrimination resulted in determination of the affected chromosomal region, which is heterozygous in phenotypic mutant G2 animals and homozygous for the C57BL/6J genotype in phenotypic wild-type G2 mice. Genotyping of only 50 G2 phenotypic mutants provides the opportunity to map the causative mutation to a specific chromosomal region. With the assignment of the number of meioses scored and the number of loci that display recombinant allelic combination, testing of the hypothesis that two loci are linked is now feasible by χ^2 -test. Linkage analysis, together with the available mouse genome sequence provides therefore the basis for positional candidate gene selection and sequencing (Balling 2001; Reeves and D'Eustachio 1999; Silver 1995).

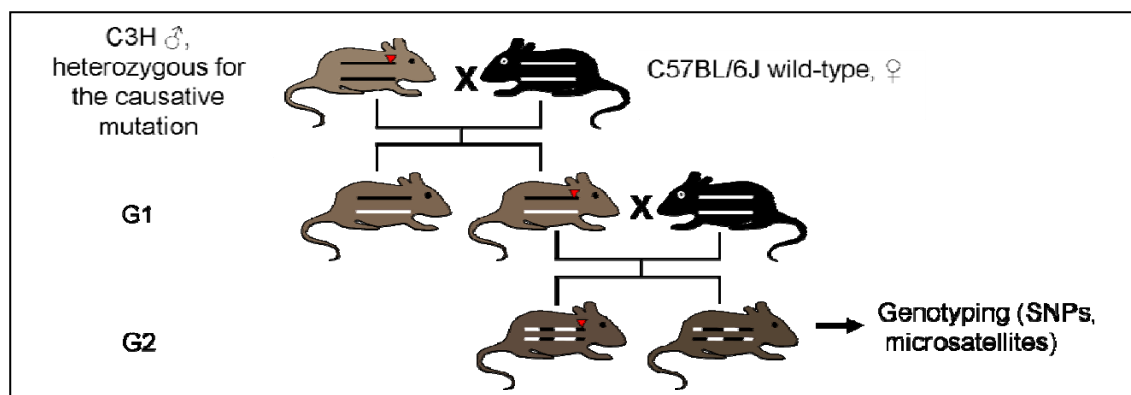


Figure 2.3: Schematic illustration of the breeding strategy for linkage analysis. The position of the causative mutation is marked by a red triangle. Modified according to Aigner *et al.* 2008.

2.3.4 Phenotype screening for diabetic mouse models

The clinical chemical screen in the Munich ENU mouse mutagenesis project was accomplished with blood samples from 90-day-old G1 and G3 offspring which were

¹ Microsatellite markers represent short but surpassing polymorphic, high density spread tandem repeats of mono-, di-, tri- or tetrameric sequences. Allelic variation manifests in differences in the number of repeats, present in a tandem array (Silver 1995).

fasted overnight. The required blood volume was yielded by puncture of the retroorbital sinus under short-term general anaesthesia. Plasma glucose concentrations from Li-heparinised blood samples were quantified by an enzymatic hexokinase assay using the reagent OSR6121 (Olympus, Germany) in the linear measurement range of 10-800 mg/dl (0.6-45 mmol/l) (Rathkolb *et al.* 2000). Since genetic and environmental influences are known to affect phenotypic characteristics (Cox and Brown 2003; Klempt *et al.* 2006), the physiological range of plasma glucose was determined in wild-type control mice. Based on the upper value of the 90% range (208 mg/dl in male mice, 201 mg/dl in female animals), mice exhibiting plasma glucose concentrations of more than 200 mg/dl in two measurements within an interval of three weeks were considered hyperglycaemic. Four hyperglycaemic mouse strains, harbouring dominant mutations have been established so far and further strains are currently tested for inheritance of the diabetic phenotype (Aigner *et al.* 2008). The successful identification of the causative mutation and the clinical and pathomorphological consequences has already been described for the strain GLS004 (Herbach *et al.* 2007). Two other hyperglycaemic mouse strains, GLS001 and GLS006, were subsequently chosen for the present study.

2.3.5 Initial characterisation of the ENU strains GLS001 and GLS006

After the confirmation of a dominant mutation being causative for the abnormal phenotype in both strains, genome-wide linkage analysis was carried out, using DNA samples of 75 G2 backcross mutants and 15 wild-type littermates for the ENU strain GLS001, and DNA samples from 70 G2 backcross mutants and 22 wild-type littermates of the ENU strain GLS006. Single nucleotide polymorphism (SNP)-based strategies were performed using a genome-wide mapping panel consisting of a total number of 136 (GLS001) and 141 (GLS006) polymorphic markers (performed in cooperation with the Institute of Experimental Genetics (Prof. Dr. M. Hrabé de Angelis, Helmholtz Zentrum München, Neuherberg). SNP analyses revealed a strong linkage ($\chi^2=64.7$; $p<0.0001$ for GLS001 mice and $\chi^2=80.2$; $p<0.0001$ for the ENU strain GLS006) of the diabetic phenotype of both strains to polymorphic markers on chromosome 11. The diabetic phenotype of GLS001 mice mapped to a marker at 14.3 Mb (reference SNP: rs13480881), that of GLS006 mice to a marker at 7.1 Mb (reference SNP: rs13480851) (chapter 9.2). Scanning the mouse genome data base (Mouse Genome Informatics, MGI; <http://www.informatics.jax.org/>) for potential

diabetes-associated candidate genes indicated the glucokinase (*Gck*) gene, which is situated within the mapping region, as a potential candidate gene for both strains. Murine *Gck*, which is located on chromosome 11 at 5.8-5.9 Mb, is comprised of 11 exons including liver- and β -cell specific variants of exon 1, and spans a total number of ~ 48.8 kb². Since the glucokinase enzyme is known to play an important role in regulation of glucose metabolism, the positional *Gck* was chosen as candidate gene for both ENU strains to undergo further sequence analysis.

2.4 Diabetes mellitus in human beings

2.4.1 Definition and description of diabetes mellitus

Diabetes mellitus is defined as a heterogeneous group of metabolic disorders characterised by hyperglycaemia resulting from defects in insulin secretion, insulin action or both. Long-term consequences of prolonged hyperglycaemia represent damage, dysfunction, and failure of various organs, especially the eyes, kidneys, nerves, heart, and blood vessels (American Diabetes Association 2009). The pathogenesis of diabetes mellitus involves various complex determinants influencing the development of this disease. At least three factors are involved in the pathogenesis of diabetes mellitus (Leahy 2005; Lehmann and Spinas 2000).

- Genetic predisposition: i.e. mutations/polymorphisms in genes, encoding for transcription factors (Weedon *et al.* 2006), mutations in genes involved in glucose metabolism (glucokinase)
- Beta cell dysfunction and failure resulting in inadequate insulin secretion
- Peripheral insulin resistance: decreased response of liver, muscle, and adipose tissue to insulin stimulus

A fourth pathogenic factor is discussed to contribute to the development of diabetes mellitus: environmental conditions like lifestyle, nutrition or infectious agents are supposed to strongly influence the development of diabetes mellitus (Leahy 2005; Lehmann and Spinas 2000).

The pathognomonic sign of diabetes mellitus represents hyperglycaemia, occasionally accompanied by polyuria, polydipsia, weight loss, sometimes with polyphagia and blurred vision. Other concomitant symptoms including impairment of

² http://www.ensembl.org/Mus_musculus/Gene/Summary?g=ENSMUSG00000041798

growth and susceptibility to certain infections can also appear. Hyperglycaemia with ketoacidosis or the nonketotic hyperosmolar syndrome represent possible life threatening consequences of uncontrolled diabetes mellitus. Further, chronic hyperglycaemia is known to be associated with long-term complications resulting from macro- and microvascular lesions. Organ-specific microvascular pathology includes retinopathy accompanied by potential loss of vision; nephropathy leading to renal failure; peripheral neuropathy; risk of foot ulcers, amputations, and Charcot joints; and autonomic neuropathy causing gastrointestinal, genitourinary, and cardiovascular symptoms, and sexual dysfunction. Atherosclerotic macrovascular lesions increase the risk of cardiovascular, peripheral arterial, and cerebrovascular disease in diabetic patients. An increase in the polyol pathway flux, enhanced formation of advanced glycation end-products (AGEs), the activation of protein kinase C (PKC), sorbitol accumulation, and myo-inositol depletion, and an accelerated hexosamine pathway are the mechanisms that are hypothesised to major account for macro- and microvascular complications in diabetes mellitus (American Diabetes Association 2009; Brownlee 2001; Kikkawa 2000).

2.4.2 Diagnostic criteria for diabetes mellitus

Diagnosis of diabetes mellitus in patients with severe hyperglycaemia or in asymptomatic persons with only slightly elevated blood glucose values requires feasible diagnostic tests (Alberti and Zimmet 1998).

According to the expert committee on the diagnosis and classification of diabetes mellitus, subjects, meeting one of the criteria stated in Table 2.2, are classified diabetic.

Table 2.2: Criteria for the diagnosis of diabetes

1. Fasting plasma glucose (FPG) ≥ 126 mg/dl (7.0 mmol/l). Fasting is defined as no caloric intake for at least 8 h.*
 2. Symptoms of hyperglycaemia and a casual plasma glucose ≥ 200 mg/dl (11.1 mmol/l). Casual is defined as any time of day without regard to time since last meal. The classic symptoms of hyperglycaemia include polyuria, polydipsia, and unexplained weight loss.
 3. 2-h plasma glucose ≥ 200 mg/dl (11.1 mmol/l) during an oral glucose tolerance test (OGTT). The test should be performed as described by the World Health Organization, using a glucose load containing the equivalent of 75 g anhydrous glucose dissolved in water.*
-

*In the absence of unequivocal hyperglycaemia, these criteria should be confirmed by repeat testing on a different day.

Although the 75-g OGTT is more sensitive and modestly more specific to diagnose diabetes than FPG, it is poorly reproducible and difficult to perform in practice. Therefore, the determination of FPG represents the preferred diagnostic test. Though the OGTT is not recommended for routine clinical use, it may be useful for further evaluation of patients in whom diabetes is still strongly suspected but who have normal FPG or impaired FPG (IFG).

An additional intermediate group of subjects whose glucose levels, although not meeting criteria for diabetes, are nevertheless too high to be considered normal has been admitted. This group is defined as having FPG levels between 100–125 mg/dl (5.6–6.9 mmol/l) or 2 h values in the OGTT of 140–199 mg/dl (7.8–11.1 mmol/l). These persons are consequently classified according to the criteria stated in Table 2.3.

Table 2.3: Classification of patients with equivocal glucose levels

FPG <100 mg/dl (5.6 mmol/l)	→ normal fasting glucose
FPG 100–125 mg/dl (5.6–6.9 mmol/l)	→ IFG (impaired fasting glucose)
FPG ≥ 126 mg/dl (7.0 mmol/l)	→ provisional diagnosis of diabetes (the diagnosis must be confirmed, as described below)
when the OGTT is used	
2-h postload glucose <140 mg/dl (7.8 mmol/l)	→ normal glucose tolerance
2-h postload glucose 140–199 mg/dl (7.8–11.1 mmol/l)	→ IGT (impaired glucose tolerance)
2-h postload glucose ≥200 mg/dl (11.1 mmol/l)	→ provisional diagnosis of diabetes (the diagnosis must be confirmed, as described below)

Patients with IFG or IGT are considered “pre-diabetic” with a relatively high risk for the development of diabetes. IFG and IGT by their own (in absence of pregnancy) do not represent clinical entities, but can be considered as intermediate stages and are associated with the metabolic syndrome, which includes obesity (abdominal or visceral obesity), dyslipidaemia of the high-triglyceride and/or low-HDL type, and hypertension.

Due to lack of global standardisation and uncertainty about diagnostic thresholds, the use of the HbA_{1c}³ for the diagnosis of diabetes has previously not been

³ Measurements of glycosylated proteins, including haemoglobin represent suitable methods to assess glycaemia. The term HbA_{1c} is used to describe stable minor haemoglobin components which are formed nonenzymatically from haemoglobin and glucose (Reynolds *et al.* 2003).

recommended. However, a worldwide move toward a standardised assay and an increasing observational evidence about the prognostic significance of HbA_{1c} will likely lead to a recommendation of HbA_{1c} as the preferred diagnostic parameter for diabetes mellitus by the International Diabetes Federation.

The criteria for abnormal glucose tolerance in gestational diabetes mellitus are adapted from Carpenter and Coustan (1982). Fasting plasma glucose levels >126 mg/dl (7.0 mmol/l) or a casual plasma glucose >200 mg/dl (11.1 mmol/l) meets the threshold for the diagnosis of diabetes. If glucose levels are equivocal, the diagnosis must be confirmed on a subsequent day (Carpenter and Coustan 1982).

2.4.3 Classification of diabetes mellitus

The classification of diabetes mellitus according to the recommendations of the American Diabetes Association (ADA) and the WHO was fundamentally revised in 1997 in order to establish a classification reflecting the aetiology and pathogenesis of diabetes mellitus. Therefore, the terms "juvenile-onset/insulin-dependent diabetes mellitus" and "maturity-onset/non-insulin-dependent diabetes mellitus" which were used to formerly distinguish between type 1 and type 2 diabetes mellitus are obsolete (Fajans 1998; Lehmann and Spinaz 2000; Murphy *et al.* 2008; Sacks 1997). According to the recommendations of the ADA and the WHO, diabetes mellitus in human beings is classified into four main groups.

- I) Type 1 diabetes (β -cell destruction, usually leading to absolute insulin deficiency)
 - Immune mediated
 - Idiopathic
- II) Type 2 diabetes (may range from predominantly insulin resistance with relative insulin deficiency to a predominantly secretory defect with insulin resistance)
- III) Other specific types
 - Genetic defects of β -cell function
 - Chromosome 12, HNF-1 α (MODY3)
 - Chromosome 7, glucokinase (MODY2)
 - Chromosome 20, HNF-4 α (MODY1)
 - Chromosome 13, insulin promoter factor-1 (IPF-1; MODY4)
 - Chromosome 17, HNF-1 β (MODY5)
 - Chromosome 2, NeuroD1 (MODY6)
 - Mitochondrial DNA and others

- Genetic defects in insulin action (type A insulin resistance, Leprechaunism, Rabson-Mendenhall syndrome, lipomatrophic diabetes and others)
- Diseases of the exocrine pancreas (pancreatitis, trauma/pancreatectomy, neoplasia, cystic fibrosis, haemochromatosis, fibrocalculous pancreatopathy and others)
- Endocrinopathies (acromegaly, Cushing's syndrome, glucagonoma, pheochromocytoma, hyperthyroidism, somatostatinoma, aldosteronoma and others)
- Drug- or chemical-induced (vacor, pentamidine, nicotinic acid glucocorticoids, thyroid hormone, diazoxide, β -adrenergic agonists, thiazides, dilantin, α -Interferon and others)
- Infections (congenital rubella, cytomegalovirus and others)
- Uncommon forms of immune-mediated diabetes ("Stiff-man" syndrome, anti-insulin receptor antibodies and others)
- Other genetic syndromes sometimes associated with diabetes (Down's syndrome, Klinefelter's syndrome, Turner's syndrome, Wolfram's syndrome, Friedreich's ataxia, Huntington's chorea, Laurence-Moon-Biedl syndrome, Myotonic dystrophy, Porphyria, Prader-Willi syndrome and others)

IV) Gestational diabetes mellitus (GDM)

Gestational diabetes mellitus (GDM) is defined as any degree of glucose intolerance with onset or first recognition during pregnancy (Metzger and Coustan 1998). Approximately 7% of all pregnancies are complicated by GDM, resulting in more than 200,000 cases annually (American Diabetes Association 2003).

2.4.4 Global burden of diabetes mellitus

During the last decades, the prevalence of diabetes mellitus in industrial nations has taken on alarming dimensions. The worldwide prevalence of diabetes mellitus among adults is estimated to advance from 4% in 1995 to 5.4% in 2025 and the worldwide prevalence of diabetes for all age groups is predicted to rise from 2.8% in 2000 to 4.4% in 2030. The total number of people suffering from diabetes mellitus is projected to rise from 171 million in 2000 to 366 million in 2030, and for adults to advance from 135 million in 1995 to 300 million in 2025 (King *et al.* 1998; Wild *et al.* 2004). A dramatic increase of about 42% - from 51 to 72 million- is predicted for

developed countries and even a 170% increase - from 84 to 228 million people - is assumed for developing countries. Thus, by the year 2025, 75% of people with diabetes mellitus will reside in developing countries. According to this exceeding increase, diabetes mellitus is already considered an “epidemic” disease (Zimmet *et al.* 2001). India, China, and the United States are considered as the countries with the highest number of people suffering from diabetes mellitus (King *et al.* 1998). In Germany, the total number of diabetic persons currently amounts to four million (population prevalence of 5%) (Federal Health Monitoring 2006; www.gbe-bund.de) and is predicted to further increase dramatically in the future (www.who.int/diabetes). Type 2 diabetes, representing 90-97% of all diabetes cases, is reported to be the most common diabetes subtype (Bjork 2001; Printz and Granner 2005). Diabetes mellitus is accompanied by a 3-4 times higher risk of death as compared to those without diabetes and people with diabetes are on average 3 times more likely hospitalised. Recent data demonstrated that, in the United States, diabetes represents the leading cause of blindness and accounts for 40% of new cases of end-stage renal disease. The risk for leg amputation is 15–40 times higher and the risk for heart disease and stroke is 2-4 times higher for people with diabetes mellitus as compared to people without diabetes (Bjork 2001). The critical rise of the prevalence of diabetes and diabetes-associated complications is accompanied by exceeding costs (Hogan *et al.* 2003). Therefore, the urgent need for elucidating the pathomechanisms of diabetes mellitus is incontestable to combat this disease.

2.5 Maturity-onset diabetes of the young (MODY)

Maturity-onset diabetes of the young (MODY) was described for the first time in 1974. R.B. Tattersall observed mild non-progressive diabetes in three families, appearing usually in juvenile subjects (in the early twenties), and he suggested that this phenotype might be inherited in a dominant Mendelian pattern (Tattersall 1974). One year later, the assumption of an autosomal dominant inheritance of MODY has been proven (Tattersall and Fajans 1975). During the following years, various MODY-associated genes have been discovered, resulting in novel subtypes of MODY.

2.5.1 Characteristics of MODY

MODY represents a clinically and genetically heterogeneous group of monogenic

disorders, characterised by an autosomal dominant mode of inheritance with high penetrance of the resulting diabetic phenotype. Affected individuals develop nonketotic diabetes due to defective insulin secretion resulting from an inherited β -cell dysfunction, whereas insulin action is usually unaffected (American Diabetes Association 2009; Fajans *et al.* 2001; Velho and Froguel 1998). Even if a great phenotypic variability is reported to appear within a MODY pedigree as well as among the individual subtypes, the MODY phenotype is characterised in general by early age of onset of the diabetic phenotype (between childhood and early adulthood but usually before an age of 25 years) (Rehman 2001; Velho and Froguel 1998). The nature of the causative mutation, as well as modifying genes that are inherited independently, and environmental factors have been described to influence the age of clinical manifestation in MODY 3 patients (Kim *et al.* 2003). MODY 2 patients are known to exhibit hyperglycaemia from birth but the disease often remains undiagnosed due to the mild diabetic phenotype (Singh 2006; Timsit *et al.* 2005). Additionally, different phenotypic outcomes are reported in patients, exhibiting identical MODY subtypes (Fajans and Bell 2006). Considering the heterogeneity among the particular MODY subtypes, concerning the age of diagnosis, the pattern of diabetic outcome, the requirement of specific treatment and the occurrence of extrapancreatic manifestations, the unifying term “MODY” would no longer fulfil the manifold spectrum of this polymorphic disease. Consequently, the current opinion according to the reconditioned classification of diabetes in 1997 is to choose the correct monogenic terms of the different forms of young-onset diabetes appropriate to their aetiology and to classify them into four groups under the main topic “Monogenic forms of β -cell dysfunction” (Murphy *et al.* 2008; Sacks 1997):

1. Diagnosis before 6 months of age (transient (TNDM) or permanent neonatal diabetes mellitus (PNDM))
2. Mild familial hyperglycaemia (e.g. due to mutations in the glucokinase gene)
3. Familial young-onset diabetes (e.g. mutations in the gene encoding the hepatocyte nuclear factor-1 β)
4. Diabetes with extrapancreatic features (like Wolfram syndrome, mutations in the hepatocyte nuclear factor-1 α -encoding gene)

However, the current classification of diabetes adheres to the established subtypes. The exact prevalence of MODY and its subtypes in particular is unknown, but

estimations suppose a worldwide prevalence for MODY of about 2-5% of all type 2 diabetic subjects (McCarthy and Froguel 2002; van Tilburg *et al.* 2001; Velho and Robert 2002). The relative prevalence of the MODY subtypes varies greatly depending on the population, but all studies clearly point out that MODY 2 and 3 account for the most cases (Chèvre *et al.* 1998; Hattersley 1998; Lindner *et al.* 1999). From the six official MODY-associated genes, five encode for tissue specific transcription factors, which are expressed in pancreatic β -cells and are known to be involved in complex regulation of genes controlling glucose homeostasis (MODY 1 and MODY 3-6) (Mitchell and Frayling ; Thomas *et al.* 2001) (Fig. 2.4).

2.5.2 MODY subtypes

Table 2.4: MODY subtypes according to the classification of the ADA and the WHO (A, B) and MODY subtypes, not yet admitted to the official classification (C).

A	MODY 1	MODY 2	MODY 3
OMIM ID	125850	125851	600496
Affected gene	<i>HNF4A</i>	<i>GCK</i>	<i>HNF1A</i>
Chromosomal location	20q12-q13.1	refer to chapter 2.7.4	12q22-qter; 12q24.2
Affected protein	Hepatocyte nuclear factor-4 α		Hepatocyte nuclear factor-1 α
Prevalence ^a	Rare		Very common
Physiological function	Regulation of hepatic and pancreatic β -cell gene expression		Controls <i>PDX1</i> , <i>HNF4A</i> , and <i>GLUT2</i> expression
Diabetic phenotype (heterozygous state)	Progressive hyperglycaemia macrosomia ⁴ , transient hypoglycaemia and/or hyperinsulinaemia		Severe diabetes, renal glucosuria pancreatic exocrine failure, increased sensitivity to sulfonylureas
Extrapancreatic manifestations	Alteration in liver triglycerides		Low renal threshold for glucose, liver adenomatosis
Diabetic complications	Frequent		Frequent
Treatment	Oral antidiabetics or insulin		Insulin or oral antidiabetics
References	(Brink 2003; Fajans <i>et al.</i> 2001; Gupta and Kaestner 2004; Hattersley 1998; Ilag <i>et al.</i> 2000; Matyka <i>et al.</i> 1998; Sladek <i>et al.</i> 1990; Stanger 2008; Winter 2003; Yamagata <i>et al.</i> 1996)		(Bellanné-Chantelot <i>et al.</i> 2008; Cerf 2006; Ellard and Colclough 2006; Kuo <i>et al.</i> 1992; Menzel <i>et al.</i> 1998; Reznik <i>et al.</i> 2004; Vaxillaire and Froguel 2008; Vesterhus <i>et al.</i> 2008a; Vesterhus <i>et al.</i> 2008b)

⁴ MODY 1 subjects exhibit macrosomia most likely as a result of prolonged exposure insulin, due to surpassing fetal production of the anabolic acting hormone insulin (Pearson *et al.* 2007).

B	MODY 4	MODY 5	MODY 6
OMIM ID	606392	137920	606394
Affected gene	<i>IPF1</i>	<i>HNF1B</i>	<i>NEUROD1</i>
Chromosomal location	13q12.1	17cen-q21.3	2q32
Affected protein	Insulin promoter factor-1	Hepatocyte nuclear factor-1 β	BETA2/NeuroD1
Prevalence ^a	Rare	Very rare	Very rare
Physiological function	Essential for embryonic pancreas development, regulation of <i>GCK</i> , <i>INS</i> , and <i>GLUT2</i> expression	Important role in embryonic development, regulates <i>HNF4A</i> expression	Essential for neuronal differentiation and pancreatic development and function
Diabetic phenotype (heterozygous state)	Diabetes mellitus, intermediate between MODY2 and MODY1	Renal cysts and diabetes (variable severity) (RCAD), partial pancreatic agenesis	Probably severe but limited data
Extrapancreatic manifestations	Unknown	Hepatic, biliary, and genitourinary manifestations, renal failure	Unknown
Diabetic complications	Unknown	Unknown	Unknown
Treatment	Oral antidiabetic treatment, insulin	Insulin	Insulin
References	(Fajans and Bell 2006; Mitchell and Frayling ; Nyunt <i>et al.</i> 2009; Stoffers <i>et al.</i> 1997a; Stoffers <i>et al.</i> 1997b; Weng <i>et al.</i> 2001; Winter 2000)	(Bellanné-Chantelot <i>et al.</i> 2004; Fajans and Bell 2006; Furuta <i>et al.</i> 2002; Haldorsen <i>et al.</i> 2008; Igarashi <i>et al.</i> 2005; Kitanaka <i>et al.</i> 2004; Ulinski <i>et al.</i> 2006; Winter 2003)	(Chao <i>et al.</i> 2007; Fajans <i>et al.</i> 2001; Lee <i>et al.</i> 1995; Liu <i>et al.</i> 2007; Malecki and Mlynarski 2008; Mitchell and Frayling ; Naya <i>et al.</i> 1997)

C	MODY 7	MODY 8	MODY 9
OMIM ID	610508	609812	612225
Affected gene	<i>KLF11</i>	<i>CEL</i>	<i>PAX4</i>
Chromosomal location	2p25	9q34.3	7q32
Affected protein	Krüppel-like factor 11	Pancreatic carboxyl-ester lipase	Paired box protein 4
Prevalence ^a	Unknown		
Physiological function	Involved in regulation of pancreatic β -cell function	Hydrolysis of cholesteryl esters, triglycerides, and lysophospholipids	Promotes differentiation of β - and δ -cells during early pancreas development
Diabetic phenotype (heterozygous state)	Diabetes mellitus	Beta cell failure and exocrine pancreas dysfunction	MODY-similar diabetic phenotype
Extrapancreatic manifestations	Unknown		
Diabetic complications			
Treatment			
References	(Bieker 2001; Neve <i>et al.</i> 2005)	(Ræder <i>et al.</i> 2006; Shamir <i>et al.</i> 1996)	(Brun <i>et al.</i> 2004; Habener <i>et al.</i> 2005; Plengvidhya <i>et al.</i> 2007; Smith <i>et al.</i> 1999; Sosa-Pineda <i>et al.</i> 1997)

^a Prevalence within the MODY population; Chromosomal locations refer to the NCBI database (<http://www.ncbi.nlm.nih.gov/>).

Novel potential MODY-associated candidate genes

Heterozygous mutations in the paired box gene 6 (*PAX6*) have previously been reported in sporadic cases of maturity-onset diabetes in human subjects (Nishi *et al.* 2005; Yasuda *et al.* 2002). The transcription factor Pax6 is known to be involved in oculo-genesis and has also been suggested to play an indispensable role in the development of the endocrine pancreas (Hanson and Van Heyningen 1995; St-Onge *et al.* 1997). The mutation carriers were therefore diagnosed of aniridia and various degrees of diabetes (Nishi *et al.* 2005; Yasuda *et al.* 2002). Another transcription factor, suggested to be essential for endocrine pancreas development with focus on α -cell differentiation (Lee *et al.* 2005), the forkhead box A2 protein (Foxa2, formerly hepatocyte nuclear factor-3 β (HNF-3 β)), may also be a candidate to cause familial hypoinsulinism-mediated diabetes mellitus. As *FOXA2* has been demonstrated to regulate the expression of *HNF1A* and *HNF4A*, which are both associated with MODY subtypes, a possible role of *FOXA2* as an elicitor of MODY has been propagated (Duncan *et al.* 1998). However, previous studies failed to associate the MODY phenotype with mutations in the *FOXA2* gene (Hinokio *et al.* 2000).

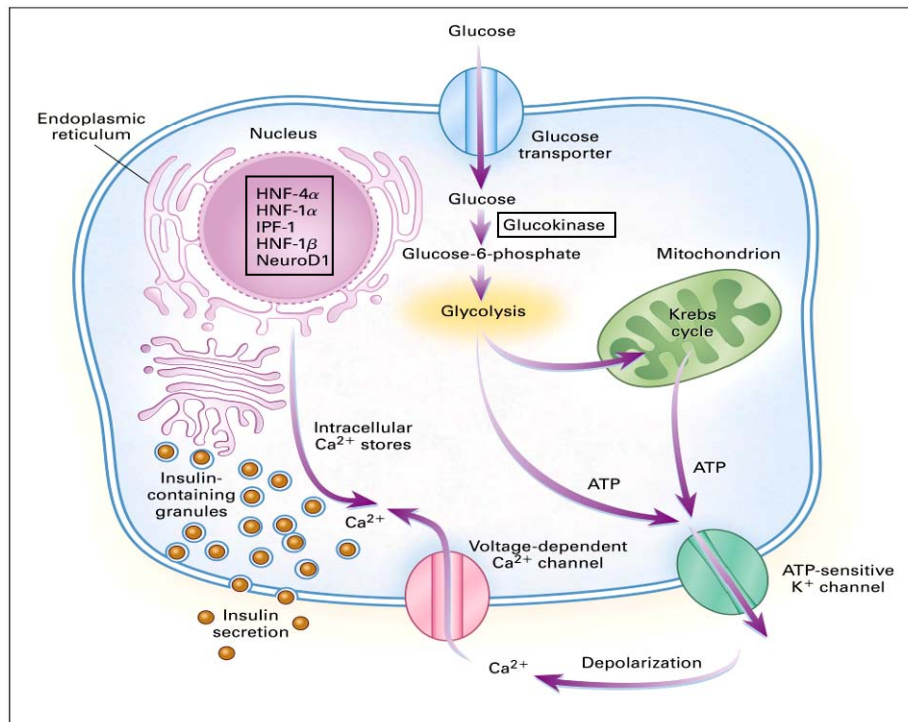


Figure 2.4: Model of the molecular mechanisms of insulin secretion in pancreatic β -cells and the proteins involved in MODY. Modified according to Fajans *et al.* 2001.

2.6 The catalytic enzyme glucokinase

2.6.1 Physiological and biochemical function of the glucokinase enzyme

The term glucokinase first appeared in the literature in 1950 and was established in 1964 to designate a glucose-phosphorylating enzyme that has been identified in rat liver tissue (Slein *et al.* 1950; Walker and Rao 1964). Mammalian glucokinase (syn. hexokinase IV; EC 2.7.1.2), as one of the four members of the hexokinase family, is capable to phosphorylate hexoses, in the order of preference glucose>mannose>2-deoxyglucose>fructose. Although all hexokinase members display a strong sequence homology, testifying of a close phylogenetic relationship, they exhibit different catalytic properties (Iynedjian 2009). In contrast to the hexokinases I-III, which have a low K_m (0.01-0.1 mM) for glucose (high affinity), the K_m for glucose of glucokinase amounts to 8.4-10 mM (low affinity). Thus, glucokinase activity can be directly influenced by plasma glucose concentrations, whereas other hexokinases are already saturated at normal plasma glucose concentrations due to their low K_m . Since the rate of substrate phosphorylation by glucokinase is dependent on extracellular glucose concentrations, the glucokinase enzyme is considered to function as a “glucose sensor”. Other kinetic characteristics of the catalytic enzyme glucokinase are a sigmoidal glucose dependency, which, together with the low glucose affinity, guarantees optimal responsiveness at physiological glucose levels. Additionally, the allosteric glucokinase enzyme exhibits a positive cooperativeness with glucose (basic kinetic properties of the glucokinase enzyme are stated in chapter 10.1). These attributes make the enzyme most sensitive to glucose level changes close to the physiological range. In contrast to other hexokinases, which are inhibited by various phosphorylated intermediates (glucose-6-phosphate, glucose-1,6-diphosphate, and 6-phosphogluconate), the glucokinase enzyme does not underlie any specific feedback inhibition by downstream products (Matschinsky 1990, 2002; Matschinsky *et al.* 1998; Winter 2000). Apart from hepatocytes, the glucokinase enzyme is also widely expressed in different endocrine and neuroendocrine cells in various tissues. Glucokinase expressing cells for example reside in the endocrine pancreas, the intestine, and in the brain (Matschinsky 2002). In the islets of Langerhans, glucokinase is predominantly expressed in the insulin-producing β -cells, but it has also been detected in glucagon-producing α -cells and in somatostatin-producing δ -cells (Heimberg *et al.* 1996; Toyoda *et al.* 1997; Toyoda *et*

al. 1999). In pancreatic β -cells, glucokinase catalyses the first, rate limiting step of glycolysis: the phosphorylation of glucose (on carbon 6 with MgATP as the second substrate) to glucose-6-phosphate (G6P). Glycolysis results in increased ATP generation in the cytoplasm, enhanced oxidative phosphorylation within the mitochondrion, and in turn to a decrease of ADP and anorganic phosphate concentrations. This shift in energy equilibrium leads to the closure of β -cell K_{ATP} channels, followed by membrane depolarisation and the opening of voltage-dependent Ca^{2+} -channels. Subsequently, increased intracytoplasmic calcium induces fusion of the insulin containing vesicles with the cytoplasmic membrane and, finally, insulin exocytosis (Winter 2003). Therefore, already minimal changes in glucokinase activity can result in serious consequences for the organism, because the threshold for glucose-induced insulin secretion is altered directly (Ilyedjian 2009; Matschinsky 2002; Postic *et al.* 2001). In hepatocytes, glucokinase stimulates glucose uptake and glycogen synthesis (Radziuk and Pye 2001). Glucokinase in neuroendocrine enteric cells (K- and L-cells) and specialised neurons (pituitary cells, neurons of various hypothalamic nuclei, of the tractus solitarius, the vagus, and of raphe nuclei) was initially thought to fulfil a function, similar to that in pancreatic β -cells (Matschinsky *et al.* 2006). However, a recent study in human MODY 2 patients proved that glucokinase, which is co-expressed with glucagon-like peptide-1 (GLP-1) and glucose-dependent insulinotropic peptide (GIP) in intestinal K-cells, does not function as the suggested “gut glucose sensor” in enteric cells of these patients (Murphy *et al.* 2009). For anterior pituitary cells as well as for glucose-excited and glucose-inhibited neurons, by contrast, the concept of a glucose sensory function of the glucokinase enzyme in the brain was reinforced (Dunn-Meynell *et al.* 2002; Zelent *et al.* 2006).

2.6.2 Regulation of glucokinase expression

The human glucokinase gene (GCK), localised on chromosome 7p15.3-15.1, is comprised of 12 exons that span ~45 kb and encode for a 52.2 kDa protein, containing 465 amino acids⁵. The glucokinase protein therefore represents a much smaller molecule than other hexokinases, being about 100 kDa in size (Ilyedjian 1993; Postic *et al.* 2001).

⁵ <http://www.ncbi.nlm.nih.gov/>

The glucokinase coding sequence is highly conserved between human, rat, and mouse with >94% sequence identity among these species (Postic *et al.* 1995). The presence of 2 different tissue specific promoters enables differential glucokinase gene regulation and transcription and results in three tissue specific variants of exon 1 (a-c). The upstream promoter is active in pancreatic β -cells and in the brain, whereas the downstream promoter activity is restrained to hepatocytes. Thus, multiple glucokinase mRNAs, resulting from alternate transcription and RNA processing, are produced from the single gene. Exon 1b and 1c are expressed in the liver, whereas exon 1a is expressed in pancreatic β -cells. Due to alternative transcription start sites, the liver- and β -cell-specific glucokinase isoforms differ in 15 amino acids at the N-terminus. Additionally, hepatic glucokinase gene expression in rats is strongly induced by refeeding after a certain fasting period, whereas β -cell-specific glucokinase expression remains stable during the fasting and refeeding state, indicating that different mechanisms might control glucokinase gene expression in liver and β -cells (Gloyn 2003; lypedjian 1993; lypedjian *et al.* 1989b; Magnuson and Shelton 1989). Hepatic glucokinase gene expression has already been proven to be induced by insulin and to be inhibited by glucagon in a cAMP-dependent manner (lynedjian 1993; lypedjian *et al.* 1989a; Nospikel and lypedjian 1992), whereas the role of sterol regulatory element binding protein-1c (SREBP-1c) as the propagated major mediator of insulin-induced hepatic glucokinase gene expression was argued recently (Foretz *et al.* 1999; Gregori *et al.* 2006). Moreover, glucokinase gene expression in the liver is controlled by multiple DNA-protein interactions like *cis*-acting DNA sequences in the liver-specific promoter that bind to various hepatocyte nuclear transcription factors (Postic *et al.* 2004).

On the posttranslational level, liver-specific glucokinase is under the control of a small high-affinity protein, the glucokinase regulatory protein (GKRP), which influences the activity as well as the subcellular compartmentation of the glucokinase enzyme. The 62 kDa GKRP acts as both a competitive inhibitor of glucokinase activity and a nuclear receptor, and regulates glucokinase translocation from the cytoplasm to the nucleus. Due to the presence of two binding sites for fructose phosphates, the interaction of GKRP with the glucokinase protein is enhanced in the presence of fructose-6-phosphate and impeded in the presence of fructose-1-phosphate. Glucose, by contrast, induces the release of the GKRP from its complex

with glucokinase and therefore reinforces enzyme activity (Baltrusch and Tiedge 2006; van Schaftingen *et al.* 1994).

The regulation of glucokinase gene expression in endocrine and neuroendocrine cells seems to be more complex and is discussed controversially. In contrast to the liver, β -cell-specific glucokinase mRNA expression seems to be more constitutive, enabling the stable regulation of glucose turnover and insulin secretion rates in pancreatic β -cells (Matschinsky *et al.* 1998). Therefore, glucokinase regulation on the transcriptional level might play a minor role in pancreatic β -cells (Baltrusch and Tiedge 2006; Heredia *et al.* 2006; Kamata *et al.* 2004). A protruding role of glucose as the main regulator of glucokinase gene transcription in pancreatic β -cells was widely accepted for a long time. However, in isolated human and rat islets, glucokinase mRNA levels were shown to be independent of the nutrition status. Further, exposure to elevated glucose concentrations impressively enhanced glucokinase protein, but not glucokinase gene expression, thereby advising the role of glucose as a potential regulating factor of glucokinase on the posttranscriptional level (Gasa *et al.* 2000; Iynedjian *et al.* 1989b; Matschinsky *et al.* 2006). In contrast to these findings, another study demonstrated that glucose is nevertheless capable to induce glucokinase mRNA expression in rat pancreatic islets (Tiedge and Lenzen 1991), and that this effect was supposed to be also mediated by insulin (Matschinsky 2002). However, glucose is considered to be an important regulator of β -cell-specific glucokinase on posttranscriptional and posttranslational levels (Chen *et al.* 1994; Matschinsky 2002). Other factors influencing glucokinase expression seem to be numerous, and the specific mechanisms involved are still not completely elucidated. Thyroid hormone, glucocorticoids, biotin, placental lactogen (PL) and retinoic acid are known potential regulators of glucokinase induction (Matschinsky 2002; Printz *et al.* 1993). Moreover, recent studies have demonstrated the regulatory function of the bifunctional enzyme 6-phosphofructo-2-kinase/fructose-2,6-bisphosphatase (PFK-2/FBPase-2) on glucokinase activity in pancreatic β -cells and on glucokinase protein expression in hepatocytes.

2.6.3 Structure-function relationship in human glucokinase

Three-dimensional modelling of the human glucokinase (Kamata *et al.* 2004; Mahalingam *et al.* 1999; St Charles *et al.* 1994) led to the discovery of the conformational transition pathway of the glucokinase enzyme during glucose

metabolism and to the identification of small allosteric activator molecules (Baltrusch and Tiedge 2006; Grimsby *et al.* 2003). The glucokinase protein consists of two domains, a large and a small one - with a glucose binding site, located in the interdomain cleft - and an allosteric binding site in the hinge region between the large and small domains. During catalysis, glucokinase undergoes greater conformational changes than hexokinases. The thermodynamically favourable inactive form (apoenzyme form) of the glucokinase, which is held in the absence of glucose is characterised by a "wide-open" (also called "super-open") form. Glucose binding to the catalytic centre induces a conformational change of the glucokinase to a more complex form, the so-called "intermediate" or "open form" that proceeds to the active "closed form" in the presence of ATP. The mechanism of the positive cooperativeness of glucokinase with glucose is based on these three conformations. Once glucose binds to the catalytic centre, the enzyme undergoes a slow transition from the wide-open to the open form with ongoing enzymatic reaction by changing to the closed form in the presence of ATP. After completion of the reaction, glucokinase turns back to the open form to release glucose-6-phosphate and ADP. Once glucokinase forms a complex with glucose during this period, the enzyme re-enters the catalytic cycle through a fast "closed-open" transition, whereas in absence of glucose binding, glucokinase returns to the super open form (Fig. 2.5). The ratio of these two transition flows, the slow and the fast cycle, is depending on the glucose concentration (the fast cycle is favoured in presence of high, the slow cycle in presence of low glucose concentrations) and the time of glucokinase remaining in the open form. The shift between the two cycles explains the catalytic characteristics of the glucokinase enzyme, especially the low affinity for glucose and the sigmoidal saturation kinetic (Baltrusch and Tiedge 2006; Heredia *et al.* 2006; Kamata *et al.* 2004).

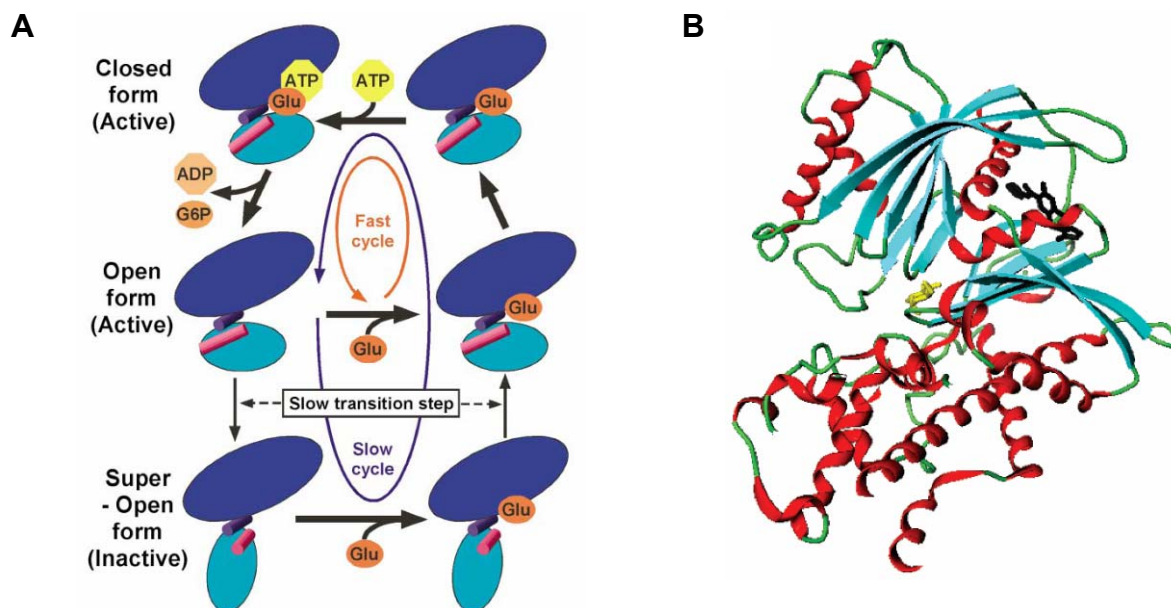


Figure 2.5: Illustration of glucokinase conformational changes (A) and protein conformation (B). Glucokinase shuttles between closed, open, and super-open form within the fast and the slow cycle (A). Ribbon drawing of the glucokinase in the closed conformation in complex with glucose (yellow) and an allosteric activator (black); helices, β -sheets, and flexible loops are coloured in red, blue, and green, respectively (B). From Heredia *et al.* 2006 and Kamata *et al.* 2004.

2.6.4 Glucokinase-associated diseases in human subjects

According to the pivotal importance of the glucokinase enzyme in glucose homeostasis, variations in the glucokinase gene (*GCK*) are predicted to have incisive impact on glucose metabolism and cause glycaemic diseases. To date, a total number of 446 naturally occurring point mutations within the coding region of *GCK* have been described, with missense mutations representing the most common defect (about 91% of all point mutations) (Osbak *et al.* 2009). *GCK* mutations are capable to cause hyperglycaemia or hypoglycaemia, resulting in three distinguishable phenotypes depending on the number of the mutated alleles and the functional consequences of the corresponding mutation (Gloyn 2003; Gloyn *et al.* 2008):

- Heterozygous gain-of-function mutations in human *GCK* cause persistent hyperinsulinaemic hypoglycaemia of infancy (PHHI), a rare disorder characterised by hypoglycaemia, present from birth, which is caused by exceeding insulin secretion. Inappropriate insulin secretion results from a reduced $S_{0.5}$ for glucose

and/or an increased V_{\max} of the glucokinase enzyme, leading to a lowered threshold for glucose-induced insulin secretion. These changes in enzyme kinetics are most often a consequence of mutations located ~20 ångstroms distal from the substrate-binding site in the region of the putative allosteric activator domain (Matschinsky *et al.* 2006; Printz and Granner 2005). The resulting phenotype can vary from chronic low fasting plasma glucose to severe persistent hypoglycaemia, accompanied by ataxia, seizures, and coma. Endocrine pancreatic manifestations of the inherited β -cell hyperfunction are characterised by β -cell hypertrophy, which can be present only in foci of hyperplastic islets or in all islets of the pancreas (Cuesta-Munoz *et al.* 2004; Pal and Miller 2009; Reinecke-Luthge *et al.* 2000).

- Homozygous loss-of-function mutations in *GCK* are associated with permanent neonatal diabetes mellitus (PNDM). Neonatal diabetes mellitus, a quite rare disease (incidence of 1:300,000–500,000 live births), can either be transient (TNDM) or permanent (PNDM) (Glaser 2008). Nevertheless, complete functional disruption of human *GCK* might be a rather rare cause of neonatal diabetes mellitus or possibly results in intra-uterine death (Edghill *et al.* 2008; Gloyn *et al.* 2002). The pathognomonic symptoms of neonatal diabetes mellitus are hyperglycaemia, usually requiring insulin treatment, hypoinsulinaemia, exocrine pancreatic manifestations, and low birth weight. However, a successful initial sulphonylurea treatment has been reported in a child with a homozygous *GCK* mutation (Fosel 1995; Glaser 2008; Turkkahraman *et al.* 2008)
- Heterozygous loss-of function mutations in *GCK* are associated with a subtype of maturity-onset diabetes of the young: MODY 2. The close linkage of the glucokinase locus to elevated fasting plasma glucose concentrations in MODY families in France and the UK was first discovered in 1992 and the hypothesis was set that defects in *GCK* potentially account for a MODY subtype and may even play a role in the pathogenesis of type 2 diabetes mellitus (Froguel *et al.* 1992; Hattersley *et al.* 1992). According to their location, *GCK* mutations can be divided into three main groups (Gloyn *et al.* 2008; St Charles *et al.* 1994; Velho *et al.* 1997).

1. Mutations of conserved active site residues may seriously impair the catalytic activity of the glucokinase.
2. Mutations, which are predicted to distort the enzyme structure and result in decreased glucokinase activity; and mutations of surface residues that eliminate interactions with other residues. These mutations are predicted to impair the structural stability or affect the conformational change induced by glucose binding to the catalytic centre, and often exert only minor effects on glucokinase activity.
3. Other mutations, that may impede interactions between glucokinase and regulatory or binding partners like GGRP. Furthermore, glucokinase mutations might affect the interplay with the bifunctional enzyme PFK/FBPase-2, which has been recently demonstrated to regulate both glucokinase activity in pancreatic β -cells and glucokinase protein expression in hepatocytes (Massa *et al.* 2004; Payne *et al.* 2005).

However, the molecular mechanisms underlying some specific mutations are not ultimately ascertained. *In vitro* studies, based on the molecular model of human glucokinase, revealed a *GCK* mutation, associated with a diabetic phenotype despite unaltered kinetic properties (Davis *et al.* 1999). Another mutation, located near the allosteric activator site and associated with familial hyperglycaemia, appeared to be kinetically activating and was therefore expected to cause hypoglycaemia rather than hyperglycaemia. Glucokinase activity of the mutated protein was proven to be refractory to allosteric activator compounds *in vitro*. Therefore, the loss of allosteric activation of the mutated glucokinase was considered to represent the key mechanism leading to the diabetic phenotype (Arden *et al.* 2007). The MODY 2 diabetic phenotype in general reflects the manifestations of a disturbed hepatic glucose clearance and a primary β -cell secretory defect due to an impaired glucose sensing and a decreased glycolytic flux in pancreatic β -cells. MODY 2 patients usually display mild, but chronic hyperglycaemia, with development of impaired fasting glucose (IFG), disturbed glucose tolerance (IGT), and increased postprandial gluconeogenesis (Velho and Froguel 1998). The defective glucokinase function in MODY 2 subjects leads to an increased threshold for glucose-induced insulin secretion in pancreatic β -cells, resulting in a disturbed glucose-induced insulin

secretion. The glucose response curve for insulin secretion exhibits a “right-shift”, whereas the first phase of insulin secretion following an intravenous glucose bolus application was proven to be well preserved in affected persons (Velho *et al.* 1992; Winter 2003). Even if some MODY 2 patients display peripheral insulin resistance, this phenomenon might be secondary to the disease rather than a direct consequence of the mutation (Clement *et al.* 1996; Hattersley and Pearson 2006). The diabetic phenotype in MODY 2 subjects may deteriorate little with age, but usually remains considerably stable due to compensatory mechanisms like overexpression of the wild-type allele (van de Bunt and Gloyn 2007). Despite being present from birth, the diabetic phenotype often remains undiagnosed for a remarkable time, because the occurrence of the disease varies, depending on the severity of glucokinase impairment, from asymptomatic mild hyperglycaemia over various degrees of glucose intolerance up to the development of persistent fasting hyperglycaemia with less than 50% of affected persons developing overt diabetes (Fajans *et al.* 2001; Velho and Froguel 1998). Due to this mild diabetic phenotype, diabetes-associated macro- and microvascular complications, overweight, and dyslipidaemia are uncommon in MODY 2 patients (Velho and Froguel 1998; Velho *et al.* 1996). Further, patients usually manage blood glucose control by diet and exercise alone, and only 1 of 50 MODY 2 patients requires insulin therapy (Fajans *et al.* 2001; Winter 2003). Defects in *GCK* can already be evident in the prenatal period. Infants with *GCK* mutations born to unaffected mothers display remarkably lower birth weights than their non-affected siblings, reflecting the effect of insulin deficiency on embryonic growth *in utero*. In contrast, unaffected children, born to a *GCK* mutation carrier, often exhibit macrosomia (van de Bunt and Gloyn 2007; Winter 2003). The worldwide prevalence of MODY is not exactly known but it is estimated that 2-5% of type 2 diabetic patients may be in fact MODY subjects. MODY 2 and MODY 3 are supposed to be the most common MODY subtypes (American Diabetes Association 2009), whereby the relative prevalence of MODY 2 varies extremely depending on the prevailing population, the applied diagnosis criteria, and the mode of patient recruitment (Massa *et al.* 2001). In European Caucasian, MODY 2 is reported to account for only 8% of all MODY cases in Germany (Lindner *et al.* 1999), for 10% in Denmark (Johansen *et al.* 2005), for 12% in Norway (Sagen *et al.* 2008), for 10-20% in the UK (Froguel *et al.* 1993; Thomson *et al.* 2003), for 31% in the Czech republic (Pruhova *et al.* 2003), for 25-41% in Spain (Barrio *et al.* 2002; Costa

et al. 2000), for 41-61% in Italy (Mantovani *et al.* 2003; Massa *et al.* 2001), and for about 50% in France (Froguel *et al.* 1993). Taken together, a worldwide population prevalence for MODY 2 of 0.04-0.1% is suggested (Gloyn 2003). However, the rare incidence of this disease and the genetic heterogeneity of the affected subjects impede detailed clinical studies in human medicine. For this reason, genetically modified animal models are essential to survey relevant clinical and pathophysiological aspects of this disease. Albeit, up to now, few advances were made in human medicine as well as in animal models, to disclose the pathomorphology of this putative mild diabetes subtype (Osbak *et al.* 2009).

2.6.5 Clinical screening criteria for MODY 2

Considering the various treatment challenges for the specific MODY subtypes, the importance of a genetic diagnosis in MODY subjects reaches more and more priority. Therefore, practice guidelines for the most common monogenic forms of diabetes caused by mutations in the *GCK*, *HNF1A*, and *HNF4A* were elaborated by the European Molecular Genetics Quality Network (EMQN), comprising clinical criteria for selection of patients for testing, methodologies, and interpretation of results (Ellard *et al.* 2008).

The following features suggest a diagnosis of a *GCK* mutation:

1. Fasting hyperglycaemia ≥ 5.5 mmol/l (99 mg/dl) (observable in 98% of MODY 2 patients), persistent (at least three separate occasions) and stable over a period of months or years.
2. HbA_{1c} typically just above the upper limit of the normal range and rarely exceeding 7.5%.
3. A small increase during OGTT [(2 h glucose) – (fasting glucose)]: 71% of patients in the large European study had an increment < 3 mmol/l (54 mg/dl) (Stride *et al.* 2002). An increase of 4.6 mmol/l (83 mg/dl) is often used to prioritise testing.
4. Parents may have "type 2 diabetes" with no complications or may not be diabetic. On testing, one parent will usually have mildly raised fasting blood glucose (range of 5.5–8 mmol/l (99-144 mg/dl)) unless the mutation has arisen *de novo*. Testing of FPG of apparently unaffected parents is important when considering a diagnosis of a glucokinase mutation.

3. Research design and methods

3.1 Animals

3.1.1 Breeding, husbandry, and analyses

The ENU strains GLS001 and GLS006⁶ were generated within Munich ENU mouse mutagenesis project on the genetic background of the inbred strain C3H. Both strains were further bred by mating male heterozygous mutants to wild-type C3H female mice. Segregation of most additional ENU-induced non-causative mutations was attained by breeding animals for more than 10 generations to wild-type C3H mice. Both strains were detected in the screen for dominant mutations, displaying elevated plasma glucose concentrations (Aigner *et al.* 2008; Hrabé de Angelis *et al.* 2000).

Animals were maintained under standard (non-barrier) conditions (21-23°C, 55 ± 3% relative humidity, 12 hours light : 12 hours dark cycle) and received standard rodent diet (Altromin C1324, Germany) and tap water *ad libitum*. After a suckling period of 21 ± 1 days, mice were weaned, weighed, and marked by ear punches. Further, tail tip biopsies for genotypic differentiation and 10 µl peripheral blood for determination of blood glucose levels were sampled from each mouse during weaning procedure. Twenty-one day-old male mice displaying *ad libitum* fed blood glucose levels ≥170 mg/dl were considered diabetic, whereas blood glucose levels ≤125 mg/dl were allocated to the wild-type phenotype. Male animals showing blood glucose concentrations >125 mg/dl and <170 mg/dl were classified susceptible for diabetes and underwent iterated blood glucose determination seven days later. The respective cut-off levels for blood glucose concentrations in female mice were 120 mg/dl and 165 mg/dl. Fasting and *ad libitum* fed blood glucoses levels of mutant mice and wild-type littermates were screened regularly within clinical tests, including oral glucose tolerance (OGTT) and intraperitoneal insulin tolerance tests (ipITT) at the indicated age. Blood samples for the determination of serum insulin levels in the fasted state and after glucose application were also collected during OGTT. Clinical investigations were carried out with at least 5 animals per sex and genotype. At the end of the

⁶ Mouse Genome Database:

GLS001: <http://www.informatics.jax.org/javawi2/servlet/WIFetch?page=markerDetail&key=382146>

GLS006: <http://www.informatics.jax.org/searchtool/Search.do?query=GLS006&submit=Quick+Search>

clinical investigation period, 4 mice per genotype and sex were sacrificed at an age of 210 days for necropsy. Four additional male mutant GLS006 mice and wild-type littermates were sacrificed at an age of 550 days. *Post mortem* investigations comprised the determination of organ weights and the procession of whole pancreata for subsequent histological and morphometric analyses. At an age of 90 days, 2 additional GLS001 mice per sex and genotype were sacrificed and pancreatic islets were isolated for Western blot analysis. Liver tissue samples for determination of glucokinase activity were also obtained from 90-day-old mice.

Homozygous mutants were generated by mating heterozygous littermates. The resulting offspring were weighed and tagged by foot pad tattoo at the first day *post partum*. Tail tip samples for DNA isolation and subsequent genotypic differentiation were collected, and litters were subsequently monitored twice a day to survey mortality rates. At an age of 3 and 21 days, body weights were determined again. Additional offspring of heterozygous mutants were sacrificed at the first day *post partum* (within the first 24 hours of life) and at an age of 1 (after the first 24 hours *post partum*) and 4 (only GLS001 mice) days to obtain blood samples for blood glucose determination. Moreover, pancreata for qualitative histological and quantitative stereological analyses and hepatic tissue for RNA isolation and subsequent quantitative real-time polymerase chain reaction (PCR), were obtained from neonatal GLS001 mice.

The total number of animals used for the respective investigations is illustrated in Table 3.1. All experiments were performed under the approval and in accordance with the guidelines of the responsible animal welfare authority (Regierung von Oberbayern).

Table 3.1: Number of GLS001 and GLS006 mice used for the respective investigations during the suckling period (A) and after weaning (B).

A	Number of animals examined					
	GLS001			GLS006		
	wt	mt, het	mt, homo	wt	mt, het	mt, homo
Investigations during the suckling period						
Body weight (days of age):						
0 (first day <i>post partum</i>)	13	18	8	16	19	18
3	13	16	7	16	20	12
Blood glucose (days of age):						
0 (first day <i>post partum</i>)	6	13	11	16	17	6
1	5	7	4	9	12	7
4	11	14	7			
Morphometric analyses of the pancreas (days of age):						
0 (first day <i>post partum</i>) (male mice)	3	4	6			

B	Number of animals examined									
	GLS001				GLS006					
	m, wt	m, het	f, wt	f, het	m, wt	m, het	m, homo	mt, wt	m, het	m, homo
Investigations after weaning										
<i>Ad libitum</i> fed body weight (days of age):										
21	5	5	5	5	7	7	7	7	7	7
30	5	5	5	5	7	7	7	7	7	7
90	10	10	10	10	7	7	7	7	7	7
175	10	10	10	10	7	7	7	7	7	7
Fasting body weight (days of age):										
30	10	10	10	10	7	7		7	7	
85	10	10	10	10	7	7		7	7	
180	10	10	10	10	7	7		7	7	
<i>Ad libitum</i> fed blood glucose (days of age):										
21	5	5	5	5	7	7	7	7	7	7
30	5	5	5	5	7	7	7	7	7	7
90	10	10	10	10	7	7	7	7	7	7
175	10	10	10	10	7	7	7	7	7	7
Fasting blood glucose (days of age):										
30	10	10	10	10	7	7		7	7	
85	10	10	10	10	7	7		7	7	
180	10	10	10	10	7	7		7	7	

OGTT (days of age):									
30	10	10	10	10	7	7	7	7	
85	10	10	10	10	7	7	7	7	
180	10	10	10	10	7	7	7	7	
ipITT (days of age):									
30	4	6	5	5	5	5	5	5	
90	10	10	10	10	7	7	7	7	
175	10	10	10	10	7	7	7	7	
Serum insulin (days of age):									
30	10	10	10	10	7	7	7	7	
85	10	10	10	10	7	7	7	7	
180	10	10	10	10	7	7	7	7	
Glucokinase activity^a (90 days of age):	2	4	2	3	4	3	2	2	2
Western blot analysis (pancreatic islets)^a (90 days of age):	2	2	2	2					
Necropsy (days of age):									
210	4	4	4	4	4	4	4	4	4
550					4	4	3		
Morphometric analyses of the pancreas (days of age):									
210	4	4	4	4					
550					4	4	3		

^a animals of both genders were matched for statistical analyses.

3.1.2 Breeding strategy for linkage analysis

GLS001 mice already underwent backcross breeding and linkage analysis in cooperation with the Institute of Experimental Genetics (Prof. Dr. Martin Hrabé de Angelis, Helmholtz Zentrum München, Neuherberg, Germany), whereas linkage analysis of the ENU strain GLS006 was part of the present study. The breeding strategy for linkage analysis of both strains has been described previously (Aigner *et al.* 2008).

Briefly, the following breeding regime was applied for GLS006 mice: Three heterozygous male phenotypic mutants (mice that were considered diabetic according to their blood glucose values) on the inbred C3H genetic background were mated to C57BL/6J female mice to produce G1 hybrid offspring. At an age of 21±1 day, G1 mice were screened for elevated blood glucose concentrations. At an age of 60 days, 8 male G1 mice that were classified diabetic were backcrossed to C57BL/6J wild-type female mice. The resulting G2 progeny were also tested for elevated blood glucose concentrations. Tail tip biopsies from total number of 75 phenotypic mutants and 25 phenotypic wild-type mice were taken in duplicates and stored at -80°C.

Linkage analysis of 70 phenotypic mutant and 22 phenotypic wild-type mice was carried out in cooperation with the Institute of Experimental Genetics as previously described (Hrabé de Angelis *et al.* 2000).

3.2 Identification of the causative mutation

3.2.1 Fine mapping in GLS001 mice

With the knowledge of the approximate chromosomal location of the causative mutation, fine mapping was carried out in GLS001 mice to further define the mutation position. For this purpose, 3 additional microsatellite markers, positioned in the previously defined chromosomal region and a fourth marker, indicating a not yet classified polymorphism in intron 7 of the glucokinase (*Gck*) gene, were applied. Genotype analysis of polymorphic markers was accomplished by Polymerase Chain Reaction (PCR), using DNA from 75 phenotypic mutant and 15 phenotypic wild-type GLS001 backcross G2 mice and 19 mice, derived from mating phenotypic mutant G2 backcross mice.

3.2.1.1 DNA isolation

DNA isolation was performed after overnight digestion of tissue samples in 400 μ l Master Mix in a heating block (Biometra TB1 Thermoblock, Whatman, Germany) at 55°C. Undigested components were separated by centrifugation (Sigma 1K15, Sigma, Germany) for 2 minutes at 15,300 rpm. DNA was precipitated after transfer of the supernatant into a sterile 1.5 ml reaction cup (Eppendorf, Germany), by addition of 400 μ l 100% isopropanol (Merck, Germany). The DNA pellet was washed twice in 70% ethanol (Merck, Germany) by vortexing. Thereafter, the DNA pellet was dried at room temperature for approximately 10 minutes. DNA was resuspended in 50-200 μ l 1xTE buffer (according to the pellet size) and incubated for 1 hour at 55°C. To ensure complete DNA dissolution, the resuspended DNA was stored at 4°C for at least 24h before further investigation.

Master Mix for DNA isolation

Cutting Buffer	375 μ l
20% SDS (Roth, Germany)	20 μ l
Proteinase K (20 mg/ml)	5 μ l

Cutting buffer

1 M Tris/HCl, pH 7.5 (Roth, Germany)	2.5 ml
0.5 M EDTA, pH 8.0 (Sigma, Germany)	5.0 ml
5 M NaCl (AppliChem, Germany)	1.0 ml
1 M DTT (Roth, Germany)	250 µl
Spermidine (500 mg/ml, Sigma, Germany)	127 µl
Ad 50 ml aqua bidest.; stored at 4°C	

TE buffer

10 mM Tris/HCl, pH 8.0 (Roth, Germany)
1 mM EDTA (Sigma, Germany)
Stored at room temperature

3.2.1.2 PCR amplification of the polymorphic sequences

PCR Master Mixes were prepared as described in Table 3.2A. The Taq DNA polymerase was stored at -20°C until it was added to the Master Mix (Taq PCR Master Mix Kit, Qiagen, Germany). Primers were synthesised by Thermo Scientific, USA. Primer sequences were obtained from the National Center for Biotechnology Information (NCBI; <http://www.ncbi.nlm.nih.gov/>). One µl of the resuspended DNA and 19 µl of the respective PCR Master Mix were mixed on ice in PCR analysis cups (Kisker, Germany). PCR reactions were performed as specified below on a Biometra® Uno II Thermocycler (Biometra, Germany). Primer sequences and cycling conditions are stated in Table 3.2 A, B. DNA from C3H and C57BL/6J wild-type mice served as positive control, H₂O was applied as quality control (no template control). PCR products were stored at 4°C (short term) or -20° (long term) until assayed.

Table 3.2: PCR conditions (A) and primer sequences (B) for amplification of the polymorphic sequences.

A

Master Mix PCR 1-4		PCR conditions	PCR 1-3	PCR 4
Aqua bidest.	8.65 µl	1. Initial denaturation 2. Denaturation 3. Annealing 4. Extension 5. Final extension 6. Hold	5 min 94°C	5 min 94°C
Q-solution	4.00 µl		45 sec 94°C	50 sec 94°C
10x buffer	2.00 µl		45 sec	50 sec
MgCl ₂	1.25 µl		45 sec 72°C	75 sec 72°C
dNTPs (1 mM)	1.00 µl		10 min 72°C	10 min 72°C
Primer sense (2 µM)	1.00 µl		∞ 4°C	∞ 4°C
Primer antisense (2 µM)	1.00 µl			
Taq Polymerase	0.10 µl			

B

PCR	Oligo name	Sequence (5'→3')	Annealing temp.	Map position ^a
1	D11Mit226_for D11Mit226_rev	AGG TGA ACT CTT TTG AAG TTT GTG AAA GGA GTG ACT GAG AAA GAC ACC	60°C	8.8 Mb
2	D11Mit2_for D11Mit2_rev	CCC CCA GCC TAC ACA CAG GCT ATT TCT CAC AGA AAG GGG	54°C	12.2 Mb
3	D11Mit78_for D11Mit78_rev	GTG GGA GAA ACC TTT ACG CA TCC TAG TGA CCA CAC TAA TTT GTG	60°C	17.8 Mb
4	Gck_17_for Gck_18_rev	TCT TCA CTG CAC AGC TGC TCC AGA ACC AGC TCA CAG ATG GCT C	62°C	5.9 Mb

^a Nucleotide positions refer to Mouse Genome Database (MGI; <http://www.informatics.jax.org/>)

3.2.1.3 Gel electrophoresis

PCR products were separated on 3% (PCR 1-3) and 4% (PCR 4) TBE agarose gels (UltraPure™ Agarose, Invitrogen, Germany) containing 10 µl/100 ml of a 1:10 diluted ethidium bromide stock solution (1%, Merck, Germany) in a gel electrophoresis chamber (Thermo Scientific Owl B2 EasyCast™ Mini Gel System, Thermo Scientific, USA). After filling the gel chamber with 1x TBE buffer, containing 9 µl/l ethidium bromide, each well was charged with 24 µl of a 1:5 mixture of PCR product and 6x loading dye. The pUC Mix Marker 8 (MBI Fermentas, Germany) served as molecular weight marker. Gel electrophoresis was run at 70 V (Biorad PowerPac 300, Bio-Rad, USA) for the first 10 minutes to enable uniform emission of PCR products from the wells. For the remaining time, electrophoresis was run at 120 V until achievement of the desired PCR product fragmentation (approximately 45-90 minutes, dependent on the respective PCR product length and the desired product fragmentation). The amplified products were visualised under UV light (Intas Gel Jet Imager, Intas Science Imaging Instruments GmbH, Germany), and a digital photograph was taken for documentation.

10x TBE stock solution

Tris base (Roth, Germany)	108 g
Boric acid (Roth, Germany)	55 g
0.5 M EDTA, pH 8.0 (Normapur, Germany)	40 ml

Ad 1000 ml aqua bidest. and autoclaved. Ready-to-use 1x TBE electrophoresis buffer was prepared by 1:10 dilution with aqua bidest.

6x loading dye

Glycerine (Roth, Germany)	3 ml
Aqua bidest.	7 ml
Bromphenol blue (Roth, Germany)	1 spatula tip

Aliquoted and stored at 4-8°C

Optional: 6x DNA Loading Dye (MBI Fermentas, Germany)

Genotypic distribution was determined (Fig. 3.1), and linkage between the diabetic phenotype and the analysed genotype for the respective polymorphic marker was statistically evaluated by chi square testing according to the equation illustrated below (Silver 1995).

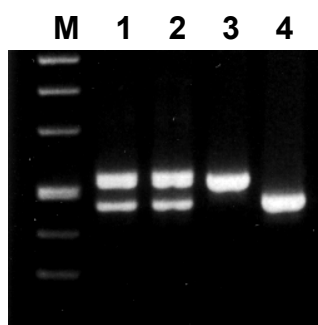


Figure 3.1. Genotypic differentiation (PCR 4) of GLS001 mice. M: Fragment size marker: marker bands represent fragment sizes of 1118, 881, 692, 501 (and 489), 404, 331 bp (from top to bottom). PCR products from mice, displaying a heterozygous genotype (1, 2) result in two visible bands of different sizes, whereas the C3H (3) C57BL/6J (4) genotypes are distinguishable by the presence of a single band of respective size.

Chi square testing of phenotypic linkage

$$\chi^2 = \frac{(\text{obs}_r - \text{exp})^2}{\text{exp}} + \frac{(\text{obs}_p - \text{exp})^2}{\text{exp}}$$

χ^2 = chi square value

obs_r = number of observed recombinant outcomes (sum of phenotypic mutant mice, heterozygous for the investigated polymorphic marker and phenotypic wild-type mice, showing the genotype of the outcross strain (C57BL/6J))

exp = expected numerical genotypic distribution (50%) ((total number of animals - number of animals that failed analysis)/2)

obs_p = number of observed parental outcomes (sum of phenotypic mutants, displaying the genotype of the outcross strain (C57BL/6J) and phenotypic wild-type mice, heterozygous for the corresponding marker)

3.2.2 Candidate gene sequencing

Sequence analysis of the candidate gene glucokinase (*Gck*) was performed on genomic DNA samples, isolated from tail tip samples. Additionally, DNase I -digested and reverse transcribed total hepatic RNA was applied. Liver tissue was obtained from mice, anaesthetised by intraperitoneal injection of 200 µl of ketamine/ xylazine mixture (1 ml 10% ketamine hydrochloride (Selectavet, Germany), 0.25 ml 2% Rompun (Bayer, Germany), 5 ml 0.9% NaCl) and killed by cervical dislocation. In GLS006 mice, tissue samples from 2 adult animals were obtained from each, phenotypic heterozygous and homozygous mutants and wild-type littermates. In GLS001 mice, breeding approaches led to the assumption that the homozygous mutation might be associated with perinatal or intrauterine death. Therefore, first sequence analysis was performed with neonatal offspring from mating heterozygous G2 backcross mice. Two animals which displayed a homozygous C3H genotype with the last polymorphic marker (positioned within the glucokinase gene) were classified as homozygous mutants and were therefore chosen for sequence analysis. Further, tissue samples from 2 adult animals were used for each phenotypic heterozygous mutants and wild-type controls on the C3H inbred genetic background.

3.2.2.1 Sample preparation for RNA and DNA isolation

DNA isolation

DNA isolation from tail tips for sequence analysis included additional steps of RNase digestion and protein precipitation in order to achieve high quality DNA. Using the Wizard[®] Genomic DNA Purification Kit (Promega, Germany), DNA was extracted after overnight digestion of tissue samples in 620 µl Master Mix at 55°C, according to manufacturer's instructions. For RNase digestion, 3 µl Ribonuclease A (RNase A (0.2 U/µl); Roche, Germany) were added to each sample, mixed by inversion for 25 times, and incubated for 20 minutes at 37°C. Afterwards, 200 µl Protein Precipitation Solution[®] (Promega, Germany) were added. After centrifugation, DNA in the supernatant was yielded by precipitation with 600 µl 100% isopropanol (Merck, Germany). The DNA pellet was washed twice with 70% ethanol (Merck, Germany), dried and resuspended in 50-150 µl (according to the pellet size) Rehydration solution[®] (Promega, Germany) at 65°C for 1 hour.

Master Mix

Nuclei Lysis Solution [®] (Promega, Germany)	500 µl
0.5 M EDTA, pH 8.0 (Normapur, Germany)	120 µl
Proteinase K (20 mg/ml)	17.5 µl

3.2.2.2 RNA isolation

Total RNA from liver tissue of GLS001 and GLS006 mice was isolated by guanidium thiocyanate-phenol-chloroform extraction. Whole liver samples from neonatal GLS001 mice, stored in RNA-later[®] RNA stabilisation reagent (Ambion, Germany) at -80°C, were obtained from the IEG. Tissue samples of about 40 mg each were transferred into a sterile and RNase-free 2 ml reaction cup (Eppendorf, Germany), containing 1 ml TRIzol[®] Reagent (Invitrogen, Germany). Hepatic tissue was subsequently homogenised for 1 minute (level D: 23,500 rpm) using a Miccra-D8 dispersing device (Art-Labortechnik, Germany). In the strain GLS006, 2 animals per phenotype (homozygous and heterozygous mutants and wild-type controls) were sacrificed under general anaesthesia (ketamine/xylacine; chapter 3.2.2) and approximately 40 mg liver tissue was stabilised in 1 ml TRIzol[®] Reagent. Samples were immediately homogenised for 1 minute on the highest level (25,000 rpm), using a Polytron PT 1200 E tissue homogeniser (Kinematica AG, Switzerland). To avoid cross contaminations, the dispersing aggregate was deterged in a series of: aqua bidest, 0.2 N NaOH, and aqua bidest. between the samples. Homogenates were stored at -80°C until assayed. RNA preparation was carried out according to the manufacturer's instruction manual. Following reagents and equipments were used: Chloroform, 100% isopropanol, 75% ethanol (Merck, Germany), sterile, RNase-free filter tips (Peske, Germany) and sterile, RNase-free reaction cups. To avoid contamination with RNases, all glassware was sterilised for 12 hours at 180°C and all buffers, except for Tris-containing solutions, were prepared with RNase-free H₂O (Invitrogen, Germany) or 0.1% DEPC-H₂O.

0.1% DEPC-H₂O

DEPC (Sigma, Germany)	1 ml
-----------------------	------

Dissolved overnight in 1000 ml H₂O by stirring, autoclaved afterwards for 3 times and stored at room temperature

The RNA pellet was resuspended in 30-100 µl RNase-free H₂O (Invitrogen, Germany) (dependent on the pellet size) for 60 minutes on an Eppendorf Thermomixer 5436 (Eppendorf, Germany) at 55°C. Resuspended RNA was further

kept on ice (short term) or was stored at -80°C (long term) until further analysis. RNA purity and total RNA amount were determined spectrophotometrically, using a NanoDrop[®] ND-1000 Spectrophotometer (NanoDrop Technologies, USA).

3.2.2.3 cDNA synthesis by reverse transcription of total hepatic RNA

Potential DNA contaminations were removed by incubation of 5 μg total RNA with 10 IU RNase-free DNase I (Roche, Germany) and 10x DNase I digestion buffer in a total reaction volume of 20 μl for 30 minutes at 37°C on an Eppendorf Thermomixer. Enzyme inactivation was carried out at 75°C for 10 minutes.

10x DNase I digestion buffer

250 mM Tris-HCl, (pH 8.3) (Roth, Germany)

375 mM KCl (Merck, Germany)

15 mM MgCl_2 (Merck, Germany)

Sterile filtered, autoclaved and aliquoted, and stored at -20°C

Four μl (1 μg) of the DNase I-digested RNA solution were applied for reverse transcription to cDNA, using M-MLV Reverse Transcriptase (M-MLV RT; Invitrogen, Germany), random primers (Invitrogen, Germany), and RNasin[®] RNase Inhibitor (Promega, Germany) in a reaction volume of 40 μl as stated in Table 3.3.

Table 3.3: cDNA synthesis from total hepatic RNA using M-MLV Reverse Transcriptase.

Step 1	Step 2	Step 3
<u>Add Master Mix 1</u>	<u>Add Master Mix 2</u>	<u>Add Master Mix 3</u>
RNase free H_2O 16 μl	RNase free H_2O 2 μl	5x first stand buffer 4 μl
Random primers 2 μl	5x first strand buffer 4 μl	M-MLV RT 1 μl
10 mM dNTPs 2 μl	0.1 M DTT 4 μl	
	RNasin [®] RNase Inhibitor 1 μl	
➤ 65°C , 5 minutes ➤ quick chill on ice	➤ 25°C , 10 minutes ➤ 37°C , 2 minutes	➤ 37°C , 50 minutes ➤ 75°C , 10 minutes ➤ chill on ice

The reverse transcription success, the integrity of the resultant cDNA, and the absence of DNA contamination were controlled by PCR, using exon-specific primers, positioned in exon 4 and 6 of the β -actin gene. Amplification of DNase I-digested and reverse transcribed RNA resulted in 613 bp PCR products, whereas the presence of genomic DNA was indicated by an additional band of 832 bp in size (Fig. 3.2). One μl of DNase I-digested, reverse transcribed RNA, RT⁻ (DNase I digested, but not reverse transcribed RNA), and DNA controls were constituted in standard PCR

reaction batches, described in 3.2.1.2. Primers were synthesised by Thermo Scientific, USA. Cycling conditions and primer sequences (Höfer 2006) are stated in Table 3.4.

Table 3.4: Cycling conditions and primer sequences for β -actin gene PCR.

PCR conditions		Oligo name	Primer Sequence (5'→3')
1.	4 min 94°C	β -actin sense β -actin antisense	GGC ATC GTG ATG GAC TCCG GCT GGA AGG TGG ACA GTG AG
2.	1 min 94°C		
3.	1 min 60°C		
4.	90 sec 72°C		
5.	10 min 72°C		
6.	∞ 4°C		

PCR products were separated by gel electrophoresis on a 1.5% TBE agarose gel as described above (chapter 3.2.1.3).

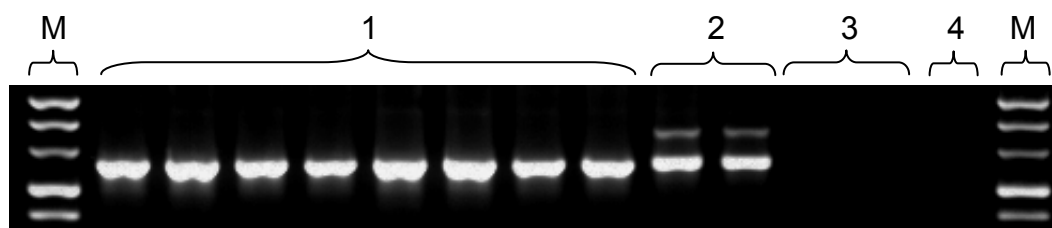


Figure 3.2: Exemplary gel electrophoresis of successfully DNase I-digested and reverse transcribed RNA after PCR-based amplification of 613 bp sequence of the β -actin gene. 1: DNase I-digested and reverse transcribed RNA; 2: DNA; 3: RT⁻ control (DNase I-digested, but not reverse transcribed RNA); 4: H₂O; M: fragment size marker (pUC mix 8; MBI Fermentas, Germany); marker bands represent fragment sizes of 1118, 881, 692, 501 (and 489), and 404 bp (from top to bottom).

3.2.2.4 PCR amplification of the candidate gene

Amplification of the complete *Gck* mRNA sequence from hepatic cDNA was performed with 5 pairs of primers, resulting in overlapping PCR products (PCR 1-5). The sizes of the resulting PCR products did not exceed 690 bp to allow reliable bidirectional sequencing. Due to alternate tissue-specific mRNA splicing, mammalian hepatic and β -cell *Gck* transcripts exhibit different sequences for exon 1 (Jetton *et al.* 1994; Liang *et al.* 1991; Magnuson and Shelton 1989; Printz *et al.* 1993). Therefore, an additional primer pair was designed to amplify the whole first exon sequence of the pancreas-specific transcript (PCR 6). Primer pairs spanning exon 9-11 failed to hybridise to cDNA of GLS001 mice. Therefore, amplification of the positional sequence was carried out with genomic DNA (PCR 7 and 8). Furthermore, the *Gck*

promoter sequence was amplified, using genomic DNA samples from homozygous and heterozygous mutants and wild-type controls of both strains. All primers were chosen without computational assistance and were synthesised by Thermo Scientific, USA.

PCRs were performed with total reaction volumes of 40 µl, containing 4 µl cDNA solution (100 ng) each (PCR 1-5) or 2 µl genomic DNA (refer to chapter 3.2.1.2). PCR reactions were run on a Mastercycler® Gradient (Eppendorf, Germany) or a Gene Amp® PCR System 9700 (Perkin Elmer, Germany) according to the cycling protocols illustrated in Table 3.5.

Table 3.5: PCR conditions for amplification of the candidate gene (A), applied primer sequences and combinations and their expected product length (B).

A

PCR 1-5			PCR 6			PCR 7			PCR 8 and 9			
1.	5 min	94°C	36 cycles	5 min	94°C	36 cycles	5 min	94°C	40 cycles	5 min	94°C	36 cycles
2.	45 sec	94°C		50 sec	94°C		50 sec	94°C		50 sec	94°C	
3.	45 sec	61°C		50 sec	64°C		50 sec	60°C		50 sec	60°C	
4.	90 sec	72°C		60 sec	72°C		100 sec	72°C		90 sec	72°C	
5.	10 min	72°C		10 min	72°C		10 min	72°C		10 min	72°C	
6.	∞	4°C		∞	4°C		∞	4°C		∞	4°C	

B

PCR	Oligo name	Sequence (5'→3')	Nucleotide position ^a	Product length (bp)
1	Gck_1_for	ACA CTC AGC CAG ACA GTC CTC	5' UTR	688
	Gck_2_rev	ACC ACA TCC ATC TCA AAG TCC	599-579	
2 ^b	Gck_7_for	ATG GCT GTG GAT ACT ACA AGG	1-21	599
3	Gck_3_for	ACA TCG TGG GAC TTC TCC GAG	539-559	675
	Gck_4_rev	TGA TGC GCA TCA CGT CCT CAC	1213-1193	
4	Gck_5_for	ATC CTT AAC ATC CTG AGC ACT C	1042-1063	498
	Gck_6_rev	TCA CTG GCT GAC TTG GCT TGC	3' UTR	
5/7 ^c	Gck_8_rev	ATG GCA TCT GGG AAA CCT GAC	3' UTR	566/1048
6	Gck_20_for	AAG AGG AAG CTG TGG CTT CAA CC	5' UTR	287
	Gck_21_rev	AGG CAT AGA CAC TTA TAG GTG GC	Intron 1	
8	Gck_22_for	AGC CGA TCC TGC TTG ATT CTC C	Intron 9	850
	Gck_24_rev	TCT CTG AAT GTT TGT GGC CTG	3' UTR	
9	Gck_25_for	ATC TCC ACT ACC CAC AAG TCT G	5' UTR	599
	Gck_26_rev	TCC TAC AGG ATC GCA CTC ATC	Intron 1	

^a Nucleotide positions according to NCBI GenBank accession nos. NM_010292 and NW_001030444, respectively. ^b Primer combinations for PCR 2 were Gck_7_for and Gck_2_rev. ^c Primer combinations used for PCR 5 and 7, respectively, included Gck_5_for and Gck_8_rev.

3.2.2.5 Purification of PCR products

PCR products were separated from unbound dNTPs and primers by either direct on-column clean-up, by microdialysis, or after gel electrophoresis.

Microdialysis

Purification of PCR products was performed with MF-Millipore Membrane Filters (#VSWP04700; Millipore, USA) (pore size: 0.025 µl). Twenty µl PCR product were pipetted on the membrane filter, floating on 0.25x TE buffer in a Petri dish (Neolab, Germany). The membrane filter was then gently stirred for 1 hour on an IKA colour squid IKAMAG[®] magnetic stirrer (IKA, Germany). Thereafter, the remaining droplet was removed from the floating membrane and transferred into a sterile, RNase-free reaction cup.

On-column purification was carried out, using the High Pure PCR Purification Kit[®] (Roche, Germany) according to the manufacturers' recommendations.

In case of additional, non-specific product amplification, PCR products were purified after gel electrophoresis on a 1.5% TBE agarose gel. To avoid cross contaminations during band excision, every second well was charged with PCR products. Thereafter, gel electrophoresis was performed as described (chapter 3.2.1.3). Bands were visualised by irradiation in the UV part of the spectrum (UV-Transilluminator FLX 20M; Biometra, Germany). The specific bands of predicted size were excised with a sterile surgical blade and were transferred into sterile, RNase-free 2 ml reaction cups. Gel slices were weighed (MJ-3000; YMC Co. Ltd., Japan), and DNA was extracted using the QIAquick[®] Gel Extraction Kit (Qiagen, Germany) according to the Kit manual. In order to enhance DNA yield, the final elution step was conducted twice.

After purification, PCR products were kept on ice (short term) or at -20°C until assayed. DNA concentration of the amplicates was quantified, using a NanoDrop[®] ND-1000 Spectrophotometer (NanoDrop Technologies, USA). Further, DNA concentration was evaluated after gel electrophoresis with a Lambda DNA/EcoRI + HindIII concentration marker, 3 (MBI Fermentas, Germany) (chapter 9.4).

3.2.2.6 Sequence analysis

According to the required DNA concentrations (Table 3.6), purified PCR products were diluted to an appropriate concentration with 1x TE, if necessary. The final reaction mixture for sequence analysis contained 5 µl of purified PCR product solution and 1 µl the corresponding *Gck*-specific primer (3 µM in 1x TE). Afterwards, PCR amplicates were sequenced bidirectionally (Sequencing service of the Gene Center, AG Blum (LMU Munich, Germany)).

Table 3.6: DNA concentrations, required for sequence analysis (adapted from the Sequencing service of the Gene Center, AG Blum, LMU Munich, Germany).

PCR product length	Purification by gel extraction	Purification by microdialysis
600 bp	20-70 ng	15-45 ng
900 bp	35-110 ng	30-60 ng
1200 bp	50-140 ng	40-75 ng

The resulting sequences were aligned with the *Gck* sequence of the mouse genome database (NM_023514 NM_010292 and NW_001030444), using the NCBI blast tool (<http://blast.ncbi.nlm.nih.gov/Blast.cgi>). The consequences of the identified genomic mutations on the glucokinase protein were evaluated by analysis of the deduced amino acid sequence (<http://www.expasy.ch/tools/dna.html>). The probability of an additional confounding mutation between the 2 polymorphic markers with the highest linkage was estimated for both strains according to the method of Keays *et al.* (<http://zeon.well.ox.ac.uk/git-bin/enuMutRat>), assuming a mutation rate of 1 in 1 Mb (Keays *et al.* 2006).

3.3 Genotyping of the identified mutations

3.3.1 Restriction fragment length polymorphism (RFLP) analysis in GLS001 mice

To establish genotyping of GLS001 mice by restriction fragment length polymorphism (RFLP) analysis, the identified mutation and flanking sequences were queried by the NEBcutter V2.0 tool, provided by New England Biolabs, UK (<http://tools.neb.com/NEBcutter2/>). The causative mutation was identified to create a novel restriction site for the restriction endonuclease BstYI (recognition site RGATCY). Therefore, primer pairs (synthesised by Thermo Scientific, USA) were designed to amplify a 343 bp fragment of the affected DNA sequence including the

mutation (Table 3.7). Incubation of PCR products with BstYI was predicted to result in restriction of the mutant allele into 2 fragments of 200 and 143 bp in size, whereas the wild-type allele remained unrestricted. PCR reaction was conducted with 1 µl DNA samples in a total reaction volume of 20 µl (chapter 3.2.1.2) in a Mastercycler® Gradient (Eppendorf, Germany) under the cycling conditions stated in Table 3.7.

Table 3.7: PCR conditions and primer sequences for genotyping of GLS001 mice.

PCR conditions	Oligo name	Sequence (5'→3')
1. 5 min 94°C	Gck_3_for Gck_16_rev	ACA TCG TGG GAC TTC TCC GAG AGG CCT GTT CTG ACT GGC TC
2. 50 sec 94°C		
3. 50 sec 62°C		
4. 80 sec 72°C		
5. 10 min 72°C		
6. ∞ 4°C		

PCR products were stored at 4°C (short term) or at -20°C (long term) until assayed. The endonuclease reaction mixture contained 12 µl Master Mix and 12 µl PCR product each. The endonuclease was kept on -20°C until added to the Master Mix. The restriction digestion was carried out at a constant temperature of 60°C for 40 minutes in a Mastercycler® Gradient (Eppendorf, Germany). Afterwards, digested PCR products were run on a 3% TBE agarose gel.

Endonuclease digestion Master Mix

Aqua bidest.	9.1 µl
NEB buffer 2 (New England Biolabs, UK)	2.4 µl
BstYI (10,000 U/ml) (New England Biolabs, UK)	0.5 µl

3.3.2 Amplification refractory mutation system PCR (ARMS PCR) in GLS006 mice
NEBcutter query of the mutant sequence in GLS006 mice did not reveal a suitable restriction site for commercially available restriction endonucleases. Thus, for allelic differentiation of GLS006 mice, an allele-specific PCR (Amplification Refractory Mutation System PCR; ARMS PCR (Newton *et al.* 1989)) was designed. The principle of an ARMS PCR is the selective amplification of either the wild-type or the mutated allele by allele-specific inner primers, bearing either the reference or the mutant base at their 3'-end. The insertion of an additional mismatch, at nt 3 of the 3'-end is predicted to increase primer specificity for the distinct alleles. If possible, ARMS PCR should be performed in a single reaction (Single Tube Allele Specific (STAS) PCR). Under established PCR conditions, the distinct inner primers recognise the allelic variation with their 3' nucleotide and, together with the

corresponding outer primer, located at different distances from the mutation, selectively amplify sequences of different size. Furthermore, an additional product of both external primers, independent of the prevailing genotype, is amplified as PCR control (Zinovieva *et al.* 1996). The product of the outer primers in GLS006 mice had a length of 343 bp, whereas the genotype-specific products displayed a total length of 238 bp (for the wild-type allele) and 147 bp (for the mutant allele) (Fig. 3.3).

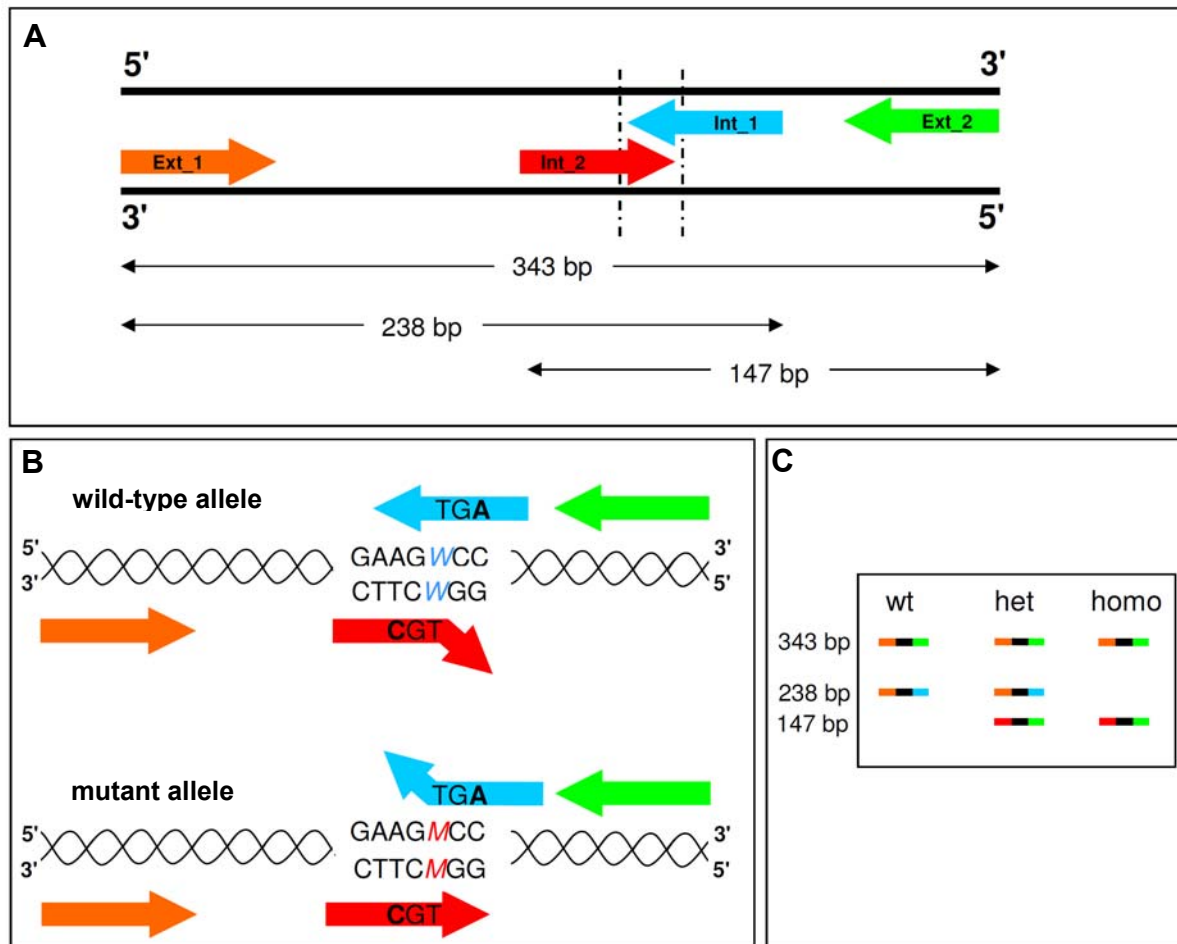


Figure 3.3: Schematic illustration of allele-specific primer hybridisation in GLS006 mice. A: Outline of both external (Ext_1 and Ext_2) and internal (Int_1 and Int_2) primers and the corresponding product lengths. B: Formation of a PCR product depended on the genotype: The mutation-specific primer (red, Int_2) failed to hybridise to the wild-type allele, whereas a PCR product resulted from wild-type specific (blue, Int_1) primer binding, and *vice versa* for the mutant allele. The appearance of a PCR product of both external primers (Ext_1 (orange) and Ext_2 (green)) is genotype-independent. Italic letters outline the position of the mutation (W, blue = reference nucleotide; M, red = mutated base); bold letters mark the auxiliary introduced mismatch. C: Predicted appearance of genotype-specific bands after gel electrophoresis. Wt = wild-type; het = heterozygous mutant; homo = homozygous mutant.

STAS PCR was carried out in a Mastercycler® Gradient (Eppendorf, Germany), using 20 µl reaction volumes, containing 1 µl sample in 19 µl PCR Master Mix. The respective cycling protocol is stated in Table 3.8. PCR products were separated according to their size by gel electrophoresis on a 3% TBE agarose gel with a GeneRuler™ 100 bp Plus DNA Ladder (Fermentas, Germany) as fragment size marker.

Table 3.8: PCR Master Mix and cycling conditions for STAS PCR in GLS006 mice.

PCR Master Mix		Cycling conditions	
Aqua bidest	3.65 µl	1. 5 min 94°C 2. 50 sec 94°C 3. 50 sec 57°C 4. 80 sec 72°C 5. 10 min 72°C 6. ∞ 4°C	36 cycles
Q-solution	4.00 µl		
10x buffer	2.00 µl		
MgCl ₂	1.25 µl		
dNTPs (1 mM)	1.00 µl		
Primer 1 sense (2 µM)	0.50 µl		
Primer 1 antisense (2 µM)	0.50 µl		
Primer 2 sense (2 µM)	3.00 µl		
Primer 2 antisense (2 µM)	3.00 µl		
Taq Polymerase	0.10 µl		

External primers (Primers 1): Gck_3_for (Ext_1); Gck_16_rev (Ext_2) (refer to chapter 3.3.1)

Internal primers (Primers 2): Primers were obtained from Eurofins MWG Operon (Germany)

Gck_1_int (antisense): 5'- TGC CGA CCT CAC ATT GGC AGT -3' ^a

Gck_2_int (sense): 5'- TGA TCT CCT GCT ACT ATG ACG T -3' ^b

^a wild-type specific; ^b mutation specific

3.4 Ex vivo studies of functional consequences of the causative mutations

3.4.1 Quantification of glucokinase enzyme activity

Since strategies for direct measurement of glucokinase enzyme have not yet been developed, an indirect fluorometric coupled assay was performed to quantify glucokinase activity in liver homogenate of 90-day-old GLS001 and GLS006 mice. Based on the phosphorylation of glucose by glucokinase enzyme to glucose-6-phosphate (G6P), which is in turn again metabolised by glucose-6-phosphate

dehydrogenase (coupled to the reduction of nicotinamide adenine dinucleotidephosphate (NADP^+)) into 6-phosphogluconate (Fig. 3.4), glucokinase activity was evaluated by spectrophotometrical quantification of the turnover rate of NADP^+ to NADPH in the presence of different glucose concentrations and excess glucose-6-phosphate dehydrogenase (G6PD) (Grupe *et al.* 1995; Hara *et al.* 1986; Trus *et al.* 1981).

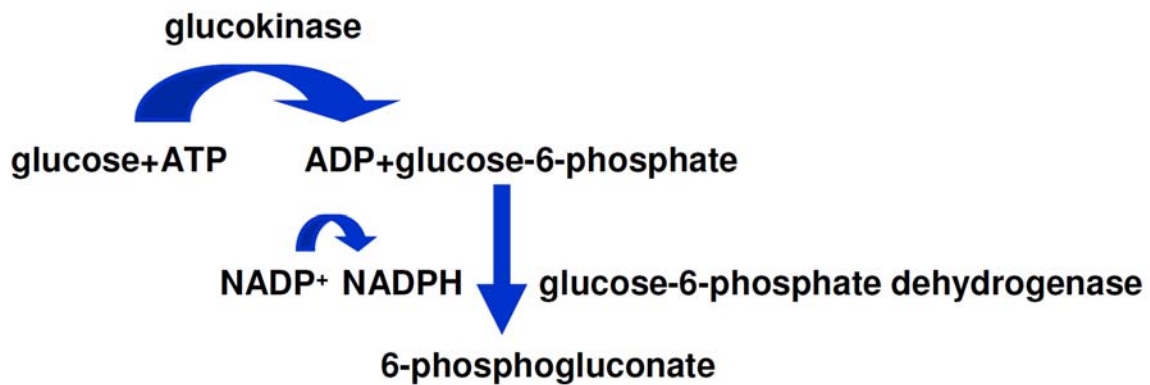


Figure 3.4: Schematic diagram of the first step of glycolysis, catalysed by glucokinase enzyme and the following downstream reactions, enabling indirect quantification of glucokinase activity.

Complicating assay specifications represent the coincident presence of other hexokinases, catalysing the identical reaction and impeding therefore separate quantification of glucokinase activity. However, the high affinity of hexokinases for glucose leads to their saturation already at low glucose concentrations (Bell *et al.* 1996). The kinetic property of hexokinases can be availed to selectively quantify glucokinase activity by assay performance in the presence of either low glucose concentrations (0.03-0.5 mM; to quantify hexokinase phosphorylation activity) or by applying glucose concentrations in a range of 6-100 mM, where hexokinases are predicted to minor contribute to glucose phosphorylation activity of the low affinity glucokinase enzyme. In order to exclude hexokinase contribution, the maximal reaction velocity (V_{\max}) for hexokinases, calculated by means of the particular reaction velocities in presence of the respective minor glucose concentrations, was subtracted from glucose phosphorylation velocities, determined by employing high glucose concentrations. The assay was performed according to a modified protocol adapted from Liang *et al.* (Liang *et al.* 1990).

3.4.1.1 Tissue sample preparation

Ad libitum fed mice were sacrificed under general anaesthesia (ketamine/xylazine mixture; 3.2.2) by cervical dislocation and liver samples of approximately 20 mg weight (weighed on a Mettler AE200 Electronic Analytical Balance, Mettler-Toledo Intl. Inc., Germany) were obtained. Tissue samples were immediately transferred into 2 ml reaction cups, containing 1 ml ice-cold 1x Homogenisation Buffer, and were homogenised for 1 minute with a Polytron PT 1200 E tissue homogeniser (Kinematica AG, Switzerland) at the highest level (25,000 rpm). Homogenates were subsequently sonicated by 7 strokes <1s each (Branson sonifier cell disruptor B15, Branson Ultrasonic Corporation, USA). Thereafter, tissue sonicates were centrifuged (75 minutes, 15,300 rpm at 4°C) and kept on ice until further assayed.

10x Homogenisation Buffer

KCl (Roth, Germany)	820 mg
K ₂ HPO ₄ (Merck, Germany)	348 mg
DTT (Roth, Germany)	77 mg
EDTA (Sigma, Germany)	29 mg

Ad 10 ml aqua bidest.; stored at 4°C and diluted 1:10 to prepare ready-to-use 1x Homogenisation Buffer

3.4.1.2 Work flow of glucokinase activity determination

Glucose phosphorylation by glucokinase was initiated by addition of 500 µl Reaction Master Mix to 20 µl liver homogenate. The reaction mixture was incubated at 30°C for 35 minutes. A total number of 11 glucose concentrations were applied, covering either the low glucose range (0.5, 0.25, 0.125, 0.06, and 0.03 mM) or the high glucose spectrum (100, 50, 25, 12, and 6 mM). Each reaction series included a reaction blank with H₂O instead of glucose. The reaction was finally stopped by pH alteration via addition of 480 µl 1M NaHCO₃ pH 9.4 and sample mixtures were transferred into disposable semi-micro PMMA cuvettes (Neolab, Deutschland). Relative absorbance of each reaction was measured at a wavelength of 340 nm after reaction blank calibration, using a SPEKOL 1500 UV/vis spectrophotometer (Analytic Jena AG, Germany).

Reaction Buffer (prepared freshly)

KCl (Roth, Germany)	298 mg
β -mercaptoethanol (Sigma, Germany)	40.3 μ l
MgCl ₂ (Merck, Germany)	28 mg
BSA (Sigma, Germany)	20 mg
NADP ⁺ (AppliChem, Germany)	15 mg
ATP (Sigma, Germany)	110 mg

Ad 20 ml 100mM Hepes pH 7.8; kept on ice until assayed

Glucose stock solutions

High glucose: 250 mM

α -D-glucose (Sigma, Germany)	0.45 g
--------------------------------------	--------

Ad 10 ml aqua bidest.; stored at 4°C (short term) or at -20°C (long term)

Low glucose: 1.25 mM

250 mM stock solution	250 μ l
-----------------------	-------------

Ad 500 ml aqua bidest.

Ready-to-use glucose solutions were prepared by serial 1:2 dilution of the corresponding stock solutions with aqua bidest. (exception: 12 and 0.06 mM glucose solutions were prepared by 48:100 dilutions of 25 and 0.125 mM glucose solutions, respectively). All glucose containing reagents were stored at 4°C (short term) or at -20°C (long term).

Glucose-6-phosphate dehydrogenase (G6PD) solution (prepared freshly)

G6PD (1000 U/ml) (Roche, Germany)	20 μ l
-----------------------------------	------------

- Centrifuge at 10,000 rpm for 45 minutes, 4°C
- Discard the supernatant, resuspend with 250 μ l ice-cold aqua bidest. and mix gently by pipetting
- Dilute 1:10 with ice-cold aqua bidest. (200 μ l resuspended G6P + 1800 μ l aqua bidest.). Assay dilution contains 8 U/ ml G6PD and is kept on ice until assayed

Reaction Master Mix

Reaction buffer	500 μ l
High/Low glucose solution/aqua bidest.	400 μ l
G6PD solution	100 μ l

Immediately applied for assay complementation

The reaction velocities per time unit (minutes) in the presence of distinct glucose concentrations were calculated according to the Beer-Lambert law, assuming a coat thickness of 1 mm for the applied cuvettes and a molar decadic extinction coefficient (ϵ) for NADPH of 6.2 L \times mmol⁻¹. The reaction velocities V for glucokinase were obtained by subtracting the maximal velocity (V_{max}) for hexokinase from the reaction

velocities, observed at the 5 high glucose concentrations. As the high affinity hexokinases follow Michaelis-Menten kinetics, the V_{max} and Michaelis constant (K_m) for hexokinases were obtained after plotting reaction velocities at low glucose concentrations vs. the respective substrate concentrations. Using a non-linear regression curve fit tool, K_m and V_{max} were calculated according to the Michaelis-Menten equation (GraphPad Prism 3.0 (GraphPad Software, USA)):

$$V = \frac{V_{max} \times [S]}{K_m + [S]}$$

V = Specific activity/substrate turnover rate in presence of the respective $[S]$

$[S]$ = Substrate concentration

V_{max} = Maximal reaction velocity

K_m = Michaelis constant

Since the absence of allostericity and cooperativeness represent prerequisites for the applicability of the Michaelis-Menten equation, kinetic characteristics of the positive cooperative behaviour displaying allosteric glucokinase enzyme were determined, applying the Hanes-Woolf plot. Performing this graphic application, the ratio of the initial substrate concentrations $[S]$ (high glucose fraction) to the reaction velocity v is plotted against the respective $[S]$. V_{max} and $S_{0.5}$ (glucose concentration that is needed to achieve the half-maximal rate of phosphorylation; $S_{0.5} \triangleq K_m$ in Michaelis-Menten equation) were calculated according to the Hanes-Woolf transformation of the Michaelis-Menten equation after data extrapolation of the linear portion of the plotting curve by best-fit linear regression adaption (GraphPad Prism 3.0 (GraphPad Software, USA)).

$$\frac{[S]}{V} = \frac{S_{0.5} + [S]}{V_{max}}$$

V = Specific activity or turnover in presence of the respective $[S]$

$[S]$ = Substrate concentration

V_{max} = Maximal reaction velocity

$S_{0.5}$ = Equivalent to Michaelis constant

All kinetic data were referred to the total protein content in the corresponding liver homogenate, determined by Bradford method (chapter 3.4.1.3).

3.4.1.3 Determination of protein contents

Total protein amounts per μl liver sonicate were determined by Bradford method. From the initial standard (1% BSA (Sigma, Germany) in phosphate buffered saline (PBS)), a serial 1:2 dilution was prepared in duplicates in a NUNC™ 96-well Optical Bottom Plate (Thermo Fisher Scientific (Nunc GmbH & Co. KG), Germany). Steady state concentrations contained 25, 12.5, 6.25, 3.13, 1.56, 0.78, 0.39, 0.20 μg BSA. One μl of the sample was added to 199 μl PBS in the first well of the plate, and diluted 1:2 in PBS in the adjacent well. Reaction was initiated by addition of 100 μl 40% Bradford reagent (Bio-Rad, Germany). After an incubation time of 5 minutes, absorbance at a wavelength of 595 nm was determined spectrophotometrically by a plate reader ((SUNRISE, Tecan, Germany) and the corresponding software (Magellan 2, Tecan, Germany).

Phosphate buffered saline (PBS)

NaCl (AppliChem, Germany)	7.95 g
Na ₂ HPO ₄ (Roth, Germany)	1.15 g
KCl (Merck, Germany)	0.20 g
KH ₂ PO ₄ (AppliChem, Germany)	0.20 g
Ad 1,000 ml distilled water	

3.4.2 Determination of glucokinase transcript abundances by quantitative real-time PCR

Real-time PCR was performed with reverse transcribed RNA, isolated from neonatal heterozygous and homozygous GLS001 mice and wild-type littermates on a 7900HT Fast Real-Time PCR System with Fast 96-Well Block Module TaqMan ABI 7900 Sequence Detection System® (Applied Biosystems, USA) and SDS Software v2.2.2. Primer pairs for amplification of the target gene (*Gck*) and the selected reference (housekeeping) genes β -actin (*Actb*) (Onishi *et al.* 2007), mitochondrial ribosomal protein S9 (*Mrps9*) (Herbach *et al.* 2009), 18S ribosomal RNA (*18s rRNA*) (Rohrl *et al.* 2008), and glyceraldehyde-3-phosphate dehydrogenase (*Gapdh*) (Siner *et al.* 2007) were chosen by Primer Express version 3.0 (Applied Biosystems), and queried by NCBI Blast software (<http://blast.ncbi.nlm.nih.gov/Blast.cgi>) (Table 3.9). Prior to application to quantitative real-time PCR, the amplification efficiencies of all primers were tested as described in chapter 9.5.

3.4.2.1 Tissue sample preparation, RNA isolation and cDNA synthesis

Mice were sacrificed by decapitation and hepatic tissue samples of approximately 30-40 mg each were immediately transferred into sterile 2 ml reaction cups, containing 1 ml TRIzol[®] Reagent. Tissue sample procession and RNA isolation was accomplished as described in chapter 3.2.2.2 and 800 ng total hepatic RNA were reverse transcribed to cDNA in a final volume of 40 μ l as stated in chapter 3.2.2.3.

3.4.2.2 Quantitative real-time PCR performance

All reactions were performed in duplicates in a total reaction volume of 25 μ l, comprising 2 μ l (40 ng) cDNA in 23 μ l Master Mix. Quantitative real-time PCR Master Mixes contained SYBR[®] Green (SensiMixPlus SYBR, Quantace Ltd, UK). For each target, sample duplicates including H₂O instead of the cDNA template, served as no template controls (NTC). All samples belonging to corresponding groups to be compared were run on identical plates. As primer pairs, specific for the internal reference transcript of *18s rRNA* and *Gapdh* did not cross intron-exon assemblies, DNase I - digested but not reverse transcribed RNA (RT⁻) samples were run simultaneously with the cDNA (RT⁺) samples and the NTCs, to evaluate genomic DNA contamination. The prepared reaction plates (ABI PRISM[®] 96-Well Optical Reaction Plate; Applied Biosystems, USA) were covered with MicroAMP[™] Optical Adhesive Films (Applied Biosystems, USA) and were then inserted into the Fast 96-Well Block Module of the real-time PCR instrument. After an initial hold of 10 minutes at 95°C, the samples were cycled 36 times at 95°C for 15 seconds, at 60°C for 30 seconds, and at 72°C for 30 seconds with a final dissociation step at the end of the run. Identical threshold lines were manually adjusted in the exponential phase of amplification for all runs, designated to be compared. Comparison of expression levels of the target transcript (*Gck*) between the genotype groups was accomplished by relative quantification of the achieved transcript abundance using the $2^{-\Delta C_T}$ method (Cohen and Kretzler 2003). After the mean C_T (= threshold cycle) for duplicate measurements of each sample was calculated for both the target (*Gck*) and the internal reference transcripts, the target transcript abundances of each sample, relative to the expression of the reference transcripts were determined. Subtracting the mean C_T value of the *Gck* transcript from the mean C_T value of the respective reference transcript revealed the corresponding ΔC_T value (ΔC_T = mean C_T (reference transcript) - mean C_T (target transcript)). Transcript abundance of the target

transcript, normalised to reference transcript expression were defined as $2^{-\text{mean}\Delta C_T}$ copies of housekeeper transcripts. The means of $2^{-\Delta C_T}$ values of all samples of the respective genotype groups were compared (mutants vs. wild-type mice; homozygous vs. heterozygous mutants), using a two-tailed unpaired Student's t-test.

SYBR Master Mix

SensiMixPlus SYBR	12.5 μ l
RNase-free H ₂ O (Invitrogen, Germany)	8.5 μ l
Primer sense (5 μ M)	1 μ l
Primer antisense (5 μ M)	1 μ l

Table 3.9: Primer sequences, applied for amplification of the target and reference transcripts.

Gene symbol/NCBI accession ID	Primer direction	Sequence (5'→3')	Product length
<i>Gck</i> (NM_010292)	sense	CGA CCG GAT GGT GGA TGA	79 bp
	antisense	TCA TTG GCG GAA AGT ACA TGG	
<i>18s rRNA</i> (XR_034450)	sense	GTA ACC CGT TGA ACC CCA TT	151 bp
	antisense	CCA TCC AAT CGG TAG TAG CG	
<i>Gapdh</i> (NM_008084)	sense	TGT GTC CGT CGT GGA TCT GA	84 bp
	antisense	CCT GCT TCA CCA CCT TCT TGA T	
<i>Actb</i> (NM_007393)	sense	GCT CTT TTC CAG CCT TCC TT	100 bp
	antisense	AGG TCT TTA CGG ATG TCA ACG	
<i>Mrps9</i> (NM_023514)	sense	CCA TCA CAC AGG ACA GAG AAC AGT	97 bp
	antisense	CTC CCT CCC CCG GAG ACT	

3.4.3 Western blot analysis

Western blot analyses were performed with isolated pancreatic islets from 90-day-old male and female heterozygous mutant GLS001 mice and wild-type littermates with regard to glucokinase and the apoptosis marker caspase-3.

3.4.3.1 Isolation and preparation of pancreatic islets

Two GLS001 mice per genotype and sex were anaesthetised by intraperitoneal injection of 200 μ l of ketamine/ xylazine mixture (chapter 3.2.2), and sacrificed by cervical dislocation. After abdominal incision, the pancreas, the bile duct and its intestinal orifice were exposed. The bile duct was ligated close to the liver and the small intestine was clamped on both sides of the bile duct orifice by artery forceps to exclude collagenase solution efflux into the intestine. A total volume of 1.8 ml collagenase solution was injected into the pancreas after cannulation of the bile duct via the small intestine by a winged infusion set (Venofix[®], B.Braun, Germany). The

bloated pancreas was cautiously removed from the adjacent tissue and transferred into a 15 ml screw-cap centrifuge tube (TTP AG, Switzerland), containing 3.75 ml perfusion solution. Immediately prior to digestion, 3.2 ml collagenase solution were added, and pancreatic tissue was digested for at least 20 minutes at 37°C under occasional gently agitation. The digested pancreas was conveyed into a Petri dish (Neolab, Germany), filled with ice cold 1x Hank's with 0.3% BSA to stop the digestion reaction. During the ongoing procedure steps, all assay components and isolated islets were kept on ice. After digestion, all visible islets (at least 250) were hand picked under a stereomicroscope (Stemi DV4, Zeiss, Germany; magnification x32) (Fig. 3.5) into a 1.5 ml reaction tube and were centrifuged for 1 minute at 1,000 rpm (1K15, Sigma, Germany). Subsequently, the supernatant was discarded and pancreatic islets were resuspended in 1 µl protein extraction buffer/6 islets. Cell membranes were destroyed by freezing at -80°C, thawing on ice for 30 minutes, followed by sonication (7 strokes <1 s each by a Branson sonifier cell disruptor B15 (Branson Ultrasonic Corporation, USA)), and lysing on ice for another 30 minutes. After centrifugation (5 minutes, 5,000 rpm), the supernatant was separated, and stored at -20°C until assayed.

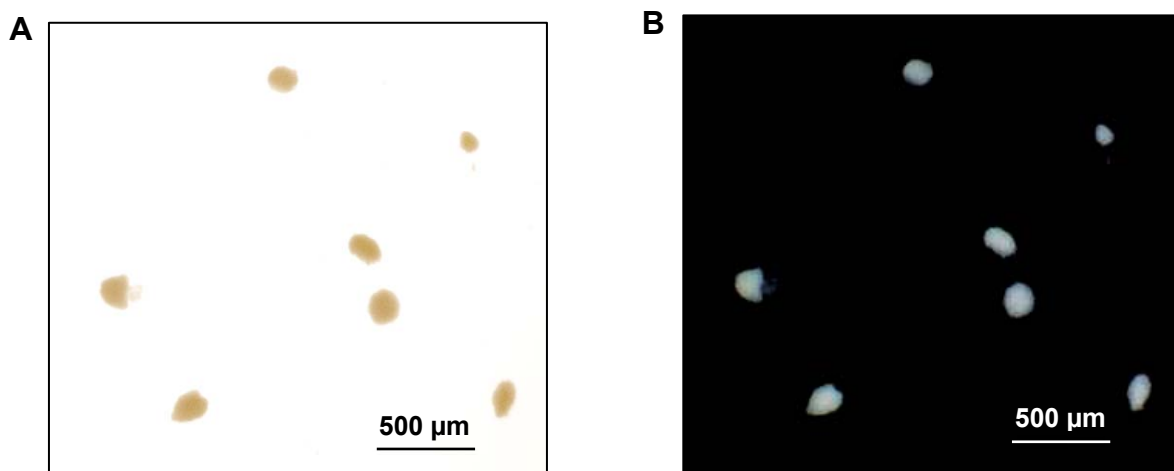


Figure 3.5: Generic appearance of hand picked pancreatic islets after collagenase I-digestion. Under transmitted light (A), pancreatic islets occurred of light brown colour, whereas under reflected light on a black background (B), islets usually represented opaque structures with discrete granulation.

4x Hank's solution

NaCl (AppliChem, Germany)	16.00 g
HEPES (Sigma, Germany)	4.76 g
KCl (Roth, Germany)	0.80 g
NaHCO ₃ (Merck, Germany)	0.70 g
KH ₂ PO ₄ (Roth, Germany)	0.12 g
Na ₂ HPO ₄ (Merck, Germany)	0.12 g
MgSO ₄ (Merck, Germany)	0.40 g
CaCl ₂ (Merck, Germany)	0.37 g
distilled water	500 ml

Stored at 4°C

1x Hank's solution

Hank's 4x	375 ml
α-D-Glucose (Sigma, Germany)	0.60 g

Adjust to pH 7.25 and keep on ice

1x Hank's with 0.3% BSA

Hank's 1x	500 ml
BSA (Sigma, Germany)	1.5 g

Perfusion solution

Hank's 1x	20 ml
CaCl ₂ 1 M (Merck, Germany)	47 μl
Hepes 1 M (Sigma, Germany)	500 μl

Kept on ice

Collagenase solution

Perfusion solution	10 ml
Collagenase type 1 (#C0130, Sigma, Germany)	20 mg

Kept on ice

Protein extraction buffer

200 mM NaCl/Tris pH 7.6	100 μl
Igepal CA 630 (ICN Biomedicals GmbH, Germany)	5 μl
300 mM EDTA	10 μl
300 mM EGTA	10 μl
100 mM PMSF	10 μl
200 mM NaOV	10 μl
1M DTT	1 μl
25x Complete	40 μl
Aqua bidest.	814 μl

Stock solutions

200 mM NaCl/Tris pH 7.6:

Tris base(Roth, Germany)	1.58 g
NaCl (AppliChem, Germany)	7.31 g

Dissolved in 30 ml aqua bidest and adjusted to pH 7.6; ad 50 ml aqua bidest

300 mM EDTA: 1.12 g EDTA (Sigma, Germany) ad 10 ml aqua bidest

300 mM EGTA: 1.41 g EDTA (Sigma, Germany) ad 10 ml aqua bidest.

100 mM PMSF: 17.4 mg PMSF (Sigma, Germany) dissolved in 1 ml isopropanol (Merck, Germany) and stored at -20°C.

200 mM NaOV: 0.92 g NaOV (ICN Biomedicals GmbH, Germany) dissolved in 20 ml distilled water and adjusted to pH 10 until the solution turns yellow. Solutions were reiterated boiled and cooled down on ice until remaining clear and of stable pH. After addition of 22.5 ml aqua bidest., the solution was aliquoted and stored at -20°C. Prior to use, solutions were boiled for 10 minutes on a heating block to remove crystallisation.

1 M DTT: 77.0 mg DTT (Roth, Germany) ad 500 µl aqua bidest.

25x Complete: Complete Protease Inhibitor Cocktail Tablets (Roche, Germany) were dissolved according to manufacturer's instructions

3.4.3.2 Sodium dodecyl sulphate polyacrylamide gel electrophoresis (SDS-PAGE)

SDS-PAGEs were performed with islet samples on 10 and 12% separating SDS gels (Table 3.10). The respective separating gels were poured into the intercept of 2 glass plates, clamped in a Mini-Protean III[®] gel casting chamber (Bio-Rad, Germany), and were immediately covered with isopropanol. After a polymerisation time of 45 minutes, isopropanol was drained and the stacking gel was casted onto the separating gel. A 10-well-comb was immediately inserted into the fluid stacking gel to create sample wells, and the stacking gel was allowed to polymerise for additional 45 minutes. Thereafter, the comb was removed, and the gel was placed into an electrophoresis cell (Protean III[®], Bio-Rad, Germany), which was then filled to the top of the inner cell with running buffer. About 1 half of the remaining buffer was disseminated in the outer cell of the electrophoresis chamber.

Protein content in the respective islet sonicates was determined by Bradford method (chapter 3.4.1.3). Islet sonicates were diluted to a total concentration of 20 µg protein/20 µl with at least equal volumes of Sample Denaturation Buffer (the maximum final volume did not exceed 20 µl). After protein denaturation for 10 minutes at 100°C, wells were charged and gel electrophoresis was run at 200 V (Biorad PowerPac 300, Bio-Rad, USA) until desired protein separation was achieved. A prestained molecular weight standard (Precision Plus Protein[™], Bio-Rad, Germany) was applied to indicate proceeding protein separation during electrophoresis.

Reducing sample buffer

Sample buffer, stock solution	475 µl
β-mercaptoethanol (Sigma, Germany)	25 µl

Sample buffer, stock solution

Tris/HCl 0.5 M, pH 6.8	1.3 ml
SDS 10% (Sigma, Germany)	2 ml
Glycerol (Merck, Germany)	1 ml
Bromphenol blue 0.05% (Merck, Germany)	0.6 ml
Aqua bidest.	4.8 ml

Table 3.10: Composition of the distinct SDS-gels.

Compound	Separating gel		Stacking gel
	10%	12%	
Aqua bidest.	4.17 ml	3.5 ml	3.05 ml
Tris HCl (1.5mM, pH 8.8)	2.50 ml	2.50 ml	-
Tris HCl (0.5mM, pH 6.8)	-	-	1.25 ml
10% SDS (Sigma, Germany)	0.1 ml	0.1 ml	0.1 ml
30% acrylamide (Roti Phenol®, Roth, Germany)	3.33 ml	4.00 ml	0.65 ml
APS 10% (Merck, Germany)*	0.05 ml	0.05 ml	0.05 ml
TEMED (Roth, Germany)*	0.01 ml	0.01 ml	0.01 ml

*added immediately before casting of the gels

Tris/HCl 0.5 M, pH 6.8

Tris base (Roth, Germany)	6.06 g
Ad 100 ml aqua bidest.	
Adjust to pH 6.8 with 1N HCl (Merck, Germany)	

Tris/HCl 1.5 M, pH 8.8

Tris base (Roth, Germany)	18.5 g
Ad 100 ml aqua bidest.	
Adjust to pH 8.8 with 1 N HCl (Merck, Germany)	

Running buffer, stock solution

Tris base (Roth, Germany)	30.3 g
Glycine (Merck, Germany)	144.0 g
Ad 1,000 ml aqua bidest.	

Running buffer

Stock solution	40 ml
SDS 10% (Sigma, Germany)	4 ml
Ad 400 ml aqua bidest.	

3.4.3.3 Blotting

After gel electrophoresis, SDS-gels were positioned onto a nitrocellulose membrane (Schleicher&Schuell, Germany), humidified with Towbin buffer. The gel-covered membrane was placed between 3 layers of absorbent paper and fibre pads each side

(both steeped in Towbin buffer) in a gel holder cassette. The cassettes were placed into the electrode module, which was then inserted in the buffer tank, containing ice cold Towbin buffer, a magnetic stir bar and a frozen cooling unit (Mini Trans-Blot Cell, Biorad, Germany). The transfer of the separated proteins was run for 90 minutes at 100 V on a magnetic stirrer (IKA, Germany). Thereafter, the nitrocellulose membrane was washed in Tris buffered saline (TBS, pH 8.3).

Towbin buffer

Tris base (Roth, Germany)	3.03 g
Glycine (Merck, Germany)	14.40 g
Methanol (neoLab, Germany)	200 ml
Distilled water	800 ml

Stored at 4°C

3.4.3.4 Western blot analysis

Detection of specific antigens was performed by Western blot analysis. Washing and incubation procedures were accomplished under consequent agitation of the membranes on a tumbling shaker (Heidolph, Germany) to allow consistent moistening of the membranes. All reaction steps were carried out at room temperature unless stated otherwise. Between the distinct incubation steps, membranes were washed 3 times for 5 minutes with TBS-T. Blocking and antibody dilution solutions either consisted of 1% BSA in TBS (for determination of glucokinase and reference (β -actin) protein levels) or TBS Blotto A (for evaluation of apoptosis).

After blocking for 1 hour, membranes were washed and incubated overnight at 4°C with the respective antibodies. Polyclonal rabbit anti-glucokinase (Abcam, Germany) antibody was diluted 1:250 in 1% BSA in TBS, monoclonal rabbit anti-caspase-3 antibody was diluted 1:1,000 in TBS Blotto A. On the following day, membranes were washed and incubated for 1 hour with a horseradish peroxidase-conjugated goat anti-rabbit IgG (Cell Signaling Technology; 1:10,000 for glucokinase detection and 1:2,000 for caspase-3 detection). After reiterate washing procedure, the membranes were tumbled for 1 minute in Luminol Reagent (Santa Cruz Biotechnology, Germany), immediately covered with an overhead transparency in a film cassette (Ortho Fine, AGFA, Germany), and then exposed to an Amersham Hyperfilm ECL (GE Healthcare, Germany) in a darkroom. Exposed films were successively processed in developer (Kodak professional developer, Kodak, USA) until

appearance of the specific bands, shortly dipped in 12% acetic acid solution, fixed (Kodak professional fixer, Kodak, USA), rinsed under running tap water and, finally, air dried. For repeated use, membranes were washed once and antibodies were detached from the membrane by incubation for 10 minutes in stripping buffer. After washing, twice in PBS for 10 minutes and twice in TBS-T for 5 minutes, membranes were ready to re-use. Protein levels of the constitutively expressed protein β -actin served as internal reference. The primary (mouse anti-actin antibody; Chemicon international, Germany) and the secondary antibody (horseradish peroxidase conjugated rabbit anti-mouse Ig; DAKO, Germany) were applied in a 1:10,000 dilution in 1% BSA in TBS.

TBS, stock solution (x10)

Tris base (Roth, Germany)	60.6 g
NaCl (AppliChem, Germany)	87.6 g
Ad 1,000 ml aqua bidest.	
Adjust to pH 7.4 with 1 N HCl (Merck, Germany)	

TBS-T

TBS, stock solution	50 ml
Aqua bidest.	450 ml
Tween 20 (Merck, Germany)	250 μ l

TBS Blotto A

TBS-T	100 ml
Non-fat dry milk (Roth, Germany)	5.0 g

Stripping buffer

Glycine (neoLab, Germany)	15 g
SDS (Sigma, Germany)	1 g
Tween 20 (Merck, Germany)	10 ml
Ad 1,000 ml distilled water	
Adjust to pH 2.2 with 37% HCl (Merck, Germany)	

3.5 Clinical analyses and tests

3.5.1 Body weights

Body weights of GLS001 and GLS006 mice were determined at the first day *post partum* (within the first 24 hours of life) and at an age of 3 days to the nearest 0.01 g, using a Mettler AE200 Electronic Analytical Balance (Mettler-Toledo Intl. Inc., Germany). During the post-weaning period, body weights of *ad libitum* fed 21-, 30-, 90-, and 175-day-old mice were quantified to the nearest 0.1 g on a Kern 440-43N

precision balance (Kern, Germany). Additionally, fasting body weights were determined at an age of 30, 85, and 180 days.

3.5.2 Blood glucose determination

Determination of blood glucose levels in GLS001 and GLS006 mice was accomplished within the first day *post partum* and at an age of 1 and 4 (only GLS001 mice) days. Blood samples from suckling mice were obtained under general anaesthesia by intraperitoneal injection of 50 μ l ketamine/xylazine mixture (chapter 3.2.2; diluted 1:4 for neonatal and 1-day-old mice, and diluted 1:2 for 4-day-old mice). After opening the eyelids, the retroorbital plexus was punctured with an open-end capillary (HITADO, Germany). Thereafter, mice were sacrificed by decapitation. During the post-weaning period, blood samples of *ad libitum* fed 21-, 30-, 90-, and 175-day-old mice were obtained from the nicked tail tip. Blood samples from fasted 30-, 85-, and 180-day-old mice were collected, applying the identical procedure. Blood glucose concentrations were quantified using a SUPER GL[®] auto analyser (HITADO, Germany) and the corresponding analysing reagents. Blood glucose levels during glucose and insulin tolerance tests were determined analogically.

3.5.3 Oral glucose tolerance tests (OGTT)

Ten GLS001 and 7 GLS006 mice per sex and genotype underwent oral glucose tolerance testing at an age of 30, 85, and 180 days. Mice were fasted overnight for 15 hours (7 pm - 10 am) and blood samples were taken from the nicked tail tip to determine basal blood glucose and serum insulin concentrations. Blood samples for serum separation were collected into 75 μ l heparinised capillary tubes and emptied into 0.5 ml reaction cups. Each mouse was administered 11.1 μ l of a 1 M glucose solution per gram mean body weight (1.8 g α -D-Glucose; Sigma, Germany), dissolved in 10 ml tap water) into the stomach via an olive probe *per os* (Eickemeyer, Germany). Blood samples for determination of blood glucose and serum insulin levels were taken 10 minutes after glucose challenge. Additional samples for blood glucose analyses were collected 20, 30, 60, 90, and 120 minutes after oral glucose application. For serum insulin quantification, blood samples were centrifuged for 10 minutes at 10,000 rpm at 4°C. Thereafter, the serum was removed and stored at -80°C until assayed. The area under the blood glucose curve was calculated, using GraphPad Prism 3.0. software (GraphPad Software, USA). The β -cell function

indices homeostasis model assessment of a: baseline insulin secretion (HOMA B) and b: insulin resistance (HOMA IR) were calculated by means of fasting blood glucose and serum insulin concentrations according to the following equations (Wallace *et al.* 2004).

$$\text{HOMA B} = (20 \times \text{FPI}) / (\text{FPG} - 3.5)$$

$$\text{HOMA IR} = (\text{FPI} \times \text{FPG}) / 22.5$$

FPI = Fasting plasma insulin (mU/L)

FPG = Fasting plasma glucose (mmol/L)

3.5.4 Serum insulin determination by Enzyme-Linked Immunosorbent Assay (ELISA)

Serum insulin levels of 30-, 85-, and 180-day-old heterozygous GLS001 and GLS006 mutants and wild-type littermates in the fasted state and 10 minutes after oral glucose application were quantified by ELISA (Ultra Sensitive Mouse Insulin ELISA Kit; Crystal Chem Inc., USA). Fasting insulin concentrations were expected to be considerably low, especially in heterozygous mutants. Therefore, the assay sensitivity was enhanced by increasing the applied sample volume up to 30 μl (depending on age, genotype and time point of blood collection during OGTT). The serum volumes, applied for serum insulin determination of the respective animal groups are listed in Table 3.11. Quantification of serum insulin levels was performed according to the manufacturer's manual, using the low range assay (0.1-6.4 ng/ml). Absorbance was determined at 450 nm (reference wavelength: 630 nm) in a plate reader (SUNRISE, Tecan, Germany) and concentrations were calculated with the associated Magellan 2 software (Tecan, Germany).

Table 3.11: Applied serum volumes for the distinct genders and genotypes and age groups.

		OGTT 30days		OGTT 85 days		OGTT 180 days	
		T ₀ (μl)	T ₁₀ (μl)	T ₀ (μl)	T ₁₀ (μl)	T ₀ (μl)	T ₁₀ (μl)
male	wild-type	20 ^a /30 ^b	10 ^a /25 ^b	30	10	30	10
	mutant	20 ^a /30 ^b	20 ^a /25 ^b	30	30	30	30
female	wild-type	20 ^a /30 ^b	10 ^a /25 ^b	30	10	30	10
	mutant	20 ^a /30 ^b	20 ^a /25 ^b	30	30	30	30

^{a, b} serum volumes applied for serum insulin determination in 30-day-old GLS001 (a) and GLS006 (b) mice, serum volumes for the remaining age groups were identical in both strains

3.5.5 Intraperitoneal insulin tolerance tests (ipITT)

Intraperitoneal insulin tolerance tests (ipITTs) were carried out with *ad libitum* fed GLS001 and GLS006 mice at the age of 30, 90, and 175 days. The test was consistently performed at 2 pm. Prior to intraperitoneal insulin application, blood samples for the determination of basal blood glucose concentrations were collected. Subsequently, each mouse was injected 0.75 I.U. insulin per kilogram body weight (Insuman[®] Rapid 40 U/ml, Aventis, Germany; appropriately diluted in 0.9% NaCl (autoclaved) to a final volume of 100-120 μ l), using a 30G x 1/2" BD Microlance 3[™] cannula (Becton Dickinson, Germany). Samples for determination of blood glucose concentrations were taken 10, 20, 30, 60, and 90 minutes after insulin application.

3.6 Necropsy and organ preparation

3.6.1 Gravimetric organ analyses

Organ weights of 210-day-old GLS001 and 210- and 550-day-old GLS006 mice were determined after exsanguination by puncture of the retroorbital plexus with a capillary tube (75 μ l capacity; Hirschmann[®] Laborgeräte, Germany) under general anaesthesia (refer to chapter 3.2.2). Mice were finally sacrificed by cervical dislocation and the skin was detached from the subcutaneous tissue. After determination of the nose-rump length, the body cavities were opened and abdominal and thoracic organs (lung, heart, thymus, liver, spleen, stomach, intestine, kidneys, adrenal glands, testes, epididymes, or ovaries) were removed and separated from the adjacent tissues. The gastrointestinal tract was weighed with and without ingesta. Organs were blotted dry on cellulose paper and weighed (Mettler AE200 Electronic Analytical Balance; Mettler-Toledo Intl. Inc., Germany). Abdominal adipose tissue weight included mesentery (without lymph node) and fat tissue from the abdominal and pelvic cave. Further, the weight of the carcass (including extremities and tail of the skinned animals) was determined. Organs, fat, and the animal carcass were fixed in 4% neutral buffered formaldehyde solution (SAV LP, Germany) at room temperature.

3.6.2 Liver preparation

Liver tissue for haematoxylin and eosin (HE), periodic acid-Schiff (PAS), and fat red staining was obtained from 4-day-old GLS001 mice. Animals were sacrificed by

decapitation under general anaesthesia (refer to chapter 3.2.2). Whole livers were divided into 2 equal tissue parts. One half was fixed in 96% ethanol, the other half was fixed overnight in 4% neutral buffered formaldehyde solution. Ethanol fixed tissue samples were cut to appropriate size, placed into plastic biopsy capsules, and processed in an Autotechnicon (Histomaster 2050/DI; Bavimed, Germany) by omitting the H₂O rinsing step to avoid glycogen elution. Tissue samples were embedded in paraffin (SAV-LP, Germany) and approximately 4 µm thick sections were cut, using a HM 315 microtome (Microm GmbH, Germany). Sections were mounted on glass slides (Engelbrecht, Germany) and dried in a heating cabinet (37°C). For fat red staining, frozen sections of formalin fixed liver tissue were cut on a freezing microtome (Frigomobil, Leitz, Germany).

3.6.3 Pancreas preparation

Pancreata were obtained from neonatal and 210-day-old GLS001 mice and from 550-day-old GLS006 mice for qualitative histological, immunohistochemical, and quantitative stereological analyses. The pancreas was separated from the adjacent tissue and weighed (Mettler AE200 Electronic Analytical Balance; Mettler-Toledo Intl. Inc., Germany). Thereafter, the pancreas was placed evenly on a biopsy pad (Bio-optica, Italy) in a plastic tissue capsule (Engelbrecht, Germany) and covered with an additional biopsy pad to avoid distortion. Formalin fixation of the pancreas was carried out by overnight incubation at room temperature.

The fixed pancreas was embedded in agar (Bacto™ Agar, Becton&Dickinson, USA) and routinely processed and embedded in paraffin (Histomaster 2050/DI; Bavimed, Germany).

The length of the embedded pancreas was determined before the whole pancreas was sliced perpendicular to its longitudinal axis into parallel sections of approximately 1 mm thickness. The first cut was positioned randomly within an interval of 1 mm length at the splenic end of the pancreas. The slices were placed into embedding moulds with the right cut surface facing downward, and paraffin embedding was finished. Paraffin sections for immunohistochemical analyses were prepared as described above (chapter 3.6.2), mounted on 3-aminopropyltriethoxy-silane-treated glass slides (Starfrost® microscope slides, Engelbrecht, Germany), and dried in a heating cabinet (Wagner&Munz GmbH, Germany) at 37°C for at least 12 hours.

3.7 Immunohistochemical procedures

3.7.1 Insulin immunostaining of pancreas sections

Immunohistochemistry of paraffin embedded pancreas sections was performed by indirect immunoperoxidase method. Pancreas sections were immunohistochemically stained for insulin to allow differentiation of insulin producing β -cells from non- β -cells.

Pancreas sections were dewaxed for 20 minutes in xylene (SAV, Germany), rehydrated in a descending alcohol series (2 x 100%, 2 x 96%, 1 x 70% ethanol), and rinsed in distilled water. Endogenous peroxidase was blocked by incubation in 1% hydrogen peroxide (neoLab, Germany) solution for 15 minutes. After washing in TBS (chapter 3.4.3.4) for 10 minutes, sections were pre-treated with rabbit normal serum (MP Biomedicals, USA; dilution 1:10, 30 minutes) to reduce non-specific binding. Subsequently, sections were incubated with guinea pig anti-swine insulin (DAKO[®], Germany), diluted 1:1,000 in TBS, for 1.5 hours at room temperature. Thereafter, tissue sections were rinsed for 10 minutes in TBS and incubated with a horseradish peroxidase conjugated rabbit anti-guinea pig IgG (DAKO[®], Germany; diluted 1:50 in TBS, containing 5% mouse serum) for 1 hour at room temperature. After washing (10 minutes), chromogen substrate (DAB, KEM-EN-TEC, Denmark) containing 0.1% H₂O₂ was added to visualise immunoreactivity. Slides were rinsed in tap water for 5 minutes, counterstained with Mayer's Haemalaun (Applichem, Germany), and washed under running tap water (5 minutes). Subsequently, the sections were dehydrated in an ascending alcohol series, cleared in xylene (SAV, Germany), and mounted under glass coverslips, using Roti[®] Histokitt II (Roth, Germany).

Hydrogen peroxide 1%

30% H ₂ O ₂ (neoLab, Germany)	6 ml
Aqua bidest.	194 ml

DAB solution

DAB pellets (KEM-EN-TEC, Denmark)	1 piece
Aqua bidest.	10 ml

Dissolved for 1 hour (protected from light), filtered, aliquoted, and stored at -20°C. Add 1 μ l 30% H₂O₂ (neoLab, Germany) per 1 ml DAB solution directly before use.

3.8 Quantitative stereological investigations of the pancreas

Quantitative stereological investigations of pancreata from neonatal and 210-day-old GLS001 and 550-day-old GLS006 mice were performed, using unbiased model-independent methods (Gundersen *et al.* 1988; Wanke *et al.* 1994) as previously described (Herbach *et al.* 2005; Herbach *et al.* 2007). As conventional tissue procession for histological analysis provokes embedding shrinkage of the organ, stereological parameters were corrected for the individual tissue shrinkage factor if possible. Due to the low weight of pancreata from neonatal mice, stereological parameters could not be corrected for individual tissue shrinkage in this age group.

3.8.1 Quantification of the pancreas volume according to Cavalieri's principle

The total volume of the embedded pancreas was evaluated stereologically according to Cavalieri's principle, applying the following equation (Gundersen *et al.* 1988):

$$V_{\text{span}} = \Sigma A_{\text{span}} \times t$$

V_{span} = Volume of the embedded (shrunken) pancreas

ΣA_{span} = Sum of all cross sectional areas of the embedded pancreas

t = Mean distance of the parallel sections (mean pancreas slice thickness)

For determination of ΣA_{pan} , the complete cut surface of H&E-stained pancreas sections was photographed (Leica DFC 320 Digital Camera System, Leica, Germany) at a final magnification of 16x (adult mice) or 25x (neonatal mice), using a M400 photomicroscope (Wild, Switzerland) or a Leitz Orthoplan microscope (Leitz Wetzlar, Germany), respectively. For calibration, an object micrometer (Zeiss-Kontron, Germany) was photographed at the same magnifications. All photographs were printed under equal conditions.

Point counting was performed with a 10 mm point counting grid photocopied onto an overhead transparency. Weibel (1979) defines a test point as the true point of intersection between the upper edge of the horizontal line of a cross, and the right-hand side edge of the vertical line of the cross (Weibel 1979). The sum of points (ΣP) hitting pancreatic tissue (endocrine and exocrine pancreas, including connective tissue of the pancreas; ΣP_{pan}), and the sum of points hitting the whole section ($\Sigma P_{\text{section}}$, including extrapancreatic tissue) were determined separately (Fig. 3.6).

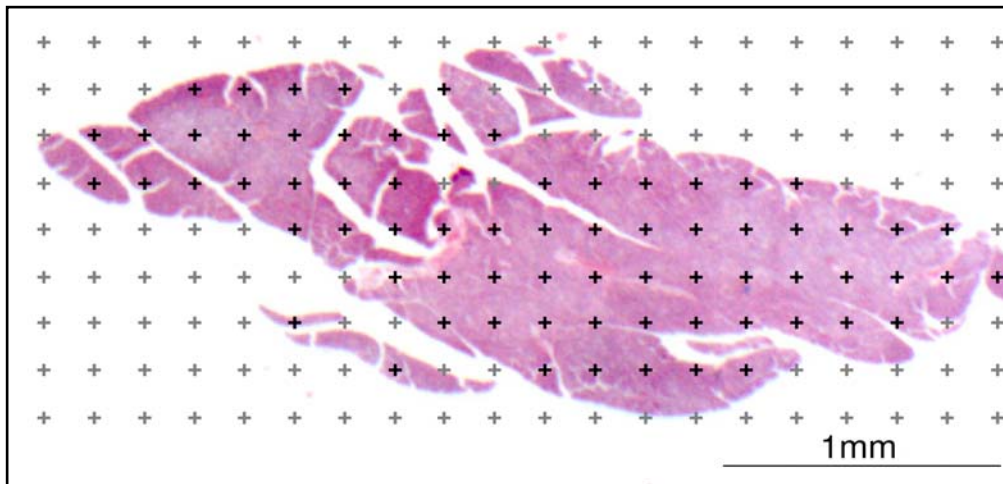


Figure 3.6: Illustration of the point counting method for determination of the sum of cross sectional areas of the pancreas (ΣA_{pan}). HE stained pancreas section, overlaid with a point counting grid (counted points are illustrated in black, $n=71$).

To calculate the volume fraction of pancreatic tissue in the section ($V_{V(\text{pan}/\text{section})}$), ΣP_{pan} was divided by $\Sigma P_{\text{section}}$. The pancreas weight was corrected for non-pancreatic tissue by multiplying the pancreas weight and $V_{V(\text{pan}/\text{section})}$.

The area corresponding to one point was determined by 30 iterate measurements, each at different positions of the point counting grid, using the Videoplan[®] image analysis system (Zeiss-Kontron, Germany) after calibration with the printed object micrometer. The mean area, equal to 1 point of the grid was obtained by dividing the sum of measured areas by the total number of measurements. The sum of cross-sectional areas of the pancreas (ΣA_{pan}) was obtained by multiplying ΣP_{pan} with the calculated mean area, equal to 1 point on the point-counting grid. The pancreas volume before embedding (V_{pan}) was calculated by dividing the pancreas weight, corrected for extrapancreatic tissue, by the specific weight of mouse pancreas (1.08 mg/mm³; (Wanke *et al.* 1994)).

3.8.1.1 Determination of the individual tissue shrinkage

The individual shrinkage factor (f_s) was calculated according to the following equation (Kluge 1994):

$$f_s = V_{\text{span}} / V_{\text{pan}}$$

f_s = Linear correction factor for embedding shrinkage

V_{span} = Volume of the embedded pancreas

V_{pan} = Pancreas volume before embedding

The respective parameters of all animals were corrected with the individual correction factor f_s .

3.8.2 Specific morphometric parameters in mice of different age groups

Morphometric evaluation of pancreas sections, immunohistochemically stained for insulin, was carried out on a Videoplan® image analysis system (Zeiss-Kontron, Germany) coupled to a light microscope (Orthoplan; Leitz, Germany) via a colour video camera (CCTV WVCD132E; Matsushita, Japan). Images of paraffin embedded pancreas sections were displayed on a colour monitor at a final magnification of x250. The sum of cross-sectional areas of islets, β -cells, and isolated β -cells ($\sum A_{\text{islets}}$, $\sum A_{\beta\text{-cells}}$, $\sum A_{\text{isol. } \beta\text{-cells}}$, respectively) was measured planimetrically by circling their outlines with a cursor on the digitising tablet of the image analysis system after calibration with an object micrometer (Zeiss, Germany). In adult mice, a subsampling was performed by systematically meandering through the section. The lateral lines of a frame displayed on the monitor were used as “allowed and forbidden lines” according to the unbiased counting rule (Gundersen 1977; Gundersen 1978). The structures in between the lines or touching the “allowed line” were measured. In neonatal mice, no subsampling was performed.

Volume fractions of the structures of interest (islets, β -cells, isolated β -cells) in the reference compartments (pancreas, islets) were calculated according to the principle of Delesse (Delesse 1847; Weibel 1979):

$$A_A = V_V$$

A_A = Estimated area fraction of a target structure in a reference compartment

V_V = Estimated volume fraction of a target structure in a reference compartment

3.8.2.1 Neonatal mice

The volume density of β -cells in the pancreas ($V_{V(\beta\text{-cells/pan})}$) was calculated by dividing $\sum A_{\beta\text{-cells}}$ by $\sum A_{\text{pan}}$. The total β -cell volume was obtained by multiplying $V_{V(\beta\text{-cells/pan})}$ and V_{pan} .

3.8.2.2 Adult mice

The volume density of islets in the pancreas ($V_{V(\text{islets/pan})}$) was calculated by dividing $\sum A_{\text{islets}}$ by $\sum A_{\text{pan}}$. The total volume of islets in the pancreas ($V_{(\text{islets,pan})}$) was attained by multiplying $V_{V(\text{islets/pan})}$ with V_{pan} .

The volume density of β -cell in the islets ($Vv_{(\beta\text{-cells/islets})}$) was determined by dividing $\sum A_{\beta\text{-cells}}$ by $\sum A_{\text{islets}}$. The total volume of β -cell in the islets ($V_{(\beta\text{-cells,islets})}$) was calculated by multiplying $Vv_{(\beta\text{-cells/islets})}$ with $V_{(\text{islets,pan})}$.

Isolated β -cells, which are considered as an indicator for islet neogenesis, are defined as single insulin-positive (insulin⁺) cells within or budding from pancreatic ducts (Fig. 3.8. A, B), scattered β -cells (Fig. 3.8. C), and extra-islet β -cell clusters (EICs; < 4 insulin⁺ cells, Fig. 3.8. D) (Bonner-Weir 2001; Butler *et al.* 2003; Kauri *et al.* 2007). The volume density of isolated β -cells in the pancreas ($Vv_{(\text{isol. } \beta\text{-cells/pan})}$) was obtained by dividing $\sum A_{\text{isol. } \beta\text{-cells}}$ by $\sum A_{\text{pan}}$. The total volume of isolated β -cells was determined by multiplying $Vv_{(\text{isol. } \beta\text{-cells/pan})}$ and V_{pan} .

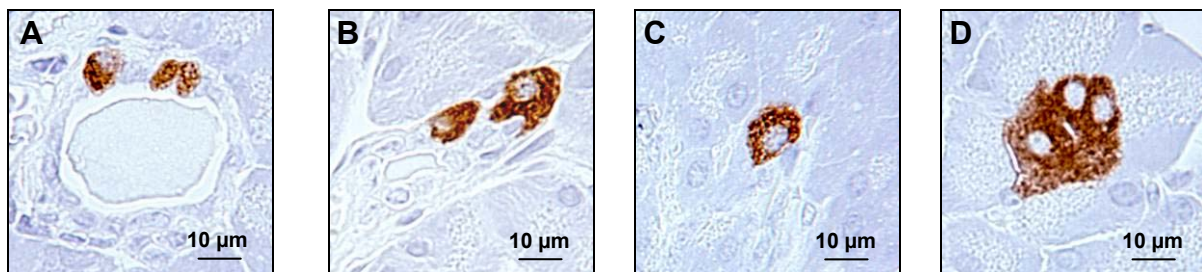


Figure 3.8: Spectrum of insulin⁺ stained pancreatic cells, classified as isolated β -cells: Insulin positive cells within (A) or budding from pancreatic ducts (B), scattered β -cells (C), and extra-islet β -cell clusters (EICs; < 4 insulin⁺ cells) (D).

3.9 Statistical analysis and data presentation

Data from all analyses displayed a normal distribution, as evinced by the Kolmogorow-Smirnov test (SPSS 16.0, SPSS GmbH Software, Germany). Therefore, means were compared by a two-tailed unpaired Student's t-test (GraphPad Prism 3.0; GraphPad Software, USA). Statistical analysis of the linkage between the diabetic phenotype of GLS001 G2 backcross mice and the examined polymorphic markers was performed by the chi²-test as described in chapter 3.2.1.3. P values <0.05 were considered significant throughout the study. Data are presented as means \pm standard deviation (SD) or standard error of the mean (SEM; calculated dividing the SD by the square root of the number of animals examined), as indicated. Data charts were generated with GraphPad Prism 3.0.

4. Results

4.1 Identification of the causative mutation

4.1.1 GLS001 mice: Munich *Gck*^{M210R} mutants

4.1.1.1 Fine mapping

In GLS001 mice, further narrowing of the chromosomal region of the causative mutation, which was already indicated by genome-wide SNP analysis, was performed by fine mapping. For this purpose, genotype analysis of 4 additional polymorphic markers, located upstream of the SNP with the highest linkage on chromosome 11 (14.3 Mb; Table 9.1) was performed. A total number of 90 GLS001 G2 backcross mice (75 phenotypic heterozygous and 15 wild-type animals) and 19 animals, resulting from mating phenotypic heterozygous G2 backcross mice, were investigated. Genotype classification for the polymorphic markers, positioned at 17.8, 12.2, 8.8, and 5.9 Mb, revealed a continuous increase of the χ^2 -values from 67.6 up to 74.1 (Table 4.1). The highest χ^2 -value, and therefore the strongest linkage to the diabetic phenotype, was observed for the polymorphic marker, located at 5.9 Mb. MGI database query for diabetes-associated candidate genes, revealed the glucokinase (*Gck*) gene, which is localised in the corresponding mapping region (5.8-5.9 Mb), as a potential candidate gene.

Table 4.1: Genotype analysis of further polymorphic DNA markers, positioned upstream of the SNP with the highest linkage.

Locus (Mb)	χ^2 -value	p-value
5.9	74.1	p<0.001
8.8	71.1	p<0.001
12.2	67.6	p<0.001
17.8	67.6	p<0.001

4.1.1.2 Candidate gene sequencing of the glucokinase (*Gck*) gene

Genomic DNA and hepatic cDNA were applied for analysis of the complete mRNA sequence of *Gck*. For this purpose, neonatal mice on the mixed C3H and C57BL/6J inbred genetic background (derived from mating phenotypic heterozygous G2

backcross mice), which were homozygous for the C3H genotype with the polymorphic marker in intron 7 of *Gck*, were analysed. Further, adult phenotypic heterozygous mutants and wild-type mice on the C3H inbred genetic background were investigated. Analyses of the sequences of the pancreas-specific exon 1 and of the *Gck* promoter of homozygous and heterozygous mutants revealed no nucleotide exchange as compared to both the mouse reference (NCBI GenBank accession no. NW_001030444) and the wild-type C3H sequence. Alignment of the hepatic *Gck* mRNA sequences of homozygous mutants with the mouse genome reference sequence (NCBI GenBank accession no. NM_010292) disclosed a defined point mutation. The identified base exchange was apparent in the bidirectional sequence analysis in all homozygous mutants examined. In contrast, wild-type controls displayed the mouse genome reference sequence (Fig. 4.1A). Evaluation of the corresponding electropherograms of heterozygous mutants, harbouring both the mutant and the wild-type sequence, a double peak was detected at the position of the mutation (Fig. 4.1B). The identified mutation represents a T→G transversion (Fig. 4.1C) at nucleotide position 629 in exon 6 of *Gck*. Translation of the mutated sequence resulted in an amino acid exchange from methionine to arginine at position 210. According to the mutation, the surrogate name GLS001 was replaced by the official term Munich *Gck*^{M210R} mutant mouse to designate this mutant strain. The probability of an additional confounding ENU-induced mutation between the last 2 polymorphic markers with the highest linkage as well as within the region upstream of the last polymorphic marker was 0.0006 and 0.0045, respectively.

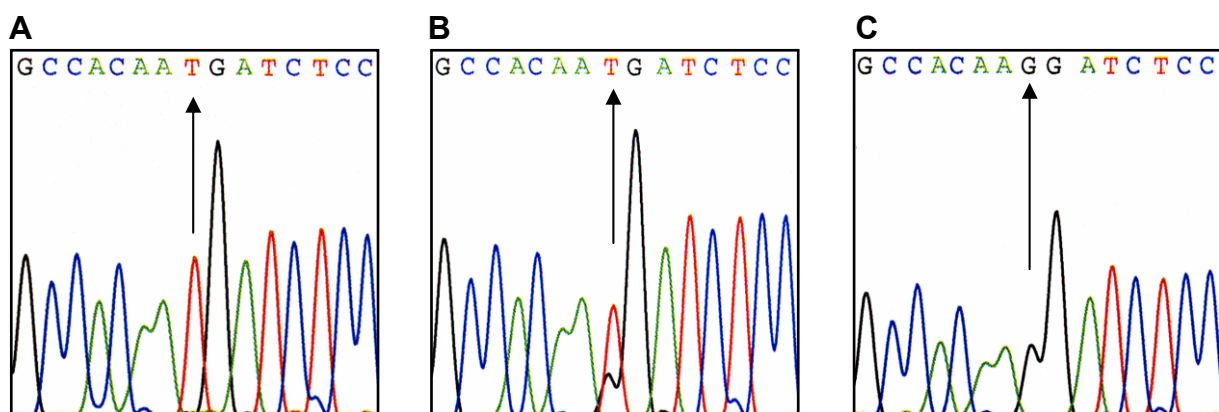


Figure 4.1: Electropherogram of the sequence analysis of *Gck* in wild-type controls (A), heterozygous (B) and homozygous Munich *Gck*^{M210R} mutants (C). The position of the base exchange at nucleotide position 629 is marked by an arrow. Wild-type mice displayed the

mouse genome reference sequence. Heterozygous mutants exhibited a double peak, whereas homozygous mutants exhibited the base exchange from T to G.

4.1.2 GLS006 mice: Munich Gck^{D217V} mutants

Since the diabetic phenotype of GLS006 mice mapped to the almost same chromosomal region as in GLS001 mice, Gck was also chosen for candidate gene analysis.

4.1.3 Candidate gene sequencing of the glucokinase (Gck) gene

Sequence analysis of Gck , accomplished with adult homozygous and heterozygous mutants and wild-type littermates on the C3H inbred genetic background was carried out as mentioned above. Sequence alignment of the complete Gck mRNA sequence disclosed an A→T transversion (Fig. 4.2) at nt 650 in exon 6 of the glucokinase gene, leading to an amino acid exchange from aspartic acid to valine at position 217. The probability of an additional confounding ENU-induced mutation between the last 2 polymorphic markers with the highest linkage as well as within the region upstream of the last polymorphic marker was 0.0019 and 0.0078, respectively. In accordance to Munich Gck^{M210R} mutants the official term Munich Gck^{D217V} mutant mouse was chosen for GLS006 mice.

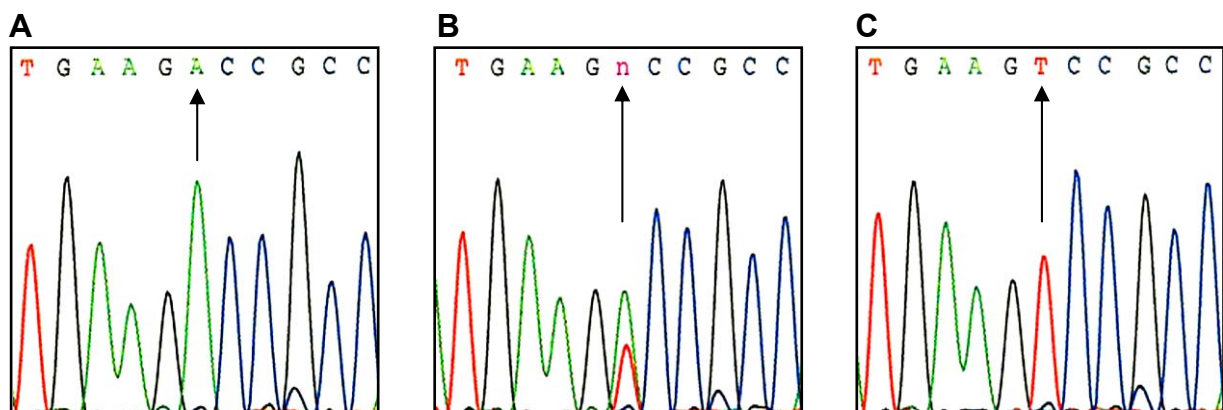


Figure 4.2: Electropherogram of the sequence analysis of Gck in wild-type controls (A), heterozygous (B) and homozygous Munich Gck^{D217V} mutants (C). The position of the base exchange at nucleotide position 650 is marked by an arrow. Wild-type mice displayed the mouse genome reference base, heterozygous mutants showed a double peak, whereas homozygous mutants exhibited the base exchange from A to T.

4.2 Allelic differentiation of mutant mice

4.2.1 Genotyping of Munich Gck^{M210R} mutants

The single base exchange from T to G in Munich Gck^{M210R} mutants created a novel restriction site for the enzyme BstYI, which displays the recognition sequence R□GATCY (R = adenine or guanine; G = guanine; A = adenine; T = thymine; C = cytosine; Y = cytosine or thymine). Thus, PCR products (343 bp) of the mutant allele were restricted into two fragments (200 and 143 bp), whereas wild-type PCR products were not restricted. Since the particular restriction fragments differ enough in size to be reliably separated even on a 1.5% electrophoresis gel, allelic differentiation of Munich Gck^{M210R} mutants was feasible by RFLP analysis (Fig. 4.3).



Figure 4.3: Genotyping of Munich Gck^{M210R} mutants by RFLP: Genotype-specific RFLP analysis resulted in a 343 bp band of the wild-type allele and in 2 fragments (200 and 143 bp) for the mutant allele. In heterozygous mutants, 3 fragments are visible. M: Fragment size marker (pUC mix 8 MBI Fermentas, Germany); marker bands represent fragment sizes of 1118, 881, 692, 501 (and 489), 404, 331, 242, 190, 147, and 111 bp (from top to bottom).

4.2.2 Genotyping of Munich Gck^{D217V} mutants

Genotyping of Munich Gck^{D217V} mutants was accomplished by selective PCR-based amplification of either the wild-type allele (in wild-type controls) or the mutant allele (in homozygous mutants), or both (in heterozygous mutants). Allelic differentiation was performed by Amplification Refractory Mutation System PCR (ARMS), which was established as single-tube allele-specific PCR (STAS PCR; chapter 3.3.2). Hybridisation of both external primers resulted in PCR-based amplification of a 343 bp fragment in both alleles. Successful amplification of this fragment therefore served as a PCR control. The allele-specific 3' nt termination and the insertion of an

additional mismatch at nt 3 upstream of the 3' end restricted primer hybridisation of both internal primers to the respective allele. Amplification of the corresponding alleles resulted in genotype-specific PCR products of 238 bp (wild-type allele) and 147 bp (mutated allele). Thus, wild-type mice and homozygous mutants were differentiated by the presence of the corresponding allele-specific DNA fragment, whereas heterozygous mutants were identified by the presence of both fragments (Fig. 4.4).



Figure 4.4: Genotyping of Munich Gck^{D217V} mutants by STAS PCR: Amplification of the control (343 bp) fragment was observed in samples from all genotypes. In heterozygous mutants, PCR products of both the mutant and the wild-type allele were apparent. In homozygous mutants and wild-type mice only one allele-specific PCR product (238 bp for the wild-type, 147 bp for the mutant allele) was detectable. M: Fragment size marker (GeneRuler™ 100 bp plus DNA Ladder; Fermentas, Germany); marker bands represent fragment sizes of 1100, 1000, 900, 800, 700, 600, 500, 400, 300, 200, and 100 bp (from top to bottom).

4.3 Functional consequences of the mutations

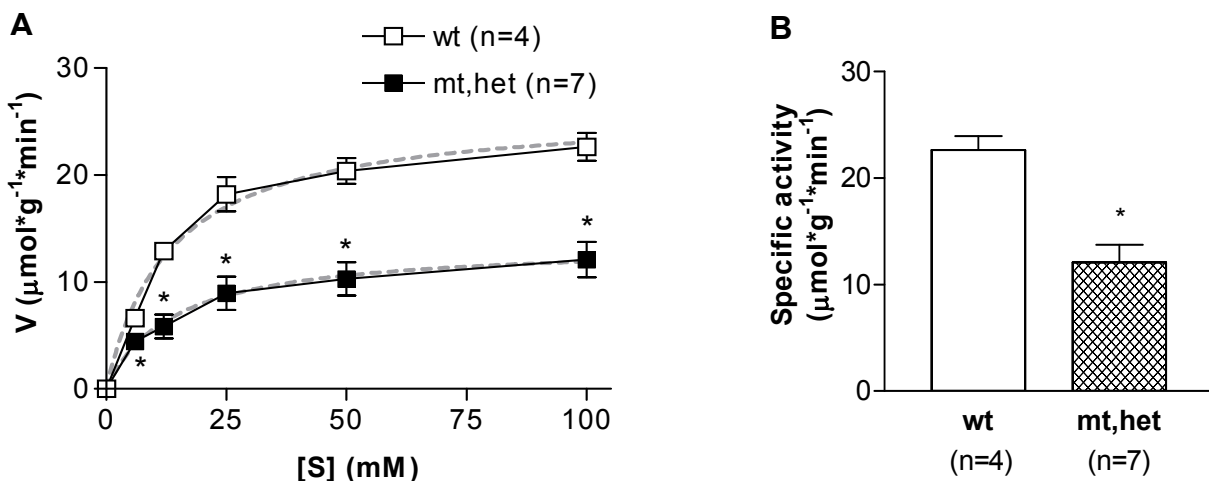
4.3.1 Quantification of glucokinase activity

Hepatic glucokinase activity was determined in 90-day-old Munich Gck^{M210R} and Gck^{D217V} mutants and wild-type littermate control mice. Plotting the distinct reaction velocities in the presence of the 5 high glucose concentrations against the respective substrate concentrations (Cornish-Bowden diagram; chapter 9.1) revealed an approximately sigmoidal appearance of the glucokinase substrate-velocity curve in mice of both strains up to a glucose concentration of about 10 mM. Nevertheless, deviance from hyperbolic Michaelis-Menten kinetics was marginal. The discrete sigmoidal glucose dependency of wild-type and mutant glucokinase of both strains

indicates a Hill coefficient slightly above 1 and therefore, a positive cooperativity with the main substrate glucose. Thus, kinetic constants of the glucokinase enzyme were determined after linear data transformation (Hanes-Woolf plot), whereby only the linear portion of the curve was employed for calculation after data extrapolation by linear regression curve fitting.

Munich Gck^{M210R} mutants

The glucokinase of heterozygous Munich Gck^{M210R} mutants exhibited a significant ($p < 0.05$) reduction of glucose turnover rate per time unit as compared to wild-type littermates at all investigated glucose concentrations (Fig. 4.5A). Substrate turnover velocity (specific glucokinase phosphorylating activity) in the presence of 100 mM glucose was decreased by about 47% in heterozygous mutants vs. wild-type controls (Fig. 4.5B). Furthermore, the maximal substrate turnover velocity (V_{max}) for glucokinase was significantly ($p < 0.05$) reduced in mutants (by about 43% vs. wild-type mice; range from 22-70%). The $S_{0.5}$ for glucokinase, reflecting glucokinase substrate affinity, was only slightly but not significantly increased in heterozygous mutants, and also the V_{max} and K_m values for the high-affinity glucose phosphorylating enzyme hexokinase did not differ significantly between mutants and wild-type littermates. On the contrary, heterozygous mutants displayed a slightly increased V_{max} for hexokinase and a by tendency decreased K_m for hexokinase (Fig. 4.5C). Taken together, murine M210R mutant glucokinase exhibited a significantly ($p < 0.05$) decreased, but only marginally right-shifted substrate-velocity curve, indicating the marked reduction of glucokinase activity in these animals as compared to wild-type mice.



	Hexokinase				Glucokinase			
	V_{max}		K_m		V_{max}		$S_{0.5}$	
	absolute	% of wt	absolute	% of wt	absolute	% of wt	absolute	% of wt
wt (n=4)	1.7 (± 0.5)		0.3 (± 0.2)		25.0 (± 1.4)		10.88 (± 1.4)	
mt, het (n=7)	2.1 (± 0.3)	122.0 (± 17.5)	0.1 ^a	34.5 (± 7.8)	14.3* (± 1.6)	57.0* (± 6.5)	13.5 (± 0.7)	123.9 (± 6.2)

Figure 4.5: Kinetic characteristics of hepatic glucokinase of 90-day-old heterozygous Munich Gck^{M210R} mutants and wild-type littermates. Illustration of the marginal differences between the original glucokinase substrate-velocity curve of wild-type mice and heterozygous mutants (without extrapolation by non-linear regression curve fitting, black line) and the hyperbolic curve (dotted grey line), resulting from non-linear regression data fitting. For all examined glucose concentrations, the substrate turnover rate by glucokinase (A) and the specific activity of glucokinase in the presence of 100mM glucose (B) was significantly decreased in heterozygous (het) mutants (mt) vs. wild-type mice (wt). The absolute ($\mu\text{mol}\cdot\text{g}^{-1}\cdot\text{min}^{-1}$) and relative (% of wild-type V_{max}) V_{max} for glucokinase was significantly decreased in mutant mice, whereas the $S_{0.5}$ for glucokinase and V_{max} and K_m for hexokinase were not significantly altered. Data represent means \pm SEM; n=number of animals examined per group; * $p<0.05$ mt, het vs. wt. ^a (± 0.01).

Munich Gck^{D217V} mutants

Quantification of glucokinase activity in liver homogenates of 90-day-old heterozygous and homozygous Munich Gck^{D217V} mutants disclosed a significant ($p<0.05$) reduction of glucose turnover velocity (specific activity in the presence of various glucose concentrations) for glucokinase in the presence of 12, 25, 50, and 100mM glucose as compared to age-matched wild-type littermates (Fig. 4.6A). Specific glucokinase activity at 100mM glucose was diminished by about 32% in heterozygous mutants, by about 90% in homozygous mutants vs. wild-type mice, and by 84% in homozygous vs. heterozygous mutants (Fig. 4.6B). The maximal glucose phosphorylating velocity (V_{max}) and the Michaelis-Menten constant (K_m) for the high-affinity glucose phosphorylating enzyme hexokinase, did not differ between the respective genotypes, whereas V_{max} for the low-affinity glucokinase enzyme was significantly diminished in both heterozygous and homozygous mutants (by about 33% in heterozygous and by about 84% in homozygous mutants vs. wild-type mice). The $S_{0.5}$ for glucokinase was only significantly ($p<0.05$) increased in homozygous vs.

heterozygous mutants and wild-type mice, but not in heterozygous mutants as compared to wild-type mice (Fig. 4.6C).

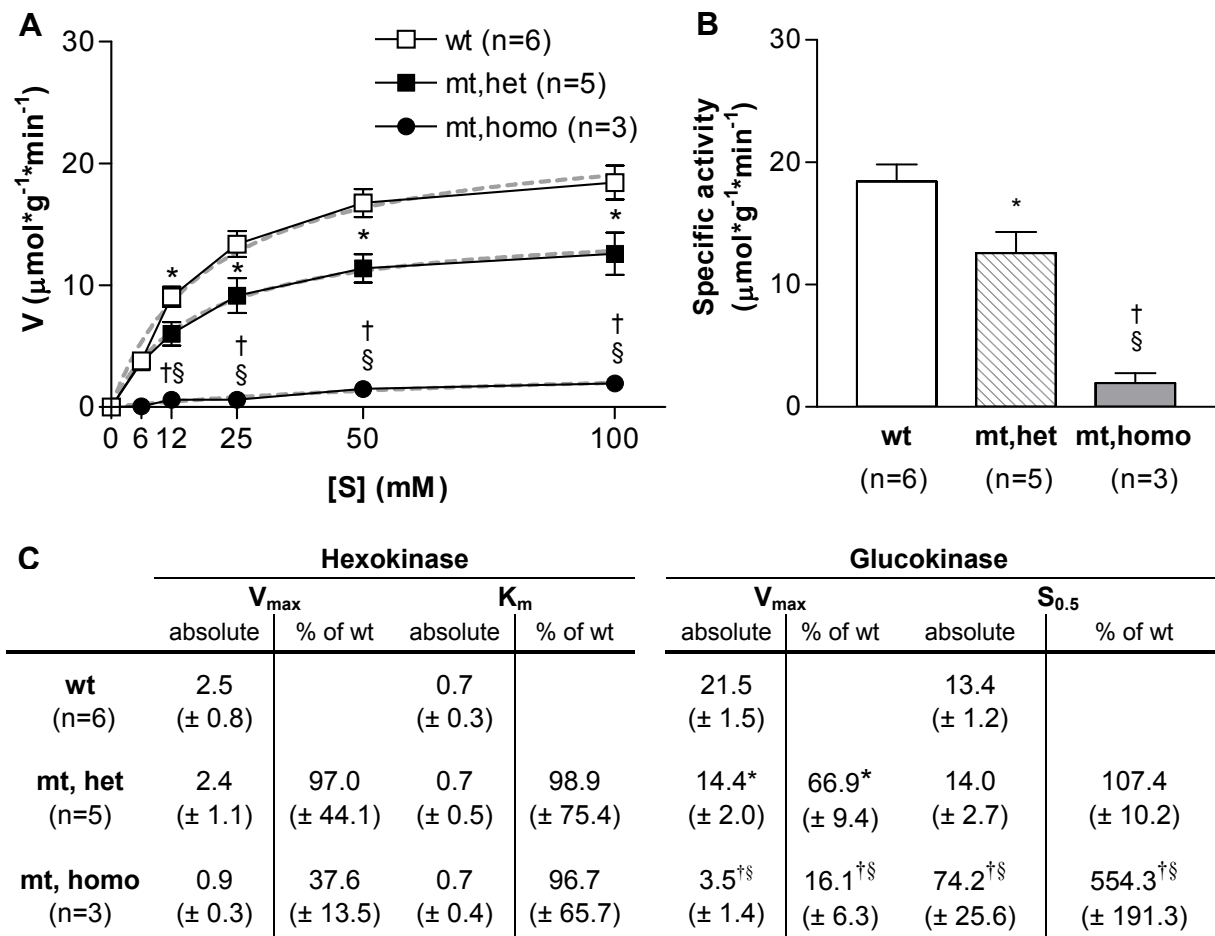
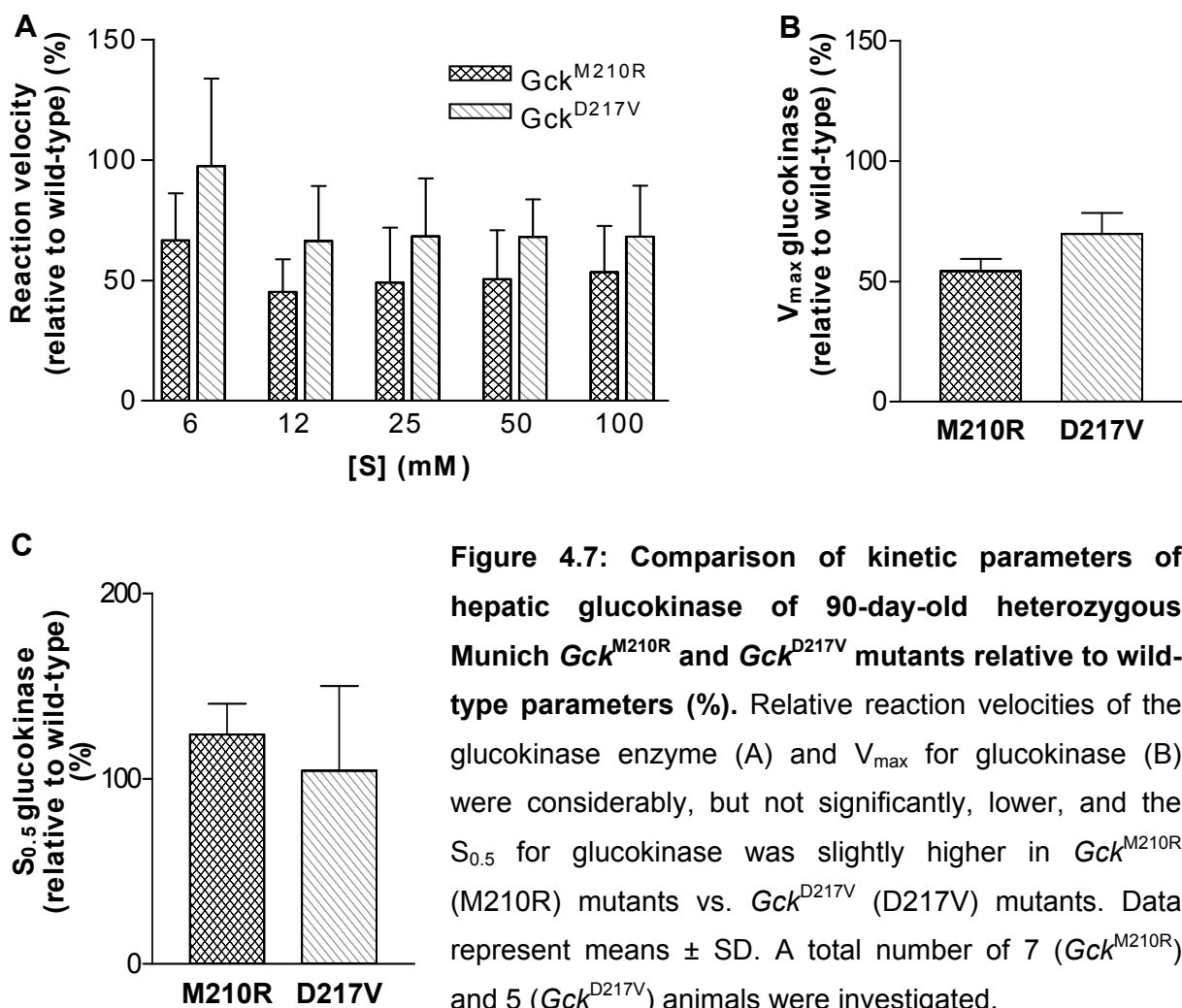


Figure 4.6: Kinetic parameters of hepatic glucokinase of 90-day-old heterozygous and homozygous Munich Gck^{D217V} mutants and wild-type mice. Substrate turnover velocity (A) was significantly decreased in heterozygous (het) and homozygous (homo) mutants (mt) vs. wild-type animals (wt) from a substrate concentration of glucose of 6 mM onwards. Note the initial insinuated sigmoidicity of the glucokinase substrate-velocity curve prior to extrapolation (black line) vs. the hyperbolic character of the fitted (dotted grey line) saturation curve. Furthermore, specific activity of glucokinase in the presence of 100 mM glucose (B) was significantly lower in mutants of both genotypes (B). The absolute ($\mu\text{mol}\cdot\text{g}^{-1}\cdot\text{min}^{-1}$) and relative (% of wild-type V_{max}) V_{max} for glucokinase was significantly diminished in heterozygous and homozygous mutant mice, whereas $S_{0.5}$ for glucokinase was only reduced in homozygous mutants (C). V_{max} and K_m values for the high-affinity hexokinases were comparable among all genotypes. Data represent means \pm SEM; n=number of animals examined per group; * p <0.05 mt, het vs. wt; [†] p <0.05 mt, homo vs. mt, het; [§] p <0.05 mt, homo vs. wt.

Comparison between glucokinase kinetic characteristics in Munich Gck^{M210R} and Gck^{D217V} mutants

The substrate turnover rate per minute, relative to wild-type mice, was marginally lower (range of 22-32%) in heterozygous Munich Gck^{M210R} mutants as compared to Gck^{D217V} mutants in the presence of all 5 glucose concentrations (Fig. 4.7A). Likewise, the maximal reaction velocity of glucokinase (V_{max}) (Fig. 4.7B) was slightly, but not significantly decreased. Further, the relative $S_{0.5}$ for glucokinase (Fig. 4.7C) was elevated by tendency in Gck^{M210R} vs. Gck^{D217V} mutants.



4.3.2 Determination of glucokinase RNA expression in Munich Gck^{M210R} mutants

The relative expression abundance of the hepatic glucokinase (Gck) transcripts of homozygous and heterozygous Munich Gck^{M210R} mutants and wild-type littermates was determined at the first day of life by quantitative real-time PCR. All primers

showed a comparable efficiency of 0.75 ± 0.02 . Moreover, the relative transcript abundances of the reference genes *Mrps9*, *Actb* and *18s rRNA* did not differ significantly among the genotype-specific groups (Fig. 4.8A), demonstrating their eligibility for quantification of the relative abundance of the target transcript. In the following, target gene expression levels were compared to *Actb* as reference transcript. The relative abundances of the *Gck* transcripts were quite low in liver samples of all genotypic groups. However, *Gck* transcript abundance, relative to *Actb*, was markedly decreased in homozygous mutants vs. wild-type littermates and heterozygous mutants ($p < 0.05$). Moreover, relative transcript abundance of *Gck* was significantly ($p < 0.05$) decreased in heterozygous mutants as compared to age-matched wild-type littermates (Fig. 4.8B).

A Primer combinations	2 ^{-ΔCT} values		
	wt (n=7)	mt, het (n=8)	mt, homo (n=7)
<i>18s rRNA</i> vs. <i>Mrps9</i> ($\times 10^4$)	3.86 (± 0.63)	3.62 (± 1.13)	3.78 (± 0.37)
<i>Mrps9</i> vs. <i>18s rRNA</i> ($\times 10^{-5}$)	2.67 (± 0.54)	2.98 (± 0.85)	2.67 (± 0.25)
<i>Actb</i> vs. <i>Mrps9</i> ($\times 10^2$)	2.39 (± 0.36)	2.37 (± 0.38)	2.15 (± 9.26)
<i>Mrps9</i> vs. <i>Actb</i> ($\times 10^{-3}$)	4.27 (± 0.79)	4.33 (± 0.27)	4.70 (± 0.62)
<i>Mrps9</i> vs. <i>Actb</i> ($\times 10^{-3}$)	1.62 (± 0.24)	1.52 (± 0.33)	1.77 (± 0.17)
<i>Actb</i> vs. <i>18s rRNA</i> ($\times 10^{-3}$)	6.27 (± 0.86)	6.85 (± 1.36)	5.70 (± 0.55)

B

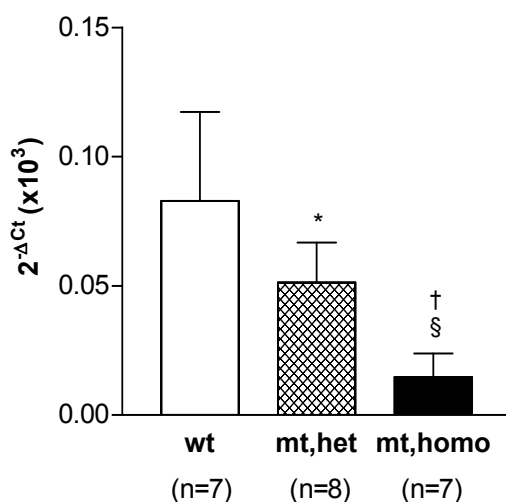


Figure 4.8: Relative transcript abundances of the applied reference genes (A) and *Gck* expression of paired liver samples from neonatal mice (B): Relative transcript abundances of *Mrps9*, *Actb* and *18s rRNA* did not significantly differ between heterozygous (het) mutants (mt), homozygous (homo) mutants, and wild-type controls (wt). (B) *Gck* expression was significantly decreased in homozygous and heterozygous mutants vs. wild-type controls. Data represent means \pm SD; n=number of animals examined; * $p < 0.05$ mt, het vs. wt; † $p < 0.05$ mt, homo vs. mt, het; § $p < 0.05$ mt, homo vs. wt.

4.3.3 Western blot analysis in Munich Gck^{M210R} mutants

4.3.3.1 Quantification of glucokinase protein levels

Glucokinase protein abundance was investigated in isolated islets of 90-day-old heterozygous mutants and sex- and age-matched wild-type littermates. The specificity of the applied antibody was considerably high, resulting in only 1 detectable band of 65 kDa, which represents the predicted molecular weight of the glucokinase protein. Staining intensity of the 65 kDa glucokinase specific band in general appeared comparable in heterozygous mutants of both genders vs. wild-type controls (Fig. 4.9A). Quantification of glucokinase protein abundance, relative to β -actin, revealed a reduction of glucokinase protein levels in heterozygous mutants by about 28% as compared to wild-type mice, but this difference was not significant (Fig 4.9B).

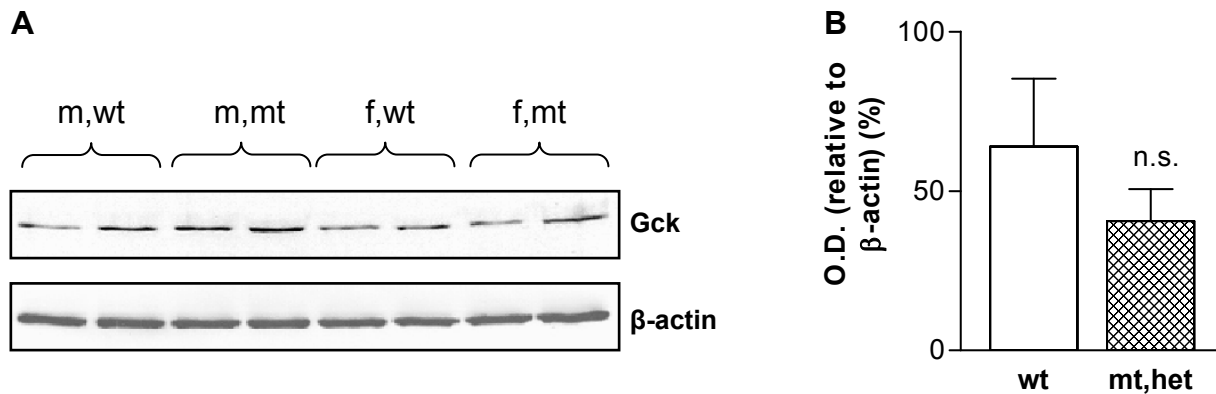


Figure 4.9: Western blot of glucokinase (A; top) in isolated pancreatic islets from 90-day-old Munich Gck^{M210R} mutants and wild-type littermates in comparison to β -actin (A; bottom) and quantification of the relative optical density (O.D.) of the specific signals (B). Staining intensity of the glucokinase-specific band in general did not differ between heterozygous (het) male (m) and female (f) mutants vs. wild-type controls (wt). Quantification of the relative abundance of the glucokinase-specific band revealed slightly, but not significantly decreased glucokinase protein levels in heterozygous mutants.

4.3.3.2 Determination of apoptosis

Intracellular cysteine proteases (caspases), especially the effector caspase-3, are major regulators of programmed cell death (apoptosis). In presence of cell death stimuli, inactive pro-caspase-3, which is usually expressed in mammalian cells, is activated by autoproteolytic procession from the inactive heterodimer into its active

heterotetrameric form, consisting of a large (~20 kDa) and a small (~10 kDa) active subunit (Porter *et al.* 1999; Thornberry *et al.* 1998). Since β -cell apoptosis is considered to represent an important aspect in pathogenesis and progression of both type 1 and type 2 diabetes mellitus (Leonardi *et al.* 2003; Thomas *et al.* 2009), apoptosis in islets of 90-day-old heterozygous Munich Gck^{M210R} mutants and wild-type littermates was investigated by Western blot analysis, using an antibody that detects both the inactive and active form of caspase-3. Lymph node homogenate was applied as positive control for the activated subunits. Pro-caspase-3 was detectable in all samples and the active large subunit of caspase-3 was also apparent in lymph node homogenate (size 17/19 kDa), whereas no band was detectable in heterozygous mutants and wild-type controls (Fig. 4.10).

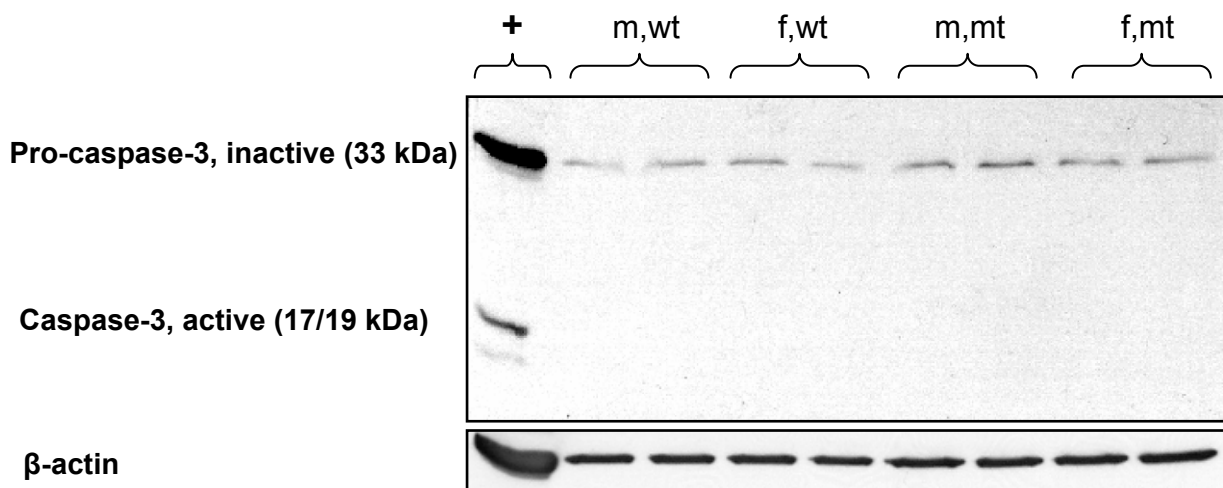


Figure 4.10: Detection of the apoptosis marker caspase-3 in lymph node homogenate (+) and pancreatic islets of 90-day-old heterozygous Munich Gck^{M210R} mutants and wild-type controls in comparison to β -actin. The 33 kDa band of pro-caspase-3 was detectable in all samples, whereas the 17/19 kDa fragment of activated caspase-3 was only apparent in lymph node homogenate but not in pancreatic islets of heterozygous male (m) and female (f) mutants (mt) and wild-type controls (wt).

4.4 Clinical findings in Munich Gck^{M210R} and Gck^{D217V} mutants

4.4.1 Basic clinical features

Body weight and blood glucose levels of homozygous and heterozygous Munich Gck^{M210R} and Gck^{D217V} mutants and wild-type littermates were first determined within the first 24 hours *post partum*. Additionally, animals were weighed at an age of 4 days and blood glucose concentrations were quantified in 1-day-old mice of both

strains and in 4-day-old Munich Gck^{M210R} mutants and wild-type littermates. Body weight and blood glucose levels of *ad libitum* fed Munich Gck^{M210R} and Gck^{D217V} mutants were determined at the day of weaning (21 days of age) and during the post-weaning period at an age of 21, 30, 90, and 175 days. Body weight and blood glucose levels after a 15 h fasting period were determined at an age of 30, 85 and 180 days.

4.4.1.1 Body weight

Munich Gck^{M210R} mutants

The birth weight of homozygous and heterozygous mutants was unaltered as compared to wild-type littermates (Fig. 4.11A). However, at an age of 3 days, homozygous mutants exhibited a markedly reduced body weight as compared to wild-type littermates (Fig. 4.11C). At this age, the body weight of homozygous mutants was almost the same as their birth weight and was by about 50% decreased vs. wild-type mice and heterozygous mutants ($p < 0.05$) (Fig. 4.11B), whereas the body weight of age-matched heterozygous mutants was unchanged. Furthermore, the fasting body weight of 30-day-old heterozygous male mutants was significantly ($p < 0.05$) reduced vs. wild-type controls. At all other time points investigated, the body weight of *ad libitum fed* and fasted heterozygous mutants of both sexes did not differ significantly from those of age- and sex-matched wild-type littermates (Table 4.2).

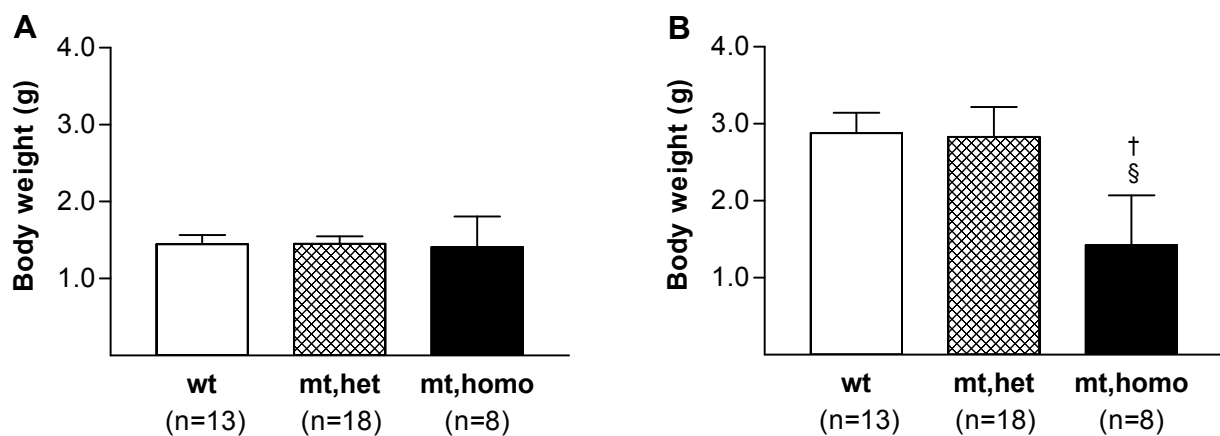


Figure 4.11: Body weight of homozygous and heterozygous neonatal (A) and 3-day-old (B) Munich Gck^{M210R} mutants vs. wild-type littermates. Birth weight was unaltered in homozygous (homo) and heterozygous (het) mutants (mt) vs. wild-type mice (wt), whereas homozygous mutants displayed a significantly reduced body weight at an age of 3 days vs. wild-type mice and heterozygous mutants (B). Data represent means \pm SD, † $p < 0.05$ mt, homo vs. mt, het; § $p < 0.05$ mt, homo vs. wt; n=number of animals examined.



Figure 4.11 C: Typical appearance of 3-day-old homozygous Munich Gck^{M210R} mutants vs. a wild-type control. Homozygous mutants displayed severe growth retardation.

Table 4.2: *Ad libitum* fed and fasting body weight of male (m) and female (f) heterozygous mutants and age- and sex-matched wild-type littermates (wt).

Group	<i>Ad libitum</i> fed body weight (g)				Fasting body weight (g)		
	Age (days)				Age (days)		
	21	30	90	175	30	85	180
m, wt	11.1 (± 2.1)	14.1 (± 1.2)	27.7 (± 2.0)	31.7 (± 2.1)	14.9 (± 1.2)	28.4 (± 1.0)	28.4 (± 2.7)
m, mt	9.6 (± 2.6)	14.3 (± 0.5)	26.9 (± 2.0)	31.2 (± 1.7)	12.5* (± 2.7)	27.0 (± 2.0)	28.6 (± 1.7)
f, wt	9.9 (± 2.7)	11.8 (± 0.6)	23.3 (± 2.0)	27.3 (± 1.6)	11.7 (± 1.8)	23.7 (± 1.0)	24.6 (± 1.8)
f, mt	8.7 (± 2.6)	11.9 (± 0.4)	21.9 (± 1.0)	25.9 (± 1.3)	10.5 (± 1.3)	22.3 (± 1.0)	23.7 (± 1.3)

Data represent means ± SD, * $p < 0.05$ m, mt vs. m, wt; a total number of 10 animals per sex and genotype were investigated except for *ad libitum* fed body weights of 21- and 30-day-old mice, which were determined from 5 animals per sex and genotype.

Munich Gck^{D217V} mutants

The body weight of neonatal and 3-day-old homozygous and heterozygous mutants did not differ from those of wild-type controls (Fig.4.12A, B). From an age of 30 days onwards, *ad libitum* fed homozygous mutants of both sexes weighed significantly ($p < 0.05$) less than wild-type mice. Additionally, the body weight of *ad libitum* fed

female homozygous mutants was significantly ($p < 0.05$) decreased vs. female heterozygous mutants from an age of 30 days onwards (Table 4.3).

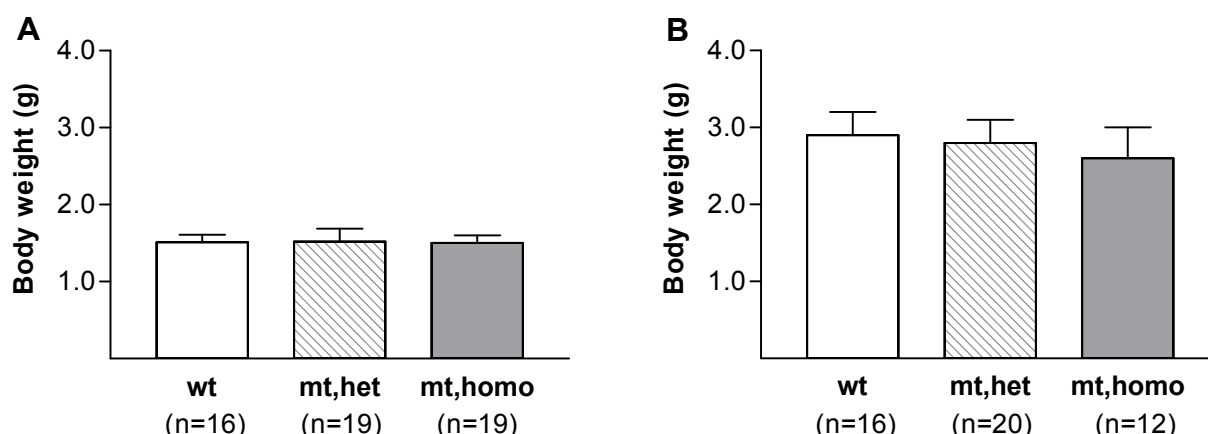


Figure 4.12: Body weight of homozygous and heterozygous Munich Gck^{D217V} mutants vs. wild-type littermates at the first day *post partum* (A) and at an age of 3 days (B). Birth weight and body weight of 3-day-old homozygous (homo) and heterozygous (het) mutants (mt) were unaltered vs. wild-type mice (wt); Data represent means \pm SD; n=number of animals examined

Table 4.3: *Ad libitum* fed and fasting body weight of male (m) and female (f) homozygous (homo) and heterozygous (het) Munich Gck^{D217V} mutants and wild-type littermates (wt).

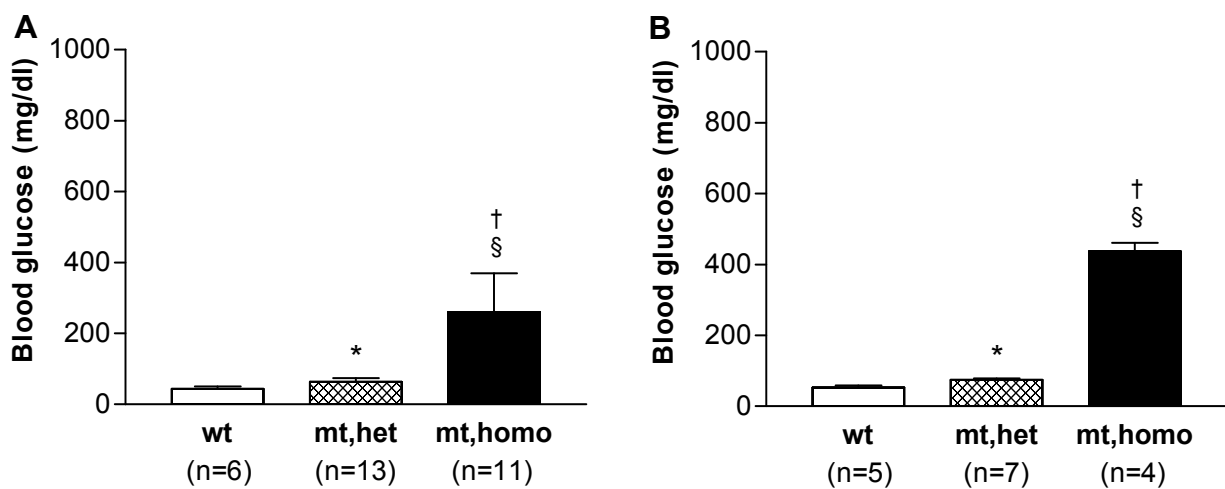
Group	<i>Ad libitum</i> fed body weight (g)				Fasting body weight (g)		
	Age (days)				Age (days)		
	21	30	90	175	30	85	180
m, wt	10.4 (± 0.5)	17.1 (± 1.7)	28.1 (± 1.7)	35.0 (± 2.7)	12.2 (± 1.5)	23.4 (± 2.3)	28.3 (± 3.2)
m, het	10.3 (± 0.9)	17.1 (± 1.7)	27.7 (± 1.9)	34.5 (± 2.9)	12.0 (± 1.4)	23.2 (± 1.1)	27.4 (± 1.6)
m, homo	10.6 (± 1.4)	14.6 [§] (± 2.4)	26.8 [§] (± 2.2)	31.7 [§] (± 1.8)	not determined		
f, wt	10.4 (± 1.3)	14.2 (± 1.1)	24.4 (± 0.9)	29.0 (± 1.2)	9.7 (± 1.3)	19.1 (± 1.4)	22.9 (± 1.3)
f, het	10.1 (± 0.5)	14.2 (± 0.8)	24.0 (± 1.3)	27.5 (± 1.4)	9.7 (± 1.1)	19.2 (± 1.6)	23.0 (± 0.7)
f, homo	8.8 (± 1.0)	12.1 ^{§†} (± 1.6)	21.3 ^{§†} (± 2.1)	26.1 ^{§†} (± 1.9)	not determined		

Data represent means \pm SD; [†] $p < 0.05$ homo vs. het; [§] $p < 0.05$ homo vs. wt; a total number of 7 animals per sex and genotype were investigated.

4.4.1.2 Blood glucose levels

Munich Gck^{M210R} mutant mouse

Determination of blood glucose levels at the first day *post partum* revealed significantly ($p < 0.05$) elevated blood glucose levels in both homozygous and heterozygous Munich Gck^{M210R} mutants as compared to wild-type controls. Blood glucose levels in neonatal homozygous mutants were 6.0- and 4.1-fold increased vs. wild-type mice and heterozygous mutants ($p < 0.05$), respectively (Fig 4.13A). Until an age of 1 day (second day *post partum*), blood glucose levels of homozygous mutants raised to 438 ± 24 mg/dl, representing a 1.7-fold increase as compared to the blood glucose levels at first day of life. Four of 5 homozygous mutants displayed glucosuria at the first day *post partum*. From the second day of life onwards, all investigated homozygous mutants displayed marked glucosuria. Blood glucose levels of heterozygous mutants and wild-type littermates remained considerably stable during the period of the first and the second day *post partum* (Fig. 4.13B). At an age of 4 days, blood glucose levels of homozygous mutants were 8.3-fold increased vs. wild-type littermates and were 5.8-times higher than in heterozygous mutants ($p < 0.05$) (Fig. 4.13C). Blood glucose levels of 4-day-old homozygous mutants were 4.0-fold increased as compared to the blood glucose concentrations at the first day *post partum*, whereas blood glucose values of heterozygous mutants remained 1.4-fold increased as compared to wild-type littermates during this period.



C

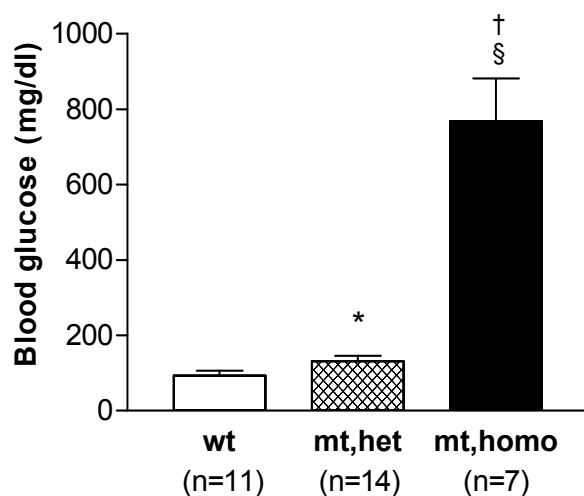


Figure 4.13: Blood glucose concentrations of neonatal (A), 1-day-old (B) and 4-day-old (C) homozygous and heterozygous Munich Gck^{M210R} mutants vs. wild-type littermates.

Blood glucose levels of homozygous (homo) and heterozygous (het) mutants (mt) were significantly elevated vs. wild-type (wt) mice. Blood glucose remained stable in mt, het but increased largely in mt, homo mt until 4 days of age. Data represent means \pm SD; * $p < 0.05$ mt, het vs. wt; † $p < 0.05$ mt, homo vs. mt, het; § $p < 0.05$ mt, homo vs. wt; n=number of animals examined.

Post-weaning blood glucose levels of *ad libitum* fed heterozygous mutants of both sexes were also significantly ($p < 0.05$) elevated vs. age- and sex-matched controls. As compared to wild-type mice, disturbances in glucose homeostasis remained almost stable from an age of 30 days onwards. Fasting blood glucose levels of heterozygous mutants were first found to be elevated at an age of 30 days and remained stable for the period of investigation (Table 4.4).

Table 4.4: *Ad libitum* fed and fasting blood glucose of male (m) and female (f) heterozygous Munich Gck^{M210R} mutants and wild-type littermates (wt).

Group	<i>Ad libitum</i> fed blood glucose levels (mg/dl)				Fasting blood glucose levels (mg/dl)		
	Age (days)				Age (days)		
	21	30	90	175	30	85	180
m, wt	99 (± 12)	106 (± 7)	131 (± 12)	112 (± 10)	84 (± 27)	86 (± 10)	86 (± 12)
m, mt	152* (± 35)	176* (± 21)	198* (± 14)	193* (± 16)	130* (± 24)	113* (± 15)	123* (± 16)
f, wt	95 (± 35)	106 (± 5)	125 (± 20)	107 (± 8)	79 (± 7)	78 (± 9)	86 (± 11)
f, mt	150* (± 36)	182* (± 22)	184* (± 32)	174* (± 11)	113* (± 13)	110* (± 11)	114* (± 1)

Data represent means \pm SD, * $p < 0.05$ mt vs. sex- and age-matched wt; a total number of 10 animals per sex and genotype were investigated except for *ad libitum* fed blood glucose of 21- and 30-day-old mice which was determined in 5 animals per sex and genotype.

Munich Gck^{D217V} mutants

Homozygous and heterozygous Munich Gck^{D217V} mutants displayed significantly ($p < 0.05$) elevated blood glucose levels already from birth. Blood glucose levels of neonatal homozygous mutants were 2.0- and 1.6-fold increased vs. wild-type littermates and heterozygous mutants, respectively. Blood glucose levels of neonatal heterozygous mutants were increased about 1.3-fold as compared to wild-type littermates (Fig. 4.14A). At an age of 1 day, blood glucose levels of homozygous mutants have raised to 125 ± 33 mg/dl (2.2-fold increase vs. wild-type), whereas the blood glucose concentrations of heterozygous mutants and wild-type mice increased slightly and to the same extent (Fig. 4.14B). At an age of 4 days, all homozygous mutants investigated displayed marked glucosuria.

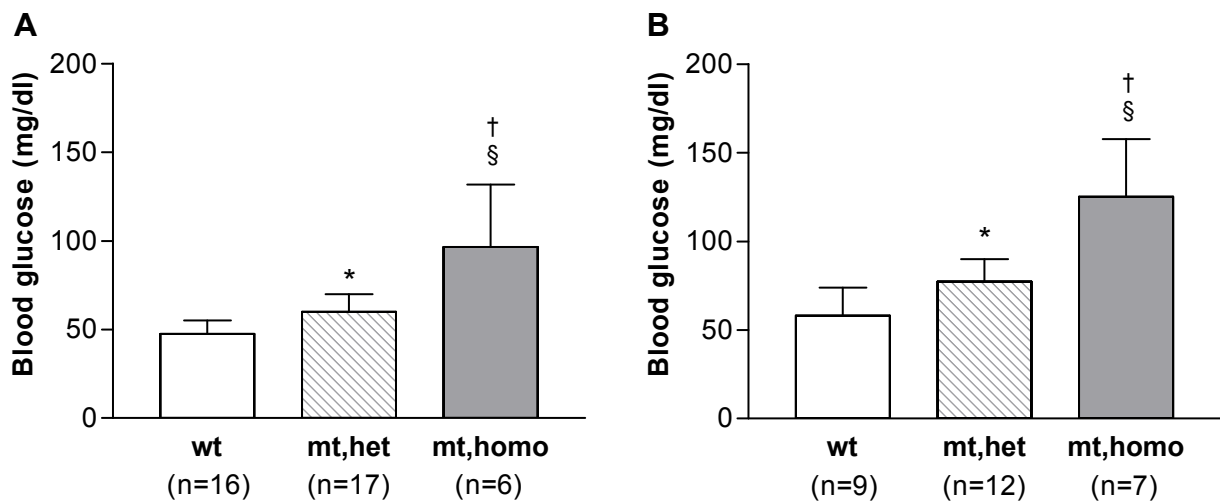


Figure 4.14: Blood glucose concentrations of neonatal (A) and 1-day-old (B) homozygous and heterozygous Munich Gck^{D217V} mutants vs. wild-type littermates.

Blood glucose levels of homozygous and heterozygous mutants were significantly elevated during the period of investigation, remaining stable in heterozygous mutants and deteriorating little in homozygous mutants. Data represent means \pm SD; * $p < 0.05$ mt, het vs. wt; † $p < 0.05$ mt, homo vs. mt, het; § $p < 0.05$ mt, homo vs. wt; n=number of animals examined.

Blood glucose levels of *ad libitum* fed homozygous mutants raised to 382 ± 36 mg/dl in male, and to 391 ± 31 mg/dl in female mice until the time of weaning (at an age of 21 days), representing a 3.3-fold increase as compared to wild-type mice, and a 2.6-fold (in female homozygous mutants) and a 2.4-fold (in homozygous male mutants) increment as compared to age and sex- matched heterozygous mutants ($p < 0.05$). Additionally, the diabetic phenotype of homozygous mutants deteriorated little until

an age of 90 days, remaining stable thenceforth. Blood glucose levels of *ad libitum* fed heterozygous mutants of both sexes were significantly elevated during all time points investigated, but remained considerably stable until and age of 175 days. Fasting blood glucose levels of heterozygous mutants of both sexes were first found to be elevated at an age of 30 days and remained stable for the period of investigation (Table 4.5).

Table 4.5: *Ad libitum* fed and fasting blood glucose levels of male (m) and female (f) heterozygous (het) and homozygous (homo) Munich Gck^{D217V} mutants and wild-type littermates (wt).

Group	<i>Ad libitum</i> fed blood glucose levels (mg/dl)				Fasting blood glucose levels (mg/dl)		
	Age (days)				Age (days)		
	21	30	90	175	30	85	180
m, wt	116 (± 16)	131 (± 11)	127 (± 5)	133 (± 13)	79 (± 10)	91 (± 12)	101 (± 15)
m, het	161* (± 29)	176* (± 8)	184* (± 14)	174* (± 22)	101* (± 13)	128* (± 13)	138* (± 23)
m, homo	382 ^{§†} (± 36)	382 ^{§†} (± 52)	462 ^{§†} (± 43)	464 ^{§†} (± 46)	not determined		
f, wt	117 (± 11)	118 (± 9)	111 (± 3)	118 (± 11)	86 (± 15)	79 (± 8)	82 (± 8)
f, het	151* (± 22)	164* (± 24)	191* (± 37)	161* (± 9)	107* (± 17)	110* (± 10)	105* (± 9)
f, homo	391 ^{§†} (± 31)	389 ^{§†} (± 34)	458 ^{§†} (± 51)	446 ^{§†} (± 44)	not determined		

Data represent means ± SD, *p<0.05 het vs. wt; †p<0.05 homo vs. het; §p<0.05 homo vs. wt; a total number of 7 animals per sex and genotype were investigated.

4.4.2 Specific clinical findings

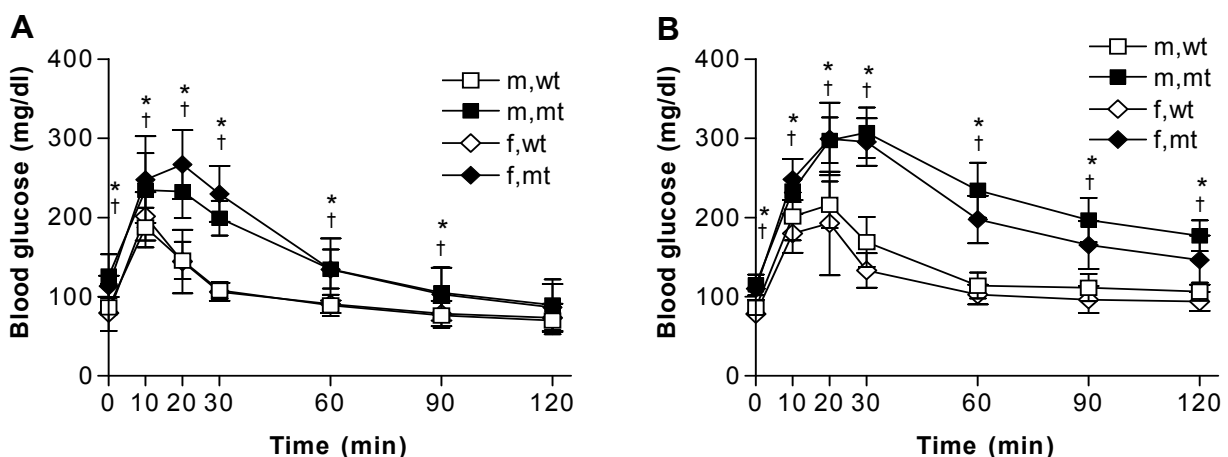
Oral glucose tolerance tests (OGTT) were accomplished in 30-, 85-, and 180-day-old heterozygous Munich Gck^{M210R} and Gck^{D217V} mutants of both sexes and wild-type littermate control mice after a 15 h fasting period. During OGTT, basal blood glucose and serum insulin levels as well as changes in blood glucose and serum insulin concentrations in response to oral glucose application were determined for subsequent calculation of β -cell function indices and the area under glucose curve. Relative changes of blood glucose concentrations after intraperitoneal insulin application (intraperitoneal insulin tolerance test; ipITT) were determined in heterozygous mutants of both strains and wild-type controls at an age of 30, 90, and

175 days, in order to assess peripheral insulin sensitivity.

4.4.2.1 Course of blood glucose levels after oral glucose application

Munich Gck^{M210R} mutant mouse

During OGTT, 30-day-old male and female heterozygous mutants showed significantly ($p < 0.05$) elevated blood glucose levels until 90 minutes after oral glucose application. At 120 minutes, blood glucose concentrations of heterozygous mutants were similar to those of wild-type mice (Fig. 4.15A). At an age of 85 and 180 days, blood glucose levels of heterozygous mutants were significantly increased at all time points during OGTT as compared to age- and sex-matched wild-type animals (Fig. 4.15B, C). Blood glucose concentrations of male heterozygous mutants reached their maximum 30 minutes after glucose application, whereas blood glucose concentrations of wild-type mice and female heterozygous mutants had already reached the maximal glucose peak at 10-20 minutes in the 2 older age groups. The area under the glucose curve (AUC) was already significantly increased in 30-day-old heterozygous mutants of both sexes, and further deteriorated with age, while the AUC of wild-type mice remained almost constant until an age of 180 days. At an age of 30 days the AUC was 1.5-fold increased in male heterozygous mutants, and was 1.6-fold higher in female mutants as compared to age- and sex-matched wild-type mice. At 180 days, the AUC was 1.9- (male) and 1.8-fold (female) increased vs. wild-type mice (Fig. 4.15D).



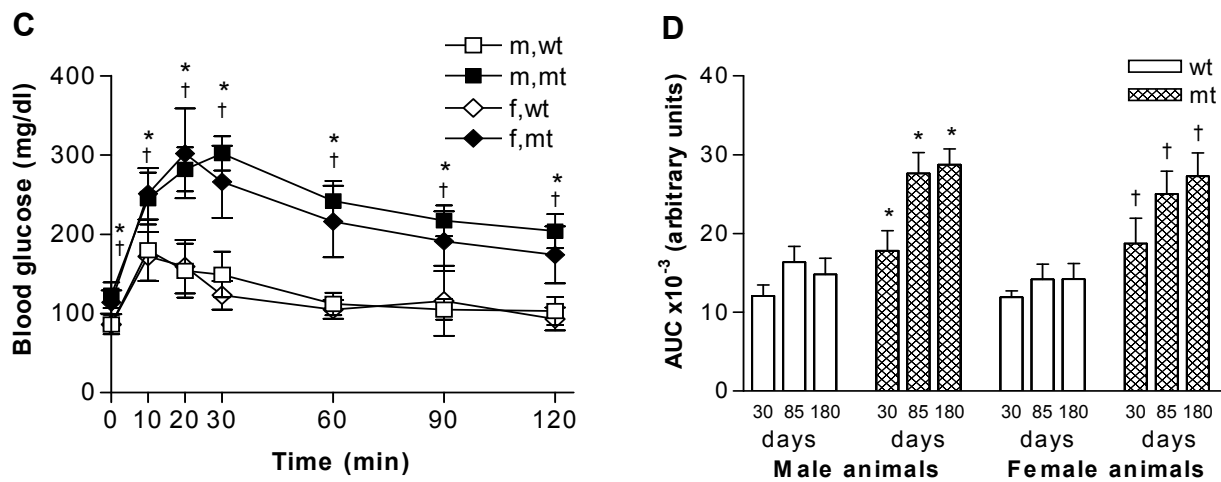


Figure 4.15: Oral glucose tolerance tests of 30- (A), 85- (B), and 180-day-old (C) Munich Gck^{M210R} mutants and wild-type control mice. (D) Area under the glucose curve (AUC) during oral glucose tolerance tests. Blood glucose levels during OGTT were significantly increased in heterozygous male (m) and female (f) mutants (mt) as compared to wild-type littermates (wt) (A-C), resulting in a significantly increased AUC (D). Data represent means \pm SD. * $p < 0.05$ m, mt vs. m, wt; † $p < 0.05$ f, mt vs. f, wt; a total number of 10 animals per sex and genotype were examined.

Munich Gck^{D217V} mutants

During the OGTT at an age of 30 days male heterozygous mutants displayed significantly elevated blood glucose levels as compared to age- and sex-matched wild-type littermates at all time points investigated, whereas blood glucose concentrations of female heterozygous mutants were only significantly increased at 30, 60, and 90 minutes after oral glucose load (Fig. 4.16A). At an age of 85 and 180 days, blood glucose levels of heterozygous mutants of both sexes were significantly elevated during all time points investigated. Additionally, 180-day-old male heterozygous mutants displayed a maximum blood glucose peak at 30 minutes and a markedly prolonged decrease of blood glucose levels after reaching the maximum, whereas blood glucose concentrations of wild-type mice and female heterozygous mutants reached the maximum levels at 10-20 minutes after glucose administration (Fig. 4.16B, C). The area under the blood glucose curve (AUC) was already increased in 30-day-old heterozygous mutants by about 1.6-fold in male, and by about 1.3-fold in female mutants vs. wild-type mice. In 85-day-old heterozygous mutants, the AUC of heterozygous mutants was increased about 1.8- (male) and 1.7-fold (female) as compared to age- and sex-matched wild-type littermates and this

increase vs. wild-type mice remained constant thereafter (Fig. 4.16D).

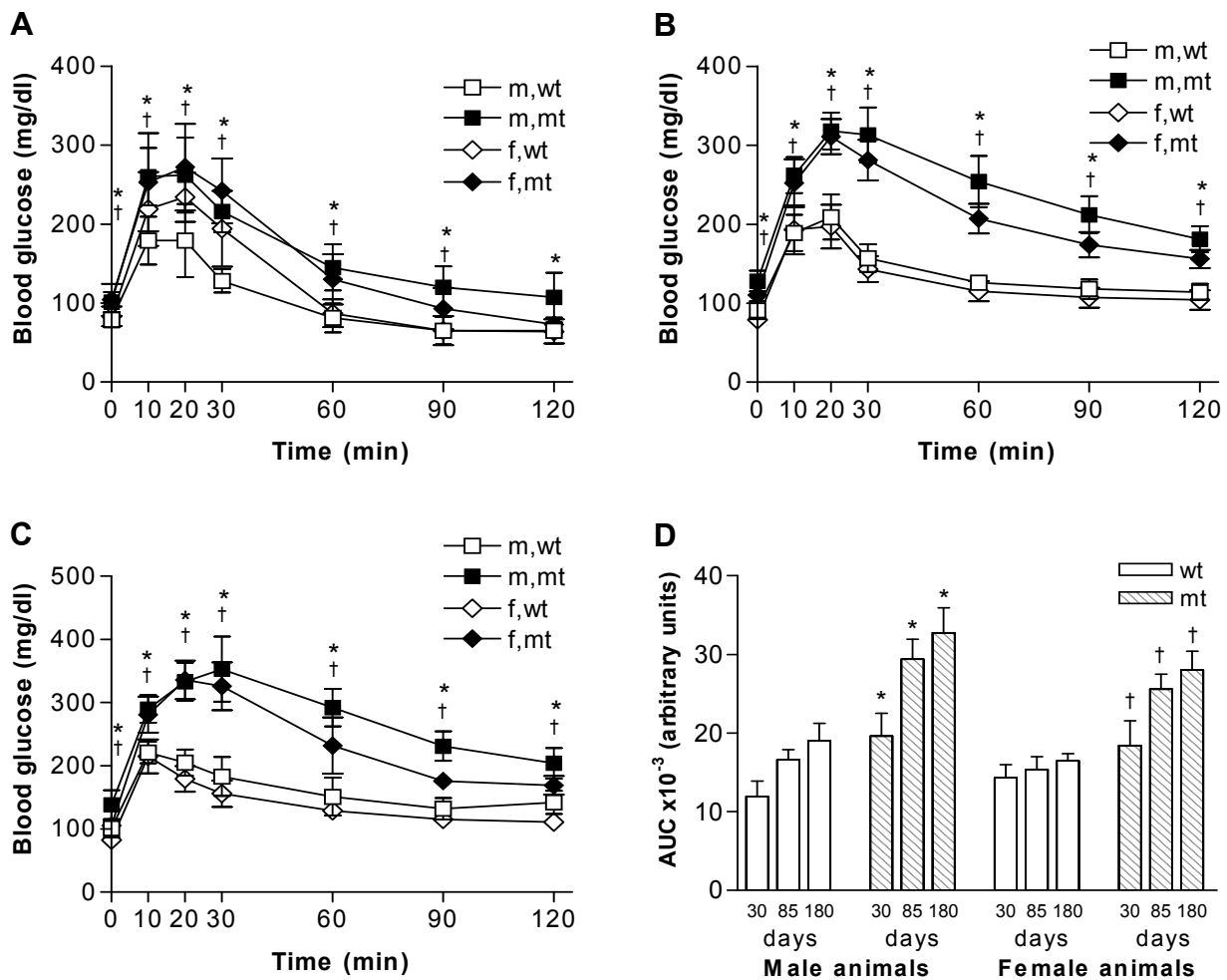


Figure 4.16: Oral glucose tolerance tests of 30- (A), 85- (B), and 180-day-old Munich Gck^{D217V} mutants and wild-type control mice (C). (D) Area under the glucose curve (AUC) during oral glucose tolerance tests. Blood glucose levels during OGTT were significantly increased in heterozygous male (m) and female (f) mutants (mt) as compared to wild-type littermates (wt) (A-C), resulting in a significantly increased AUC (D). Data represent means \pm SD; * p <0.05 m, mt vs. m, wt; † p <0.05 f, mt vs. f, wt; a total number of 7 animals per sex and genotype were examined.

4.4.2.2 Serum insulin

Munich Gck^{M210R} mutant mouse

Serum insulin quantification by ELISA revealed unchanged basal (fasting) serum insulin concentrations in 30-day-old male, and in 30-, 85-, and 180-day-old female heterozygous mutants as compared to wild-type controls. At an age of 85 days, fasting serum insulin levels of male heterozygous mutants were found to be

decreased by about 50%, at an age of 180 days by about 57% ($p < 0.05$) vs. wild-type littermates (Fig. 4.17A). Glucose-induced insulin secretion (difference of fasting insulin levels and insulin concentrations 10 minutes after glucose administration) was reduced by about 54-56% in male ($p < 0.05$), and by about 53-71% ($p < 0.05$) in female mutants vs. wild-type mice (Fig. 4.17B).

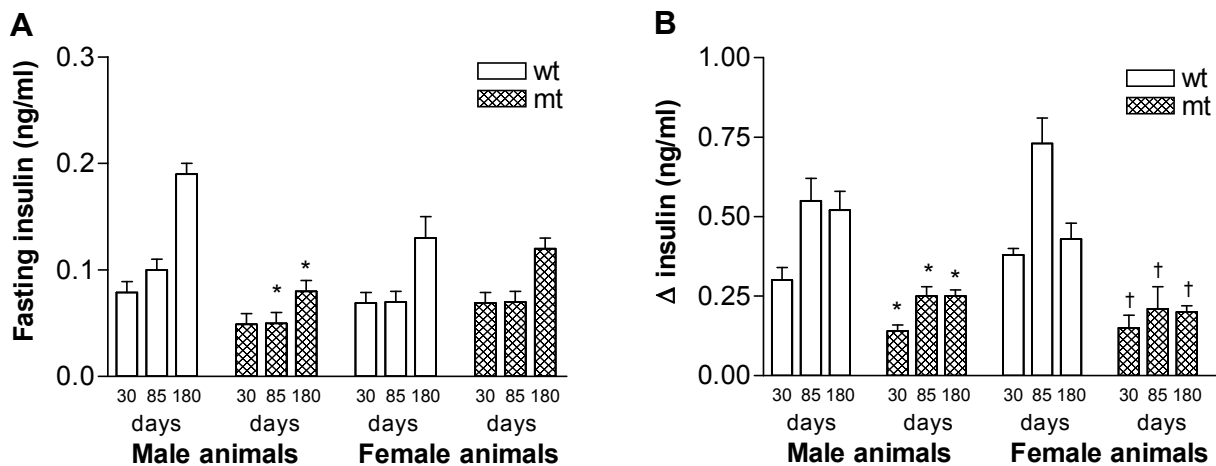


Figure 4.17: Fasting serum insulin concentrations (A) and glucose-induced insulin secretion (Δ insulin = serum insulin concentrations 10 minutes after oral glucose bolus application minus fasting insulin levels) (B) in 30-, 85-, and 180-day-old Munich Gck^{M210R} mutants and wild-type control mice. Fasting serum insulin concentrations were significantly decreased in 85- and 180-day-old male heterozygous mutants (mt) vs. wild-type mice (wt). Additionally, glucose-induced insulin secretion was significantly decreased in heterozygous mutants of both genders vs. wild-type controls. Data represent means \pm SEM; number of animals examined per group: $n=10$; * $p < 0.05$ m, mt vs. m, wt; † $p < 0.05$ f, mt vs. f, wt.

Munich Gck^{D217V} mutant mouse

Fasting serum insulin levels were decreased in heterozygous Munich Gck^{D217V} mutants of both sexes as compared to wild-type littermates, but reached a significant level only in 30- and 180-day-old male, and in 30-day-old female mutants ($p < 0.05$) (Fig. 4.18A). At an age of 30 days, glucose-induced insulin secretion in heterozygous mutants was unaltered (104% of the wild-type delta insulin levels in male, and 93% in female mutants). However, from an age of 85 days onwards, heterozygous mutants of both genders displayed significantly ($p < 0.05$) reduced insulin secretion after oral glucose administration. At an age of 85 days, delta insulin levels were decreased by about 46% in male, and by about 56% in female mutants, whereas in 180-day-old

mutants, this parameter was decreased by about 56% in male, and by about 80% in female mutants as compared to age- and sex-matched wild-type controls (Fig. 4.18B).

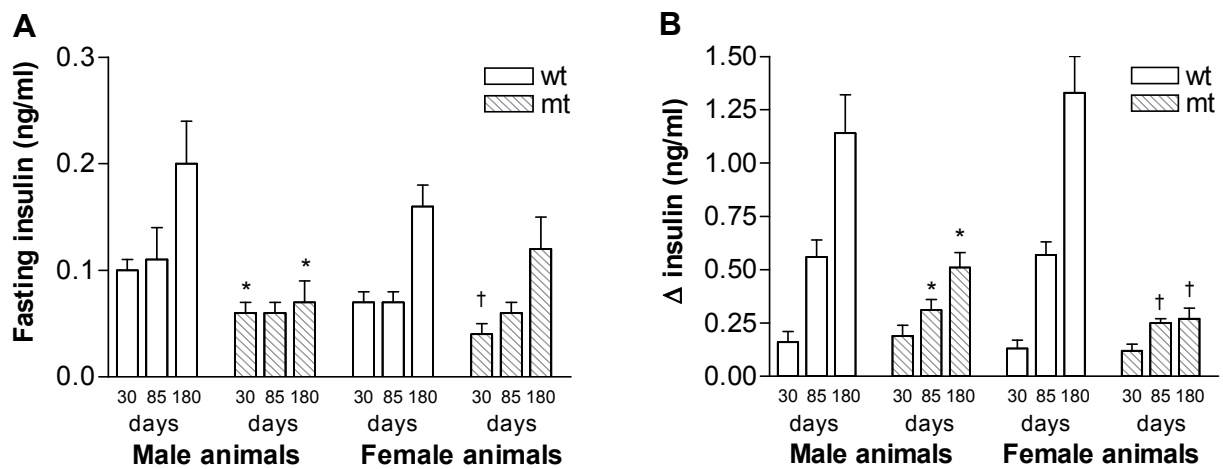


Figure 4.18: Fasting serum insulin concentrations (A) and glucose-induced insulin secretion (delta insulin = serum insulin concentrations 10 minutes after oral glucose bolus application minus fasting insulin levels) (B) in 30-, 85-, and 180-day-old Munich Gck^{D217V} mutants and wild-type control mice. Fasting serum insulin concentrations were decreased in heterozygous mutants (mt) vs. wild-type mice (wt). From an age of 85 days onwards, both genders displayed significantly reduced insulin secretion after oral glucose administration vs. wild-type controls. Data represent means \pm SEM; a total number of 7 animals per sex and genotype were examined; * $p < 0.05$ m, mt vs. m, wt; † $p < 0.05$ f, mt vs. f, wt.

4.4.2.3 Beta cell function indices

The homeostasis model assessments of baseline insulin secretion (HOMA B) and of insulin resistance (HOMA IR) were calculated by means of fasting blood glucose and serum insulin levels from heterozygous Munich Gck^{M210R} and Gck^{D217V} mutants and wild-type littermates, obtained in the course of OGTTs at an age of 30, 85, and 180 days.

Munich Gck^{M210R} mutant mouse

The HOMA B was significantly ($p < 0.05$) reduced in male heterozygous mutants of all examined age groups (range from 77-82% diminution) and in 30- and 180-day-old female heterozygous mutants (by about 74%-82%) vs. wild-type controls (Fig. 4.19A). In contrast, the HOMA IR was not significantly altered in mutants of both

genders as compared to wild-type mice (Fig. 4.19B).

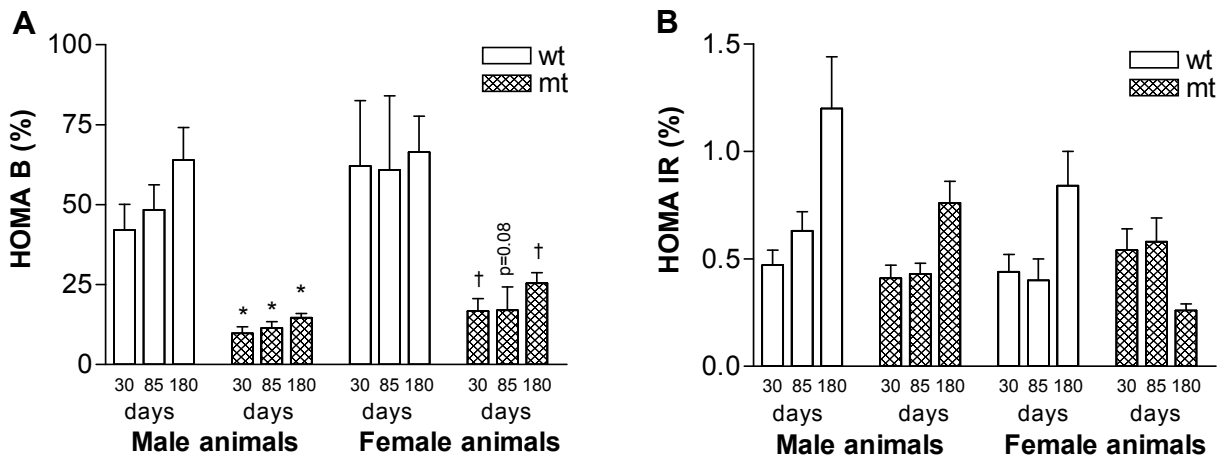


Figure 4.19: Homeostasis model assessment of baseline insulin secretion (HOMA B) (A) and insulin resistance (HOMA IR) (B) in 30-, 85-, and 180-day-old Munich Gck^{M210R} mutants and wild-type control mice. The HOMA B was decreased in heterozygous mutants (mt) of both sexes, whereas the HOMA IR was not significantly altered as compared to wild-type controls (wt). Data represent means \pm SEM. A total number of 10 animals per sex and genotype were investigated; * $p < 0.05$ m, mt vs. m, wt; † $p < 0.05$ f, mt vs. f, wt.

Munich Gck^{D217V} mutant mouse

The HOMA B of heterozygous mutants was 75-83% decreased in all examined age groups (Fig. 4.20A). The HOMA IR of heterozygous mutants of both sexes was not significantly altered vs. wild-type controls at all time points investigated. In male heterozygous mutants, the insulin resistance index even appeared slightly decreased vs. wild-type mice, at all time points investigated (Fig 4.20B).

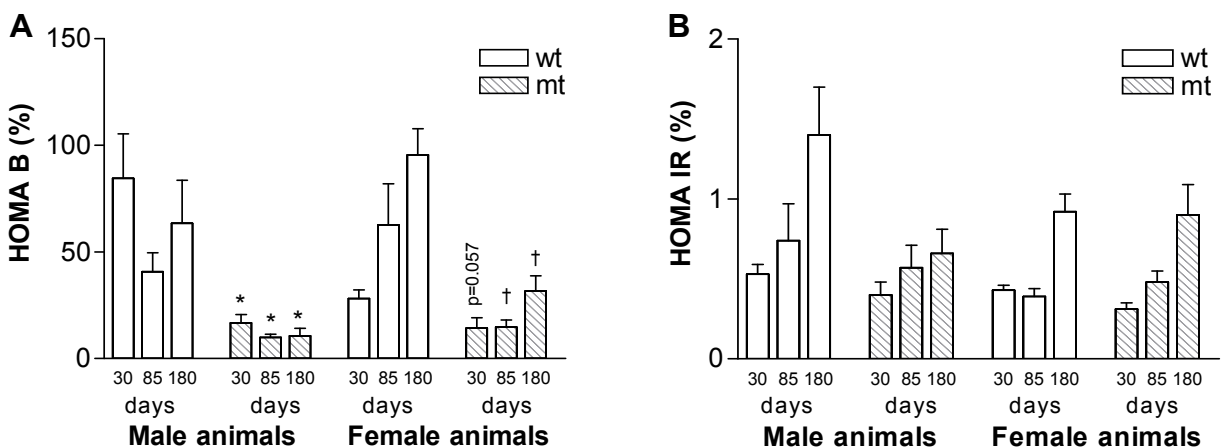


Figure 4.20: Homeostasis model assessment of baseline insulin secretion (HOMA B) (A) and insulin resistance (HOMA IR) (B) in 30-, 85-, and 180-day-old Munich Gck^{D217V} mutants and wild-type control mice.

mutants and wild-type control mice. The HOMA B was decreased in heterozygous mutants (mt) of both sexes, whereas the HOMA IR was comparable to wild-type controls (wt) or slightly decreased. Data represents mean \pm SD. A total number of 7 animals per sex and genotype were investigated; * $p < 0.05$ m, mt vs. m, wt; † $p < 0.05$ f, mt vs. f, wt.

4.4.2.4 Intraperitoneal insulin tolerance test (ipITT)

Munich Gck^{M210R} mutant mouse

At an age of 30 days, blood glucose decrease during ipITT was comparable between heterozygous mutants and wild-type mice (Fig. 4.21A), while 90- and 175-day-old male mutants showed a significantly ($p < 0.05$) less pronounced decrease of blood glucose levels from basal, 10 and 90 minutes, and 10 and 20 minutes after intraperitoneal insulin application, respectively (Fig. 4.21B, C). In contrast, relative blood glucose decrease relative from basal was unchanged in female heterozygous mutants of all investigated age groups as compared to age- and sex-matched wild-type littermates (Fig. 4.21A-C).

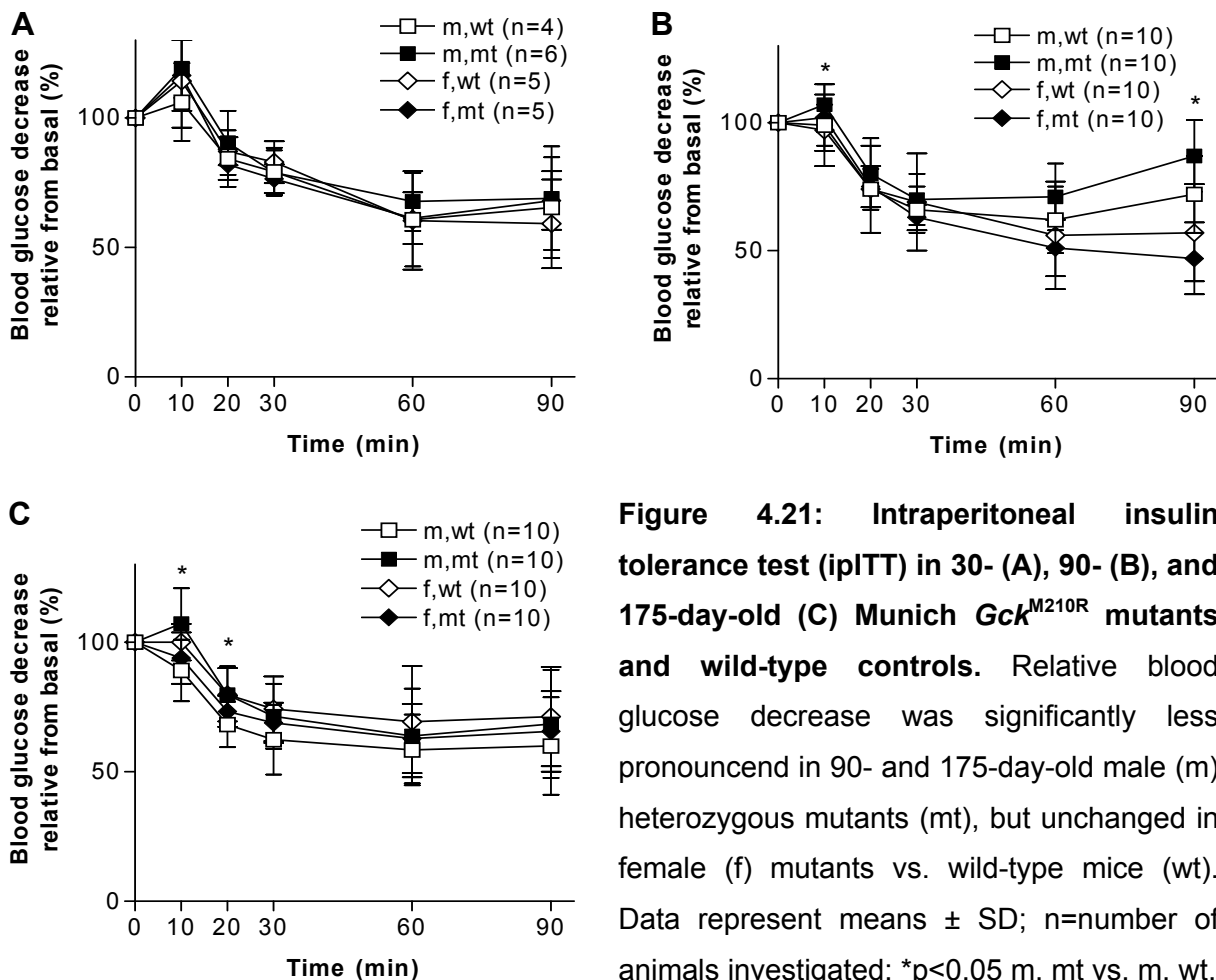


Figure 4.21: Intraperitoneal insulin tolerance test (ipITT) in 30- (A), 90- (B), and 175-day-old (C) Munich *Gck^{M210R}* mutants and wild-type controls. Relative blood glucose decrease was significantly less pronounced in 90- and 175-day-old male (m) heterozygous mutants (mt), but unchanged in female (f) mutants vs. wild-type mice (wt). Data represent means \pm SD; n=number of animals investigated; * $p < 0.05$ m, mt vs. m, wt.

Munich Gck^{D217V} mutants

In 30- and 90-day-old male heterozygous Munich Gck^{D217V} mutants, blood glucose decrease 10 minutes after intraperitoneal insulin application was less pronounced as compared to wild-type mice (Fig. 4.22A, B). At 175 days of age, course of blood glucose decrease was unchanged in heterozygous male mutants vs. wild-type mice, at all time points investigated. In contrast, age-matched female heterozygous mutants displayed a significantly less pronounced decrease of relative blood glucose levels from basal, 10 and 20 minutes after insulin challenge as compared to wild-type controls (Fig. 4.22C).

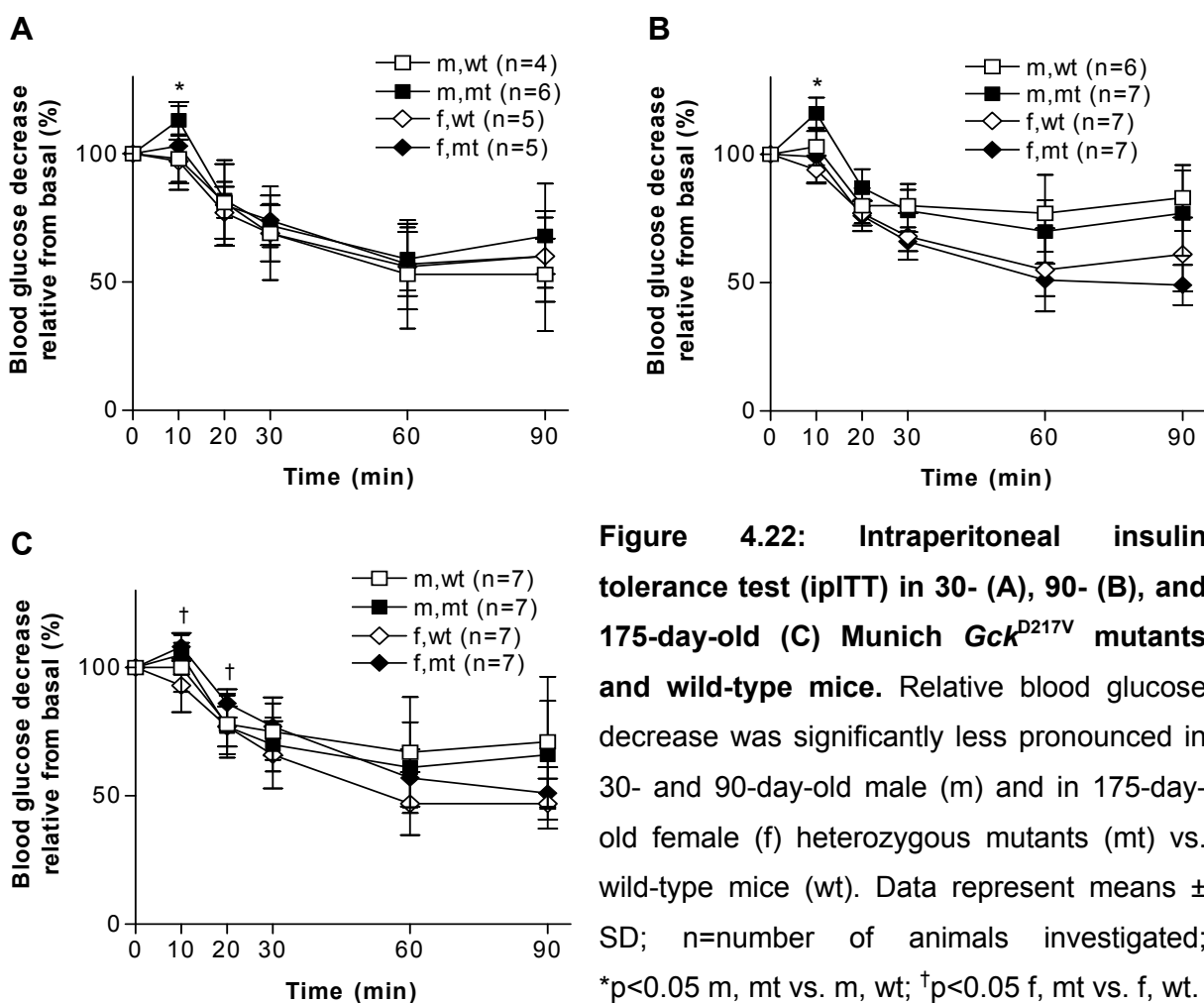


Figure 4.22: Intra-peritoneal insulin tolerance test (ipITT) in 30- (A), 90- (B), and 175-day-old (C) Munich Gck^{D217V} mutants and wild-type mice. Relative blood glucose decrease was significantly less pronounced in 30- and 90-day-old male (m) and in 175-day-old female (f) heterozygous mutants (mt) vs. wild-type mice (wt). Data represent means \pm SD; n=number of animals investigated; * $p < 0.05$ m, mt vs. m, wt; † $p < 0.05$ f, mt vs. f, wt.

4.4.3 Comparison of clinical parameters of both strains

For comparison of phenotypic features of Munich Gck^{M210R} and Gck^{D217V} mutants, clinical parameters were expressed relative to the respective sex-, and age-matched wild-type littermates.

4.4.3.1 Body weight of neonatal and 3-day-old mutants

Relative birth weight of heterozygous and homozygous Munich Gck^{M210R} and Gck^{D217V} mutants did not differ (Fig.4.23A). However, at an age of 3 days, the relative body weight of homozygous Gck^{M210R} mutants was about 46% ($p<0.05$) lower vs. homozygous Gck^{D217V} mutants (Fig 4.23B).

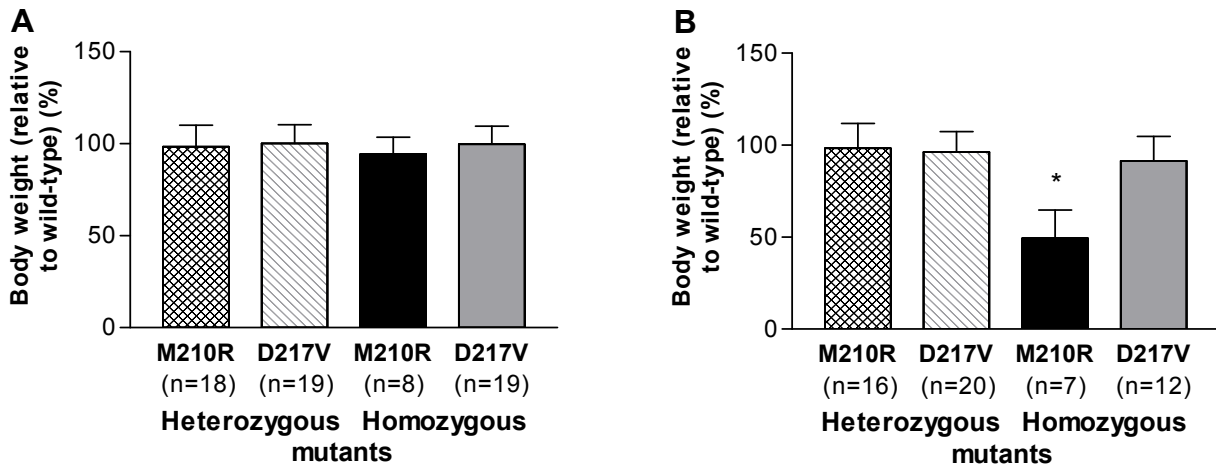


Figure 4.23: Body weight of neonatal (A) and 3-day-old (B) heterozygous and homozygous Munich Gck^{M210R} (M210R) and Gck^{D217V} (D217V) mutants, illustrated as percent of wild-type body weight. Relative birth weight of mutants (mt) of both strains was comparable, whereas 3-day-old homozygous Gck^{M210R} mutants (M210R) showed a significantly reduced relative body weight as compared to homozygous Gck^{D217V} (D217V) mutants. Data represent means \pm SD; n=number of animals investigated. * $p<0.05$ M210R mt, homozygous vs. D217V mt, homozygous

4.4.3.2 Blood glucose levels of neonatal and 1-day-old mutants

Blood glucose levels, relative to wild-type controls, of neonatal and 1-day-old heterozygous mutants did not differ between Munich Gck^{M210R} and Gck^{D217V} mutants (Fig. 4.24A, B). Relative blood glucose concentrations were about 2.9- and 3.8-fold higher in neonatal and 1-day-old homozygous Gck^{M210R} mutants vs. homozygous Gck^{D217V} mutants, respectively (Fig. 4.24A, B).

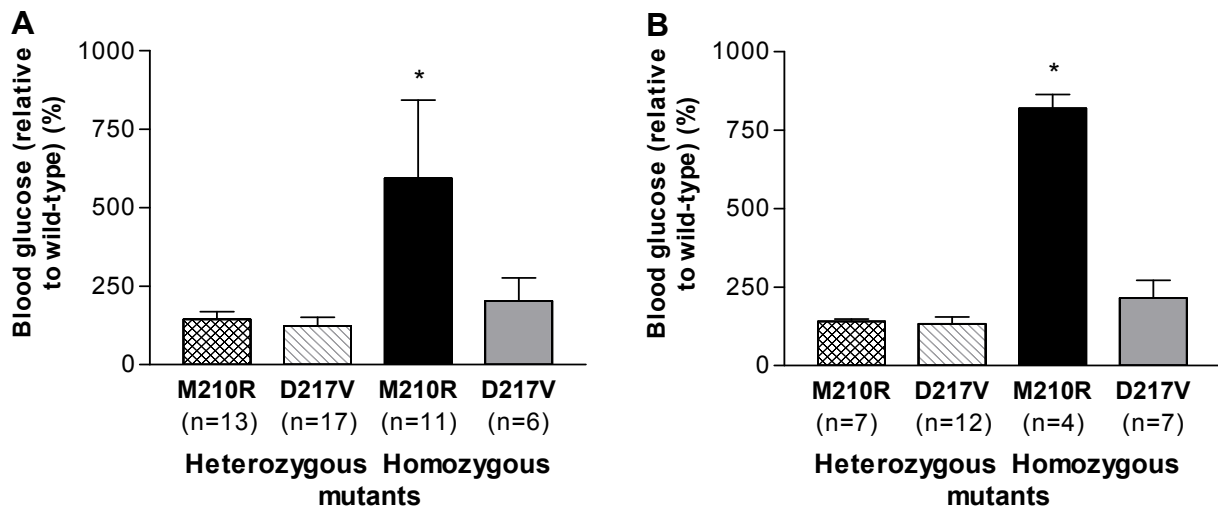


Figure 4.24: Blood glucose levels of neonatal (A) and 1-day-old (B) heterozygous and homozygous Munich *Gck*^{M210R} (M210R) and *Gck*^{D217V} (D217V) mutants, illustrated as percent of wild-type blood glucose levels. Blood glucose levels of heterozygous mutants (mt) of both strains were comparable, whereas neonatal and 1-day-old homozygous *Gck*^{M210R} mutants (M210R) exhibited significantly higher relative blood glucose concentrations than homozygous *Gck*^{D217V} (D217V) mutants. Data represent means \pm SD; n=number of animals investigated; *p<0.05 M210R mt, homozygous vs. D217V mt, homozygous.

4.4.3.3 Glucose tolerance in heterozygous mutants

The area under the glucose curve (AUC), relative to wild-type controls, did not significantly differ in 30- and 85-day-old male and female heterozygous mutants of both strains, whereas at an age of 180 days, the relative AUC was significantly higher in male *Gck*^{M210R} mutants as compared to age- and sex-matched *Gck*^{D217V} mutants (Fig. 4.25).

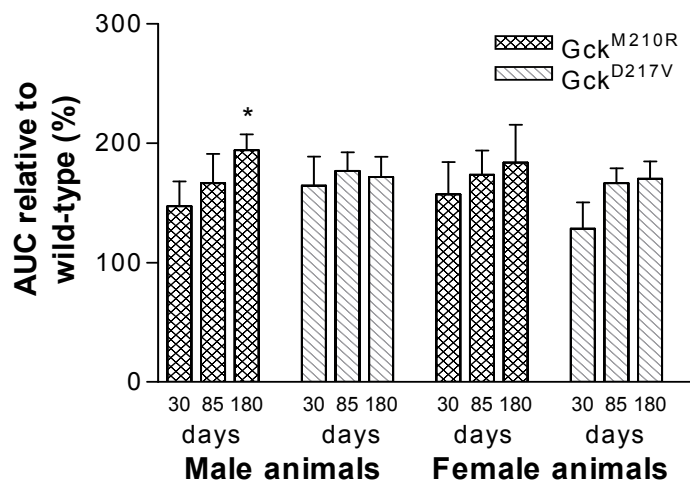


Figure 4.25: Area under the blood glucose curve (AUC) during oral glucose tolerance

tests of 30-, 85-, and 180-day-old male and female heterozygous Munich Gck^{M210R} and Gck^{D217V} mutants, presented as percentage of wild-type AUC. The relative AUC of 180-day-old male Gck^{M210R} mutants was significantly higher as compared to male Gck^{D217V} mutants. Data represent means \pm SD; number of animals investigated per sex: Gck^{M210R} mutants: 10; Gck^{D217V} mutants: 7; * $p < 0.05$ male Gck^{M210R} mutants vs. male Gck^{D217V} mutants.

4.4.3.4 Serum insulin levels in heterozygous mutants

Munich Gck^{M210R} and Gck^{D217V} mutants of both genders displayed comparable fasting serum insulin concentrations relative to wild-type controls in all examined age groups (Fig. 4.26A), whereas delta insulin secretion, relative to wild-type littermates, was significantly ($p < 0.05$) lower in 30-day-old male and in 30- and 85-day-old female Gck^{M210R} mutants vs. Gck^{D217V} mutants. However, at an age of 180-days, glucose-induced insulin secretion relative to wild-type controls was significantly lower in female Gck^{D217V} mutants as compared to age- and sex-matched Gck^{M210R} mutants (Fig. 4.26B).

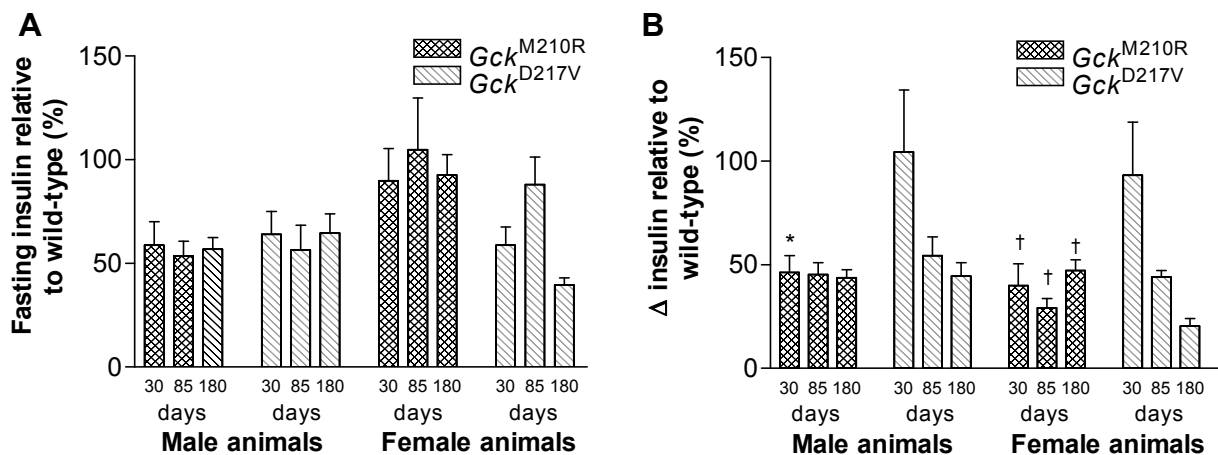


Figure 4.26: Fasting serum insulin concentrations (A) and delta insulin secretion after glucose application (B) of 30-, 85-, and 180-day-old male and female heterozygous Munich Gck^{M210R} and Gck^{D217V} mutants, relative to wild-type serum insulin concentrations (%). Relative fasting serum insulin concentrations did not differ between mutants of both strains, whereas delta insulin secretion relative to wild-type mice was significantly lower in 30-day-old male, and in 30- and 85-day-old female Gck^{M210R} mutants but higher in 180-day-old female Gck^{M210R} mutants vs. sex-matched Gck^{D217V} mutants. Data represent means \pm SEM; number of animals investigated per sex: Gck^{M210R} mutants: n=10; Gck^{D217V} mutants: n=7; * $p < 0.05$ male Gck^{M210R} mutants vs. male Gck^{D217V} mutants; $\dagger p < 0.05$ female Gck^{M210R} vs. female Gck^{D217V} mutants.

4.4.3.5 Homeostasis model assessment of baseline insulin secretion (HOMA B)

The β -cell function index, relative to wild-type mice was not significantly different comparing age- and sex-matched heterozygous mutants of both strains (Fig. 4.27)

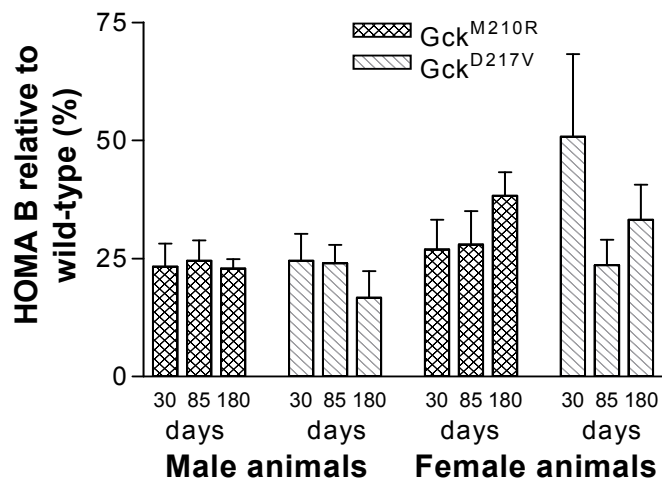


Figure 4.27: Homeostasis model assessment of baseline insulin secretion (HOMA B) of 30-, 85-, and 180-day-old male and female heterozygous Munich Gck^{M210R} and Gck^{D217V} mutants, relative to wild-type. The HOMA B index relative to wild-type mice of both strains was comparable. Data represent means \pm SEM; number of animals investigated per sex: Gck^{M210R} mutants: n=10; Gck^{D217V} mutants: n=7.

4.5 Survival studies in Munich Gck^{M210R} and Gck^{D217V} mutants

Munich Gck^{M210R} mutant mouse

The survival rates of heterozygous and homozygous Munich Gck^{M210R} mutants and wild-type littermates were determined from the first day *post partum* until an age of 365 days. Mice of all genotypes were born as expected according to the Mendelian pattern of inheritance. At the first day *post partum*, 2 of 6 male homozygous mutants died within the first 6 hours of life. During the following days, 2 male homozygous mutants deceased at 4 days of age, the other 2 male homozygous mutants died at an age of 5 and 6 days (Fig. 4.28A). Within the group of female homozygous mutants, 3 of 4 mice died between an age of 5 and 6 days, the last homozygous littermate died at 6 days of age (Fig. 4.28B). All homozygous mutants showed reduced body condition, marked glucosuria, and hyperglycaemia within the first 4 days of life as described in chapter 4.4.1.1 and 4.4.1.2. Homozygous mutants displayed a significantly reduced life span as compared to wild-type mice and

heterozygous mutants and were suspected to have died of severe diabetes mellitus with an average survival period of 4 days. Pathological organ findings in homozygous mutants are described in chapter 4.7.

One male heterozygous mutant deceased at an age of 4 days, one female heterozygous mutant died at an age of 7 days. The affected animals displayed reduced body condition and low body weight during the days *ante mortem*, so that asthenia might be causal for the early death of these animals. Post-weaning, 1 of 10 male wild-type mice died at 134 days of age without any obvious organ alteration. One of 10 female wild-type and 1/9 male heterozygous mutant mice were euthanised at the age of 174 and 287 days, respectively, due to severely reduced body condition and malignant tumours (lymphoma).

In summary, the survival rate of heterozygous Munich Gck^{M210R} mutants of both genders was comparable to wild-type littermates, while homozygous mutants exhibited a markedly constrained life span.

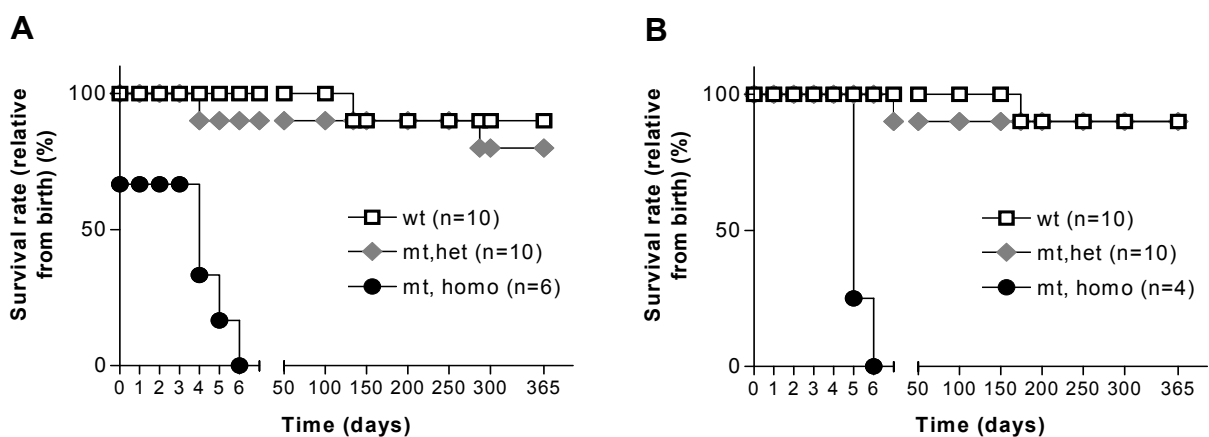


Figure 4.28: Survival rates of male (A) and female (B) heterozygous and homozygous Munich Gck^{M210R} mutants and wild-type littermates. While homozygous (homo) mutants (mt) died until an age of 6 days, life span of heterozygous mutants (het) was not constrained as compared to wild-type controls (wt). Data represent percentage of live animals out of all mice born per group; n=number of animals examined per group.

Munich Gck^{D217V} mutant mouse

The mean survival period of heterozygous and homozygous Munich Gck^{D217V} mutants and wild-type littermates was determined from the first day *post partum* until an age of 200 days. Mice of all 3 genotypes and both genders were born in the

expected pattern of Mendelian inheritance. One of 10 male homozygous mutants and 1 of 10 female wild-type mice died at an age of 1 day. One of 10 male heterozygous mutants displayed low birth weight, growth retardation, and died at an age of 8 days, most likely as a consequence of general weakness and energy poverty (Fig. 4.29A, B). None of the remaining animals deceased until an age of 200 days and the animal collective will be under ongoing survey until an age of 365 days.

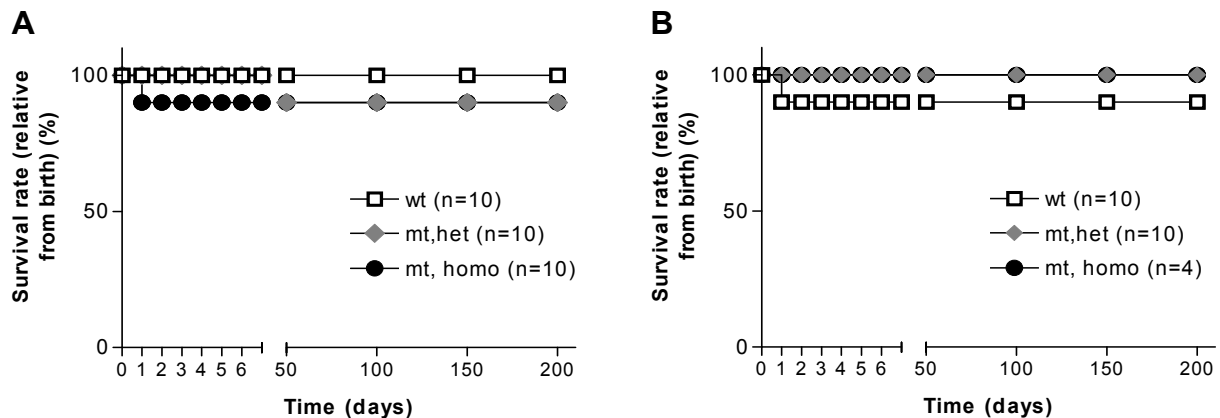


Figure 4.29: Survival rates of male (A) and female (B) heterozygous and homozygous Munich Gck^{D217V} mutants and wild-type littermates. Life span of heterozygous (het) and homozygous (homo) mutants (mt) was not constrained as compared to wild-type controls (wt). Data represent percentage of living mice out of all mice born per group. A total number of 10 animals per sex and genotype were investigated.

4.6 Organ weights

Organ weights were determined in 210-day-old heterozygous Munich Gck^{M210R} and Gck^{D217V} mutants of both sexes and wild-type littermates as controls. Absolute kidney weight of male heterozygous Gck^{D217V} mutants was significantly increased vs. sex-matched wild-type controls. However, kidney weight relative to the body weight was unaltered in these animals vs. wild-type mice ($2.01 \pm 0.13\%$ vs. $1.88 \pm 0.12\%$). Further, the absolute and relative weights of the intestine filled with ingesta and without ingesta were inconsiderably increased in female Munich Gck^{D217V} mutants as compared to wild-type mice. Other absolute (Table 4.6) and relative organ weights (data not shown) of heterozygous mutants of both strains and genders were comparable to those of wild-type mice.

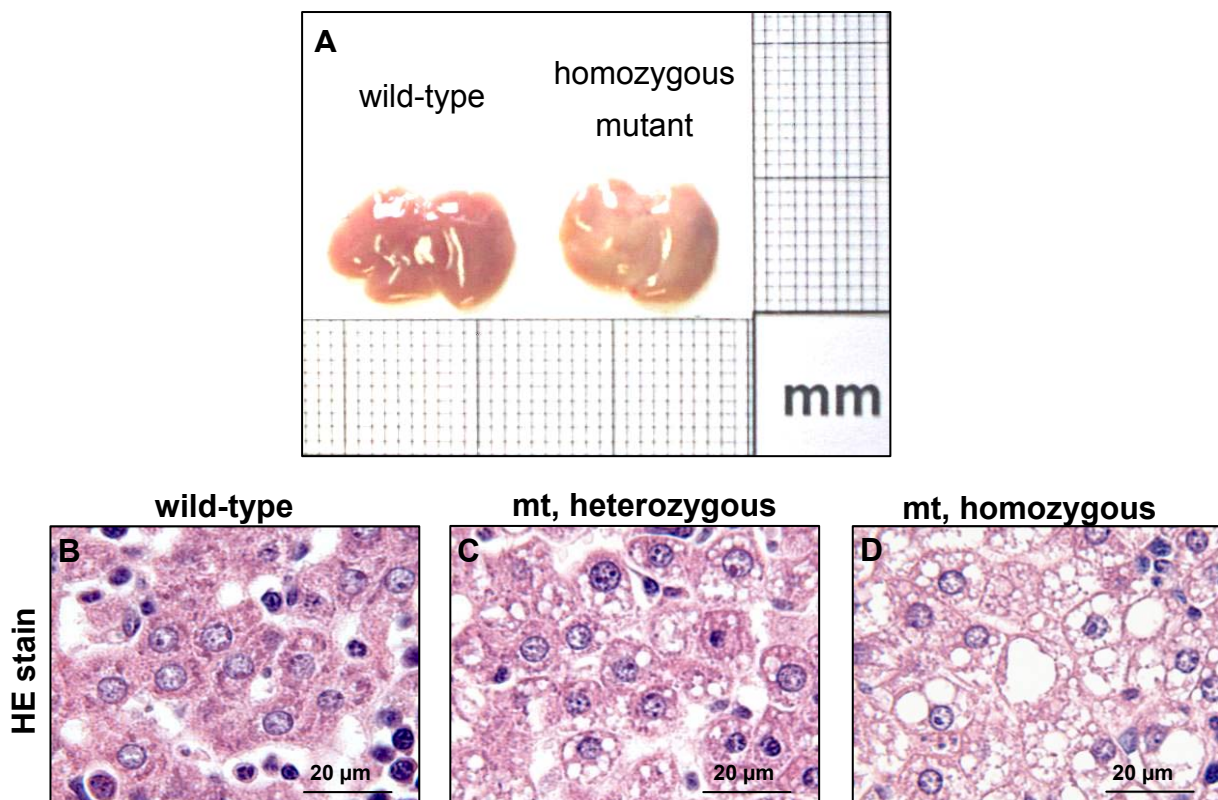
Table 4.6: Organ weights of 210-day-old male (m) and female (f) heterozygous Munich *Gck*^{M210R} and *Gck*^{D210V} mutants (mt) and wild-type littermates (wt).

Organ	Munich <i>Gck</i> ^{M210R} mutant mouse				Munich <i>Gck</i> ^{D210V} mutant mouse			
	m, wt	m, mt	f, wt	f, mt	m, wt	m, mt	f, wt	f, mt
Carcass (g)	15.4 (± 1.1)	15.1 (± 0.7)	14.3 (± 0.3)	13.8 (± 0.3)	14.7 (± 0.5)	15.3 (± 0.9)	12.6 (± 0.5)	12.4 (± 0.3)
GIT (filled with ingesta) (g)	3.8 (± 0.2)	3.4 (± 0.3)	3.5 (± 0.5)	3.4 (± 0.3)	2.4 (± 0.2)	2.4 (± 0.2)	2.2 (± 0.1)	2.4 [†] (± 0.2)
GIT (without ingesta) (g)	2.0 (± 0.1)	1.9 (± 0.1)	1.9 (± 0.1)	2.0 (± 0.1)	1.6 (± 0.1)	1.7 (± 0.2)	1.5 (± 0.1)	1.8 [†] (± 0.1)
Abdominal fat (mg)	406 (± 163)	430 (± 114)	317 (± 135)	425 (± 123)	523 (± 169)	669 (± 537)	246 (± 137)	295 (± 95)
Mesentery (mg)	251 (± 54)	239 (± 16)	149 (± 72)	275 (± 86)	215 (± 56)	278 (± 81)	208 (± 50)	168 (± 34)
Liver (g)	1.6 (± 0.1)	1.5 (± 0.1)	1.4 (± 0.1)	1.5 (± 0.1)	1.2 (± 0.1)	1.3 (± 0.1)	1.1 (± 0.1)	1.1 (± 0.1)
Kidney (mg)	589 (± 69)	561 (± 65)	514 (± 120)	475 (± 192)	526 (± 24)	602 ^a (± 47)	316 (± 13)	323 (± 16)
Spleen (mg)	82 (± 14)	85 (± 5)	106 (± 10)	118 (± 8)	64 (± 9)	70 (± 6)	81 (± 7)	90 (± 20)
Lung (mg)	160 (± 15)	172 (± 12)	177 (± 12)	173 (± 18)	150 (± 4)	149 (± 6)	130 (± 15)	133 (± 13)
Heart (mg)	153 (± 14)	144 (± 11)	131 (± 4)	128 (± 5)	163 (± 23)	152 (± 12)	132 (± 3)	124 (± 13)
Adrenal glands (mg)	5.1 (± 0.8)	4.8 (± 0.8)	7.2 (± 1.5)	7.7 (± 1.1)	5.6 (± 1.2)	5.4 (± 2.2)	5.9 (± 0.6)	5.3 (± 0.5)
Thymus (mg)	22 (± 3)	24 (± 2)	34 (± 8)	25 (± 4)	20 (± 4)	25 (± 1)	26 (± 5)	22 (± 7)
Testes (mg)	160 (± 4)	145 (± 4)			143 (± 10)	135 (± 1)		
Epididymes (mg)	70 (± 8)	69 (± 5)			57 (± 5)	56 (± 7)		
Ovaries (mg)			17 (± 5)	18 (± 6)			14 (± 2)	15 (± 4)

Data represent means ± SD. A total number of 4 animals per sex and genotype were examined. *p<0.05 male mutant (m, mt) vs. male wild-type (wt); [†]p<0.05 female (f) mutant vs. f, wt. ^a relative kidney weight of m, mt was unaltered vs. wt, m.

4.7 Analysis of specific organ alterations in Munich Gck^{M210R} mutants

Necropsy of 4-day-old homozygous and heterozygous Munich Gck^{M210R} mutants and wild-type littermates disclosed genotype-dependent gross liver alterations. Livers of homozygous mutants showed a pale beige colour vs. dark red-brown livers of heterozygous mutants and wild-type control mice (Fig. 4.30A). Histological analysis of haematoxylin-eosin (HE) stained liver sections from 4-day-old mice revealed normal hepatic tissue of wild-type mice (Fig. 4.30B), discrete vacuolisation of hepatocytes in heterozygous mutants (Fig. 4.30C), and extensive hepatocyte vacuolisation in homozygous mutants (Fig. 4.30D). In frozen liver sections from wild-type mice, stained for neutral lipids, only singular and small fat droplets (Fig. 4.30E) were identified, whereas fat accumulation in the liver of heterozygous mutants was more pronounced (Fig. 4.30F). Liver sections of homozygous mutants, by contrast, displayed massive hepatocellular deposition of large fat droplets, reflecting marked hepatic steatosis (Fig. 4.30G). Furthermore, high amounts of glycogen granules were observable in periodic acid-Schiff (PAS) stained liver sections of wild-type mice (Fig. 4.30H), whereas glycogen storage was obviously reduced in heterozygous mutants (Fig. 4.30I) and almost undetectable in homozygous mutants (Fig. 4.30J).



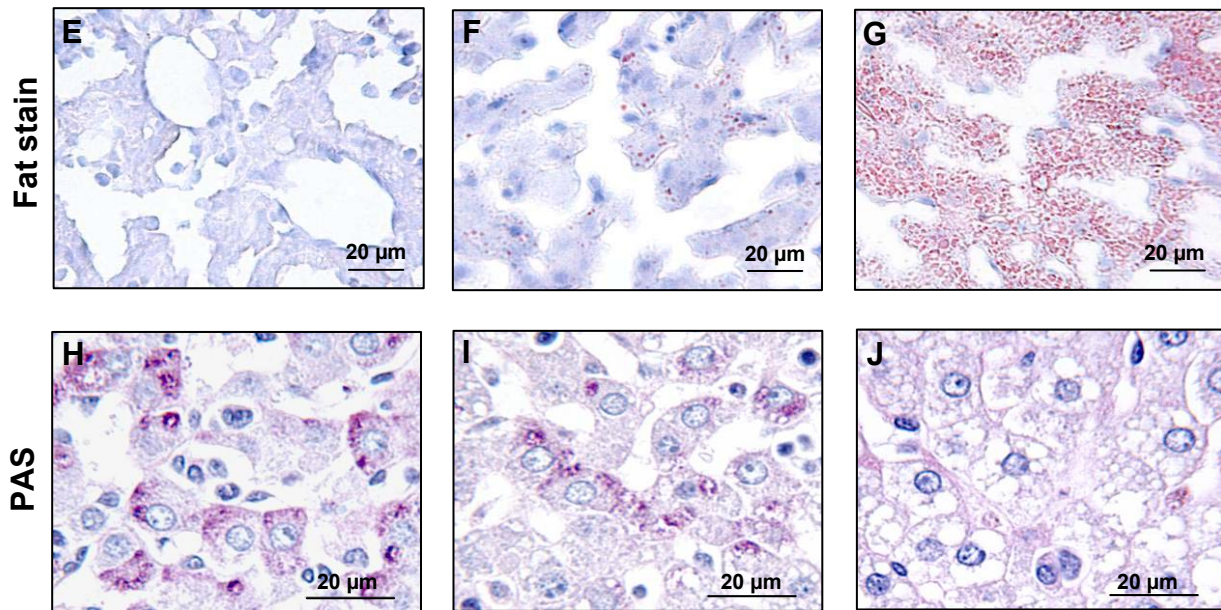


Figure 4.30: Gross appearance of livers from a 4-day-old homozygous Munich Gck^{M210R} mutant and a wild-type littermate (A). B-J: liver sections of a wild-type mouse (B, E, H); a heterozygous mutant (C, F, I), and a homozygous (D, G, J) mutant, paraffin embedded, stained with HE (B-D) or PAS (H-J), and Fat red staining of frozen liver tissue (E-G). Grossly, the liver of the homozygous mutant appeared markedly lighter in colour vs. the wild-type mouse. Histology revealed slight vacuolisation and lipid droplets in hepatocytes of heterozygous mutants (C, F) and marked vacuolisation and lipid accumulation in hepatocytes of homozygous mutants (D, G). Additionally, hepatocytes of heterozygous mutants exhibited discrete (I), those of homozygous mutants striking glycogen depletion (J), vs. wild-type mice (H).

4.8 Qualitative histological evaluation of the endocrine pancreas

4.8.1 Munich Gck^{M210R} mutants

4.8.1.1 Pancreata from neonatal mice

Due to the premature morphologic organisation of pancreatic islets in neonatal mice, the predominance of cumulative, duct-associated pancreatic islets, and the presence of widespread, connective tissue-similar, fibrous cords, islet demarcation was difficult to define at this age. Haematoxylin-eosin (HE) as well as connective tissue staining (Masson's trichrome stain modified according to Goldner and Weigert) and immunohistochemical staining for insulin could not reveal a defined pancreatic islet contour (Fig 4.31A-C). Therefore, with regard to subsequent quantitative histological

analysis of the pancreas sections, pancreatic islets could not serve as reference compartment at this age group. However, immunohistochemical staining for insulin of pancreas sections of neonatal mice suggested comparable profiles of insulin positive stained β -cell areas in homozygous and heterozygous Munich Gck^{M210R} mutants vs. wild-type littermates (Fig. 4.32A-C).

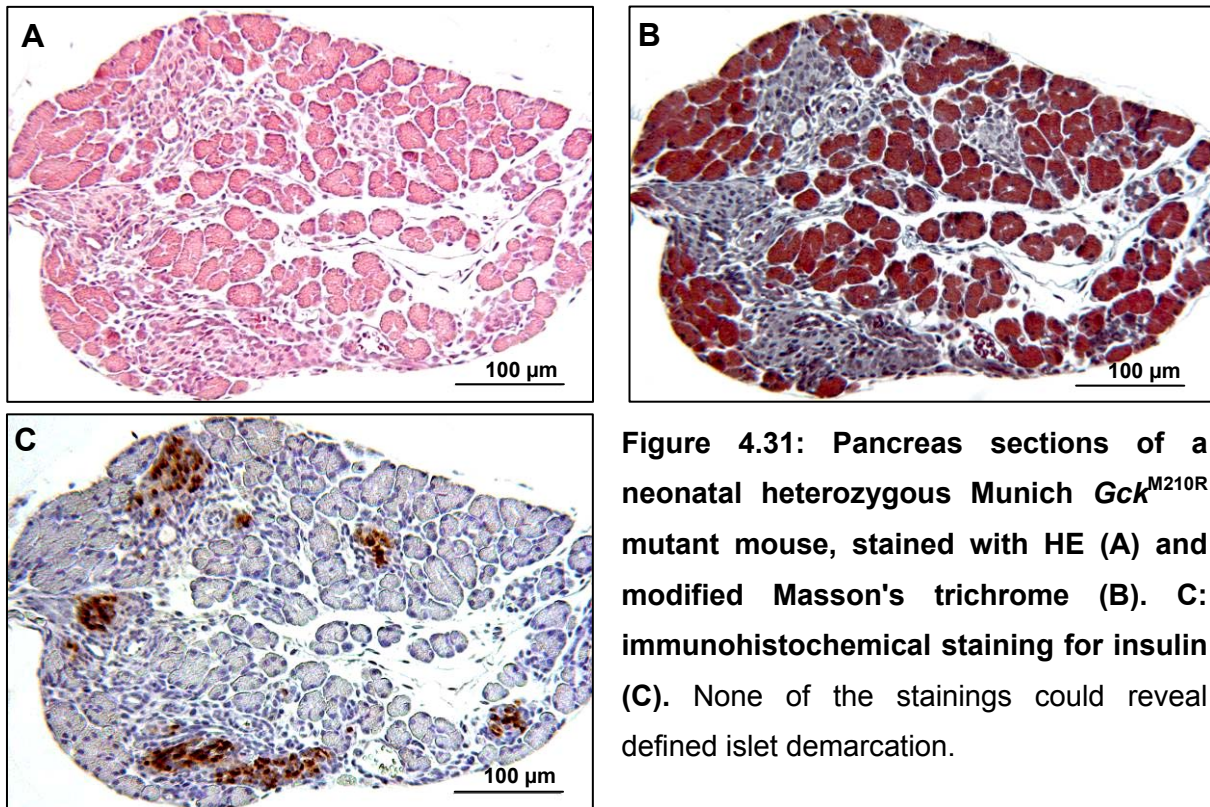


Figure 4.31: Pancreas sections of a neonatal heterozygous Munich Gck^{M210R} mutant mouse, stained with HE (A) and modified Masson's trichrome (B). C: immunohistochemical staining for insulin (C). None of the stainings could reveal defined islet demarcation.

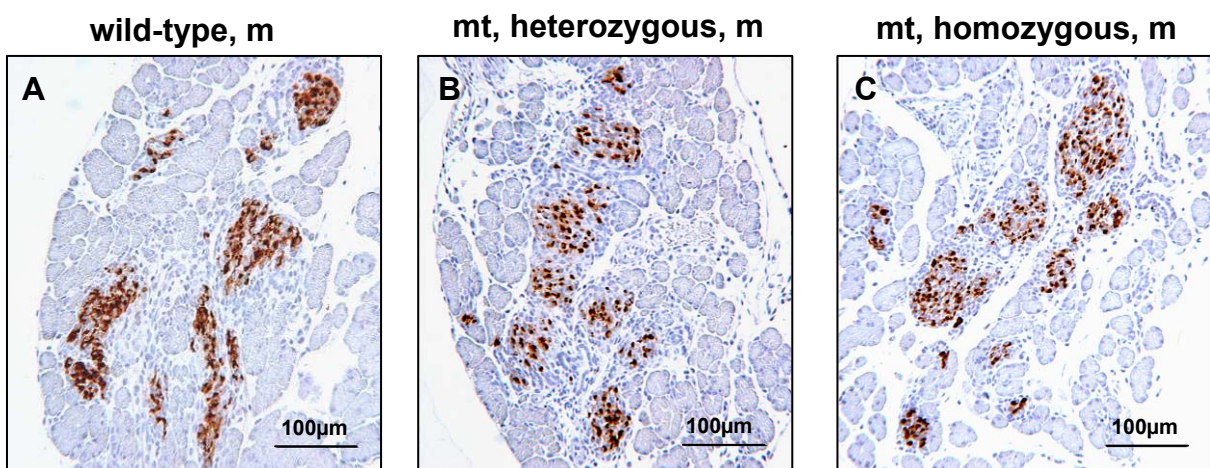


Figure 4.32: Pancreas sections from neonatal heterozygous (B) and homozygous (C) Munich Gck^{M210R} mutants (mt) and a wild-type control animal (A) in an immunohistochemical staining for insulin. The cross-sectional area of β -cells immunostained for insulin appeared unaltered among the different genotypes.

4.8.1.2 Pancreata from 210-day-old mice

Considering gross morphology and histological appearance, pancreata from 210-day-old heterozygous mutants of both sexes were unaltered as compared to wild-type littermates and no evidence for the presence of any inflammatory event in the pancreatic islets was detectable in these animals. Insulin-immunostaining of pancreas sections from heterozygous mutants revealed typical islet composition and distribution of insulin⁺ stained cells within the islets. Additionally, β -cell staining intensity for insulin was also comparable to control mice and the relative amount of insulin⁺ cells seemed to be unaltered vs. wild-type mice. However, the cross-sectional area of pancreatic islets appeared conspicuously smaller in male heterozygous mutants as compared to wild-type control mice (Fig. 4.33 A-D).

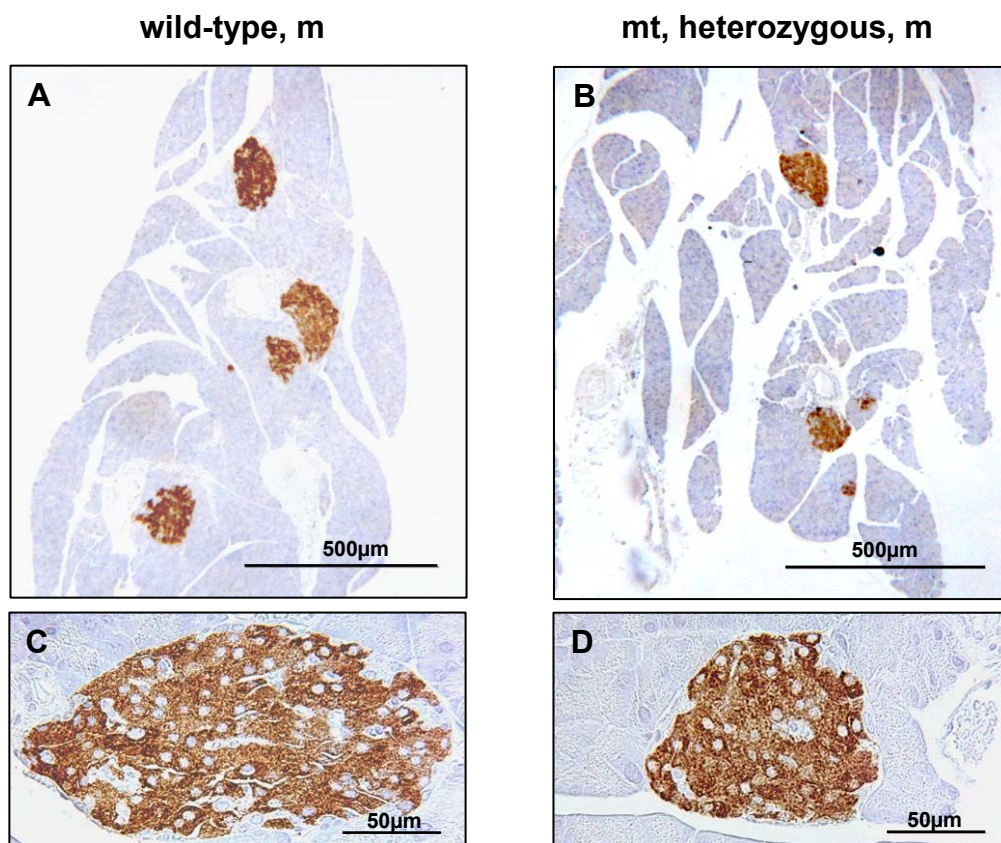


Figure 4.33: Pancreas sections of a 210-day-old male (m) heterozygous Munich Gck^{M210R} mutant (mt) and a male wild-type mouse immunostained for insulin. Staining intensity and the distribution of the insulin producing β -cells in the islets did not differ between male heterozygous mutants (B, D) and male wild-type controls (A, C). Broad overview over pancreas sections (A, B) and exemplary depiction of single islets (C, D) revealed the impression that islet area was considerably smaller in male heterozygous mutants vs. the wild-type control.

4.8.2 Munich Gck^{D217V} mutants

4.8.2.1 Pancreata from 550-day-old mice

Macroscopically and histologically, pancreata from 550-day-old heterozygous and homozygous Munich Gck^{D217V} mutants appeared normal and no evidence for any inflammatory event in the islets was observable. Staining intensity of insulin⁺ β -cells and their distribution in pancreatic islets was comparable to wild-type mice. However, the broached area of pancreatic islets appeared strikingly decreased in male homozygous mutants as compared to wild-type mice and heterozygous mutants. Additionally, the amount of insulin producing β -cells was slightly reduced in heterozygous mutants, and considerably less insulin expressing cells were detectable in homozygous mutants as compared to wild-type mice (Fig. 4.34 A-F)

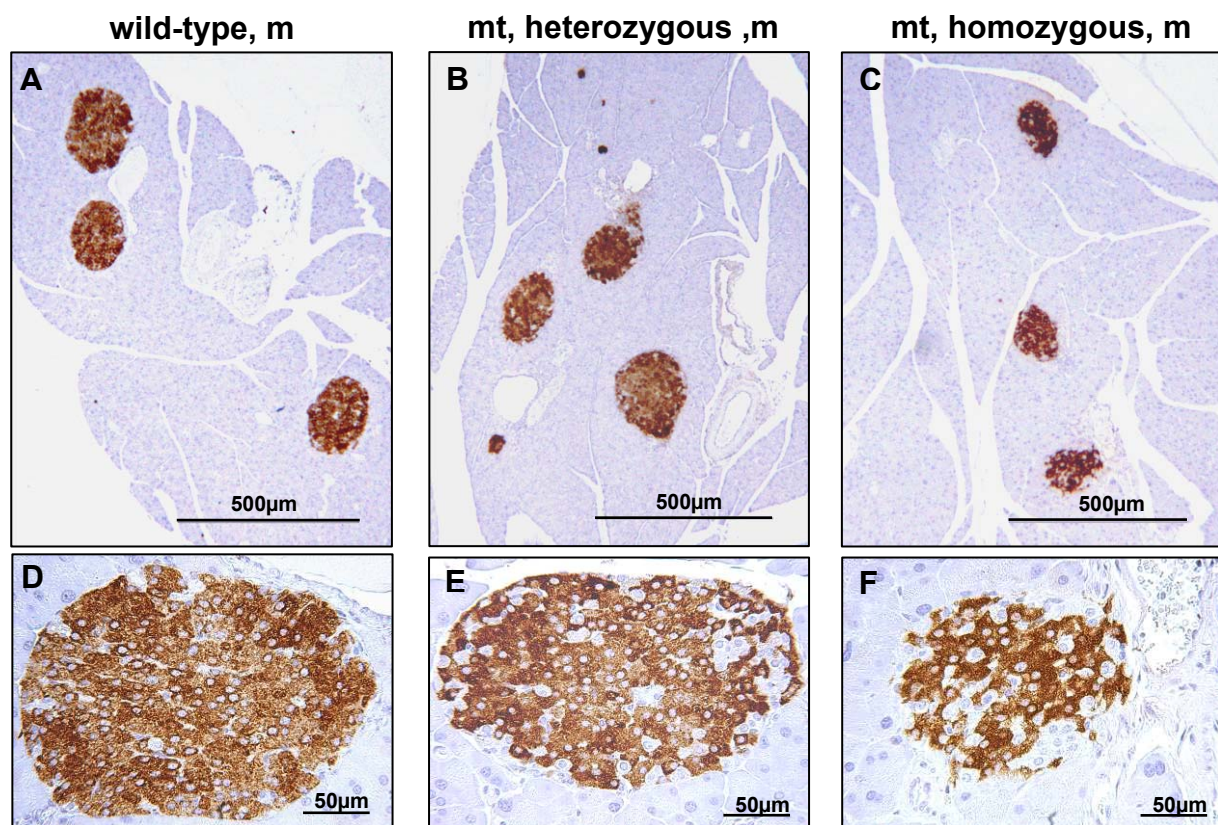


Figure 4.34: Pancreas sections from 550-day-old male heterozygous and homozygous Munich Gck^{D217V} mutants and a wild-type control immunohistochemically stained for insulin. As already visible in a minor magnification (A-C), the cross sectional areas of islets appeared comparable in male (m) heterozygous mutants (mt) and wild-type mice, but were considerably smaller in homozygous mutants. Higher magnification of these sections (D-F) also suggested conspicuously reduced β -cell content in pancreatic islets of homozygous and heterozygous mutants.

4.9 Quantitative stereological analysis of the endocrine pancreas

4.9.1 Munich Gck^{M210R} mutants

4.9.1.1 Stereological findings in pancreata from neonatal male mice

At the first day *post partum*, the pancreas volume ($V_{(pan)}$, Fig. 4.35A) of male heterozygous and homozygous Munich Gck^{M210R} mutants was unaltered as compared to wild-type littermates. Even if the volume density of β -cells in the pancreas ($Vv_{(\beta\text{-cells}/pan)}$; Fig 4.35B) and the total β -cell volume ($V_{(\beta\text{-cells},pan)}$; Fig. 4.35C) of heterozygous and homozygous mutants did not significantly deviate from wild-type controls, both parameters were decreased by tendency in homozygous mutants at this age.

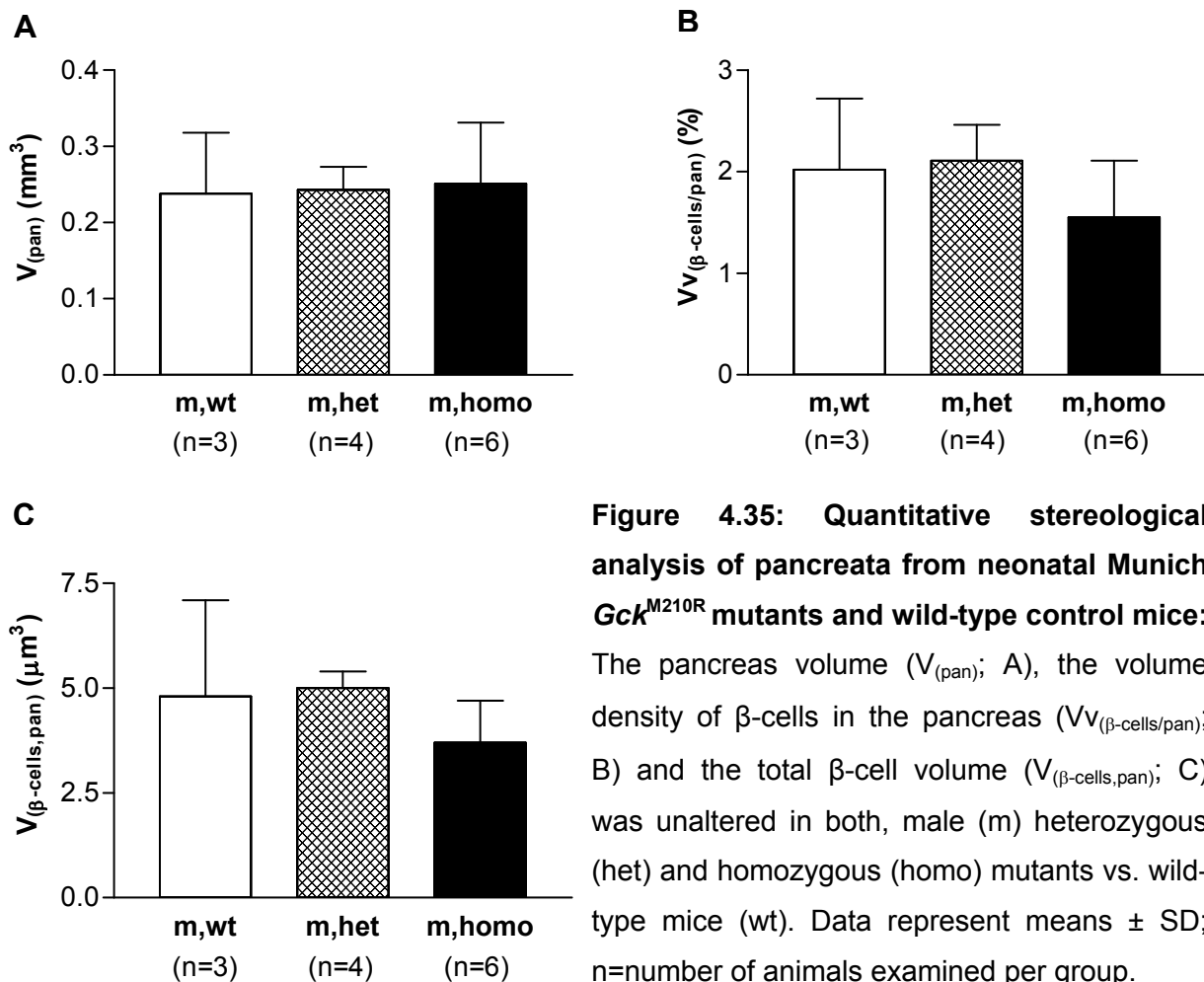
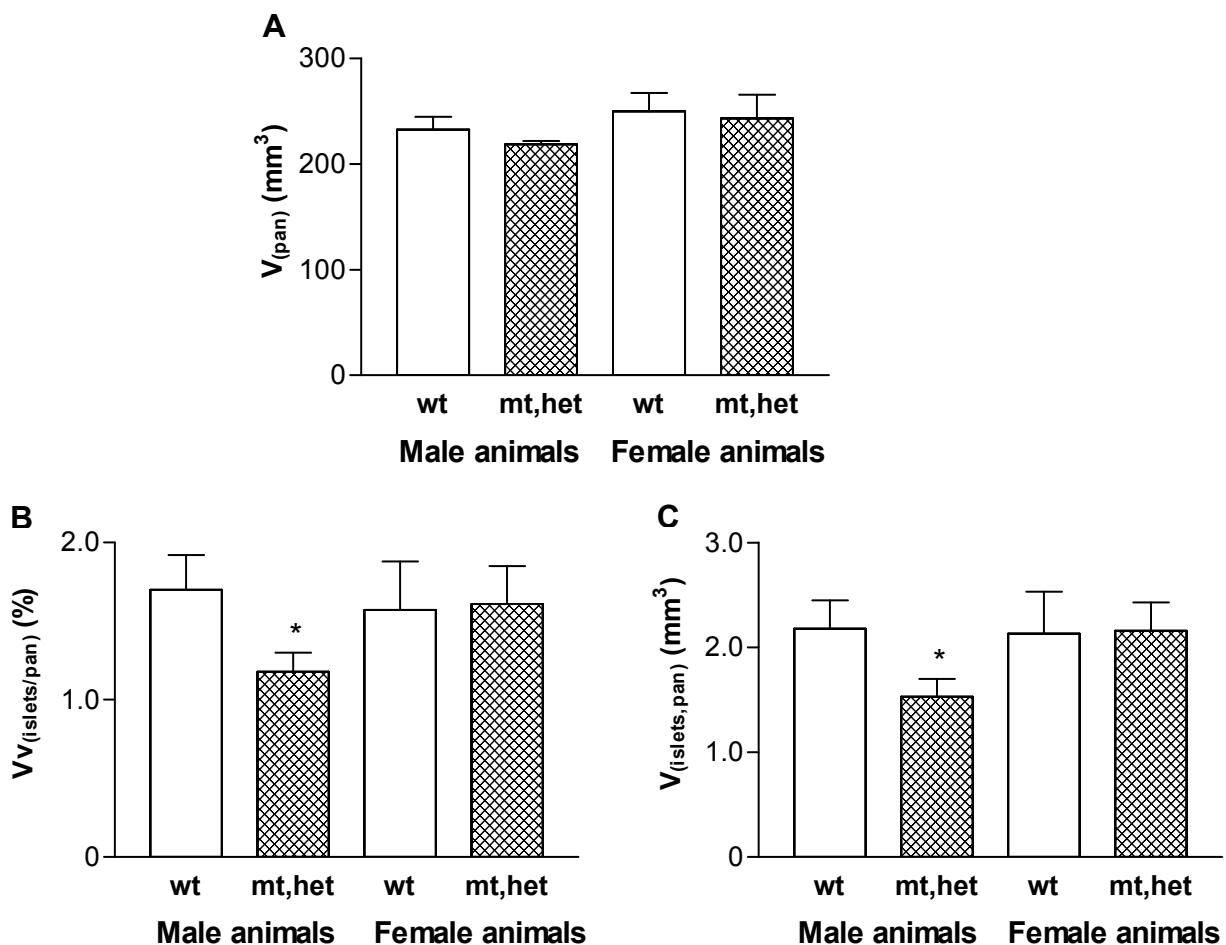


Figure 4.35: Quantitative stereological analysis of pancreata from neonatal Munich Gck^{M210R} mutants and wild-type control mice: The pancreas volume ($V_{(pan)}$; A), the volume density of β -cells in the pancreas ($Vv_{(\beta\text{-cells}/pan)}$; B) and the total β -cell volume ($V_{(\beta\text{-cells},pan)}$; C) was unaltered in both, male (m) heterozygous (het) and homozygous (homo) mutants vs. wild-type mice (wt). Data represent means \pm SD; n=number of animals examined per group.

4.9.1.2 Quantitative stereological parameters of pancreata from 210-day-old mutants

The pancreas volume ($V_{(pan)}$, Fig. 4.36A) was unaltered in 210-day-old heterozygous mutants of both genders as compared to wild-type mice. The volume density of islets in the pancreas ($Vv_{(islets/pan)}$; Fig. 4.36B) was significantly ($p < 0.05$) decreased by about 25% (range from 18-36%) in male, but not female heterozygous mutants, whereas the volume density of β -cells in the islets ($Vv_{(\beta\text{-cells/islets})}$ Fig. 4.36D) was unaltered in mutants of both genders. Consistent with these findings, male mutants exhibited reduced total islet ($V_{(islets,pan)}$; Fig. 4.36C) and total β -cell volumes ($V_{(\beta\text{-cells, islets})}$; Fig. 4.36E) by about 25% and 33% ($p < 0.05$), respectively, whereas these parameters were unchanged in female heterozygous mutants as compared to age- and sex-matched wild-type littermates. Additional quantification of isolated β -cells in pancreata from male mice revealed a significant ($p < 0.05$) reduction of the volume density of isolated β -cells in the pancreas ($Vv_{(isolated \beta\text{-cells/pan})}$; Fig. 4.36F) by about 33% in male heterozygous mutants vs. wild-type controls. Analogically, the total volume of isolated β -cells ($V_{(isolated \beta\text{-cells,pan})}$; Fig. 4.36G) was diminished by about 31% in these animals.



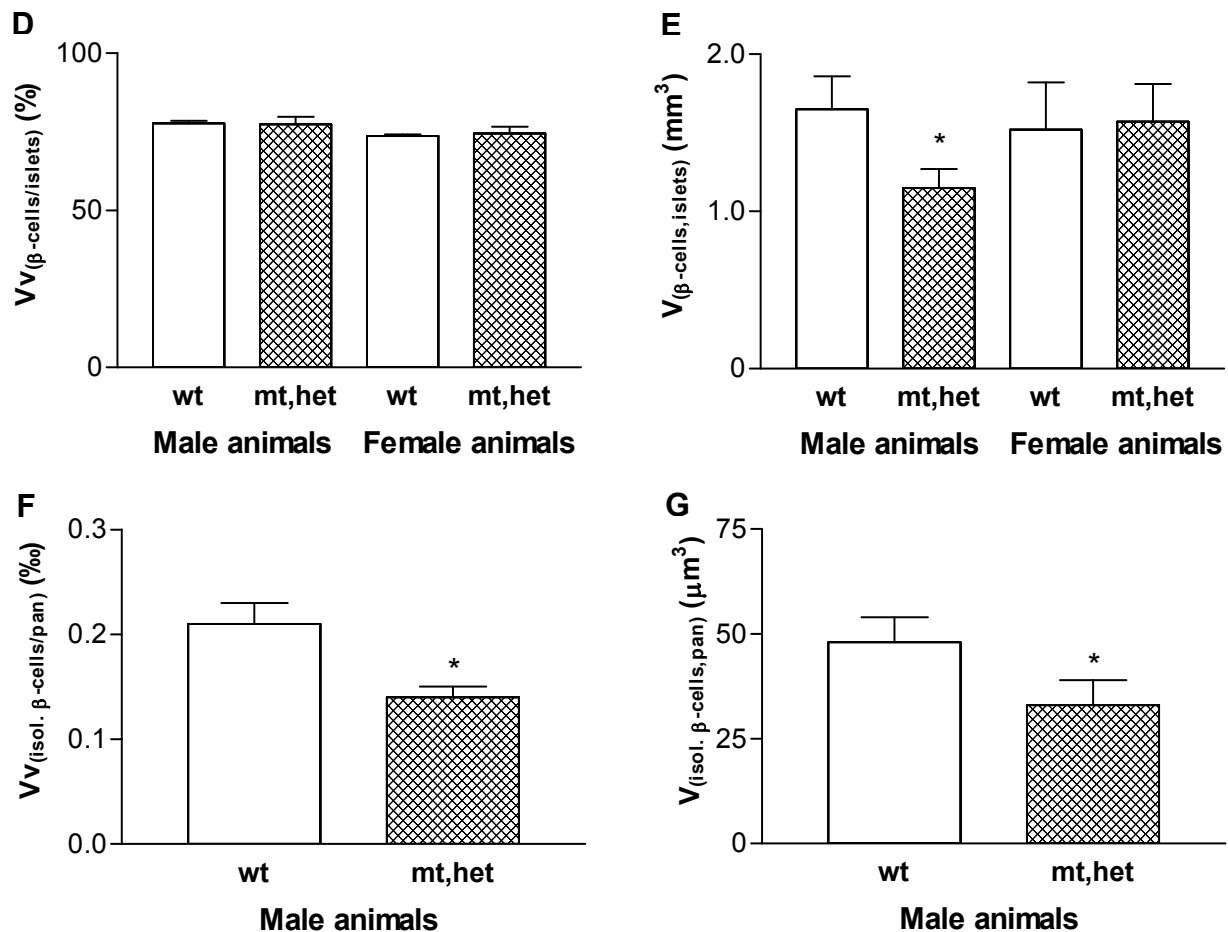


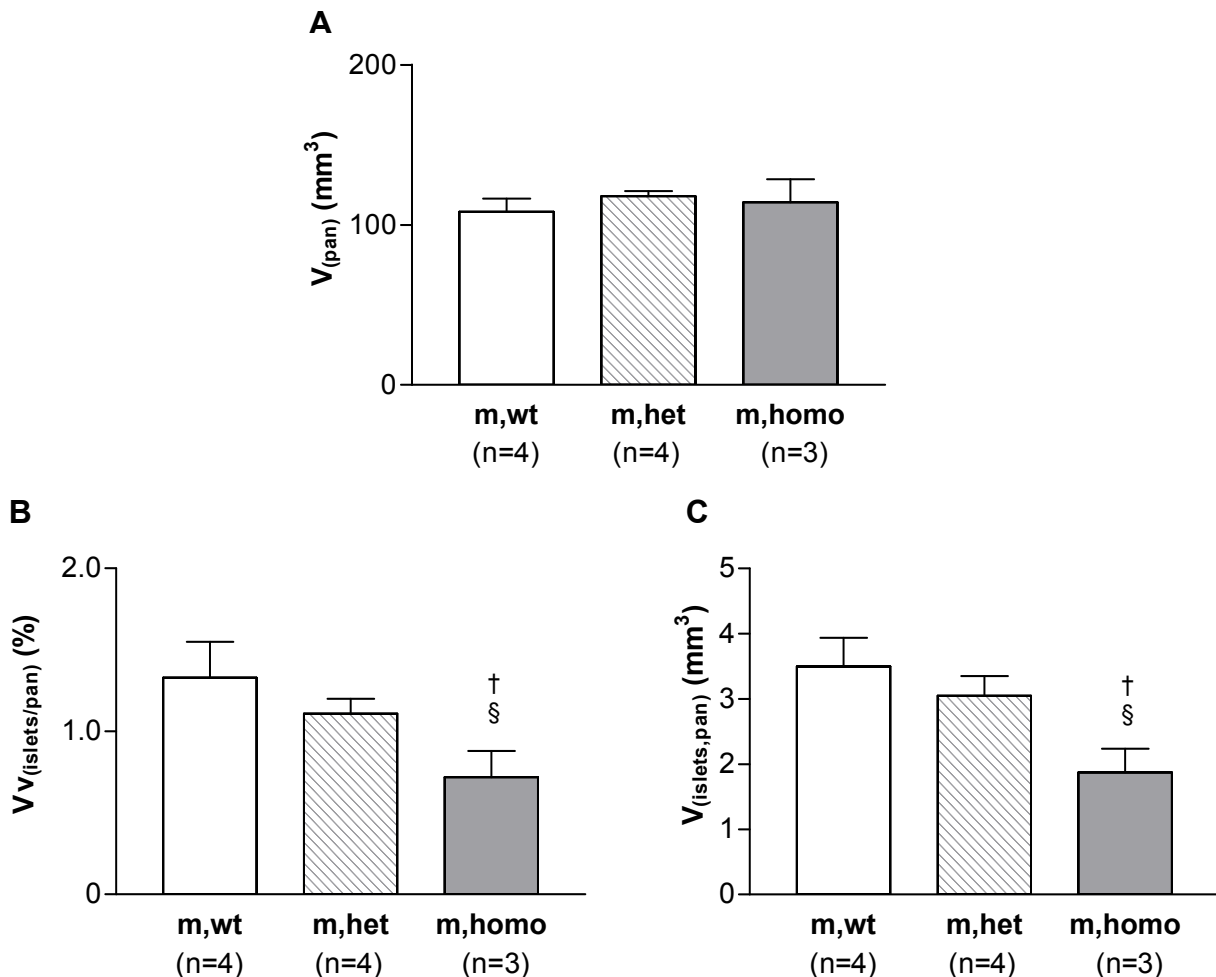
Figure 4.36: Quantitative stereological evaluation of pancreas sections from 210-day-old heterozygous Munich Gck^{M210R} mutants and wild-type littermates. The pancreas volume ($V_{(\text{pan})}$; A) and the volume density of β -cells in the islets ($Vv_{(\beta\text{-cells/islets})}$; D) were unaltered in male (m) and female (f) mutants (mt) vs. wild-type mice (wt), whereas the volume densities of islets ($Vv_{(\text{islets/pan})}$; B) and of isolated β -cells ($Vv_{(\text{isolated } \beta\text{-cells/pan})}$; F) in the pancreas, as well as the total volumes of islets ($V_{(\text{islets,pan})}$; C), β -cells ($V_{(\beta\text{-cells,islets})}$; E) and isolated β -cells ($V_{(\text{isolated } \beta\text{-cells,pan})}$; G) were significantly decreased in male mutants. Data represent means \pm SD. A total number of 4 animals per sex and genotype were examined. * $p < 0.05$ m, mt vs. m, wt.

4.9.2 Munich Gck^{D217V} mutants

4.9.2.1 Stereological findings in pancreata from 550-day-old male mice

At an age of 550 days, the pancreas volume ($V_{(\text{pan})}$, Fig. 4.37A) was comparable between male heterozygous and homozygous Munich Gck^{D217V} mutants and age- and sex-matched wild-type littermates. The volume density of the islets in the pancreas ($Vv_{(\text{islets/pan})}$; Fig. 4.37B) in homozygous mutants was reduced by about 45%

as compared to wild-type mice, and by about 35% vs. heterozygous mutants, whereas $V_{V(islets/pan)}$ was unaltered in heterozygous mutants. Further, homozygous and heterozygous mutants exhibited a significantly ($p < 0.05$) reduced volume density of the β -cells in the islets ($V_{V(\beta-cells/islets)}$, Fig. 4.37D). However, this reduction was marginal, especially in heterozygous mutants (diminution by about 14% in homozygous mutants and by about 6% in heterozygous mutants as compared to wild-type mice). Additionally, the total islet ($V_{(islets,pan)}$; Fig. 4.37C) and β -cell volumes ($V_{(\beta-cells,islets)}$; Fig. 4.37E) of homozygous mutants were significantly ($p < 0.05$) decreased by about 47% and 54%, respectively as compared to wild-type mice. In contrast to homozygous mutants, heterozygous mutants exhibited an unaltered $V_{(islets,pan)}$ and an only slightly reduced $V_{(\beta-cells,islets)}$.



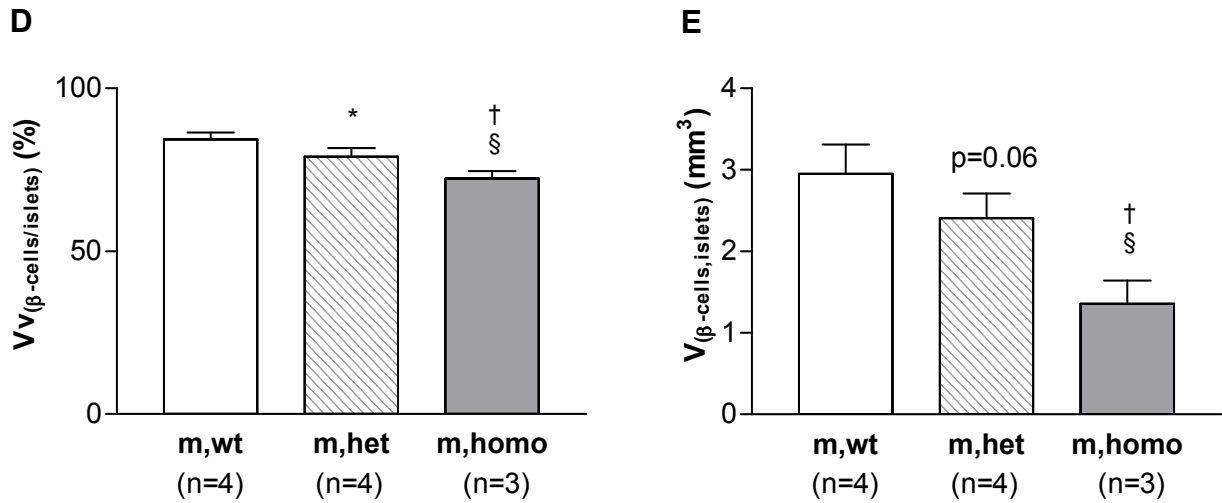


Figure 4.37: Quantitative stereological parameters of pancreas sections from 550-day-old male heterozygous and homozygous Munich Gck^{D217V} mutants and wild-type animals. The pancreas volume ($V_{(pan)}$; A) did not differ between mice of all genotypes. The volume density of the islets in the pancreas ($Vv_{(islets/pan)}$; B), the volume density of the β -cells in the islets ($Vv_{(\beta\text{-cells/islets})}$; D), and, consequentially, the total islet ($V_{(islets,pan)}$; C) and β -cell volumes ($V_{(\beta\text{-cells,islets})}$; E) were significantly decreased in male (m) homozygous mutants vs. wild-type mice (wt) and heterozygous mutants (het), whereas in heterozygous mutants only $Vv_{(\beta\text{-cells/islets})}$ was significantly diminished. Data represent means \pm SD; n=number of animals investigated per genotype. * $p < 0.05$ het vs. wt; † $p < 0.05$ homo vs. het; § $p < 0.05$ homo vs. wt.

5. Discussion

In the present study, two hyperglycaemic mutant mouse strains, which were detected in the clinical-chemical screen for dominant mutations within the Munich ENU mouse mutagenesis project, were investigated. The location and nature of the respective causative mutations were characterised, as well as the resulting diabetic phenotype and the pathomorphological features of both strains were investigated. Both strains were established by breeding diabetic heterozygous mutants for more than 10 generations onto the inbred C3H genetic background, which is supposed to be a diabetes-resistant strain (Leiter *et al.* 1999). This led to the loss of most additional ENU-induced non-causative mutations and excluded eventual phenotypic influences of these mutations. Standardisation of animal husbandry and treatment, randomisation of animal and biological material selection for investigations, and uniformisation of sample materials, concerning origin and mode of processing were emphasised in this study.

5.1 Genetic aspects

Low-resolution SNP genotyping of GLS001 and GLS006 mice and subsequent high-resolution linkage analysis of GLS001 mice mapped the diabetic phenotype of both strains to polymorphic DNA markers on chromosome 11 at 5.9 and 7.1 Mb, respectively. The mouse genome database query for positional diabetes-associated genes revealed the glucokinase (*Gck*) gene as potential candidate gene for sequencing. Sequence analysis of *Gck* revealed a defined point mutation in exon 6 of *Gck* in both strains. The ENU strain GLS001 exhibited a T to G transversion at nucleotide position (nt) 629, leading to an amino acid exchange from methionine to arginine at position 210. In GLS006 mice an A to T transversion at nt 650 was identified, thereby resulting in an amino acid exchange from aspartic acid to valine at position 217. According to the respective missense mutations, the laboratory names GLS001 and GLS006 were replaced by the official terms Munich *Gck*^{M210R} and *Gck*^{D217V} mutant mouse. Mutations in the human glucokinase (*GCK*) gene are associated with 2 distinct phenotypic traits. Mutations can either cause hypoglycaemia (when activating glucokinase function) or hyperglycaemia (when impairing glucokinase function). While heterozygous inactivating mutations are

reported to cause maturity-onset diabetes of the young, type 2 (MODY 2), homozygous mutations are associated with neonatal diabetes mellitus (NDM) (Gloyn 2003). Four M210 mutations and 1 D217 mutation have already been detected in human diabetic subjects, whereas base exchanges at these two positions have not yet been detected in other animal models so far. Referring to the missense mutation M210 in human subjects, the base exchanges from methionine to lysine (M210K) has been discovered to cause MODY 2 and NDM, whereas the mutations M210T, M210V, and M210I (amino acid exchange to threonine, to valine, or to isoleucine, respectively) have only been identified in families with MODY features. At position D217, only the amino acid exchange from aspartic acid to glutamic acid (D217E) has been reported to be associated with MODY 2 (Njolstad *et al.* 2001; Osbak *et al.* 2009; Sagen *et al.* 2006; Velho *et al.* 1997). Various knockout mouse models for MODY 2 have already been generated by targeted global or tissue-specific disruption of *Gck* (Bali *et al.* 1995; Grupe *et al.* 1995; Postic *et al.* 2001; Postic *et al.* 1999; Terauchi *et al.* 1995) (<http://www.informatics.jax.org/>). However, monogenic diseases like MODY 2 in human beings usually arise from single point mutations and include a broad spectrum of phenotypic outcomes depending on the position and the nature of the mutation. Knockout strategies which target complete ablation of the respective gene transcript, might fail to produce animal models that recapitulate human disease phenotypes. Therefore, animal models exhibiting naturally occurring or induced mutations represent additional useful tools to dissect specific gene functions (Clark *et al.* 1994; Oliver *et al.* 2007; Peltonen and McKusick 2001). A total number of 15 ENU-induced glucokinase mutant mouse strains have been generated in various ENU-driven mutagenesis projects (Fenner *et al.* 2009; Inoue *et al.* 2004; Toyé *et al.* 2004) (<http://www.informatics.jax.org/>). In the screen for dominant mutations of the RIKEN mutagenesis project (RIKEN BioResources Center), 12 of 17 mouse strains exhibiting hyperglycaemia were identified to bear single-base pair substitutions in *Gck* (<http://www.brc.riken.jp/lab/gsc/mouse/>). This predominance of ENU-induced *Gck* mutations might be due to the high penetrance of *Gck* defects, a great sensitivity of the glucokinase protein to amino acid exchanges or may arise from the fact that *Gck* haploinsufficiency leads to abnormal phenotypic traits (Inoue *et al.* 2004). Another probable explanation for the plenitude of *Gck* mutations, identified in screens for hyperglycaemia in other ENU mutagenesis projects, might be founded in the structural properties of *Gck*. Exhibiting a surpassing coding sequence length

(1,398 bp vs. 1,137 bp median coding sequence for the mouse genome), a high exon number (11 exons vs. a median exon number of 6), and an above-average G+C-content (57.3% vs. a median G+C-content of about 45%), *Gck* may be more frequently targeted by ENU-induced base exchanges than other genes for statistical reasons (Barbaric *et al.* 2007).

The occurrence of the diabetic phenotype in both Munich *Gck*^{M210R} and *Gck*^{D217V} mutants remained unaltered in ensuing generations, giving proof of the heritability and the complete penetrance of the abnormal phenotype. Together with the linkage analysis carried out and the revelation of the functional consequences of the respective mutations, these findings indicate that the identified missense mutations in *Gck* are causative for the diabetic phenotype of both mouse strains.

The induction of different mutations in the same gene represents an extremely powerful tool to address the question of gene and protein function (Justice *et al.* 1999). An impressive example of an allelic series is the quaking locus. Prior to ENU mutagenesis, the quaking locus was defined by a single spontaneous allele, characterised by quaking and seizures as a result of defective CNS myelination in homozygous mutants. The identification of novel ENU-induced alleles indicated an additional involvement of quaking in embryogenesis (Justice and Bode 1988; Sidman *et al.* 1964).

Since the causative mutations in Munich *Gck*^{M210R} and *Gck*^{D217V} mutants are located in a distance of only 7 amino acids to each other, the creation of an allelic series in these mouse strains represents an extremely valuable genetic resource for detailed dissection of the impact of alterations at different amino acid residues of the glucokinase protein on phenotypic and pathomorphologic traits.

5.2 Functional consequences of the mutations

5.2.1 Glucokinase activity

The glucose phosphorylation rate by glucokinase in liver homogenate of 90-day-old mice was considerably reduced in heterozygous mutants of both strains, whereas the activity of other hexokinases and their affinity for glucose was not altered. Impairment of glucokinase substrate turnover rate was slightly more pronounced in Munich *Gck*^{M210R} than in *Gck*^{D217V} mutants (relative reduction of about 43% in M210R vs.

33% in D217V mutants). In homozygous *Gck*^{D217V} mutants, glucokinase activity and the affinity for glucose were severely reduced, indicating the striking impact of the mutation on glucokinase function when present on both alleles. Enzyme activity studies with recombinant M210K mutant glucokinase already revealed a reduction of glucokinase activity for heterozygous mutations, comparable to the reduction observed in Munich *Gck*^{M210R} mutants. The catalytic activity of the recombinant glucokinase, homozygous for the mutation M210K, was almost undetectable (about 0.16% of wild-type enzyme activity), whereas the $S_{0.5}$ was about 7-fold increased (Aguilar-Bryan and Bryan 2008; Njolstad *et al.* 2001; Sagen *et al.* 2006). The $S_{0.5}$, reflecting the affinity of the glucokinase enzyme for its main substrate glucose, was unaltered in heterozygous *Gck*^{D217V} and was only slightly increased in *Gck*^{M210R} mutants. However, compensatory *in vivo* mechanisms might mask a reduced affinity of the mutant glucokinase to glucose in both strains. Attenuation of inhibitory effects of the glucokinase regulatory protein, which binds to hepatic glucokinase and decreases its affinity for glucose (Agius *et al.* 2001), is thought to represent a possible compensatory adaptation to increase the glycolytic flux of glucose through the mutated glucokinase enzyme (Sturis *et al.* 1994; Veiga-da-Cunha *et al.* 1996). The effect of *Gck* haploinsufficiency on glucokinase activity has already been demonstrated for heterozygous global, liver- and β -cell specific *Gck* knockout mouse models, which displayed different degrees of glucokinase activity impairment. However, mice that lack one *Gck* allele either in the liver or in liver and pancreatic β -cells exhibit a reduction of glucokinase activity by less than 50%, thereby implying the presence of potential compensatory mechanisms. This assumption is emphasised by the observation that human MODY 2 patients, especially those who bear a *GCK* mutation which is associated with severe reduction of glucokinase activity, exhibit a less constrained insulin secretion than expected (Sturis *et al.* 1994). Compensation might be achieved by increased transcription of the wild-type allele, increased translation or stability of the wild-type *Gck* mRNA, or by post-translational mechanisms (Bali *et al.* 1995; Grupe *et al.* 1995; Postic *et al.* 1999). Five of seven published ENU-induced glucokinase mutant mouse strains, which underwent glucokinase activity testing, exhibited a decreased glucose phosphorylating capacity, suggesting that diabetes-associated ENU-induced *Gck* mutations in mice might commonly affect glucokinase activity. Even if only 30% of the naturally occurring *GCK* mutations in subjects with hyperglycaemia have been characterised kinetically,

the majority of the analysed mutations are associated with abnormal glucokinase kinetics. Therefore, mutations in GCK are supposed to predominantly exert their functional consequences by altering glucokinase activity (Gloyn *et al.* 2008; Osbak *et al.* 2009).

5.2.2 Glucokinase RNA expression

Hepatic glucokinase mRNA is reported to be barely present in foetal or neonatal rats. The initial intake of carbohydrates during the suckling-weaning period, coupled with an increase of insulin and a decline of glucagon levels, seems to be the first stimulus for significant glucokinase RNA and protein expression (Bossard *et al.* 1993; Girard *et al.* 1992). Consequentially, relative abundance of the *Gck* transcript was appreciably low in neonatal Munich *Gck*^{M210R} mutant mice, independent of the prevailing genotype. Despite consistent low *Gck* mRNA levels, hepatic *Gck* transcript abundance was strikingly reduced in homozygous mutants, and was also remarkably decreased in heterozygous mutants as compared to wild-type littermates. Reduced glucokinase mRNA levels have also been observed to occur as a consequence of ENU-induced glucokinase mutations in two other hyperglycaemic mouse strains (M-702 and M-475). Furthermore, glucokinase activity in these two mutant mouse strains was decreased to an extent, almost comparable to that in Munich *Gck*^{M210R} mutants. However, M-702 and M-475 mutants exhibited nonsense mutations, introducing premature stop codons. Therefore, the authors suggested that the introduction of premature stop codons might cause mRNA degradation by the nonsense-mediated mRNA decay (NMD) pathway and, consequentially, reduced glucokinase activity. The NMD pathway represents a quality-control mechanism to protect the organism from deleterious dominant-negative or gain-of-function effects, initiated by truncated proteins (Frischmeyer and Dietz 1999; Inoue *et al.* 2004). Therefore, a potential role of the NMD pathway in elimination of mutant mRNA of Munich *Gck*^{M210R} mutants, thereby leading to decreased *Gck* mRNA levels in these animals, cannot be excluded. However, as missense mutations in the glucokinase gene are thought to exert their effects predominantly by altering glucokinase activity and are supposed to unlikely exert dominant negative effects, a potential involvement of the NMD pathway might be argued (Arden *et al.* 2007; Gloyn *et al.* 2008; Takeda *et al.* 1993). In fact, it seems more likely that the reduction of *Gck* mRNA levels in Munich *Gck*^{M210R} mutants might represent an indirect consequence of the mutation-associated

reduced glucokinase activity. As hepatic *Gck* expression is known to be regulated and induced by insulin (Gregori *et al.* 2006; lynesjian *et al.* 1989a; Nospikel and lynesjian 1992), decreased glucokinase activity and therefore, reduced insulin secretion are most likely to account for the downregulation of *Gck* in Munich *Gck*^{M210R} mutants.

5.2.3 Glucokinase protein levels

Western blot analysis from isolated pancreatic islets of 90-day-old heterozygous Munich *Gck*^{M210R} mutants revealed a reduction of glucokinase protein levels of about 28% as compared to wild-type mice, even if this difference was not significant. Reduced glucokinase protein expression has been shown to occur in five of seven investigated glucokinase mutant mouse strains, derived from other ENU mutagenesis projects, whereby only two of these strains (M702 and M-475) exhibited coincident reduction of glucokinase activity and *Gck* expression. From a total number of four mutant mouse strains that bear a reduced glucokinase activity, three strains coincidentally displayed reduced glucokinase protein levels. These findings indicate that in ENU-induced *Gck* mutant mice, reduction of glucokinase activity is often accompanied by diminution of glucokinase protein abundance (Inoue *et al.* 2004; Toye *et al.* 2004).

5.3 Phenotypic characteristics

5.3.1 Heterozygous mutants

Heterozygous mutants of both strains displayed comparable, slightly elevated blood glucose levels already from birth. Consistent with these findings, in human MODY 2 subjects, the diabetic phenotype is proposed to be usually present from birth even if often diagnosed later in life due to its mild peculiarity (Froguel *et al.* 1992; Murphy *et al.* 2008). Blood glucose concentrations deteriorated little until an age of 90 days, remaining stable thenceforth. The diabetic phenotype of Munich *Gck*^{M210R} and *Gck*^{D217V} mutants was mainly characterised by chronic but stable fasting hyperglycaemia from an age of 30 days onwards, accompanied by disturbed glucose tolerance. In mutants of both strains, the area under the blood glucose curve (AUC) during oral glucose tolerance tests was already increased at an age of 30 days. However, in Munich *Gck*^{M210R} mutants of both genders the AUC relative to wild-type

mice further increased with age and was significantly higher in 180-day-old male Gck^{M210R} than in Gck^{D217V} mutants, whereas the AUC of Gck^{D217V} mutants remained stable from an age of 85 days onwards. These findings suggest a trend to a more accelerated diabetic phenotype in Gck^{M210R} than in Gck^{D217V} mutants, which is not unreasonable, considering the slightly stronger diminution of glucokinase activity in Gck^{M210R} mutants.

Since the glucokinase enzyme catalyses the first, rate-limiting step of glycolysis and functions as a glucose sensor in pancreatic β -cells, mutations that alter the enzyme's activity are predicted to affect insulin secretion due to direct alteration of the threshold for glucose-induced insulin secretion (Bedoya *et al.* 1986; Magnuson and Matschinsky 2004). Due to the genetic β -cell secretory defect, MODY 2 subjects usually display altered insulin secretory response to glucose, characterised by a lowered and right-shifted dose-response curve during intravenous glucose tolerance tests. Nevertheless, the first phase of insulin secretion is thought to remain preserved (Bell and Polonsky 2001; Byrne *et al.* 1994; van Haeften *et al.* 1991). Impairment of fasting insulin levels in MODY 2 subjects seems to appear occasionally but is not considered as a common characteristic of the MODY 2 phenotype (Froguel *et al.* 1993; Velho *et al.* 1992). Furthermore, reflecting the β -cell function defect, the HOMA of baseline insulin secretion (HOMA B) is reduced in MODY 2 patients (Martin *et al.* 2008; Murphy *et al.* 2009). Similar to human MODY 2, glucose-induced insulin secretion and the HOMA B were significantly reduced in heterozygous Munich Gck^{M210R} and Gck^{D217V} mutants. Decreased insulin secretion was first detected in 30-day-old Munich Gck^{M210R} mutants, whereas onset of disturbed glucose-induced insulin secretion in Gck^{D217V} mutants was at an age of 85 days. Fasting insulin levels, by contrast, were only diminished in male but not female Munich Gck^{M210R} mutants, probably reflecting the slightly more pronounced diabetic phenotype of male mutants. The phenomenon of sexual dimorphism has been described for several diabetic rodent models (Louet *et al.* 2004) and also appears in human diabetes mellitus (Gale and Gillespie 2001). A positive impact of 17β -oestradiol has been postulated to account for the milder diabetic phenotype in female gender (Le May *et al.* 2006; Louet *et al.* 2004). In contrast, fasting insulin levels of Munich Gck^{D217V} mutants were only slightly and not consistently diminished, and no gender dependency was observable. Furthermore, recapitulating the distinct degrees of glucokinase activity

reduction, reduction of delta insulin secretion relative to wild-type mice was considerably more pronounced in Munich Gck^{M210R} than in Gck^{D217V} mutants for the main period of investigation. Defects of glucose-induced insulin secretion have also been proven to arise from other ENU-induced Gck mutations and are generic findings in heterozygous global and β -cell specific, but not in liver-specific Gck knockout mouse models (Bali *et al.* 1995; Grupe *et al.* 1995; Inoue *et al.* 2004; Postic *et al.* 1999). Fasting insulin levels in these mouse models were either not specified (Inoue *et al.* 2004; Toye *et al.* 2004) or were not significantly altered (Bali *et al.* 1995; Grupe *et al.* 1995; Postic *et al.* 1999). However, age groups for determination of insulin levels in Gck knockout mice were quite inhomogeneous (Postic *et al.* 1999), and fasting insulin levels were also appreciably reduced in these animals (Terauchi *et al.* 1995).

The role of insulin resistance in long-term evolution of disorders, like monogenic forms of β -cell dysfunction is discussed controversially. Some authors defend the distinction of MODY from type 2 diabetes mellitus by the absence of characteristics of the metabolic syndrome (i.e. among others insulin resistance) (Argawal *et al.* 2002; Murphy *et al.* 2008). Nevertheless, the broad opinion has been established that even if insulin resistance does not represent the primary genetic defect in MODY, impaired insulin sensitivity may contribute to chronic hyperglycaemia in some MODY subtypes (Hattersley and Pearson 2006; Winter 2003). Studies from 125 MODY 2 patients and 14 unaffected first-degree relatives revealed lowered insulin sensitivity in some GCK -deficient probands (Clement *et al.* 1996). Furthermore, long-term follow-up studies showed that MODY 2 patients, whose glucose tolerance deteriorated over time, displayed a significantly decreased HOMA of insulin sensitivity (HOMA %S) as compared to those with impaired but stable glucose tolerance (Martin *et al.* 2008). In contrast to the HOMA B, which was markedly decreased in heterozygous Munich Gck^{M210R} and Gck^{D217V} mutants, the HOMA of insulin resistance, indicating insulin sensitivity, was unaltered in both strains and even appeared slightly decreased in male heterozygous Gck^{D217V} mutants. In contrast, heterozygous male Munich Gck^{M210R} mutants exhibited a delayed response to exogenous insulin from an age of 90 days onwards. Although the HOMA of beta cell function indices were developed to assess β -cell function in human beings (Katz *et al.* 2000; Wallace *et al.* 2004), a linear correlation between insulin sensitivity,

determined during hyperinsulinaemic euglycaemic clamp studies in insulin resistant mice, and the surrogate index HOMA IR has been shown (Lee *et al.* 2008). Thus, male Munich Gck^{M210R} mutants should not be considered insulin resistant, whereas the presence of slightly impaired insulin sensitivity might not be argued. Munich Gck^{D217V} mutants of both genders also displayed a less pronounced decrease of blood glucose levels relative from basal after intraperitoneal insulin application, but in contrast to male Munich Gck^{M210R} mutants, the delayed response did not occur consistently. Taken together with the even decreased HOMA IR, insulin sensitivity seemed not to be constrained in mutants of this strain, albeit mildly impaired insulin sensitivity can not be definitely excluded. Consistent with these findings, sensitivity to exogenous insulin has been reported to be normal or slightly decreased in other ENU-induced Gck mutants (Inoue *et al.* 2004). In Gck knockout mice, by contrast, observations concerning insulin sensitivity vary in dependence on the prevailing nature of Gck disruption. While enhanced insulin sensitivity was suggested for global Gck deficiency, mild insulin resistance was detected in mice lacking hepatic Gck . In these mice, additional metabolic disturbances due to the loss of liver Gck were suggested to lead to impaired peripheral glucose utilisation and insulin action (Grupe *et al.* 1995; Postic *et al.* 1999).

5.3.2 Homozygous mutants

Homozygous or compound⁷ heterozygous mutations in human GCK are known to be associated with low birth weight and neonatal diabetes mellitus (NDM) (Osbak *et al.* 2009; Porter and Barrett 2005; Waterfield and Gloyn 2008). In contrast to the common findings in NDM subjects, birth weights of homozygous Munich Gck^{M210R} and Gck^{D217V} mutants were unaltered. However, homozygous Gck^{M210R} mutants exhibited marked growth retardation and barely gained weight within the first days *post partum*, whereas body weight development of homozygous Gck^{D217V} mutants was unaltered in the first days of life. As it has already been proven *in vitro* (Njolstad *et al.* 2001), homozygous M210 mutations are predicted to strikingly lower glucokinase activity, so that a similar reduction can be assumed for homozygous Munich Gck^{M210R} mutants. Therefore, the disability to secrete adequate quantities of insulin, which is widely known to be one of the most important growth determinants

⁷ Compound heterozygous mutations are characterised by the presence of 2 different mutant alleles at the 2 copies of an appointed locus (Silver 1995).

during early postnatal development (Avery *et al.* 2005), most likely accounts for the reduced postnatal growth in homozygous Gck^{M210R} mutants. Studies in growth retarded homozygous mice that lack the β -cell-specific isoform of Gck showed that insulin or oral antidiabetic treatment resulted in body weight gain almost comparable to wild-type mice (Terauchi *et al.* 1995). From the age of weaning - with the beginning of carbohydrate intake - homozygous Munich Gck^{D217V} mutants also exhibited delayed body weight gain as compared to heterozygous mutants and wild-type mice. As hepatic glucokinase activity is known to dramatically increase during the suckling-weaning transition in rats (Walker and Holland 1965), it is not unreasonable to suppose that growth retardation in Gck^{D217V} mutants might initially manifest during the post-weaning period due to the expected higher residual activity of the mutant glucokinase enzyme in homozygous Munich Gck^{D217V} mutants as compared to Munich Gck^{M210R} mutants. Blood glucose levels of neonatal homozygous mutants were markedly increased, whereby homozygous Munich Gck^{M210R} mutants exhibited dramatic hyperglycaemia already at birth with daunting aggravation of the diabetic phenotype within the first days of life. Homozygous Gck^{D217V} mutants exhibited lower blood glucose levels and a less pronounced increase of blood glucose concentrations than homozygous Munich Gck^{M210R} mutants. The phenotypic differences between Gck^{M210R} and Gck^{D217V} mutants may be explained by the differences in the severity of glucokinase enzyme impairment, which is known to correlate with the degree of hyperglycaemia (Lowe 1998). The different degrees of hyperglycaemia also influenced life span. While homozygous Gck^{M210R} mutants showed a significantly reduced life span and died not later than at 6 days of age, life span was not constrained in homozygous Gck^{D217V} mutants. As downstream products of glucose metabolism enter the mitochondrial respiratory chain, which uses them to generate adenosine triphosphate (ATP) (Langin 2001), the glucokinase enzyme exerts a crucial impact on energy metabolism in cells. Therefore, homozygous Gck^{M210R} mutants likely died from fatal energy deprivation and hyperglycaemia, rising up from presumably marginal glucokinase activity. Survival studies in homozygous Gck -deficient mice demonstrated a crucial effect of global or β -cell-specific, but not of hepatic Gck ablation on animal viability. Mice that lack either the β -cell-specific or both isoforms developed marked hyperglycaemia and growth retardation, comparable to homozygous Munich Gck^{M210R} mutants, and died *in utero* or between day 3 and 7 *post partum* (Bali *et al.* 1995; Postic *et al.* 2001). The

complete loss of hepatic *Gck* was neither lethal nor exerted any effect on body weight development and resulted only in mild hyperglycaemia (Bali *et al.* 1995; Grupe *et al.* 1995; Postic *et al.* 1999; Terauchi *et al.* 1995). Other ENU-induced *Gck* mutant mouse strains either exhibited similar perinatal lethality, which was thought to result from extreme hyperglycaemia and growth retardation, or survived at least 5 to 12 weeks, depending on the mutation (Inoue *et al.* 2004; Toyé *et al.* 2004). These data emphasise either strong and specific or combined effects of *Gck* mutations on glucokinase structure and/or function (exon skipping, distortion of the glucokinase protein, impairment of glucokinase activity, reduction of glucokinase RNA and protein expression (Inoue *et al.* 2004)) to account for the different phenotypic outcomes and survival rates in the affected mouse models. Even if blood glucose levels of homozygous Munich *Gck*^{D217V} mutants were strongly increased from the time point of weaning onwards, disturbances in glucose homeostasis deteriorated very little with age, and blood glucose concentrations remained considerably stable. A study in human NDM patients recently demonstrated the occurrence of divergent phenotypes due to different *GCK* mutations. The authors suggested that less deleterious diabetic phenotypes might be associated with residual glucokinase activity, high enough to keep β -cells viable and to marginally preserve insulin secretion (Bakri *et al.* 2004). Thus, glucokinase activity in homozygous Munich *Gck*^{D217V} mutants, which still owed 16% of the wild-type enzyme activity, would be sufficient to prevent fatal hypoinsulinaemia and enable marginal but stable maintenance of blood glucose homeostasis. In contrast, the phosphorylation activity in homozygous *Gck*^{M210R} mutants, which is suggested to be almost absent (Aguilar-Bryan and Bryan 2008) would not be sufficient to preserve animal viability.

5.4 Specific organ alterations

5.4.1 Liver

Homozygosity in Munich *Gck*^{M210R} mutants was not only associated with fatal hyperglycaemia, growth retardation, and perinatal death, but also led to hepatic alterations. Under normal conditions, hyperglycaemia inhibits hepatic glucose production and stimulates hepatic glucose uptake and glycogen synthesis by enhancing glucose phosphorylation rate and thereby, the flux through glucokinase (Postic *et al.* 2001; Radziuk and Pye 2001). Due to impaired hepatic glucose

phosphorylation capacity, livers from 4-day-old homozygous Gck^{M210R} mutants were almost depleted of glycogen, reflecting almost absent glycogenesis in these animals. With regard to the protruding role of glycogen in the energy metabolism of neonates (Cornblath and Schwartz 1976), an additional fatal consequence of a defective glucokinase function on postnatal development is emphasised. Homozygous Gck^{M210R} mutants also exhibited vast hepatocyte vacuolisation, and fat red staining revealed massive steatosis. Mice that totally lack insulin (generated by targeted ablation of the Insulin 1 (*Ins1*) and Insulin 2 (*Ins2*) gene) exhibited similar perinatal hepatic steatosis that was rescued by insulin application (Duvillie *et al.* 1997). Thus, the fatty liver phenotype in homozygous Munich Gck^{M210R} mutants most likely resulted from insufficient insulin secretion. Hepatic lipid accumulation may arise from the lack of NAD^+ regeneration from downstream metabolites (pyruvate) of glycolysis in the tricarboxylic acid cycle (TCA or Krebs cycle). As β -oxidation of fatty acids requires NADH as coenzyme, inhibition of this catabolic pathway might be causative for steatosis, observed in homozygous Munich Gck^{M210R} mutants (Moradpour 2006). Glycogen deprivation and steatosis also occurred in homozygous global or β -cell-specific *Gck* knockout mice, and was diagnosed in two of three ENU-induced *Gck* mutant strains that exhibited perinatal lethality. In the respective knockout models, steatosis was additionally accompanied by hypertriglyceridaemia and hypercholesterinaemia (Grupe *et al.* 1995; Inoue *et al.* 2004; Postic *et al.* 1999). In contrast to the identified liver changes of homozygous Munich Gck^{M210R} mutants and other mouse models of deficient glucokinase function, hepatic steatosis and decreased glycogen content were absent in the two homozygous M210K carriers (Njolstad *et al.* 2001). However, hypertriglyceridaemia and hypercholesterinaemia have been reported to occur, albeit representing a rare complication, in MODY 2 subjects (Velho *et al.* 1997). Therefore, it cannot be excluded that the same alterations may represent common features in homozygous *GCK* mutation carriers, but have not yet been diagnosed due to the minor prevalence of *GCK*-NDM and the resulting lack of clinical studies (Edghill *et al.* 2008; Osbak *et al.* 2009; Vaxillaire *et al.* 2002).

5.4.2 Endocrine pancreas

Although in human beings, the “glucokinase disease” MODY 2 represents a well known diabetic phenotype, few perceptions about the pathomorphology of this

putative mild disorder and the impact of glucokinase gene mutations on the integrity of the endocrine pancreas are existing (Zelent *et al.* 2005). Even though morphologic alterations of the endocrine pancreas are reported to arise in some MODY subtypes (Johnson 2007), knowledge about the specific impact of glucokinase gene mutations on endocrine pancreatic integrity and mass is bare. The occurrence of endocrine pancreas alterations in other MODY subtypes emerges from the crucial involvement of the affected transcription factors in elementary pathways of pancreas development and maintenance and their implication in β -cell differentiation and/or apoptosis (Johnson 2007). Even if β -cell depletion, as observable in other MODY subtypes, has been speculated to be absent in MODY 2 patients, particular studies about the influence of glucokinase aberrations on maintenance, adaption, and turnover of the endocrine pancreatic mass are lacking.

Glucose has already been shown to represent a critical determinant of endocrine pancreas mass by influencing β -cell replication and apoptosis in a time and dose-dependent fashion (Alonso *et al.* 2007; Kim *et al.* 2005). Therefore, Gck^{M210R} mutants and wild-type littermates were chosen to first undergo qualitative histological and quantitative stereological analysis of the pancreas at the first day *post partum* to exclude the influence of phenotypic traits such as hyperglycaemia. The total pancreas and β -cell volumes did not significantly differ between the respective genotypes, although a marginally reduced β -cell mass was identified in homozygous Munich Gck^{M210R} mutants. These findings indicate that the identified mutation, especially in heterozygous mutants, does not affect endocrine pancreas development and integrity, albeit, a subtle, but not decisively identifiable effect on β -cell mass in homozygous mutants might not be excluded. By contrast, male heterozygous mutants at an age of 210 days exhibited an about 30% reduced total islet and total β -cell volume as compared to wild-type mice. Both parameters were unchanged in female mutants, whose β -cells are probably protected by 17β -oestradiol (Le May *et al.* 2006). Since the total β -cell volume was unaltered in neonatal heterozygous mutants, islet and β -cell mass reduction in adult male mutants is not a direct consequence of the causative mutation. Isolated β -cells (single, scattered insulin⁺ cells, endocrine cells budding from ducts and extra-islet insulin⁺ cell clusters (EICs) are considered as a parameter for new islet formation (Bonner-Weir 2001; Butler *et al.* 2003; Herbach *et al.* 2005; Kauri *et al.* 2007). Thus, a coincident reduction of the

total volume of isolated β -cells of male heterozygous mutants of about 30% suggests that reduced islet- and β -cell mass, observed in male mutants, emerge from impaired islet neogenesis. This assumption is supported by the absence of any apoptotic event in pancreatic islets of 90-day-old heterozygous Munich Gck^{M210R} mutants, as evinced by Western blot analysis of the inactive and active form of caspase-3. Nevertheless, detection and quantification of apoptosis in β -cells has already been reported to represent a real challenge. Although the process of β -cell destruction is extended over weeks or months, only few (2-7%) apoptotic β -cells are likely to be observable even in mouse models of severe β -cell destruction (Augstein *et al.* 1998; O'Brien *et al.* 1996). The difficulty in quantification of β -cell apoptosis is supposed to result from the nature of apoptosis kinetics. Apoptosis is an extremely rapid process, with only few minutes elapsing from initiation to complete disintegration of the cell (Butler *et al.* 2003). Immediate clearance of apoptotic cells by phagocytosis is also known to be executed in an accelerated fashion, although the time frame varies depending on the respective tissue (Coles *et al.* 1993; Platt *et al.* 1998; Tanaka 2005). For this reason one might hypothesise that in case of only moderate β -cell destruction, apoptosis may be undetectable.

Over the last decades there is increasing evidence that, from embryogenesis to adulthood, the endocrine pancreas represents a dynamic, in adult life slowly renewing tissue. Beta cell mass is determined by the balance between replication, neogenesis and apoptosis - under physiological conditions and in response to varying secretory demand (Ackermann and Gannon 2007; Nielsen *et al.* 2001). The factors involved in regulating β -cell mass are numerous (Ackermann and Gannon 2007), but the potent stimulatory effect of glucose and insulin on expansion of β -cell mass *in vivo* (Bernard *et al.* 1999; Paris *et al.* 2003) and *in vitro* (Rabinovitch *et al.* 1982; Schuppin *et al.* 1993) substantiates a central impact of glucose metabolism and insulin-signalling pathway on endocrine pancreatic mass expansion. Islet neogenesis and β -cell proliferation from pre-existing β -cells are reported to be the main mechanisms of these adaptive changes (Ackermann and Gannon 2007; Bouwens and Kloppel 1996; Paris *et al.* 2004).

For one of these mechanisms, glucokinase has already been shown to be essential. Mice, haploinsufficient for pancreatic Gck , failed to increase β -cell mass in response to a high-fat diet, whereas wild-type controls developed compensatory β -cell

hyperplasia. However, in contrast to Munich Gck^{M210R} mutant mice, no reduction of β -cell mass or islet size was detected in β -cell-specific heterozygous Gck knockout mice vs. wild-type mice when fed a standard chow (Terauchi *et al.* 2007). As the genetic background has a great influence on the occurrence of an aberrant phenotype (Andrikopoulos *et al.* 2005), these different observations might be explained by the different genetic background of the Gck mutants. Additionally, parameters of islet neogenesis and the influence of complete absence of β -cell glucokinase on the integrity of the endocrine pancreas were not investigated in these knockout models.

Recent studies suggest a detrimental influence of glucokinase on endocrine pancreas mass dynamics by demonstrating that glucokinase is involved in glucotoxicity-induced β -cell death via induction of Bad dephosphorylation and Bax- and Bad-mediated apoptosis (Danial *et al.* 2003; Danial *et al.* 2008; Kim *et al.* 2005). Lee *et al.* (2009) specified the critical role of glucokinase in metabolic stress-related apoptosis by evincing that impairment of mitochondrial function *in vitro* (MIN6N8 cells) leads to glucokinase downregulation, defective insulin secretion and apoptosis. These events could be blocked by either antioxidant treatment or glucokinase overexpression (Lee *et al.* 2009; Tsuruzoe *et al.* 1998). The coincident reduction of islet- and β -cell mass without altered volume fraction of β -cells in islets of male heterozygous Munich Gck^{M210R} mutants would imply that whole islets were destroyed by apoptosis. In contrast, selective β -cell destruction is considered to represent the final outcome in type 1 and 2 diabetes mellitus in human beings (Andre-Schmutz *et al.* 1999; Cnop *et al.* 2005; Yoon *et al.* 2003). Therefore, impaired islet neogenesis rather than enhanced apoptosis most likely accounts for islet and β -cell mass reduction in male heterozygous Munich Gck^{M210R} mutants.

Male heterozygous Munich Gck^{D217V} mutants at an age of 550 days displayed an only marginal reduction of the total islet and β -cell volumes, reflecting the slightly milder diabetic phenotype as compared to Munich Gck^{M210R} mutants. Morphologic alterations of the endocrine pancreas of male homozygous mutants were more pronounced and mainly characterised by considerably reduced islet and β -cell mass and an only slightly decreased volume fraction of β -cells in the islets.

Oxidative-stress mediated apoptosis, arising from insulin resistance and chronic

overstimulation of β -cells by hyperglycaemia, is considered to represent one of the most important contributors to β -cell loss in type 2 diabetes mellitus (Cnop *et al.* 2005; Donath *et al.* 2005; Mandrup-Poulsen 2003; Rhodes 2005). In contrast, the relevance of glucotoxicity in the pathogenesis of MODY 2 is discussed controversially. On the one hand it has been shown that insulin sensitivity and insulin secretion can almost be restored by exposure of pancreatic islets, isolated from *Gck*-deficient mice, to high glucose concentrations for 48-96 hours (Sreenan *et al.* 1998). On the other hand, enhanced apoptosis and downregulation of the glucokinase gene were observed after exposure of MIN6 cells and primary islet cells to high glucose concentrations for the same period (Kim *et al.* 2005). Nevertheless, the lack of detailed *in vivo* studies about the effect of long-term exposure to mild hyperglycaemia on endocrine pancreas integrity and the absence of morphometric data from *Gck*-deficient mice or homozygous *Gck* mutants of other ENU mouse strains, impede definite interpretation of the morphologic alterations in Munich *Gck*^{D217V} mutants. However, as a time- and dose dependent detrimental influence of excess glucose on pancreatic β -cell viability was proposed (Kim *et al.* 2005; Robertson *et al.* 2003), increased apoptosis, arising from prolonged exposure of β -cells to elevated glucose levels, might be causative for the reduction of β -cell mass at least in homozygous Munich *Gck*^{D217V} mutants.

Considering the early onset of hyperglycaemia, the severity of the diabetic phenotype and the stable maintenance of strikingly elevated blood glucose levels throughout life, islet and β -cell mass reduction was appreciably moderate in homozygous *Gck*^{D217V} mutants. Other diabetic mouse models, displaying comparable degrees of glycaemia developed considerably more accentuated endocrine pancreas alterations in a shorter period of time. Two mutations in the insulin 2 gene (*Ins2*), both leading to the loss of disulfide bonds within the insulin molecule, have been reported in mouse models of severe, progressive hyperglycaemia and extensive β -cell depletion: the Akita mouse and the Munich *Ins2*^{C95S} mutant mouse. Male heterozygous Munich *Ins2*^{C95S} mutants at an age of 180 days exhibited a strikingly reduced islet and β -cell volume and an 80% reduced β -cell volume fraction. The accelerated β -cell depletion in islets of this mouse model in opposition to the relative discrete β -cell loss in homozygous Munich *Gck*^{D217V} mutants suggests additional specific effects that trigger β -cell loss in *Ins2* mutants. As both *Ins2* mutations are predicted to induce

misfolding of the mutated protein, endoplasmic reticulum stress was supposed to major account for the β -cell loss and the progression of hyperglycaemia in both mouse models (Herbach *et al.* 2007; Wang *et al.* 1999; Yoshioka *et al.* 1997; Zuber *et al.* 2004). A current study with insulin treated male Munich $Ins2^{C95S}$ mutants stresses the additional involvement of chronic hyperglycaemia in the development of β -cell damage in this mouse model (personal communication Sabine Kautz and Dr. Nadja Herbach). Even if endoplasmic reticulum stress and components of the unfolded protein response are considered to play an important part in triggering β -cell apoptosis in diabetes mellitus (Eizirik *et al.* 2008; Waterfield and Gloyn 2008), glucokinase mutations have not been reported to induce protein misfolding in human beings and rodent models so far. Thus, the potential absence of endoplasmic reticulum stress in homozygous Munich Gck^{D217V} mutants might account for the considerable stable phenotype and the relatively moderate reduced islet- and β -cell masses. However, a possible participation of disturbed islet neogenesis, as it is supposed to account for endocrine mass alterations in male heterozygous Munich Gck^{M210R} mutants, may also play a role in Munich Gck^{D217V} mutants. Thus, further investigations are necessary to allocate the impact of Gck mutations and the associated different degrees of hyperglycaemia to the identified endocrine pancreas alterations.

Taken together, glucokinase may have an important impact on the balance between β -cell renewal and death and, therefore, on endocrine pancreas plasticity.

5.5 Conclusion and further prospects

The creation of two Gck alleles in the ENU strains GLS001 (Munich Gck^{M210R} mutant mouse) and GLS006 (Munich Gck^{D217V} mutant mouse) and the resulting phenotypic similarities and differences provide the opportunity to analyse specific effects of distinct, but closely neighboured mutations in Gck , and to elucidate the complexity of the “glucokinase disease” concerning clinical and pathomorphological aspects. Both profoundly characterised mutant mouse strains provided unforeseen insights into the undiscovered pathomorphology of Gck mutations. Furthermore, this study represents the first report of unrestricted life span of homozygous Gck mutants. The viability of homozygous Munich Gck^{D217V} mutants therefore enables detailed long-term studies to elucidate clinical and pathomorphological aspects of human NDM.

Monogenic diabetes in general is supposed to be often misdiagnosed as type 1 or type 2 diabetes mellitus (Singh 2006). Further, the inheritance of a *GCK* mutation in human beings does not exclude the concurrent development of type 2 diabetes mellitus later in life, which occurs at a similar prevalence in those with *GCK* mutations as in the general population (up to 50% of the affected persons develop overt diabetes (Murphy *et al.* 2008; Olek 2006)). For this reason, even if large-scale population studies are lacking, the number of undiagnosed MODY 2 patients might be higher than estimated. A recent study with 798 human subjects at high risk for MODY unveiled the difficulties to distinguish *GCK*-mutation from non-mutation carriers by means of clinical diagnostic criteria alone. Further, in case of rigid application of the 4 screening criteria for MODY, elaborated by the European Molecular Genetics Quality Network (EMQN) (refer to chapter 2.6.5) (Ellard *et al.* 2008), none of the participating *GCK*-mutation carriers would have been identified as MODY 2 patient (Gloyn *et al.* 2009). These findings emphasise the assumption that MODY 2 in human subjects might be often misdiagnosed or even may remain undiagnosed. The molecular definition of the genetic aetiology, especially in MODY 2 subjects, allows the development of specific treatment regimes and provides the opportunity to reliably prevent long-term disease progression. Therefore, some authors emphasise the indispensability of genetic testing not only in specific risk populations (familiar history of diabetes, asymptomatic fasting hyperglycaemia etc.) (Codner *et al.* 2006; Osbak *et al.* 2009; Singh 2006). Further, small molecule activators of the glucokinase enzyme are not only applicable in therapy of MODY 2, but are also considered to represent potential therapeutics for other forms of diabetes mellitus (Matschinsky 2009; Sarabu and Grimsby 2005; Sarabu *et al.* 2007). Thus, both profoundly characterised *Gck* mutant mouse models are thought to be valuable to study the roles of *Gck*, disturbed glucose homeostasis and mild hyperglycemia in endocrine pancreatic mass dynamics, for the development of strategies for early diagnosis, and the development of potential novel therapeutics. Consequentially, both mouse strains represent sophisticated models for translational diabetes research.

Further clarification of the specific and/or combined functional consequences of the respective *Gck* mutations in both ENU-induced mutant strains will require additional investigations of *Gck* mRNA and protein levels in both liver and pancreatic β -cells of

90-day-old mice to allocate the results to glucokinase activity levels. Additionally, an intraperitoneal glucose tolerance test should be considered to assess the first phase of glucose-induced insulin secretion, which is usually preserved in MODY 2 patients. Addressing the question of serum insulin levels in suckling mice, especially in homozygous mutants, represents another extremely interesting task. The absence of apoptosis in pancreatic islets of Munich Gck^{M210R} mutants should be further verified by histological methods (e.g. TdT-mediated dUTP-biotin nick end labelling; TUNEL). Moreover, morphometric evaluation of the endocrine pancreas from 4-day-old homozygous Munich Gck^{M210R} mutants, which displayed already fatal hyperglycaemia at this age, may be performed to examine the effect of short-term but extremely surpassing glucose levels on postnatal pancreas development in these animals.

6. Summary

Several diabetic mouse strains have been generated in the Munich ENU (*N*-ethyl-*N*-nitrosourea) mouse mutagenesis screen, representing suitable models for functional genome analysis in diabetes research. The aim of the present study was to identify the causative mutation of two of these strains (GLS001 and GLS006) and to characterise the resulting diabetic phenotype. For phenotypic characterisation, diabetic GLS001 and GLS006 mice were bred on the C3HeB/FeJ inbred genetic background. The causative mutation was mapped to a defined chromosomal region by linkage analysis. Subsequently, candidate gene sequence analysis was performed to identify the respective mutations. Clinical and pathomorphological analyses comprised regular screening of glucose homeostasis, determination of body and organ weights, and qualitative histological and quantitative stereological investigations of the pancreas. Specification of the functional consequences of the respective mutations was carried out with isolated pancreatic islets and liver homogenate from homozygous and heterozygous mutants and wild-type littermates by quantitative real-time PCR, Western blot analysis, and determination of glucokinase activity. Linkage analysis mapped the diabetic phenotype of both strains to a polymorphic marker on chromosome 11 at 5.9 and 7.1 Mb, respectively. Candidate gene sequencing of the positional glucokinase (*Gck*) gene disclosed a missense mutation in exon 6 of *Gck* in both strains. The ENU strain GLS001 bears a T to G transversion at nucleotide position 629 of *Gck*, leading to an amino acid exchange from methionine to arginine at position 210 (Munich *Gck*^{M210R} mutant mouse), whereas in GLS006 mice, an A to T transversion at nucleotide position 650 was identified, resulting in an amino acid exchange from aspartic acid to valine at position 217 (Munich *Gck*^{D217V} mutant mouse). Analogous mutations in human beings are associated with two autosomal dominant hereditary forms of diabetes mellitus. Heterozygous mutations are associated with maturity-onset diabetes of the young, type 2 (MODY 2), whereas homozygous mutations lead to neonatal diabetes mellitus (NDM). The mutations of both strains resulted in a significantly decreased hepatic glucokinase activity, whereas islet glucokinase protein abundance was unaltered in Munich *Gck*^{M210R} mutants. Further, *Gck* transcript abundance was appreciably decreased in neonatal Munich *Gck*^{M210R} mutants. Heterozygous mutants of both strains exhibited a MODY

2-like diabetic phenotype, characterised by mild, non-progressive fasting hyperglycaemia, a disturbed glucose tolerance, and an impaired glucose-induced insulin secretion. Further, male heterozygous Munich Gck^{M210R} mutants exhibited a delayed response to exogenous insulin, whereas insulin sensitivity was almost unaltered in Munich Gck^{D217V} mutants. In contrast to heterozygous mutants, homozygous mutants displayed strongly elevated blood glucose levels already from birth. Homozygous Munich Gck^{M210R} mutants showed growth retardation, liver steatosis, and a dramatic deterioration of hyperglycaemia within the first days *post partum*, leading to premature death within the first six days of life. In contrast, Munich Gck^{D217V} mutants exhibited normal postnatal development, blood glucose increase was less accentuated, and life span of homozygous Gck^{D217V} mutants was not restrained. Quantitative stereological analyses revealed a 30% reduction of islet and β -cell mass in male, but not female heterozygous Munich Gck^{M210R} mutants at an age of 210 days. The additional reduction of the total volume of isolated beta cells and the absence of apoptosis indicated that disturbed islet neogenesis might be causative for islet mass reduction in male Munich Gck^{M210R} mutants. The total islet and β -cell volumes were considerably decreased in 550-day-old male homozygous Munich Gck^{D217V} mutants, whereas these changes were only discrete in male heterozygous mutants. The coincident slight reduction of the volume fraction of β -cells in the islets of homozygous mutants indicated an additional selective β -cell loss, most likely as a consequence of prolonged exposure to elevated blood glucose levels.

Regarding the assumed number of undiagnosed MODY 2 patients and the lack of detailed clinical studies in human beings, these profoundly characterised diabetic mouse strains represent valuable models for the functional analysis of Gck . Further, both models enable long-term studies of relevant aspects of human MODY 2/NDM, the elaboration of strategies for early diagnosis, and the development of new treatment strategies.

7. Zusammenfassung

Klinische und pathomorphologische Charakterisierung zweier diabetischer Mausmodelle aus dem Münchener ENU-Mausmutageneseprojekt

Im Münchener ENU- (*N*-ethyl-*N*-nitrosoharnstoff) Mausmutageneseprojekt wurden mehrere diabetische Mauslinien generiert, die wertvolle Tiermodelle für die funktionale Genomforschung darstellen. Ziel der vorliegenden Studie war es, zwei dieser diabetischen Mauslinien (GLS001 und GLS006) hinsichtlich der zugrunde liegenden Mutationen und des daraus resultierenden diabetischen Phänotypes klinisch und pathomorphologisch zu untersuchen. Heterozygote Mutanten der Linien GLS001 und GLS006 wurden auf dem genetischen Hintergrund des Inzuchtstammes C3HeB/FeJ gezüchtet. Nach Eingrenzung der chromosomalen Lokalisation der ursächlichen Mutationen durch die Kopplungsanalyse erfolgte die Auswahl und Sequenzierung des Kandidatengens, die zur Identifizierung der Mutationen führte. Die klinische und pathomorphologische Untersuchung umfasste die regelmäßige Analyse Diabetes-relevanter Parameter, die Bestimmung von Körper- und Organgewichten, sowie qualitativ-histologische und quantitativ-stereologische Untersuchungen des Pankreas. Die funktionalen Auswirkungen der Mutationen wurden in isolierten Pankreasinseln und Leberhomogenat mittels quantitativer real-time PCR, Westernblotanalysen, und Glucokinase-Enzymaktivitätsbestimmung spezifiziert. Die Kopplungsanalyse ergab bei Mutanten beider Mauslinien eine eindeutige Kopplung des diabetischen Phänotyps zu polymorphen DNA-Markern auf dem Chromosom 11 im Bereich von 5,9 beziehungsweise 7,1 Mb. Bei der Sequenzierung des Kandidatengens Glucokinase (*Gck*) wurde bei beiden Mauslinien eine definierte Punktmutation im Exon 6 des *Gck* identifiziert. Bei der ursächlichen Mutation der ENU-Mauslinie GLS001 handelt es sich um eine T zu G Transversion an Nukleotidposition 629, welche zu einem Aminosäureaustausch von Methionin zu Arginin an Position 210 führt (Munich *Gck*^{M210R} Mutante). Die ENU-Linie GLS006 besitzt eine A zu T Transversion an Nukleotidposition 650, die zu einem Aminosäureaustausch von Asparaginsäure zu Valin an Position 217 führt (Munich *Gck*^{D217V} Mutante). Entsprechende Mutationen führen beim Menschen zu zwei verschiedenen, autosomal dominant vererbten Formen des Diabetes mellitus. Heterozygote Mutationen führen zu maturity-onset diabetes of the young, type 2

(MODY 2), wohingegen homozygote Mutationen mit neonatalem Diabetes mellitus (NDM) assoziiert sind. Die Mutationen sind bei beiden mutanten Mauslinien mit einer signifikanten Reduktion der Glucokinase-Enzymaktivität verbunden, wohingegen die Glucokinase-Proteinmenge in den Pankreasinseln von Munich Gck^{M210R} Mutanten unverändert war. Bei neonatalen Munich Gck^{M210R} Mutanten führt die Mutation darüber hinaus zu einer deutlich reduzierten Gck Transkriptabundanz. Heterozygote Mutanten beider Mauslinien entwickelten einen milden, dem MODY 2 des Menschen ähnlichen diabetischen Phänotyp, der charakterisiert ist durch konstant erhöhte Nüchternblutglukose, eine gestörte Glukosetoleranz und eine verminderte glukoseinduzierte Insulinsekretion. Außerdem zeigten männliche heterozygote Munich Gck^{M210R} Mutanten eine leicht verzögerte Senkung der Blutglukosewerte nach Insulinapplikation, wohingegen die Insulinsensitivität bei Munich Gck^{D217V} Mutanten nicht merklich eingeschränkt war. Homozygote Mutanten hingegen entwickelten einen stärker ausgeprägten diabetischen Phänotyp mit stark erhöhten Blutglukosewerten vom Zeitpunkt der Geburt an. Homozygote Munich Gck^{M210R} Mutanten zeigten Wachstumsverzögerung, Lebersteatose, eine dramatische Progression der Hyperglykämie und starben innerhalb der ersten sechs Lebenstage. Bei homozygoten Munich Gck^{D217V} Mutanten hingegen war die postnatale Entwicklung nicht verändert, der Anstieg der Blutglukosewerte war geringer ausgeprägt und die Lebensdauer war nicht eingeschränkt. Die quantitativ-stereologische Untersuchung des Pankreas ergab eine 30%ige Reduktion der Insel- und Betazellmasse bei männlichen, nicht jedoch bei weiblichen heterozygoten Munich Gck^{M210R} Mutanten in einem Alter von 210 Tagen im Vergleich zu Wildtyp-Kontrolltieren. Die gleichzeitige Reduktion des Gesamtvolumens der isolierten Betazellen und das Fehlen erhöhter Apoptoseaktivität weisen darauf hin, dass eine gestörte Inselneogenese ursächlich für die Reduktion des Gesamtinsel- und Betazellvolumens sein könnte. Bei homozygoten Munich Gck^{D217V} Mutanten in einem Alter von 550 Tagen war die Insel- und Betazellmasse deutlich, bei heterozygoten Mutanten nur geringgradig reduziert. Der leicht verminderte Volumenanteil der Betazellen in den Inseln bei homozygoten Mutanten weist darüber hinaus auf einen zusätzlichen selektiven Betazellverlust hin, der Folge der anhaltenden Exposition der Betazellen gegenüber erhöhten Blutglukosewerten sein könnte.

In Anbetracht der geschätzten Dunkelziffer nicht diagnostizierter MODY 2 Patienten

und dem Mangel an detaillierten klinischen Studien stellen beide ausführlich charakterisierten Mauslinien wertvolle Modelle für funktionale Studien des *Gck* dar. Weiterhin können beide Modelle für Langzeitstudien relevanter Aspekte des humanen MODY 2/NDM, für die Erarbeitung von Strategien zur Früherkennung und die Entwicklung potenzieller neuer Therapeutika dienen.

8. References

- Acevedo-Arozena, A., Wells, S., Potter, P., Kelly, M., Cox, R.D. and Brown, S.D. (2008) ENU mutagenesis, a way forward to understand gene function. *Annu Rev Genomics Hum Genet* 9, 49-69.
- Ackermann, A.M. and Gannon, M. (2007) Molecular regulation of pancreatic β -cell mass development, maintenance, and expansion. *J Mol Endocrinol* 38, 193-206.
- Agius, L., Aiston, S., Mukhtar, M. and Iglesia, N.d.I. (2001) GKRP/GK: Control of metabolic fluxes in hepatocytes. In: *Glucokinase and Glycaemic Disease: From Basics to Novel Therapeutics*
Eds: F.M. Matschinsky and M.A. Magnuson, Karger, Basel. pp 208-221.
- Aguilar-Bryan, L. and Bryan, J. (2008) Neonatal diabetes mellitus. *Endocr Rev* 29, 265-291.
- Aigner, B., Rathkolb, B., Herbach, N., Hrabé de Angelis, M., Wanke, R. and Wolf, E. (2008) Diabetes models by screen for hyperglycaemia in phenotype-driven ENU mouse mutagenesis projects. *Am J Physiol Endocrinol Metab* 294, E232-240.
- Alberti, K.G. and Zimmet, P.Z. (1998) Definition, diagnosis and classification of diabetes mellitus and its complications. Part 1: Diagnosis and classification of diabetes mellitus provisional report of a WHO consultation. *Diabet Med* 15, 539-553.
- Alonso, L.C., Yokoe, T., Zhang, P., Scott, D.K., Kim, S.K., O'Donnell, C.P. and Garcia-Ocana, A. (2007) Glucose infusion in mice: a new model to induce β -cell replication. *Diabetes* 56, 1792-1801.
- American Diabetes Association, T. (2003) Gestational diabetes mellitus. *Diabetes Care* 26 Suppl 1, S103-105.
- American Diabetes Association, T. (2009) Diagnosis and classification of diabetes mellitus. In: *Diabetes Care*. pp S62-67.
- Andre-Schmutz, I., Hindelang, C., Benoist, C. and Mathis, D. (1999) Cellular and molecular changes accompanying the progression from insulinitis to diabetes. *Eur J Immunol* 29, 245-255.
- Andrikopoulos, S., Massa, C.M., Aston-Mourney, K., Funkat, A., Fam, B.C., Hull, R.L., Kahn, S.E. and Proietto, J. (2005) Differential effect of inbred mouse strain (C57BL/6, DBA/2, 129T2) on insulin secretory function in response to a high fat diet. *J Endocrinol* 187, 45-53.
- Arden, C., Trainer, A., de la Iglesia, N., Scougall, K.T., Gloyn, A.L., Lange, A.J., Shaw, J.A., Matschinsky, F.M. and Agius, L. (2007) Cell biology assessment of glucokinase mutations V62M and G72R in pancreatic β -cells: evidence for cellular instability of catalytic activity. *Diabetes* 56, 1773-1782.

Argawal, S.K., Khatri, S., Prakash, N., Singh, N.P., Anuradha, S. and Prakash, A. (2002) Maturity-onset diabetes of the young. *Journal, Indian Academy of Clinical Medicine* 3, 271-277.

Argmann, C.A., Dierich, A. and Auwerx, J. (2006) Uses of forward and reverse genetics in mice to study gene function. *Curr Protoc Mol Biol* Chapter 29, Unit 29A 21.

Augstein, P., Elefanty, A.G., Allison, J. and Harrison, L.C. (1998) Apoptosis and β -cell destruction in pancreatic islets of NOD mice with spontaneous and cyclophosphamide-accelerated diabetes. *Diabetologia* 41, 1381-1388.

Avery, G.B., MacDonald, M.G., Mullett, M.D. and Seshia, M.M.K. (2005) *Avery's neonatology: pathophysiology & management of the newborn* Lipinkott Williams&Wilkins, Philadelphia, USA.

Bakri, D., Gershoni-Baruch, R. and Shehadeh, N. (2004) Permanent neonatal diabetes. *Isr Med Assoc J* 6, 290-291.

Bali, D., Svetlanov, A., Lee, H.W., Fusco-DeMane, D., Leiser, M., Li, B., Barzilai, N., Surana, M., Hou, H., Fleischer, N. and et al. (1995) Animal model for maturity-onset diabetes of the young generated by disruption of the mouse glucokinase gene. *J Biol Chem* 270, 21464-21467.

Balling, R. (2001) ENU mutagenesis: analysing gene function in mice. *Annu Rev Genomics Hum Genet* 2, 463-492.

Balling, R., Hrabé de Angelis, M., Schughart, K. and Wolf, E. (1998) We need more mutants: plans for a large scale ENU mouse mutagenesis screen. In: *OECD Proceedings: Novel systems for the study of human diseases*, Ed: C. Candea., OECD Publishing, Paris, France. pp 103-111.

Baltrusch, S. and Tiedge, M. (2006) Glucokinase regulatory network in pancreatic β -cells and liver. *Diabetes* 55, S55-S64.

Barbaric, I., Wells, S., Russ, A. and Dear, T.N. (2007) Spectrum of ENU-induced mutations in phenotype-driven and gene-driven screens in the mouse. *Environ Mol Mutagen* 48, 124-142.

Barrio, R., Bellanne-Chantelot, C., Moreno, J.C., Morel, V., Calle, H., Alonso, M. and Mustieles, C. (2002) Nine novel mutations in maturity-onset diabetes of the young (MODY) candidate genes in 22 spanish families. *J Clin Endocrinol Metab* 87, 2532-2539.

Beck, J.A., Lloyd, S., Hafezparast, M., Lennon-Pierce, M., Eppig, J.T., Festing, M.F. and Fisher, E.M. (2000) Genealogies of mouse inbred strains. *Nat Genet* 24, 23-25.

Bedell, M.A., Jenkins, N.A. and Copeland, N.G. (1997) Mouse models of human disease. Part I: techniques and resources for genetic analysis in mice. *Genes Dev* 11, 1-10.

Bedoya, F.J., Matschinsky, F.M., Shimizu, T., O'Neil, J.J. and Appel, M.C. (1986) Differential regulation of glucokinase activity in pancreatic islets and liver of the rat. *J Biol Chem* 261, 10760-10764.

Beier, D.R. (2000) Sequence-based analysis of mutagenised mice. *Mamm Genome* 11, 594-597.

Bell, G.I., Pilkis, S.J., Weber, I.T. and Polonsky, K.S. (1996) Glucokinase mutations, insulin secretion, and diabetes mellitus. *Annu Rev Physiol* 58, 171-186.

Bell, G.I. and Polonsky, K.S. (2001) Diabetes mellitus and genetically programmed defects in β -cell function. *Nature* 414, 788-791.

Bellanné-Chantelot, C., Carette, C., Riveline, J.P., Valero, R., Gautier, J.F., Larger, E., Reznik, Y., Ducluzeau, P.H., Sola, A., Hartemann-Heurtier, A., Lecomte, P., Chaillous, L., Laloi-Michelin, M., Wilhem, J.M., Cuny, P., Duron, F., Guerci, B., Jeandidier, N., Mosnier-Pudar, H., Assayag, M., Dubois-Laforgue, D., Velho, G. and Timsit, J. (2008) The type and the position of *HNF1A* mutation modulate age at diagnosis of diabetes in patients with maturity-onset diabetes of the young (MODY)-3. *Diabetes* 57, 503-508.

Bellanné-Chantelot, C., Chauveau, D., Gautier, J.F., Dubois-Laforgue, D., Clauin, S., Beaufile, S., Wilhelm, J.M., Boitard, C., Noel, L.H., Velho, G. and Timsit, J. (2004) Clinical spectrum associated with hepatocyte nuclear factor-1 β mutations. *Ann Intern Med* 140, 510-517.

Bernard, C., Berthault, M.F., Saulnier, C. and Ktorza, A. (1999) Neogenesis vs. apoptosis as main components of pancreatic β -cell mass changes in glucose-infused normal and mildly diabetic adult rats. *FASEB J* 13, 1195-1205.

Bieker, J.J. (2001) Krüppel-like factors: three fingers in many pies. *J Biol Chem* 276, 34355-34358.

Bisswanger, H. (2008) *Enzyme kinetics: principles and methods*, Wiley-VCH, Weinheim.

Bjork, S. (2001) The cost of diabetes and diabetes care. *Diabetes Res Clin Pract* 54 Suppl 1, S13-18.

Bonner-Weir, S. (2001) Beta cell turnover: its assessment and implications. *Diabetes* 50 Suppl 1, S20-24.

Bossard, P., Parsa, R., Decaux, J.F., Iynedjian, P. and Girard, J. (1993) Glucose administration induces the premature expression of liver glucokinase gene in newborn rats. Relation with DNase-I-hypersensitive sites. *Eur J Biochem* 215, 883-892.

Bouwens, L. and Kloppel, G. (1996) Islet cell neogenesis in the pancreas. *Virchows Arch* 427, 553-560.

- Brink, C. (2003) Promoter elements in endocrine pancreas development and hormone regulation. *Cell Mol Life Sci* 60, 1033-1048.
- Brown, S.D. and Balling, R. (2001) Systematic approaches to mouse mutagenesis. *Curr Opin Genet Dev* 11, 268-273.
- Brown, S.D., Hancock, J.M. and Gates, H. (2006) Understanding mammalian genetic systems: the challenge of phenotyping in the mouse. *PLoS Genet* 2, e118.
- Brown, S.D. and Peters, J. (1996) Combining mutagenesis and genomics in the mouse-closing the phenotype gap. *Trends Genet* 12, 433-435.
- Brownlee, M. (2001) Biochemistry and molecular cell biology of diabetic complications. *Nature* 414, 813-820.
- Brun, T., Franklin, I., St-Onge, L., Bignon-Laubert, A., Schoenle, E.J., Wollheim, C.B. and Gauthier, B.R. (2004) The diabetes-linked transcription factor PAX4 promotes β -cell proliferation and survival in rat and human islets. *J. Cell Biol.* 167, 1123-1135.
- Buetow, K.H., Edmonson, M., MacDonald, R., Clifford, R., Yip, P., Kelley, J., Little, D.P., Strausberg, R., Koester, H., Cantor, C.R. and Braun, A. (2001) High-throughput development and characterisation of a genomewide collection of gene-based single nucleotide polymorphism markers by chip-based matrix-assisted laser desorption/ionisation time-of-flight mass spectrometry. *Proc Natl Acad Sci U S A* 98, 581-584.
- Butler, A.E., Janson, J., Bonner-Weir, S., Ritzel, R., Rizza, R.A. and Butler, P.C. (2003) Beta cell deficit and increased β -cell apoptosis in humans with type 2 diabetes. *Diabetes* 52, 102-110.
- Byrne, M.M., Sturis, J., Clement, K., Vionnet, N., Pueyo, M.E., Stoffel, M., Takeda, J., Passa, P., Cohen, D., Bell, G.I. and et al. (1994) Insulin secretory abnormalities in subjects with hyperglycaemia due to glucokinase mutations. *J Clin Invest* 93, 1120-1130.
- Carpenter, M.W. and Coustan, D.R. (1982) Criteria for screening tests for gestational diabetes. *Am J Obstet Gynecol* 144, 768-773.
- Cerf, M.E. (2006) Transcription factors regulating β -cell function. *Eur J Endocrinol* 155, 671-679.
- Chao, C.S., Loomis, Z.L., Lee, J.E. and Sussel, L. (2007) Genetic identification of a novel NeuroD1 function in the early differentiation of islet α -, PP and ϵ -cells. *Dev Biol* 312, 523-532.
- Chen, C., Hosokawa, H., Bumbalo, L.M. and Leahy, J.L. (1994) Regulatory effects of glucose on the catalytic activity and cellular content of glucokinase in the pancreatic β -cell. Study using cultured rat islets. *J Clin Invest* 94, 1616-1620.

- Chèvre, J.C., Hani, E.H., Boutin, P., Vaxillaire, M., Blanché, H., Vionnet, N., Pardini, V.C., Timsit, J., Larger, E., Charpentier, G., Beckers, D., Maes, M., Bellanné-Chantelot, C., Velho, G. and Froguel, P. (1998) Mutation screening in 18 Caucasian families suggest the existence of other MODY genes. *Diabetologia* 41, 1017-1023.
- Clark, A.J., Bissinger, P., Bullock, D.W., Damak, S., Wallace, R., Whitelaw, C.B. and Yull, F. (1994) Chromosomal position effects and the modulation of transgene expression. *Reprod Fertil Dev* 6, 589-598.
- Clement, K., Pueyo, M.E., Vaxillaire, M., Rakotoambinina, B., Thuillier, F., Passa, P., Froguel, P., Robert, J.J. and Velho, G. (1996) Assessment of insulin sensitivity in glucokinase-deficient subjects. *Diabetologia* 39, 82-90.
- Cnop, M., Welsh, N., Jonas, J.C., Jorns, A., Lenzen, S. and Eizirik, D.L. (2005) Mechanisms of pancreatic β -cell death in type 1 and type 2 diabetes: many differences, few similarities. *Diabetes* 54 Suppl 2, S97-107.
- Codner, E., Deng, L., Perez-Bravo, F., Roman, R., Lanzano, P., Cassorla, F. and Chung, W.K. (2006) Glucokinase mutations in young children with hyperglycaemia. *Diabetes Metab Res Rev* 22, 348-355.
- Coghill, E.L., Hugill, A., Parkinson, N., Davison, C., Glenister, P., Clements, S., Hunter, J., Cox, R.D. and Brown, S.D. (2002) A gene-driven approach to the identification of ENU mutants in the mouse. *Nat Genet* 30, 255-256.
- Cohen, C.D. and Kretzler, M. (2003) Gene expression analysis of microdissected renal biopsies. In: *Renal Disease: Techniques and Protocols*, Eds: M. Goligorsky and N. Totowa, Humana Press. pp 285-293.
- Coles, H.S., Burne, J.F. and Raff, M.C. (1993) Large-scale normal cell death in the developing rat kidney and its reduction by epidermal growth factor. *Development* 118, 777-784.
- Collins, F.S., Green, E.D., Guttmacher, A.E. and Guyer, M.S. (2003a) A vision for the future of genomics research. *Nature* 422, 835-847.
- Collins, F.S., Morgan, M. and Patrinos, A. (2003b) The Human Genome Project: lessons from large-scale biology. *Science* 300, 286-290.
- Concepcion, D., Seburn, K.L., Wen, G., Frankel, W.N. and Hamilton, B.A. (2004) Mutation rate and predicted phenotypic target sizes in ethylnitrosourea-treated mice. *Genetics* 168, 953-959.
- Cordes, S.P. (2005) *N*-ethyl-*N*-nitrosourea Mutagenesis: Boarding the mouse mutant express. *Microbiol. Mol. Biol. Rev.* 69, 426-439.
- Cornblath, M. and Schwartz, R. (1976) *Disorders of Carbohydrate Metabolism in Infancy*, W.B. Saunders Co., Philadelphia and London.

- Cornish-Bowden, A. and Càrdenas, M.L. (2004) Glucokinase: a monomeric enzyme with positive cooperativity. In: *Glucokinase and Glycaemic Disease: From Basics to Novel Therapeutics*, Eds: F.M. Matschinsky and M.A. Magnuson, Karger, Basel. pp 125-134.
- Costa, A., Bescos, M., Velho, G., Chevre, J., Vidal, J., Sesmilo, G., Bellanne-Chantelot, C., Froguel, P., Casamitjana, R., Rivera-Fillat, F., Gomis, R. and Conget, I. (2000) Genetic and clinical characterisation of maturity-onset diabetes of the young in Spanish families. *Eur J Endocrinol* 142, 380-386.
- Cox, R.D. and Brown, S.D. (2003) Rodent models of genetic disease. *Curr Opin Genet Dev* 13, 278-283.
- Cuesta-Munoz, A.L., Huopio, H., Otonkoski, T., Gomez-Zumaquero, J.M., Nanto-Salonen, K., Rahier, J., Lopez-Enriquez, S., Garcia-Gimeno, M.A., Sanz, P., Soriguer, F.C. and Laakso, M. (2004) Severe persistent hyperinsulinaemic hypoglycaemia due to a *de novo* glucokinase mutation. *Diabetes* 53, 2164-2168.
- Danial, N.N., Gramm, C.F., Scorrano, L., Zhang, C.Y., Krauss, S., Ranger, A.M., Datta, S.R., Greenberg, M.E., Licklider, L.J., Lowell, B.B., Gygi, S.P. and Korsmeyer, S.J. (2003) BAD and glucokinase reside in a mitochondrial complex that integrates glycolysis and apoptosis. *Nature* 424, 952-956.
- Danial, N.N., Walensky, L.D., Zhang, C.Y., Choi, C.S., Fisher, J.K., Molina, A.J., Datta, S.R., Pitter, K.L., Bird, G.H., Wikstrom, J.D., Deeney, J.T., Robertson, K., Morash, J., Kulkarni, A., Neschen, S., Kim, S., Greenberg, M.E., Corkey, B.E., Shirihai, O.S., Shulman, G.I., Lowell, B.B. and Korsmeyer, S.J. (2008) Dual role of proapoptotic BAD in insulin secretion and β -cell survival. *Nat Med* 14, 144-153.
- Davies, K. and Wynshaw-Boris, A. (2009) Human genetics: conceptual and practical advances in the post-genome era. *Current Opinion in Genetics & Development* 19, 193-195.
- Davis, E.A., Cuesta-Munoz, A., Raoul, M., Buettger, C., Sweet, I., Moates, M., Magnuson, M.A. and Matschinsky, F.M. (1999) Mutants of glucokinase cause hypoglycaemia and hyperglycaemia syndromes and their analysis illuminates fundamental quantitative concepts of glucose homeostasis. *Diabetologia* 42, 1175-1186.
- Delesse, M.A. (1847) Procède mecanique pour determiner la composition des roches. *C. R. Acad. Sci. (Paris)* 25, 544-545.
- Desaintes, C. (2008) Research on animal model organisms funded by the European Commission's framework programmes. *Dis Model Mech* 1, 209-212.
- Donath, M.Y., Ehses, J.A., Maedler, K., Schumann, D.M., Ellingsgaard, H., Eppler, E. and Reinecke, M. (2005) Mechanisms of β -cell death in type 2 diabetes. *Diabetes* 54 Suppl 2, S108-113.

Duncan, S.A., Navas, M.A., Dufort, D., Rossant, J. and Stoffel, M. (1998) Regulation of a transcription factor network required for differentiation and metabolism. *Science* 281, 692-695.

Dunn-Meynell, A.A., Routh, V.H., Kang, L., Gaspers, L. and Levin, B.E. (2002) Glucokinase is the likely mediator of glucosensing in both glucose-excited and glucose-inhibited central neurons. *Diabetes* 51, 2056-2065.

Duvillie, B., Cordonnier, N., Deltour, L., Dandoy-Dron, F., Itier, J.M., Monthieux, E., Jami, J., Joshi, R.L. and Bucchini, D. (1997) Phenotypic alterations in insulin-deficient mutant mice. *Proc Natl Acad Sci U S A* 94, 5137-5140.

Edghill, E.L., Flanagan, S.E., Patch, A.M., Boustred, C., Parrish, A., Shields, B., Shepherd, M.H., Hussain, K., Kapoor, R.R., Malecki, M., MacDonald, M.J., Stoy, J., Steiner, D.F., Philipson, L.H., Bell, G.I., Hattersley, A.T. and Ellard, S. (2008) Insulin mutation screening in 1,044 patients with diabetes: mutations in the INS gene are a common cause of neonatal diabetes but a rare cause of diabetes diagnosed in childhood or adulthood. *Diabetes* 57, 1034-1042.

Eizirik, D.L., Cardozo, A.K. and Cnop, M. (2008) The role for endoplasmic reticulum stress in diabetes mellitus. *Endocr Rev* 29, 42-61.

Ellard, S., Bellanne-Chantelot, C. and Hattersley, A.T. (2008) Best practice guidelines for the molecular genetic diagnosis of maturity-onset diabetes of the young. *Diabetologia* 51, 546-553.

Ellard, S. and Colclough, K. (2006) Mutations in the genes encoding the transcription factors hepatocyte nuclear factor-1 α (*HNF1A*) and -4 α (*HNF4A*) in maturity-onset diabetes of the young. *Hum Mutat* 27, 854-869.

Fajans, S.S. (1998) Revised etiologic classification of diabetes. *Diabetes Care* 21, 466-467.

Fajans, S.S. and Bell, G.I. (2006) Phenotypic heterogeneity between different mutations of MODY subtypes and within MODY pedigrees. *Diabetologia* 49, 1106-1108.

Fajans, S.S., Bell, G.I. and Polonsky, K.S. (2001) Molecular mechanisms and clinical pathophysiology of maturity-onset diabetes of the young. *N Engl J Med* 345, 971-980.

Favor, J., Neuhäuser-Klaus, A., Ehling, U.H., Wulff, A. and van Zeeland, A.A. (1997) The effect of the interval between dose applications on the observed specific-locus mutation rate in the mouse following fractionated treatments of spermatogonia with ethylnitrosourea. *Mutation Research/Fundamental and Molecular Mechanisms of Mutagenesis* 374, 193-199.

Favor, J., Sund, M., Neuhauser-Klaus, A. and Ehling, U.H. (1990) A dose-response analysis of ethylnitrosourea-induced recessive specific-locus mutations in treated spermatogonia of the mouse. *Mutat Res* 231, 47-54.

Fenner, D., Odili, S., Takahashi, J.S., Matschinsky, F.M. and Bass, J. (2009) Insight into glucokinase diabetes from ENU mutagenesis. *Diabetes Suppl.* 1 58, A308.

Foretz, M., Guichard, C., Ferre, P. and Foufelle, F. (1999) Sterol regulatory element binding protein-1c is a major mediator of insulin action on the hepatic expression of glucokinase and lipogenesis-related genes. *Proc Natl Acad Sci U S A* 96, 12737-12742.

Fosel, S. (1995) Transient and permanent neonatal diabetes. *Eur J Pediatr* 154, 944-948.

Frischmeyer, P.A. and Dietz, H.C. (1999) Nonsense-mediated mRNA decay in health and disease. *Hum Mol Genet* 8, 1893-1900.

Froguel, P., Vaxillaire, M., Sun, F., Velho, G., Zouali, H., Butel, M.O., Lesage, S., Vionnet, N., Clement, K., Fougerousse, F. and et al. (1992) Close linkage of glucokinase locus on chromosome 7p to early-onset non-insulin-dependent diabetes mellitus. *Nature* 356, 162-164.

Froguel, P., Zouali, H., Vionnet, N., Velho, G., Vaxillaire, M., Sun, F., Lesage, S., Stoffel, M., Takeda, J., Passa, P. and et al. (1993) Familial hyperglycaemia due to mutations in glucokinase. Definition of a subtype of diabetes mellitus. *N Engl J Med* 328, 697-702.

Furuta, H., Furuta, M., Sanke, T., Ekawa, K., Hanabusa, T., Nishi, M., Sasaki, H. and Nanjo, K. (2002) Nonsense and missense mutations in the human hepatocyte nuclear factor-1 β gene (TCF2) and their relation to type 2 diabetes in Japanese. *J Clin Endocrinol Metab* 87, 3859-3863.

Gale, E.A. and Gillespie, K.M. (2001) Diabetes and gender. *Diabetologia* 44, 3-15.

Garfield, S.A., Malozowski, S., Chin, M.H., Narayan, K.M., Glasgow, R.E., Green, L.W., Hiss, R.G. and Krumholz, H.M. (2003) Considerations for diabetes translational research in real-world settings. *Diabetes Care* 26, 2670-2674.

Gary, T.L. and Brancati, F.L. (2004) Strategies to curb the epidemic of diabetes and obesity in primary care settings. *J Gen Intern Med* 19, 1242-1243.

Gasa, R., Fabregat, M.E. and Gomis, R. (2000) The role of glucose and its metabolism in the regulation of glucokinase expression in isolated human pancreatic islets. *Biochem Biophys Res Commun* 268, 491-495.

Girard, J., Decaux, J.F. and Bossard, P. (1992) Regulation of the initial expression of hepatic phosphoenolpyruvate carboxykinase and glucokinase genes during development. *Diabete Metab* 18, 74-80.

Glaser, B. (2008) Insulin mutations in diabetes: the clinical spectrum. *Diabetes* 57, 799-800.

- Gloyn, A.L. (2003) Glucokinase (*GCK*) mutations in hyper- and hypoglycaemia: maturity-onset diabetes of the young, permanent neonatal diabetes, and hyperinsulinaemia of infancy. *Hum Mutat* 22, 353-362.
- Gloyn, A.L., Ellard, S., Shield, J.P., Temple, I.K., Mackay, D.J., Polak, M., Barrett, T. and Hattersley, A.T. (2002) Complete glucokinase deficiency is not a common cause of permanent neonatal diabetes. *Diabetologia* 45, 290.
- Gloyn, A.L., Tribble, N.D., van de Bunt, M., Barrett, A. and Johnson, P.R. (2008) Glucokinase (*GCK*) and other susceptibility genes for β -cell dysfunction: the candidate approach. *Biochem Soc Trans* 36, 306-311.
- Gloyn, A.L., van de Bunt, M., Stratton, I.M., Lonie, L., Tucker, L., Ellard, S. and Holman, R.R. (2009) Prevalence of *GCK* mutations in individuals screened for fasting hyperglycaemia. *Diabetologia* 52, 172-174.
- Gregori, C., Guillet-Deniau, I., Girard, J., Decaux, J.F. and Pichard, A.L. (2006) Insulin regulation of glucokinase gene expression: evidence against a role for sterol regulatory element binding protein 1 in primary hepatocytes. *FEBS Lett* 580, 410-414.
- Griffiths, A.J.F., Gelbart, W.M., Miller, J.H. and Lewontin, R.C. (1999) Gene mutations. In: *Modern Genetic Analysis*, Eds: J. Miller and R. Lewontin, W H Freeman & Co, New York.
- Grimsby, J., Sarabu, R., Corbett, W.L., Haynes, N.E., Bizzarro, F.T., Coffey, J.W., Guertin, K.R., Hilliard, D.W., Kester, R.F., Mahaney, P.E., Marcus, L., Qi, L., Spence, C.L., Tengi, J., Magnuson, M.A., Chu, C.A., Dvornozniak, M.T., Matschinsky, F.M. and Grippo, J.F. (2003) Allosteric activators of glucokinase: potential role in diabetes therapy. *Science* 301, 370-373.
- Grupe, A., Hultgren, B., Ryan, A., Ma, Y.H., Bauer, M. and Stewart, T.A. (1995) Transgenic knockouts reveal a critical requirement for pancreatic β -cell glucokinase in maintaining glucose homeostasis. *Cell* 83, 69-78.
- Guenet, J.L. (2004) Chemical mutagenesis of the mouse genome: an overview. *Genetica* 122, 9-24.
- Gundersen, H.J. (1977) Notes on the estimation of the numerical density of arbitrary profiles: The edge effect. *J. Microsc*, 219-223.
- Gundersen, H.J. (1978) Estimators of the number of objects per area unbiased by edge effects. *Microsc Acta* 81, 107-117.
- Gundersen, H.J., Bendtsen, T.F., Korbo, L., Marcussen, N., Moller, A., Nielsen, K., Nyengaard, J.R., Pakkenberg, B., Sorensen, F.B., Vesterby, A. and et al. (1988) Some new, simple and efficient stereological methods and their use in pathological research and diagnosis. *APMIS* 96, 379-394.

- Gupta, R.K. and Kaestner, K.H. (2004) HNF-4 α : from MODY to late-onset type 2 diabetes. *Trends Mol Med* 10, 521-524.
- Habener, J.F., Kemp, D.M. and Thomas, M.K. (2005) Minireview: transcriptional regulation in pancreatic development. *Endocrinology* 146, 1025-1034.
- Haldorsen, I.S., Vesterhus, M., Raeder, H., Jensen, D.K., Sovik, O., Molven, A. and Njolstad, P.R. (2008) Lack of pancreatic body and tail in *HNF1B* mutation carriers. *Diabet Med* 25, 782-787.
- Hanson, I. and Van Heyningen, V. (1995) Pax6: more than meets the eye. *Trends Genet* 11, 268-272.
- Hara, H., Miwa, I. and Okuda, J. (1986) Inhibition of rat liver glucokinase by alloxan and ninhydrin. *Chem Pharm Bull (Tokyo)* 34, 4731-4737.
- Hattersley, A.T. (1998) Maturity-onset diabetes of the young: clinical heterogeneity explained by genetic heterogeneity. *Diabetic Medicine* 15, 15-24.
- Hattersley, A.T. and Pearson, E.R. (2006) Minireview: pharmacogenetics and beyond: the interaction of therapeutic response, β -cell physiology, and genetics in diabetes. *Endocrinology* 147, 2657-2663.
- Hattersley, A.T., Turner, R.C., Patel, P., O'Rahilly, S., Wainscoat, J.S., Permutt, M.A., Tanazawa, Y., Chin, K.C. and Watkins, P. (1992) Linkage of type 2 diabetes to the glucokinase gene. *The Lancet* 339, 1307-1310.
- Heimberg, H., De Vos, A., Moens, K., Quartier, E., Bouwens, L., Pipeleers, D., van Schaffingen, E., Madsen, O. and Schuit, F. (1996) The glucose sensor protein glucokinase is expressed in glucagon-producing α -cells. *Proc Natl Acad Sci U S A* 93, 7036-7041.
- Herbach, N., Goeke, B., Schneider, M., Hermanns, W., Wolf, E. and Wanke, R. (2005) Overexpression of a dominant negative GIP receptor in transgenic mice results in disturbed postnatal pancreatic islet and β -cell development. *Regul Pept* 125, 103-117.
- Herbach, N., Rathkolb, B., Kemter, E., Pichl, L., Klafken, M., Hrabé de Angelis, M., Halban, P.A., Wolf, E., Aigner, B. and Wanke, R. (2007) Dominant-negative effects of a novel mutated *Ins2* allele causes early-onset diabetes and severe β -cell loss in Munich *Ins2*^{C95S} mutant mice. *Diabetes* 56, 1268-1276.
- Herbach, N., Schairer, I., Blutke, A., Kautz, S., Siebert, A., Goke, B., Wolf, E. and Wanke, R. (2009) Diabetic kidney lesions of GIPR^{dn} transgenic mice: podocyte hypertrophy and thickening of the GBM precede glomerular hypertrophy and glomerulosclerosis. *Am J Physiol Renal Physiol* 296, F819-829.
- Heredia, V.V., Thomson, J., Nettleton, D. and Sun, S. (2006) Glucose-induced conformational changes in glucokinase mediate allosteric regulation: transient kinetic analysis. *Biochemistry* 45, 7553-7562.

Hinokio, Y., Horikawa, Y., Furuta, H., Cox, N.J., Iwasaki, N., Honda, M., Ogata, M., Iwamoto, Y. and Bell, G.I. (2000) Beta cell transcription factors and diabetes: no evidence for diabetes-associated mutations in the hepatocyte nuclear factor-3 β gene (*HNF3B*) in Japanese patients with maturity-onset diabetes of the young. *Diabetes* 49, 302-305.

Hitotsumachi, S., Carpenter, D.A. and Russell, W.L. (1985) Dose-repetition increases the mutagenic effectiveness of *N*-ethyl-*N*-nitrosourea in mouse spermatogonia. *Proc Natl Acad Sci U S A* 82, 6619-6621.

Höfer, M. (2006) *Effects of a carbohydrate restricted diet on the metabolic state and progressive pancreatic β -cell loss in transgenic mice expressing a dominant negative GIP receptor*, Ludwig Maximilian University of Munich, Munich.

Hogan, P., Dall, T. and Nikolov, P. (2003) Economic costs of diabetes in the US in 2002. *Diabetes Care* 26, 917-932.

Hrabé de Angelis, M., Adler, A., Beckers, J., Gailus-Durner, V., Imai, K., Soewarto, D. and Wagner, S. (2004) Mouse Genomics. In: *The Laboratory Mouse: Handbook of Experimental Animals*, Ed: G.R.B. Hans J. Hedrich, Elsevier Academic Press. pp 47-60.

Hrabé de Angelis, M. and Balling, R. (1998) Large scale ENU screens in the mouse: genetics meets genomics. *Mutat Res* 400, 25-32.

Hrabé de Angelis, M., Flaswinkel, H., Fuchs, H., Rathkolb, B., Soewarto, D., Marschall, S., Heffner, S., Pargent, W., Wuensch, K., Jung, M., Reis, A., Richter, T., Alessandrini, F., Jakob, T., Fuchs, E., Kolb, H., Kremmer, E., Schaeble, K., Rollinski, B., Roscher, A., Peters, C., Meitinger, T., Strom, T., Steckler, T., Holsboer, F., Klopstock, T., Gekeler, F., Schindewolf, C., Jung, T., Avraham, K., Behrendt, H., Ring, J., Zimmer, A., Schughart, K., Pfeffer, K., Wolf, E. and Balling, R. (2000) Genome-wide, large-scale production of mutant mice by ENU mutagenesis. *Nat Genet* 25, 444-447.

Hrabé de Angelis, M., Michel, D., Wagner, S., Becker, S. and Beckers, J. (2007) Chemical Mutagenesis in Mice. In: *The mouse in biomedical research, Volume 1; 2nd edition*, , Eds: J. Fox, S. Barthold, M. Davisson, C.E. Newcomer, F.W. Quimby and A. Smith, Academic Press, Salt Lake City, USA. pp 225-260.

Human Genome Sequencing, C. (2004) Finishing the euchromatic sequence of the human genome. *Nature* 431, 931-945.

Igarashi, P., Shao, X., McNally, B.T. and Hiesberger, T. (2005) Roles of HNF-1 β in kidney development and congenital cystic diseases. *Kidney Int* 68, 1944-1947.

Ilag, L.L., Tabaei, B.P., Herman, W.H., Zawacki, C.M., D'Souza, E., Bell, G.I. and Fajans, S.S. (2000) Reduced pancreatic polypeptide response to hypoglycaemia and amylin response to arginine in subjects with a mutation in the HNF-4 α /MODY1 gene. *Diabetes* 49, 961-968.

Inoue, M., Sakuraba, Y., Motegi, H., Kubota, N., Toki, H., Matsui, J., Toyoda, Y., Miwa, I., Terauchi, Y., Kadowaki, T., Shigeyama, Y., Kasuga, M., Adachi, T., Fujimoto, N., Matsumoto, R., Tsuchihashi, K., Kagami, T., Inoue, A., Kaneda, H., Ishijima, J., Masuya, H., Suzuki, T., Wakana, S., Gondo, Y., Minowa, O., Shiroishi, T. and Noda, T. (2004) A series of maturity-onset diabetes of the young, type 2 (MODY2) mouse models generated by a large-scale ENU mutagenesis program. *Hum Mol Genet* 13, 1147-1157.

Ilyedjian, P.B. (1993) Mammalian glucokinase and its gene. *Biochem J* 293 (Pt 1), 1-13.

Ilyedjian, P.B. (2009) Molecular physiology of mammalian glucokinase. *Cell Mol Life Sci* 66, 27-42.

Ilyedjian, P.B., Jotterand, D., Nospikel, T., Asfari, M. and Pilot, P.R. (1989a) Transcriptional induction of glucokinase gene by insulin in cultured liver cells and its repression by the glucagon-cAMP system. *J. Biol. Chem.* 264, 21824-21829.

Ilyedjian, P.B., Pilot, P.R., Nospikel, T., Milburn, J.L., Quaade, C., Hughes, S., Ucla, C. and Newgard, C.B. (1989b) Differential expression and regulation of the glucokinase gene in liver and islets of Langerhans. *Proc Natl Acad Sci U S A* 86, 7838-7842.

Jetton, T.L., Liang, Y., Pettepher, C.C., Zimmerman, E.C., Cox, F.G., Horvath, K., Matschinsky, F.M. and Magnuson, M.A. (1994) Analysis of upstream glucokinase promoter activity in transgenic mice and identification of glucokinase in rare neuroendocrine cells in the brain and gut. *J Biol Chem* 269, 3641-3654.

Johansen, A., Ek, J., Mortensen, H.B., Pedersen, O. and Hansen, T. (2005) Half of clinically defined maturity-onset diabetes of the young patients in Denmark do not have mutations in *HNF4A*, *GCK*, and *TCF1*. *J Clin Endocrinol Metab* 90, 4607-4614.

Johnson, J. (2007) Pancreatic β -cell apoptosis in maturity-onset diabetes of the young. *Canadian Journal of Diabetes* 31, 67-74.

Justice, M.J. and Bode, V.C. (1988) Three ENU-induced alleles of the murine quaking locus are recessive embryonic lethal mutations. *Genet Res* 51, 95-102.

Justice, M.J., Noveroske, J.K., Weber, J.S., Zheng, B. and Bradley, A. (1999) Mouse ENU mutagenesis. *Hum Mol Genet* 8, 1955-1963.

Kamata, K., Mitsuya, M., Nishimura, T., Eiki, J. and Nagata, Y. (2004) Structural basis for allosteric regulation of the monomeric allosteric enzyme human glucokinase. *Structure* 12, 429-438.

Katz, A., Nambi, S.S., Mather, K., Baron, A.D., Follmann, D.A., Sullivan, G. and Quon, M.J. (2000) Quantitative insulin sensitivity check index: a simple, accurate method for assessing insulin sensitivity in humans. *J Clin Endocrinol Metab* 85, 2402-2410.

Kauri, L.M., Wang, G.S., Patrick, C., Bareggi, M., Hill, D.J. and Scott, F.W. (2007) Increased islet neogenesis without increased islet mass precedes autoimmune attack in diabetes-prone rats. *Lab Invest* 87, 1240-1251.

Keays, D.A., Clark, T.G. and Flint, J. (2006) Estimating the number of coding mutations in genotypic- and phenotypic-driven *N*-ethyl-*N*-nitrosourea (ENU) screens. *Mamm Genome* 17, 230-238.

Kennedy, C.L. and O'Bryan, M.K. (2006) *N*-ethyl-*N*-nitrosourea (ENU) mutagenesis and male fertility research. *Hum Reprod Update* 12, 293-301.

Kikkawa, R. (2000) Chronic complications in diabetes mellitus. *Br J Nutr* 84 Suppl 2, S183-185.

Kile, B.T. and Hilton, D.J. (2005) The art and design of genetic screens: mouse. *Nat Rev Genet* 6, 557-567.

Kim, S.-H., Ma, X., Klupa, T., Powers, C., Pezzolesi, M., Warram, J.H., Rich, S.S., Krolewski, A.S. and Doria, A. (2003) Genetic modifiers of the age at diagnosis of diabetes (MODY3) in carriers of hepatocyte nuclear factor-1 α mutations map to chromosomes 5p15, 9q22, and 14q24. *Diabetes* 52, 2182-2186.

Kim, W.H., Lee, J.W., Suh, Y.H., Hong, S.H., Choi, J.S., Lim, J.H., Song, J.H., Gao, B. and Jung, M.H. (2005) Exposure to chronic high glucose induces beta-cell apoptosis through decreased interaction of glucokinase with mitochondria: downregulation of glucokinase in pancreatic β -cells. *Diabetes* 54, 2602-2611.

King, H., Aubert, R.E. and Herman, W.H. (1998) Global burden of diabetes, 1995-2025: prevalence, numerical estimates, and projections. *Diabetes Care* 21, 1414-1431.

Kitanaka, S., Miki, Y., Hayashi, Y. and Igarashi, T. (2004) Promoter-specific repression of hepatocyte nuclear factor (HNF)-1 β and HNF-1 α transcriptional activity by an HNF-1 β missense mutant associated with Type 5 maturity-onset diabetes of the young with hepatic and biliary manifestations. *J Clin Endocrinol Metab* 89, 1369-1378.

Klempt, M., Rathkolb, B., Fuchs, E., de Angelis, M.H., Wolf, E. and Aigner, B. (2006) Genotype-specific environmental impact on the variance of blood values in inbred and F1 hybrid mice. *Mamm Genome* 17, 93-102.

Kluge, H.D. (1994) *Quantitative morphologische Untersuchung am Pankreas Wachstumshormon-transgener Mäuse*, Ludwig Maximilian University of Munich, München.

Korf, B. (1995) Molecular diagnosis (2). *N Engl J Med* 332, 1499-1502.

Kuo, C.J., Conley, P.B., Chen, L., Sladek, F.M., Darnell, J.E., Jr. and Crabtree, G.R. (1992) A transcriptional hierarchy involved in mammalian cell-type specification. *Nature* 355, 457-461.

Langin, D. (2001) Diabetes, insulin secretion, and the pancreatic β -cell mitochondrion. *N Engl J Med* 345, 1772-1774.

Le May, C., Chu, K., Hu, M., Ortega, C.S., Simpson, E.R., Korach, K.S., Tsai, M.J. and Mauvais-Jarvis, F. (2006) Oestrogens protect pancreatic β -cells from apoptosis and prevent insulin-deficient diabetes mellitus in mice. *Proc Natl Acad Sci U S A* 103, 9232-9237.

Leahy, J.L. (2005) Pathogenesis of type 2 diabetes mellitus. *Arch Med Res* 36, 197-209.

Lee, C.S., Sund, N.J., Behr, R., Herrera, P.L. and Kaestner, K.H. (2005) Foxa2 is required for the differentiation of pancreatic α -cells. *Dev Biol* 278, 484-495.

Lee, J.E., Hollenberg, S.M., Snider, L., Turner, D.L., Lipnick, N. and Weintraub, H. (1995) Conversion of *Xenopus* ectoderm into neurons by NeuroD, a basic helix-loop-helix protein. *Science* 268, 836-844.

Lee, J.W., Kim, W.H., Lim, J.H., Song, E.H., Song, J., Choi, K.Y. and Jung, M.H. (2009) Mitochondrial dysfunction: glucokinase downregulation lowers interaction of glucokinase with mitochondria, resulting in apoptosis of pancreatic β -cells. *Cell Signal* 21, 69-78.

Lee, S., Muniyappa, R., Yan, X., Chen, H., Yue, L.Q., Hong, E.G., Kim, J.K. and Quon, M.J. (2008) Comparison between surrogate indexes of insulin sensitivity and resistance and hyperinsulinaemic euglycaemic clamp estimates in mice. *Am J Physiol Endocrinol Metab* 294, E261-270.

Lehmann, R. and Spinas, G.A. (2000) Screening, diagnosis and management of diabetes mellitus and diabetic complications. *Ther Umsch* 57, 12-21.

Leiter, E.H., Gerling, I.C. and Flinn, J.C. (1999) Spontaneous insulin-dependent diabetes in non-obese diabetic mice: comparisons with experimentally induced IDDM In: *Experimental models of diabetes*, Ed: J.H. McNeill, CRC Press, Florida, USA.

Liang, Y., Jetton, T.L., Zimmerman, E.C., Najafi, H., Matschinsky, F.M. and Magnuson, M.A. (1991) Effects of alternate RNA splicing on glucokinase isoform activities in the pancreatic islet, liver, and pituitary. *J Biol Chem* 266, 6999-7007.

Liang, Y., Najafi, H. and Matschinsky, F.M. (1990) Glucose regulates glucokinase activity in cultured islets from rat pancreas. *J Biol Chem* 265, 16863-16866.

Lindblad-Toh, K., Winchester, E., Daly, M.J., Wang, D.G., Hirschhorn, J.N., Laviolette, J.P., Ardlie, K., Reich, D.E., Robinson, E., Sklar, P., Shah, N., Thomas, D., Fan, J.B., Gingeras, T., Warrington, J., Patil, N., Hudson, T.J. and Lander, E.S.

(2000) Large-scale discovery and genotyping of single-nucleotide polymorphisms in the mouse. *Nat Genet* 24, 381-386.

Lindner, T.H., Cockburn, B.N. and Bell, G.I. (1999) Molecular genetics of MODY in Germany. *Diabetologia* 42, 121-123.

Liu, L., Furuta, H., Minami, A., Zheng, T., Jia, W., Nanjo, K. and Xiang, K. (2007) A novel mutation, Ser159Pro in the NeuroD1/BETA2 gene contributes to the development of diabetes in a Chinese potential MODY family. *Mol Cell Biochem* 303, 115-120.

Louet, J.F., LeMay, C. and Mauvais-Jarvis, F. (2004) Antidiabetic actions of oestrogen: insight from human and genetic mouse models. *Curr Atheroscler Rep* 6, 180-185.

Lowe, W. (1998) Diabetes mellitus. In: *Principles of molecular medicine*, Ed: J.L. Jameson, Humana Press, Totowa, USA.

Macchiarini, F., Manz, M.G., Palucka, A.K. and Shultz, L.D. (2005) Humanised mice: are we there yet? *J Exp Med* 202, 1307-1311.

Magnuson, M.A. and Matschinsky, F.M. (2004) Glucokinase as a glucose sensor: Past, present and future. In: *Glucokinase and Glycaemic Disease: From Basics to Novel Therapeutics*, Eds: F.M. Matschinsky and M.A. Magnuson, Karger, Basel. pp 1-17.

Magnuson, M.A. and Shelton, K.D. (1989) An alternate promoter in the glucokinase gene is active in the pancreatic β -cell. *J Biol Chem* 264, 15936-15942.

Mahalingam, B., Cuesta-Munoz, A., Davis, E.A., Matschinsky, F.M., Harrison, R.W. and Weber, I.T. (1999) Structural model of human glucokinase in complex with glucose and ATP: implications for the mutants that cause hypo- and hyperglycaemia. *Diabetes* 48, 1698-1705.

Malecki, M.T. and Mlynarski, W. (2008) Monogenic diabetes: implications for therapy of rare types of disease. *Diabetes Obes Metab* 10, 607-616.

Mandrup-Poulsen, T. (2003) Apoptotic signal transduction pathways in diabetes. *Biochem Pharmacol* 66, 1433-1440.

Mantovani, V., Salardi, S., Cerreta, V., Bastia, D., Cenci, M., Ragni, L., Zucchini, S., Parente, R. and Cicognani, A. (2003) Identification of eight novel glucokinase mutations in Italian children with maturity-onset diabetes of the young. *Hum Mutat* 22, 338.

Martin, D., Bellanne-Chantelot, C., Deschamps, I., Froguel, P., Robert, J.J. and Velho, G. (2008) Long-term follow-up of oral glucose tolerance test-derived glucose tolerance and insulin secretion and insulin sensitivity indexes in subjects with glucokinase mutations (MODY2). *Diabetes Care* 31, 1321-1323.

- Massa, L., Baltrusch, S., Okar, D.A., Lange, A.J., Lenzen, S. and Tiedge, M. (2004) Interaction of 6-phosphofructo-2-kinase/fructose-2,6-bisphosphatase (PFK-2/FBPase-2) with glucokinase activates glucose phosphorylation and glucose metabolism in insulin-producing cells. *Diabetes* 53, 1020-1029.
- Massa, O., Meschi, F., Cuesta-Munoz, A., Caumo, A., Cerutti, F., Toni, S., Cherubini, V., Guazzarotti, L., Sulli, N., Matschinsky, F.M., Lorini, R., Iafusco, D. and Barbetti, F. (2001) High prevalence of glucokinase mutations in Italian children with MODY. Influence on glucose tolerance, first-phase insulin response, insulin sensitivity and BMI. Diabetes Study Group of the Italian Society of Paediatric Endocrinology and Diabetes (SIEDP). *Diabetologia* 44, 898-905.
- Matschinsky, F.M. (1990) Glucokinase as glucose sensor and metabolic signal generator in pancreatic β -cells and hepatocytes. *Diabetes* 39, 647-652.
- Matschinsky, F.M. (2002) Regulation of pancreatic β -cell glucokinase: from basics to therapeutics. *Diabetes* 51 Suppl 3, S394-404.
- Matschinsky, F.M. (2009) Assessing the potential of glucokinase activators in diabetes therapy. *Nat Rev Drug Discov* 8, 399-416.
- Matschinsky, F.M., Glaser, B. and Magnuson, M.A. (1998) Pancreatic β -cell glucokinase: closing the gap between theoretical concepts and experimental realities. *Diabetes* 47, 307-315.
- Matschinsky, F.M., Magnuson, M.A., Zelent, D., Jetton, T.L., Doliba, N., Han, Y., Taub, R. and Grimsby, J. (2006) The network of glucokinase-expressing cells in glucose homeostasis and the potential of glucokinase activators for diabetes therapy. *Diabetes* 55, 1-12.
- Matyka, K.A., Beards, F., Appleton, M., Ellard, S., Hattersley, A. and Dunger, D.B. (1998) Genetic testing for maturity-onset diabetes of the young in childhood hyperglycaemia. *Arch Dis Child* 78, 552-554.
- McCarthy, M.I. and Froguel, P. (2002) Genetic approaches to the molecular understanding of type 2 diabetes. *Am J Physiol Endocrinol Metab* 283, E217-225.
- Menzel, R., Kaisaki, P.J., Rjasanowski, I., Heinke, P., Kerner, W. and Menzel, S. (1998) A low renal threshold for glucose in diabetic patients with a mutation in the hepatocyte nuclear factor-1 α (HNF-1 α) gene. *Diabet Med* 15, 816-820.
- Mitchell, S.M.S. and Frayling, T.M. The role of transcription factors in maturity-onset diabetes of the young. *Molecular Genetics and Metabolism* 77, 35-43.
- Moore, K.J. (1999) Utilisation of mouse models in the discovery of human disease genes. *Drug Discov Today* 4, 123-128.
- Moradpour, D. (2006). In: *Klinische Pathophysiologie*, Eds: W. Siegenthaler and H.E. Blum, Thieme, Stuttgart. pp 859-887.

- Mouse Genome Sequencing, I.C. (2009) Lineage-specific biology revealed by a finished genome assembly of the mouse. *PLoS Biol* 7, e1000112.
- Murphy, R., Ellard, S. and Hattersley, A.T. (2008) Clinical implications of a molecular genetic classification of monogenic β -cell diabetes. *Nat Clin Pract Endocrinol Metab* 4, 200-213.
- Murphy, R., Tura, A., Clark, P.M., Holst, J.J., Mari, A. and Hattersley, A.T. (2009) Glucokinase, the pancreatic glucose sensor, is not the gut glucose sensor. *Diabetologia* 52, 154-159.
- Nagy, A., Gertsens, M., Vintersten, K. and Behringer, R. (2003) *Manipulating the mouse embryo: A laboratory manual*, 3. edn., Cold Spring Harbor Laboratory Press, Oxford, UK and New York, USA.
- Naya, F.J., Huang, H.P., Qiu, Y., Mutoh, H., DeMayo, F.J., Leiter, A.B. and Tsai, M.J. (1997) Diabetes, defective pancreatic morphogenesis, and abnormal enteroendocrine differentiation in *BETA2/neuroD*-deficient mice. *Genes Dev* 11, 2323-2334.
- Neve, B., Fernandez-Zapico, M.E., Ashkenazi-Katalan, V., Dina, C., Hamid, Y.H., Joly, E., Vaillant, E., Benmezroua, Y., Durand, E., Bakaher, N., Delannoy, V., Vaxillaire, M., Cook, T., Dallinga-Thie, G.M., Jansen, H., Charles, M.A., Clement, K., Galan, P., Hercberg, S., Helbecque, N., Charpentier, G., Prentki, M., Hansen, T., Pedersen, O., Urrutia, R., Melloul, D. and Froguel, P. (2005) Role of transcription factor KLF11 and its diabetes-associated gene variants in pancreatic β -cell function. *Proc Natl Acad Sci U S A* 102, 4807-4812.
- Newton, C.R., Graham, A., Heptinstall, L.E., Powell, S.J., Summers, C., Kalsheker, N., Smith, J.C. and Markham, A.F. (1989) Analysis of any point mutation in DNA. The amplification refractory mutation system (ARMS). *Nucleic Acids Res* 17, 2503-2516.
- Nguyen, D. and Xu, T. (2008) The expanding role of mouse genetics for understanding human biology and disease. *Dis Model Mech* 1, 56-66.
- Nielsen, J.H., Galsgaard, E.D., Moldrup, A., Friedrichsen, B.N., Billestrup, N., Hansen, J.A., Lee, Y.C. and Carlsson, C. (2001) Regulation of β -cell mass by hormones and growth factors. *Diabetes* 50 Suppl 1, S25-29.
- Nishi, M., Sasahara, M., Shono, T., Saika, S., Yamamoto, Y., Ohkawa, K., Furuta, H., Nakao, T., Sasaki, H. and Nanjo, K. (2005) A case of novel *de novo* paired box gene 6 (*PAX6*) mutation with early-onset diabetes mellitus and aniridia. *Diabet Med* 22, 641-644.
- Njolstad, P.R., Sovik, O., Cuesta-Munoz, A., Bjorkhaug, L., Massa, O., Barbetti, F., Undlien, D.E., Shiota, C., Magnuson, M.A., Molven, A., Matschinsky, F.M. and Bell, G.I. (2001) Neonatal diabetes mellitus due to complete glucokinase deficiency. *N Engl J Med* 344, 1588-1592.

- Nolan, P.M., Hugill, A. and Cox, R.D. (2002) ENU mutagenesis in the mouse: application to human genetic disease. *Brief Funct Genomic Proteomic* 1, 278-289.
- Nouspikel, T. and Iynedjian, P.B. (1992) Insulin signalling and regulation of glucokinase gene expression in cultured hepatocytes. *Eur J Biochem* 210, 365-373.
- Noveroske, J.K., Weber, J.S. and Justice, M.J. (2000) The mutagenic action of *N*-ethyl-*N*-nitrosourea in the mouse. *Mamm Genome* 11, 478-483.
- Nyunt, O., Wu, J.Y., McGown, I.N., Harris, M., Huynh, T., Leong, G.M., Cowley, D.M. and Cotterill, A.M. (2009) Investigating maturity-onset diabetes of the young. *Clin Biochem Rev* 30, 67-74.
- O'Brien, B.A., Harmon, B.V., Cameron, D.P. and Allan, D.J. (1996) Beta cell apoptosis is responsible for the development of IDDM in the multiple low-dose streptozotocin model. *J Pathol* 178, 176-181.
- O'Brien, T.P. and Frankel, W.N. (2004) Moving forward with chemical mutagenesis in the mouse. *J Physiol* 554, 13-21.
- Olek, K. (2006) Maturity-onset diabetes of the young: an update. *Clin Lab* 52, 593-598.
- Oliver, P.L., Bitoun, E. and Davies, K.E. (2007) Comparative genetic analysis: the utility of mouse genetic systems for studying human monogenic disease. *Mamm Genome* 18, 412-424.
- Onishi, T., Okawa, R., Ogawa, T., Shintani, S. and Ooshima, T. (2007) *Phex* mutation causes the reduction of *npt2b* mRNA in teeth. *J Dent Res* 86, 158-162.
- Osbak, K.K., Colclough, K., Saint-Martin, C., Beer, N.L., Bellanné-Chantelot, C., Ellard, S. and Gloyn, A.L. (2009) Update on mutations in glucokinase (*GCK*), which cause maturity-onset diabetes of the young, permanent neonatal diabetes, and hyperinsulinaemic hypoglycaemia. *Hum Mutat*.
- Paigen, K. (2003) One hundred years of mouse genetics: An intellectual history. II. The molecular revolution (1981-2002). *Genetics* 163, 1227-1235.
- Pal, P. and Miller, B.G. (2009) Activating mutations in the human glucokinase gene revealed by genetic selection. *Biochemistry* 48, 814-816.
- Papathanasiou, P. and Goodnow, C.C. (2005) Connecting mammalian genome with phenome by ENU mouse mutagenesis: gene combinations specifying the immune system. *Annu Rev Genet* 39, 241-262.
- Paris, M., Bernard-Kargar, C., Berthault, M.-F., Bouwens, L. and Ktorza, A. (2003) Specific and combined effects of insulin and glucose on functional pancreatic β -cell mass in vivo in adult rats. *Endocrinology* 144, 2717-2727.

Paris, M., Turrel-Cuzin, C., Plachot, C. and Ktorza, A. (2004) Review: pancreatic β -cell neogenesis revisited. *Exp Diabetes Res* 5, 111-121.

Payne, V.A., Arden, C., Wu, C., Lange, A.J. and Agius, L. (2005) Dual role of phosphofructokinase-2/fructose biphosphatase-2 in regulating the compartmentation and expression of glucokinase in hepatocytes. *Diabetes* 54, 1949-1957.

Pearson, E.R., Boj, S.F., Steele, A.M., Barrett, T., Stals, K., Shield, J.P., Ellard, S., Ferrer, J. and Hattersley, A.T. (2007) Macrosomia and hyperinsulinaemic hypoglycaemia in patients with heterozygous mutations in the HNF4A gene. *PLoS Med* 4, e118.

Peltonen, L. and McKusick, V.A. (2001) Genomics and Medicine: Dissecting human disease in the postgenomic era. *Science* 291, 1224-1229.

Platt, N., da Silva, R.P. and Gordon, S. (1998) Recognising death: the phagocytosis of apoptotic cells. *Trends Cell Biol* 8, 365-372.

Plengvidhya, N., Kooptiwut, S., Songtawee, N., Doi, A., Furuta, H., Nishi, M., Nanjo, K., Tantibhedhyangkul, W., Boonyasrisawat, W., Yenchitsomanus, P.T., Doria, A. and Banchuin, N. (2007) PAX4 mutations in Thais with maturity onset-diabetes of the young. *J Clin Endocrinol Metab* 92, 2821-2826.

Porter, J.R. and Barrett, T.G. (2005) Monogenic syndromes of abnormal glucose homeostasis: clinical review and relevance to the understanding of the pathology of insulin resistance and β -cell failure. *J Med Genet* 42, 893-902.

Postic, C., Decaux, J.-F. and Girard, J. (2004) Regulation of hepatic glucokinase gene expression. In: *Glucokinase and Glycaemic Disease: From Basics to Novel Therapeutics*. , Eds: F.M. Matschinsky and M.A. Magnuson, Karger Basel. pp 180-192.

Postic, C., Niswender, K.D., Decaux, J.F., Parsa, R., Shelton, K.D., Gouhot, B., Pettepher, C.C., Granner, D.K., Girard, J. and Magnuson, M.A. (1995) Cloning and characterisation of the mouse glucokinase gene locus and identification of distal liver-specific DNase I hypersensitive sites. *Genomics* 29, 740-750.

Postic, C., Shiota, M. and Magnuson, M.A. (2001) Cell-specific roles of glucokinase in glucose homeostasis. *Recent Prog Horm Res* 56, 195-217.

Postic, C., Shiota, M., Niswender, K.D., Jetton, T.L., Chen, Y., Moates, J.M., Shelton, K.D., Lindner, J., Cherrington, A.D. and Magnuson, M.A. (1999) Dual roles for glucokinase in glucose homeostasis as determined by liver and pancreatic β -cell-specific gene knock-outs using Cre recombinase. *J. Biol. Chem.* 274, 305-315.

Printz, R.L. and Granner, D.K. (2005) Tweaking the glucose sensor: adjusting glucokinase activity with activator compounds. *Endocrinology* 146, 3693-3695.

- Printz, R.L., Magnuson, M.A. and Granner, D.K. (1993) Mammalian glucokinase. *Annu Rev Nutr* 13, 463-496.
- Pruhova, S., Ek, J., Lebl, J., Sumnik, Z., Saudek, F., Andel, M., Pedersen, O. and Hansen, T. (2003) Genetic epidemiology of MODY in the Czech republic: new mutations in the MODY genes HNF-4 α , GCK and HNF-1 α . *Diabetologia* 46, 291-295.
- Rabinovitch, A., Quigley, C., Russell, T., Patel, Y. and Mintz, D.H. (1982) Insulin and multiplication stimulating activity (an insulin-like growth factor) stimulate islet (β -cell) replication in neonatal rat pancreatic monolayer cultures. *Diabetes* 31, 160-164.
- Radziuk, J. and Pye, S. (2001) Hepatic glucose uptake, gluconeogenesis and the regulation of glycogen synthesis. *Diabetes Metab Res Rev* 17, 250-272.
- Ræder, H., Johansson, S., Holm, P.I., Haldorsen, I.S., Mas, E., Sbarra, V., Neramoen, I., Eide, S.A., Grevle, L., Bjorkhaug, L., Sagen, J.V., Aksnes, L., Sovik, O., Lombardo, D., Molven, A. and Njolstad, P.R. (2006) Mutations in the *CEL* VNTR cause a syndrome of diabetes and pancreatic exocrine dysfunction. *Nat Genet* 38, 54-62.
- Rathkolb, B., Decker, T., Fuchs, E., Soewarto, D., Fella, C., Heffner, S., Pargent, W., Wanke, R., Balling, R., Hrabé de Angelis, M., Kolb, H.J. and Wolf, E. (2000) The clinical-chemical screen in the Munich ENU mouse mutagenesis project: screening for clinically relevant phenotypes. *Mamm Genome* 11, 543-546.
- Reeves, R.H. and D'Eustachio, P. (1999) Genetic and Comparative Mapping in Mice. In: *Genome Analysis: A Laboratory Manual Series 4*, Eds: B. Birren, E.D. Green, P. Hieter, S. Klapholz, R.M. Myers, H. Riethman and J. Roskams, Cold Spring Harbor Laboratory Press, U.S.
- Rehman, H.U. (2001) Diabetes mellitus in the young. *J R Soc Med* 94, 65-67.
- Reinecke-Luthge, A., Koschoreck, F. and Kloppel, G. (2000) The molecular basis of persistent hyperinsulinaemic hypoglycaemia of infancy and its pathologic substrates. *Virchows Arch* 436, 1-5.
- Reynolds, T.M., Smellie, W.S.A. and Twomey, P.J. (2003) Tests of glycaemia in diabetes. *Diabetes Care* 26, s106-s108.
- Reznik, Y., Dao, T., Coutant, R., Chiche, L., Jeannot, E., Clauin, S., Rousselot, P., Fabre, M., Oberti, F., Fatome, A., Zucman-Rossi, J. and Bellanne-Chantelot, C. (2004) Hepatocyte nuclear factor-1 α gene inactivation: cosegregation between liver adenomatosis and diabetes phenotypes in two maturity-onset diabetes of the young (MODY) 3 families. *J Clin Endocrinol Metab* 89, 1476-1480.
- Rhodes, C.J. (2005) Type 2 diabetes—a matter of β -cell life and death? *Science* 307, 380-384.

- Robertson, R.P., Harmon, J., Tran, P.O., Tanaka, Y. and Takahashi, H. (2003) Glucose toxicity in β -cells: type 2 diabetes, good radicals gone bad, and the glutathione connection. *Diabetes* 52, 581-587.
- Rohrl, J., Yang, D., Oppenheim, J.J. and Hehlhans, T. (2008) Identification and biological characterisation of mouse β -defensin 14, the orthologue of human β -defensin 3. *J Biol Chem* 283, 5414-5419.
- Rosenthal, N. and Brown, S. (2007) The mouse ascending: perspectives for human-disease models. *Nat Cell Biol* 9, 993-999.
- Rossant, J. and McKerlie, C. (2001) Mouse-based phenogenomics for modelling human disease. *Nat Rev Genet* 2, 502-507.
- Russ, A., Stumm, G., Augustin, M., Sedlmeier, R., Wattler, S. and Nehls, M. (2002) Random mutagenesis in the mouse as a tool in drug discovery. *Drug Discov Today* 7, 1175-1183.
- Russell, W.L., Kelly, E.M., Hunsicker, P.R., Bangham, J.W., Maddux, S.C. and Phipps, E.L. (1979) Specific-locus test shows ethylnitrosourea to be the most potent mutagen in the mouse. *Proc Natl Acad Sci U S A* 76, 5818-5819.
- Sacks, D.B. (1997) Implications of the revised criteria for diagnosis and classification of diabetes mellitus. *Clin Chem* 43, 2230-2232.
- Sagen, J.V., Bjorkhaug, L., Molnes, J., Raeder, H., Grevle, L., Sovik, O., Molven, A. and Njolstad, P.R. (2008) Diagnostic screening of MODY2/GCK mutations in the Norwegian MODY Registry. *Pediatr Diabetes* 9, 442-449.
- Sagen, J.V., Odili, S., Bjorkhaug, L., Zelent, D., Buettger, C., Kwagh, J., Stanley, C., Dahl-Jorgensen, K., de Beaufort, C., Bell, G.I., Han, Y., Grimsby, J., Taub, R., Molven, A., Sovik, O., Njolstad, P.R. and Matschinsky, F.M. (2006) From clinicogenetic studies of maturity-onset diabetes of the young to unraveling complex mechanisms of glucokinase regulation. *Diabetes* 55, 1713-1722.
- Sakuraba, Y., Sezutsu, H., Takahashi, K.R., Tsuchihashi, K., Ichikawa, R., Fujimoto, N., Kaneko, S., Nakai, Y., Uchiyama, M., Goda, N., Motoi, R., Ikeda, A., Karashima, Y., Inoue, M., Kaneda, H., Masuya, H., Minowa, O., Noguchi, H., Toyoda, A., Sakaki, Y., Wakana, S., Noda, T., Shiroishi, T. and Gondo, Y. (2005) Molecular characterisation of ENU mouse mutagenesis and archives. *Biochem Biophys Res Commun* 336, 609-616.
- Sanderson, B.J. and Shield, A.J. (1996) Mutagenic damage to mammalian cells by therapeutic alkylating agents. *Mutat Res* 355, 41-57.
- Sarabu, R. and Grimsby, J. (2005) Targeting glucokinase activation for the treatment of type 2 diabetes—a status review. *Curr Opin Drug Discov Devel* 8, 631-637.

Sarabu, R., Taub, R. and Grimsby, J. (2007) Glucokinase activation - a strategy for T2D therapy: recent developments. *Drug Discovery Today: Therapeutic Strategies* 4, 111-115.

Schimenti, J. and Bucan, M. (1998) Functional genomics in the mouse: phenotype-based mutagenesis screens. *Genome Res* 8, 698-710.

Schuppin, G.T., Bonner-Weir, S., Montana, E., Kaiser, N. and Weir, G.C. (1993) Replication of adult pancreatic-beta cells cultured on bovine corneal endothelial cell extracellular matrix. *In Vitro Cell Dev Biol Anim* 29A, 339-344.

Shamir, R., Johnson, W.J., Morlock-Fitzpatrick, K., Zolfaghari, R., Li, L., Mas, E., Lombardo, D., Morel, D.W. and Fisher, E.A. (1996) Pancreatic carboxyl ester lipase: a circulating enzyme that modifies normal and oxidised lipoproteins in vitro. *J Clin Invest* 97, 1696-1704.

Shibuya, T. and Morimoto, K. (1993) A review of the genotoxicity of 1-ethyl-1-nitrosourea. *Mutat Res* 297, 3-38.

Sidman, R.L., Dickie, M.M. and Appel, S.H. (1964) Mutant mice (quaking and jimpy) with deficient myelination in the central nervous system. *Science* 144, 309-311.

Silver, L.M. (1995) *Mouse Genetics: Concepts and applications*, Oxford University press, Oxford, UK and New York, USA.

Siner, J.M., Jiang, G., Cohen, Z.I., Shan, P., Zhang, X., Lee, C.G., Elias, J.A. and Lee, P.J. (2007) VEGF-induced heme oxygenase-1 confers cytoprotection from lethal hypoxia in vivo. *FASEB J* 21, 1422-1432.

Singh, R. (2006) The importance of making a genetic diagnosis of diabetes. *Canadian Journal of Diabetes* 30, 183-190.

Sladek, F.M., Zhong, W.M., Lai, E. and Darnell, J.E., Jr. (1990) Liver-enriched transcription factor HNF-4 is a novel member of the steroid hormone receptor superfamily. *Genes Dev* 4, 2353-2365.

Slein, M.W., Cori, G.T. and Cori, C.F. (1950) A comparative Study of hexokinase from yeast and animal tissues. *J. Biol. Chem.* 186, 763-779.

Smith, S.B., Ee, H.C., Connors, J.R. and German, M.S. (1999) Paired-homeodomain transcription factor PAX4 acts as a transcriptional repressor in early pancreatic development. *Mol. Cell. Biol.* 19, 8272-8280.

Smits, B.M.G., Haag, J.D., Gould, M.N. and Cuppen, E. (2008) Rat knockout and mutant models. In: *Sourcebook of Models for Biomedical Research*, Ed: P.M. Conn, Humana Press, Totowa, USA. pp 171-178.

Soewarto, D., Fella, C., Teubner, A., Rathkolb, B., Pargent, W., Heffner, S., Marschall, S., Wolf, E., Balling, R., Hrabé and de Angelis, M. (2000) The large-scale Munich ENU mouse mutagenesis screen. *Mamm Genome* 11, 507-510.

Sosa-Pineda, B., Chowdhury, K., Torres, M., Oliver, G. and Gruss, P. (1997) The Pax4 gene is essential for differentiation of insulin-producing β -cells in the mammalian pancreas. *Nature* 386, 399-402.

Spradling, A., Ganetsky, B., Hieter, P., Johnston, M., Olson, M., Orr-Weaver, T., Rossant, J., Sanchez, A. and Waterston, R. (2006) New roles for model genetic organisms in understanding and treating human disease: report from the 2006 Genetics Society of America meeting. *Genetics* 172, 2025-2032.

Sreenan, S.K., Cockburn, B.N., Baldwin, A.C., Ostrega, D.M., Levisetti, M., Grupe, A., Bell, G.I., Stewart, T.A., Roe, M.W. and Polonsky, K.S. (1998) Adaptation to hyperglycaemia enhances insulin secretion in glucokinase mutant mice. *Diabetes* 47, 1881-1888.

St-Onge, L., Sosa-Pineda, B., Chowdhury, K., Mansouri, A. and Gruss, P. (1997) Pax6 is required for differentiation of glucagon-producing α -cells in mouse pancreas. *Nature* 387, 406-409.

St Charles, R., Harrison, R.W., Bell, G.I., Pilkis, S.J. and Weber, I.T. (1994) Molecular model of human β -cell glucokinase built by analogy to the crystal structure of yeast hexokinase B. *Diabetes* 43, 784-791.

Stanford, W.L., Cohn, J.B. and Cordes, S.P. (2001) Gene-trap mutagenesis: past, present and beyond. *Nat Rev Genet* 2, 756-768.

Stanger, B.Z. (2008) HNF4A and diabetes: injury before insult? *Diabetes* 57, 1461-1462.

Stoffers, D.A., Ferrer, J., Clarke, W.L. and Habener, J.F. (1997a) Early-onset type-II diabetes mellitus (MODY4) linked to *IPF1*. *Nat Genet* 17, 138-139.

Stoffers, D.A., Zinkin, N.T., Stanojevic, V., Clarke, W.L. and Habener, J.F. (1997b) Pancreatic agenesis attributable to a single nucleotide deletion in the human *IPF1* gene coding sequence. *Nat Genet* 15, 106-110.

Stride, A., Vaxillaire, M., Tuomi, T., Barbetti, F., Njølstad, P.R., Hansen, T., Costa, A., Conget, I., Pedersen, O., Søvik, O., Lorini, R., Groop, L., Froguel, P. and Hattersley, A.T. (2002) The genetic abnormality in the β -cell determines the response to an oral glucose load. *Diabetologia* 45, 427-435.

Sturis, J., Kurland, I.J., Byrne, M.M., Mosekilde, E., Froguel, P., Pilkis, S.J., Bell, G.I. and Polonsky, K.S. (1994) Compensation in pancreatic β -cell function in subjects with glucokinase mutations. *Diabetes* 43, 718-723.

Takeda, J., Gidh-Jain, M., Xu, L.Z., Froguel, P., Velho, G., Vaxillaire, M., Cohen, D., Shimada, F., Makino, H., Nishi, S. and et al. (1993) Structure/function studies of human β -cell glucokinase. Enzymatic properties of a sequence polymorphism, mutations associated with diabetes, and other site-directed mutants. *J Biol Chem* 268, 15200-15204.

- Tanaka, M. (2005) Apoptotic cell clearance by phagocytes. *International Congress Series* 1285, 55-59.
- Tattersall, R.B. (1974) Mild familial diabetes with dominant inheritance. *Q J Med* 43, 339-357.
- Tattersall, R.B. and Fajans, S.S. (1975) A difference between the inheritance of classical juvenile-onset and maturity-onset type diabetes of young people. *Diabetes* 24, 44-53.
- Terauchi, Y., Sakura, H., Yasuda, K., Iwamoto, K., Takahashi, N., Ito, K., Kasai, H., Suzuki, H., Ueda, O., Kamada, N. and et al. (1995) Pancreatic β -cell-specific targeted disruption of glucokinase gene. Diabetes mellitus due to defective insulin secretion to glucose. *J Biol Chem* 270, 30253-30256.
- Terauchi, Y., Takamoto, I., Kubota, N., Matsui, J., Suzuki, R., Komeda, K., Hara, A., Toyoda, Y., Miwa, I., Aizawa, S., Tsutsumi, S., Tsubamoto, Y., Hashimoto, S., Eto, K., Nakamura, A., Noda, M., Tobe, K., Aburatani, H., Nagai, R. and Kadowaki, T. (2007) Glucokinase and IRS-2 are required for compensatory β -cell hyperplasia in response to high-fat diet-induced insulin resistance. *J Clin Invest* 117, 246-257.
- Thomas, H., Jaschowitz, K., Bulman, M., Frayling, T.M., Mitchell, S.M., Roosen, S., Lingott-Frieg, A., Tack, C.J., Ellard, S., Ryffel, G.U. and Hattersley, A.T. (2001) A distant upstream promoter of the HNF-4 α gene connects the transcription factors involved in maturity-onset diabetes of the young. *Hum Mol Genet* 10, 2089-2097.
- Thomson, K.L., Gloyn, A.L., Colclough, K., Batten, M., Allen, L.I.S., Beards, F., Hattersley, A.T. and Ellard, S. (2003) Identification of 21 novel glucokinase mutations in UK and European Caucasians with maturity-onset diabetes of the young (MODY). *Human Mutation* 22, 417.
- Tiedge, M. and Lenzen, S. (1991) Regulation of glucokinase and GLUT-2 glucose-transporter gene expression in pancreatic β -cells. *Biochem J* 279 (Pt 3), 899-901.
- Timsit, J., Bellanné-Chantelot, C., Dubois-Laforgue, D. and Velho, G. (2005) Diagnosis and management of maturity-onset diabetes of the young. *Treat Endocrinol* 4, 9-18.
- Toye, A.A., Moir, L., Hugill, A., Bentley, L., Quarterman, J., Mijat, V., Hough, T., Goldsworthy, M., Haynes, A., Hunter, A.J., Browne, M., Spurr, N. and Cox, R.D. (2004) A new mouse model of type 2 diabetes, produced by *N*-ethyl-nitrosourea mutagenesis, is the result of a missense mutation in the glucokinase gene. *Diabetes* 53, 1577-1583.
- Toyoda, Y., Yoshie, S., Fujita, T., Ito, Y., Nonogaki, T. and Miwa, I. (1997) Glucokinase is located in secretory granules of pancreatic δ -cells. *FEBS Lett* 415, 281-284.

- Toyoda, Y., Yoshie, S., Shironoguchi, H. and Miwa, I. (1999) Glucokinase is concentrated in insulin-secretory granules of pancreatic β -cells. *Histochem Cell Biol* 112, 35-40.
- Trus, M.D., Zawalich, W.S., Burch, P.T., Berner, D.K., Weill, V.A. and Matschinsky, F.M. (1981) Regulation of glucose metabolism in pancreatic islets. *Diabetes* 30, 911-922.
- Tsuruzoe, K., Araki, E., Furukawa, N., Shirotani, T., Matsumoto, K., Kaneko, K., Motoshima, H., Yoshizato, K., Shirakami, A., Kishikawa, H., Miyazaki, J. and Shichiri, M. (1998) Creation and characterization of a mitochondrial DNA-depleted pancreatic β -cell line: impaired insulin secretion induced by glucose, leucine, and sulfonylureas. *Diabetes* 47, 621-631.
- Turkkahraman, D., Bircan, I., Tribble, N.D., Akcurin, S., Ellard, S. and Gloyn, A.L. (2008) Permanent neonatal diabetes mellitus caused by a novel homozygous (T168A) glucokinase (*GCK*) mutation: initial response to oral sulphonylurea therapy. *J Pediatr* 153, 122-126.
- Ulinski, T., Lescure, S., Beaufils, S., Guignonis, V., Decramer, S., Morin, D., Clauin, S., Deschenes, G., Bouissou, F., Bensman, A. and Bellanné-Chantelot, C. (2006) Renal phenotypes related to hepatocyte nuclear factor-1 β (*TCF2*) mutations in a pediatric cohort. *J Am Soc Nephrol* 17, 497-503.
- van de Bunt, M. and Gloyn, A.L. (2007) Monogenic disorders of the pancreatic β -cell: personalising treatment for rare forms of diabetes and hypoglycaemia. *Personalized Medicine* 4, 247-259.
- van Haeften, T.W., van Maarschalkerweerd, W.W., Gerich, J.E. and van der Veen, E.A. (1991) Decreased insulin secretory capacity and normal pancreatic β -cell glucose sensitivity in non-obese patients with NIDDM. *Eur J Clin Invest* 21, 168-174.
- van Harten, A.M. (1998) *Mutation breeding: theory and practical applications*, Cambridge University Press, Cambridge, UK.
- van Schaftingen, E., Detheux, M. and Veiga da Cunha, M. (1994) Short-term control of glucokinase activity: role of a regulatory protein. *FASEB J* 8, 414-419.
- van Tilburg, J., van Haeften, T.W., Pearson, P. and Wijmenga, C. (2001) Defining the genetic contribution of type 2 diabetes mellitus. *J Med Genet* 38, 569-578.
- Vaxillaire, M. and Froguel, P. (2008) Monogenic diabetes in the young, pharmacogenetics and relevance to multifactorial forms of type 2 diabetes. *Endocr Rev* 29, 254-264.
- Vaxillaire, M., Samson, C., Cave, H., Metz, C., Froguel, P. and Polak, M. (2002) Glucokinase gene mutations are not a common cause of permanent neonatal diabetes in France. *Diabetologia* 45, 454-455.

- Veiga-da-Cunha, M., Xu, L.Z., Lee, Y.H., Marotta, D., Pilkis, S.J. and van Schaffingen, E. (1996) Effect of mutations on the sensitivity of human β -cell glucokinase to liver regulatory protein. *Diabetologia* 39, 1173-1179.
- Velho, G., Blanche, H., Vaxillaire, M., Bellanne-Chantelot, C., Pardini, V.C., Timsit, J., Passa, P., Deschamps, I., Robert, J.J., Weber, I.T., Marotta, D., Pilkis, S.J., Lipkind, G.M., Bell, G.I. and Froguel, P. (1997) Identification of 14 new glucokinase mutations and description of the clinical profile of 42 MODY-2 families. *Diabetologia* 40, 217-224.
- Velho, G. and Froguel, P. (1998) Genetic, metabolic and clinical characteristics of maturity-onset diabetes of the young. *Eur J Endocrinol* 138, 233-239.
- Velho, G., Froguel, P., Clement, K., Pueyo, M.E., Rakotoambinina, B., Zouali, H., Passa, P., Cohen, D. and Robert, J.J. (1992) Primary pancreatic β -cell secretory defect caused by mutations in glucokinase gene in kindreds of maturity-onset diabetes of the young. *Lancet* 340, 444-448.
- Velho, G. and Robert, J.J. (2002) Maturity-onset diabetes of the young (MODY): genetic and clinical characteristics. *Horm Res* 57 Suppl 1, 29-33.
- Velho, G., Vaxillaire, M., Boccio, V., Charpentier, G. and Froguel, P. (1996) Diabetes complications in NIDDM kindreds linked to the MODY3 locus on chromosome 12q. *Diabetes Care* 19, 915-919.
- Vesterhus, M., Haldorsen, I.S., Raeder, H., Molven, A. and Njolstad, P.R. (2008a) Reduced pancreatic volume in hepatocyte nuclear factor-1A-maturity-onset diabetes of the young. *J Clin Endocrinol Metab* 93, 3505-3509.
- Vesterhus, M., Raeder, H., Johansson, S., Molven, A. and Njolstad, P.R. (2008b) Pancreatic exocrine dysfunction in maturity-onset diabetes of the young type 3. *Diabetes Care* 31, 306-310.
- Walker, D.G. and Holland, G. (1965) The development of hepatic glucokinase in the neonatal rat. *Biochem J* 97, 845-854.
- Walker, D.G. and Rao, S. (1964) The role of glucokinase in the phosphorylation of glucose by rat liver. *Biochem J* 90, 360-368.
- Wallace, T.M., Levy, J.C. and Matthews, D.R. (2004) Use and abuse of HOMA modelling. *Diabetes Care* 27, 1487-1495.
- Wang, J., Takeuchi, T., Tanaka, S., Kubo, S.K., Kayo, T., Lu, D., Takata, K., Koizumi, A. and Izumi, T. (1999) A mutation in the insulin 2 gene induces diabetes with severe pancreatic β -cell dysfunction in the Mody mouse. *J Clin Invest* 103, 27-37.
- Wanke, R., Weis, S., Kluge, D., Kahnt, E., Schenck, E., Brem, G. and Herrmanns, W. (1994) Morphometric evaluation of the pancreas of growth hormone-transgenic mice. *Acta Stereologica*, 3-8.

Waterfield, T. and Gloyn, A.L. (2008) Monogenic β -cell dysfunction in children: clinical phenotypes, genetic etiology and mutational pathways. *Pediatric Health* 2, 517-532.

Weedon, M.N., McCarthy, M.I., Hitman, G., Walker, M., Groves, C.J., Zeggini, E., Rayner, N.W., Shields, B., Owen, K.R., Hattersley, A.T. and Frayling, T.M. (2006) Combining information from common type 2 diabetes risk polymorphisms improves disease prediction. *PLoS Med* 3, e374.

Weibel, E.R. (1979) *Stereological methods: Practical methods for biological morphometry* Academic Press.

Weng, J., Macfarlane, W.M., Lehto, M., Gu, H.F., Shepherd, L.M., Ivarsson, S.A., Wibell, L., Smith, T. and Groop, L.C. (2001) Functional consequences of mutations in the MODY4 gene (*IPF1*) and coexistence with MODY3 mutations. *Diabetologia* 44, 249-258.

Wild, S., Roglic, G., Green, A., Sicree, R. and King, H. (2004) Global prevalence of diabetes: estimates for the year 2000 and projections for 2030. *Diabetes Care* 27, 1047-1053.

Winter, W.E. (2000) Molecular and biochemical analysis of the MODY syndromes. *Pediatr Diabetes* 1, 88-117.

Winter, W.E. (2003) Newly defined genetic diabetes syndromes: maturity-onset diabetes of the young. *Rev Endocr Metab Disord* 4, 43-51.

Woychik, R.P., Klebig, M.L., Justice, M.J., Magnuson, T.R. and Avner, E.D. (1998) Functional genomics in the post-genome era. *Mutat Res* 400, 3-14.

Xing, C., Schumacher, F.R., Xing, G., Lu, Q., Wang, T. and Elston, R.C. (2005) Comparison of microsatellites, single-nucleotide polymorphisms (SNPs) and composite markers derived from SNPs in linkage analysis. *BMC Genet* 6 Suppl 1, S29.

Yamagata, K., Furuta, H., Oda, N., Kaisaki, P.J., Menzel, S., Cox, N.J., Fajans, S.S., Signorini, S., Stoffel, M. and Bell, G.I. (1996) Mutations in the hepatocyte nuclear factor-4 α gene in maturity-onset diabetes of the young (MODY1). *Nature* 384, 458-460.

Yasuda, T., Kajimoto, Y., Fujitani, Y., Watada, H., Yamamoto, S., Watarai, T., Umayahara, Y., Matsuhisa, M., Gorogawa, S., Kuwayama, Y., Tano, Y., Yamasaki, Y. and Hori, M. (2002) *PAX6* mutation as a genetic factor common to aniridia and glucose intolerance. *Diabetes* 51, 224-230.

Yoon, K.H., Ko, S.H., Cho, J.H., Lee, J.M., Ahn, Y.B., Song, K.H., Yoo, S.J., Kang, M.I., Cha, B.Y., Lee, K.W., Son, H.Y., Kang, S.K., Kim, H.S., Lee, I.K. and Bonner-Weir, S. (2003) Selective β -cell loss and α -cell expansion in patients with type 2 diabetes mellitus in Korea. *J Clin Endocrinol Metab* 88, 2300-2308.

Yoshioka, M., Kayo, T., Ikeda, T. and Koizumi, A. (1997) A novel locus, Mody4, distal to D7Mit189 on chromosome 7 determines early-onset NIDDM in nonobese C57BL/6 (Akita) mutant mice. *Diabetes* 46, 887-894.

Zelent, D., Golson, M.L., Koeberlein, B., Quintens, R., van Lommel, L., Buettger, C., Weik-Collins, H., Taub, R., Grimsby, J., Schuit, F., Kaestner, K.H. and Matschinsky, F.M. (2006) A glucose sensor role for glucokinase in anterior pituitary cells. *Diabetes* 55, 1923-1929.

Zelent, D., Najafi, H., Odili, S., Buettger, C., Weik-Collins, H., Li, C., Doliba, N., Grimsby, J. and Matschinsky, F.M. (2005) Glucokinase and glucose homeostasis: proven concepts and new ideas. *Biochem Soc Trans* 33, 306-310.

Zimmet, P., Alberti, K.G. and Shaw, J. (2001) Global and societal implications of the diabetes epidemic. *Nature* 414, 782-787.

Zinovieva, N., Vasicek, D., Aigner, B., Müller, M. and Brem, G. (1996) Short communication: single tube allele specific (STAS) PCR for direct determination of the mutation in the porcine ryanodine receptor gene associated with malignant hyperthermia. *Animal Biotechnology* 7(2), 173-177.

Zuber, C., Fan, J.Y., Guhl, B. and Roth, J. (2004) Misfolded proinsulin accumulates in expanded pre-Golgi intermediates and endoplasmic reticulum subdomains in pancreatic β -cells of Akita mice. *FASEB J* 18, 917-919.

9. Attachment

9.1 Basic glucokinase enzyme kinetics and their extrapolation to studies

Deviant from other members of the hexokinase family, the catalytic enzyme glucokinase exhibits profoundly unexpected structural and kinetic properties. Unlike other hexokinases, which follow Michaelis-Menten kinetics, the glucokinase is reported to exhibit sigmoidal substrate dependency. The sigmoidicity of the substrate saturation curve (= cooperativeness of the enzyme with a ligand) is described by the Hill coefficient n_H ($n_H > 1$ indicates a positive cooperativity). Even displaying the kinetic behaviour of a monomeric enzyme, glucokinase displays a slightly positive ($n_H = 1.7$) cooperativeness (= strength of a substrate-enzyme interaction, depending on the number of subunits, already occupied by substrate molecules) with its main substrate glucose (Bisswanger 2008; Cornish-Bowden and Cárdenas 2004; Matschinsky 2002). Due to exhibition of allostericity, the application of the Michaelis-Menten theory to determine kinetic characteristics of the glucokinase is therefore obsolete. Representing critical attempts to understand kinetic enzyme behaviour, the maximal reaction velocity (V_{max}) and the the glucose level at the half-maximal activity rate ($S_{0.5} \triangleq K_m$ in the Michaelis-Menten equation and indicates the substrate affinity of the respective enzyme) for the glucokinase enzyme may be determined by two distinct approaches (Matschinsky *et al.* 1998) (Fig. 9.1)

- Extrapolation of sigmoidal glucokinase substrate-velocity curves by linear regression would result in kinetic constants, slightly deviant from the intrinsic kinetic characteristics. However, particularly in studies of crude tissue extracts from pancreatic islets or liver, a linear transformation of the Michaelis-Menten equation, approximating $S_{0.5}$ or V_{max} values by extrapolation, is feasible. The Hanes-Woolf plot (ratio of substrate concentration to reaction velocity is plotted against the respective substrate concentration) is predicted to be the most suitable plot for this purpose with the error usually being small due to genuine application of the substrate concentrations on the x-axis. The slope of the regression line indicates $1/V_{max}$, the y-intercept is equal to $S_{0.5}/V_{max}$ (Matschinsky *et al.* 1998).

- The Hill equation, a linear transformation of the Michaelis-Menten kinetics is propagated to be best to illustrate glucose phosphorylation by glucokinase:

$$V = \frac{S^{n_H} \cdot V_{\max}}{S^{n_H} + S_{0.5}^{n_H}}$$

V = The specific substrate turnover rate at a given substrate concentration

S = Corresponding substrate concentration

n_H = Hill coefficient

V_{\max} = Maximal specific enzyme activity

$S_{0.5}$ = Respective glucose level at the half-maximal substrate turnover rate

However, application of the Hill equation requires the knowledge of V_{\max} , which has to be determined by other methods, mentioned above.

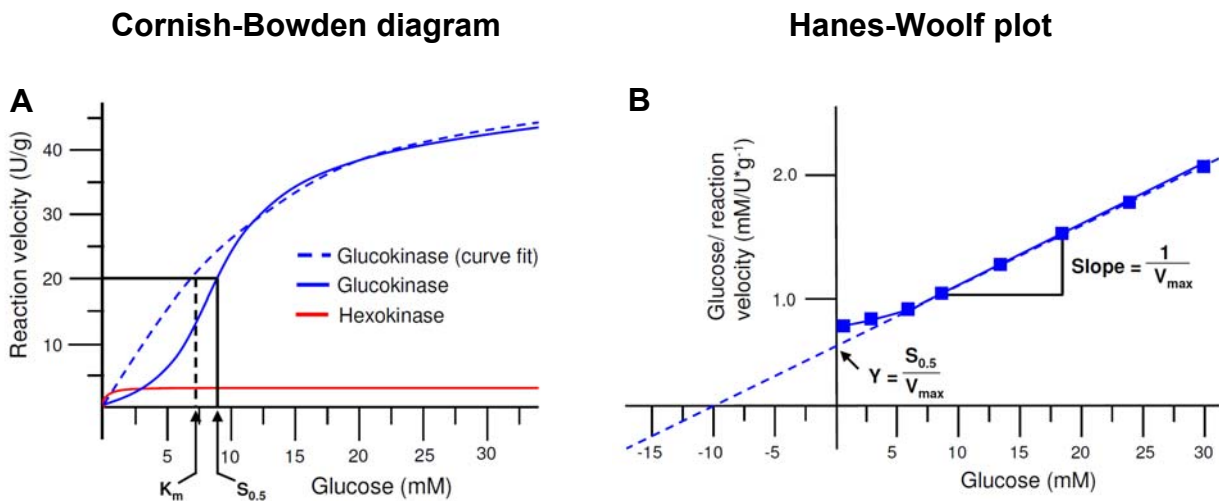


Figure 9.1: Kinetic concepts of glucokinase and their extrapolation for kinetic studies.

A: Direct-linear illustration (reaction velocity as a function of the substrate concentration; Cornish-Bowden diagram) of the substrate saturation curves of glucokinase (blue lines) and the high-affinity hexokinases (red line). Extrapolation of the reaction velocities of glucokinase by non-linear regression (hyperbolic curve (dashed blue line)) may result in misleading kinetic constants, as stated for the half-maximal saturation glucose concentrations (K_m and $S_{0.5}$, respectively). Due to the intrinsically sigmoidal behaviour of the glucokinase saturation curve (continuous line), glucose concentrations where glucokinase displays half-maximal saturation ($S_{0.5}$) would be higher than after extrapolation (K_m). While other hexokinases are saturated already at low glucose concentrations (low K_m), glucokinase enzyme exhibits low glucose affinity (high K_m and $S_{0.5}$, respectively). B: The Hanes-Woolf plot (ratio of substrate

concentration to reaction velocity as a function of the respective substrate concentrations) is practicable to determine kinetic constants (V_{max} , $S_{0.5}$) of the glucokinase enzyme. However, due to non-linearity of the original curve (continuous line) up to a glucose concentration of about 8-10 mM, extrapolation of measurement data by linear regression (dashed line) would lead to results for V_{max} and $S_{0.5}$, slightly deviant from the intrinsic kinetic characteristics of the glucokinase enzyme.

9.2 Low resolution mapping results

The causative mutations in GLS001 and GLS006 mice were mapped to a defined chromosomal region by linkage analysis. For this purpose, the distribution of mice, displaying either a heterozygous (het) or the outcross (ocr = C57BL/6J) genotype with the respective polymorphic marker (SNP) was applied to evaluate the linkage (indicated by χ^2 values) between the diabetic phenotype and the corresponding DNA marker (Table 9.1 and 9.2).

9.2.1 GLS001 mice

Table 9.1: Low resolution mapping results in GLS001 G2 backcross mice.

Chromosome	Locus (Mb)	RefSNP	Success rate	Het	Ocr	χ^2 value	P-value
1	29.94	rs3706618	100.00	48	42	0.00	>0.01
	44.08	rs13459182	95.56	46	40	0.74	>0.01
	63.05	rs3688436	100.00	46	44	0.18	>0.01
	74.62	rs3090522	98.89	43	46	0.10	>0.01
	90.37	rs3684025	97.78	41	47	0.00	>0.01
	109.28	rs13476046	98.89	41	48	0.01	>0.01
	119.66	rs3672659	97.78	38	50	0.05	>0.01
	135.04	rs8250085	100.00	41	49	0.04	>0.01
	149.63	rs6264289	98.89	41	48	0.10	>0.01
	156.81	rs4222732	98.89	42	47	0.28	>0.01
	177.06	rs3702990	97.78	43	45	0.00	>0.01
189.21	rs13476297	100.00	46	44	0.00	>0.01	
2	13.39	rs13476352	100.00	44	46	0.18	>0.01
	37.71	rs3022883	100.00	42	48	0.00	>0.01
	57.61	rs3663027	98.89	43	46	0.01	>0.01
	71.17	rs4223216	98.89	40	49	0.55	>0.01
	102.83	rs13476672	98.89	42	47	2.53	>0.01
	118.95	rs8279353	100.00	48	42	0.18	>0.01
	131.74	rs4223511	100.00	47	43	0.04	>0.01
	149.20	rs3675393	98.89	49	40	0.55	>0.01

3	10.82	rs3689058	95.56	37	49	3.77	>0.01
	30.01	rs3683804	97.78	39	49	1.64	>0.01
	43.70	rs4223943	100.00	42	48	0.71	>0.01
	54.66	rs3719338	97.78	44	44	0.41	>0.01
	70.09	rs13477178	100.00	47	43	0.04	>0.01
	79.72	rs4136771	97.78	46	42	0.41	>0.01
	103.41	rs13477302	95.56	45	41	0.05	>0.01
	113.13	rs6207837	95.56	45	41	0.05	>0.01
	132.56	rs4136518	96.67	40	47	0.93	>0.01
	150.02	rs3718378	100.00	46	44	0.18	>0.01
152.99	rs3686068	98.89	41	48	0.28	>0.01	
4	35.40	rs3703981	97.78	40	48	0.73	>0.01
	45.87	rs3719264	98.89	48	41	1.90	>0.01
	61.09	rs3686083	98.89	50	39	1.90	>0.01
	91.41	rs3703756	100.00	50	40	1.60	>0.01
	106.91	rs3664637	100.00	47	43	0.40	>0.01
	122.32	rs3682306	96.67	45	42	0.29	>0.01
	143.67	rs13478035	100.00	46	44	0.18	>0.01
5	21.18	rs3023036	97.78	44	44	0.41	>0.01
	30.47	rs3718492	100.00	47	43	0.40	>0.01
	60.37	rs3724321	98.89	49	40	1.36	>0.01
	75.65	rs4225300	97.78	47	41	1.64	>0.01
	89.33	rs3700063	95.56	46	40	2.98	>0.01
	90.80	rs3717237	100.00	48	42	2.84	>0.01
	101.81	rs8256225	98.89	50	39	4.96	>0.01
	118.75	rs4138867	98.89	53	36	8.19	<0.01
137.21	rs4225537	98.89	50	39	1.90	>0.01	
6	43.80	rs3703696	98.89	50	39	1.90	>0.01
	55.14	rs3688612	98.89	50	39	1.90	>0.01
	73.00	rs13478817	98.89	49	40	1.36	>0.01
	86.41	rs3656641	98.89	47	42	0.55	>0.01
	98.69	rs3702663	100.00	47	43	0.40	>0.01
	114.97	rs3720170	97.78	47	41	0.18	>0.01
	125.74	rs3701869	95.56	48	37	0.95	>0.01
	139.64	rs3679077	98.89	50	39	0.91	>0.01
7	8.35	rs4226424	100.00	48	42	0.00	>0.01
	27.77	rs3668793	100.00	46	44	0.18	>0.01
	37.07	rs4226613	97.78	43	45	0.00	>0.01
	53.08	rs4226645	100.00	45	45	0.04	>0.01
	67.43	rs4226725	100.00	48	42	0.18	>0.01
	77.59	rs3656285	97.78	46	42	0.05	>0.01
	87.14	rs6387510	95.56	43	43	0.05	>0.01

	102.74	rs3654133	100.00	49	41	0.40	>0.01
	130.17	rs13479566	98.89	49	40	0.55	>0.01
8	9.76	rs13479604	98.89	44	45	0.10	>0.01
	30.33	rs3661862	98.89	42	47	0.10	>0.01
	46.24	rs13479741	98.89	41	48	0.28	>0.01
	54.58	rs3723574	98.89	42	47	0.10	>0.01
	75.96	rs6282879	100.00	38	52	0.71	>0.01
	94.99	rs4227350	97.78	38	50	0.41	>0.01
	107.26	rs3666037	100.00	39	51	0.40	>0.01
	122.74	rs4227428	98.89	42	47	0.01	>0.01
9	32.69	rs3716375	100.00	52	38	1.60	>0.01
	64.69	rs3664300	98.89	49	40	0.10	>0.01
	80.00	rs6213724	95.56	52	34	0.74	>0.01
	94.44	rs3699737	98.89	51	38	0.55	>0.01
	114.04	rs3693662	97.78	44	44	0.41	>0.01
10	8.30	rs4228101	98.89	44	45	0.28	>0.01
	29.03	rs3710662	98.89	46	43	1.90	>0.01
	65.70	rs3725109	100.00	43	47	0.04	>0.01
	76.58	rs13480657	100.00	42	48	0.00	>0.01
	89.25	rs3673574	100.00	41	49	0.40	>0.01
	89.40	rs4139881	100.00	41	49	0.40	>0.01
	99.23	rs4228444	100.00	42	47	0.10	>0.01
	118.09	rs13480784	98.89	43	46	0.01	>0.01
11	14.27	rs13480881	97.78	72	15	64.66	<0.0001
	30.00	rs3718377	98.89	65	24	44.60	<0.0001
	44.79	rs13481004	98.89	62	26	28.41	<0.0001
	59.00	rs3691800	100.00	58	32	11.38	<0.0001
	76.08	rs3693943	100.00	58	32	6.40	>0.01
	94.04	rs16783394	100.00	47	43	0.04	>0.01
	104.00	rs3153214	100.00	49	41	0.04	>0.01
12	30.94	rs3723945	98.89	57	32	2.53	>0.01
	45.92	rs6379858	98.89	57	32	2.53	>0.01
	60.74	rs3686891	98.89	53	36	1.36	>0.01
	72.18	rs13481543	98.89	51	38	0.10	>0.01
	87.96	rs3684493	98.89	47	42	0.55	>0.01
	103.43	rs6390948	100.00	44	46	0.18	>0.01
13	30.26	rs6376513	98.89	43	46	0.91	>0.01
	44.56	rs6249046	98.89	47	42	0.28	>0.01
	62.21	rs3712411	98.89	42	47	1.36	>0.01
	70.66	rs4229908	97.78	41	46	0.56	>0.01
	89.63	rs3709305	97.78	44	44	0.00	>0.01

14	10.72	rs4230190	98.89	50	39	0.28	>0.01
	26.12	rs3724311	97.78	48	40	0.41	>0.01
	46.05	rs3726218	98.89	47	42	0.55	>0.01
	78.28	rs3668028	97.78	43	45	0.00	>0.01
	91.55	rs3688255	98.89	43	46	0.01	>0.01
15	5.00	rs4230638	98.89	47	42	0.55	>0.01
	29.48	rs3656493	100.00	48	42	0.18	>0.01
	45.47	rs13482548	100.00	51	39	1.11	>0.01
	57.35	rs3702158	100.00	48	42	0.00	>0.01
	79.44	rs3667621	100.00	48	42	0.00	>0.01
16	10.57	rs4161352	97.78	46	42	0.05	>0.01
	27.39	rs3694564	100.00	46	44	0.00	>0.01
	46.55	rs4182798	100.00	48	42	0.18	>0.01
	54.66	rs3687272	100.00	47	43	0.04	>0.01
	74.91	rs3663889	100.00	43	47	0.40	>0.01
	86.18	rs4212526	100.00	41	49	0.40	>0.01
17	10.00	rs13482869	98.89	43	46	0.10	>0.01
	30.35	rs3684143	97.78	47	41	1.64	>0.01
	41.24	rs4231493	100.00	48	42	1.60	>0.01
	61.51	rs3725261	98.89	50	39	3.25	>0.01
	79.55	rs2020834	98.89	54	35	4.96	>0.01
18	9.43	rs3725581	100.00	52	38	0.18	>0.01
	30.29	rs3664296	96.67	50	37	0.10	>0.01
	43.72	rs13483329	98.89	48	41	0.10	>0.01
	58.98	rs3713935	100.00	46	44	0.18	>0.01
	77.29	rs3705890	100.00	47	43	0.40	>0.01
19	10.17	rs13483528	98.89	44	44	0.05	>0.01
	24.37	rs3717368	100.00	44	46	0.18	>0.01
	29.58	rs6238842	100.00	38	52	0.71	>0.01
	47.45	rs3674914	96.67	42	45	0.01	>0.01

SNPs refer to the NCBI database (<http://www.ncbi.nlm.nih.gov/>)

9.2.2 GLS006 mice

Table 9.2: SNP genotyping results of GLS006 G2 backcross mice.

Chromosome	Locus (Mb)	RefSNP	Success rate	Het	Ocr	χ^2 value	P value
1	5.11	rs13475703	93.00	45	40	0.29	>0.01
	23.48	rs13475764	97.00	46	43	1.36	>0.01
	38.09	rs13475818	96.00	46	42	1.64	>0.01
	48.20	rs13475854	93.00	41	45	1.16	>0.01

	76.19	rs3678148	96.00	43	45	1.14	>0.01
	81.73	rs30712373	96.00	46	42	1.64	>0.01
	95.16	rs13475986	95.00	46	41	0.93	>0.01
	116.68	rs13476065	98.00	43	47	0.00	>0.01
	144.12	rs30942489	100.00	42	50	0.17	>0.01
	172.66	rs33777727	98.00	39	46	1.42	>0.01
	195.08	rs13499691	96.00	41	47	0.41	>0.01
	14.32	rs13476355	96.00	35	53	1.14	>0.01
	20.21	rs27120459	97.00	28	55	2.71	>0.01
	37.00	rs13476434	96.00	39	49	0.05	>0.01
	50.65	rs13476490	95.00	38	49	0.01	>0.01
2	70.83	rs13476567	96.00	44	44	0.18	>0.01
	95.61	rs3679193	96.00	47	41	0.05	>0.01
	114.23	rs27441842	96.00	48	39	0.01	>0.01
	129.49	rs27257388	96.00	48	40	0.00	>0.01
	169.33	rs13476909	93.00	47	39	0.05	>0.01
	181.63	rs3691120	96.00	44	44	0.00	>0.01
	7.68	rs29657774	96.00	44	44	0.18	>0.01
	26.28	rs13477026	95.00	43	44	0.01	>0.01
	36.89	rs3151604	96.00	44	44	0.18	>0.01
	52.51	rs3685081	95.00	44	43	0.10	>0.01
3	69.55	rs13477178	96.00	41	47	0.05	>0.01
	89.03	rs8259135	93.00	44	41	0.01	>0.01
	103.28	rs13477302	93.00	45	41	0.42	>0.01
	109.00	rs13477321	96.00	48	40	0.73	>0.01
	129.56	rs16799508	93.00	51	35	3.77	>0.01
	142.68	rs13477460	96.00	44	44	0.18	>0.01
	10.97	rs27731305	96.00	51	37	7.68	<0.01
	22.44	rs13477603	96.00	53	35	7.68	<0.01
	35.22	rs27781503	96.00	50	38	4.55	>0.01
4	62.74	rs3718270	96.00	48	40	4.55	>0.01
	86.81	rs28056583	93.00	41	45	1.16	>0.01
	101.16	rs28307021	96.00	41	47	2.23	>0.01
	133.12	rs13477989	96.00	43	45	0.41	>0.01
	141.90	rs3711383	96.00	44	44	0.18	>0.01
5	14.03	rs13481347	96.00	44	44	0.73	>0.01
	24.86	rs13478148	98.00	40	50	0.18	>0.01
	41.07	rs13478204	98.00	42	48	0.04	>0.01
	55.63	rs13478263	96.00	44	43	0.29	>0.01
	67.96	rs29635956	100.00	45	47	0.39	>0.01
	79.39	rs31585424	96.00	46	42	0.73	>0.01
	103.34	rs13478429	97.00	43	46	0.01	>0.01

	127.16	rs13478514	95.00	42	45	0.10	>0.01
	145.01	rs4225559	95.00	38	49	0.10	>0.01
6	4.78	rs13478606	96.00	41	47	0.41	>0.01
	26.14	rs13478670	96.00	42	46	0.73	>0.01
	35.97	rs3023067	97.00	42	45	0.93	>0.01
	72.33	rs13478816	96.00	45	43	1.14	>0.01
	85.89	rs13478872	96.00	45	43	0.41	>0.01
	102.23	rs13478935	98.00	52	38	0.04	>0.01
	115.23	rs13478987	96.00	50	38	0.00	>0.01
	144.45	rs13479084	100.00	47	41	0.41	>0.01
7	5.23	rs13479108	93.00	35	51	2.28	>0.01
	28.11	rs13479164	96.00	41	47	2.23	>0.01
	51.83	rs16793422	96.00	39	48	0.29	>0.01
	60.70	rs13479256	93.00	40	45	0.01	>0.01
	73.17	rs16805799	96.00	44	44	0.00	>0.01
	100.08	rs4226783	96.00	48	40	0.18	>0.01
	110.34	rs13479437	96.00	48	40	0.73	>0.01
	124.03	rs13479476	93.00	48	37	0.95	>0.01
	140.06	rs13479537	96.00	50	38	2.91	>0.01
8	9.76	rs13479604	95.00	44	43	4.15	>0.01
	28.02	rs13479662	96.00	43	45	3.68	>0.01
	48.19	rs13479741	93.00	44	42	1.67	>0.01
	60.52	rs13479782	99.00	45	44	2.53	>0.01
	70.85	rs13479814	96.00	43	45	2.23	>0.01
	90.66	rs6264181	93.00	45	41	0.42	>0.01
	103.43	rs13479952	100.00	62	20	3.95	>0.01
		116.69	rs13479998	93.00	44	42	0.19
9	13.23	rs13480073	96.00	46	42	0.18	>0.01
	37.50	rs3023207	96.00	48	40	0.00	>0.01
	57.67	rs13480217	97.00	46	43	0.10	>0.01
	80.06	rs13480299	96.00	46	42	0.73	>0.01
	96.23	rs3673055	96.00	42	45	0.01	>0.01
		110.96	rs13480418	95.00	41	46	0.01
10	8.19	rs13480484	95.00	39	48	0.01	>0.01
	22.64	rs13480541	96.00	39	49	0.05	>0.01
	34.30	rs13480578	100.00	34	58	0.17	>0.01
	57.47	rs13480619	95.00	37	50	0.10	>0.01
	68.91	rs13480638	96.00	41	47	2.23	>0.01
	84.15	rs13480678	95.00	36	51	0.93	>0.01
	99.48	rs8258500	96.00	37	51	1.14	>0.01
		117.84	rs13480784	97.00	39	50	0.28

11	7.11	rs13480851	96.00	68	20	80.18	<0.0001
	21.62	rs13480905	96.00	63	25	62.23	<0.0001
	32.23	rs26822879	100.00	65	27	41.78	<0.0001
	53.99	rs26982471	100.00	55	37	12.57	<0.0001
	62.81	rs13481061	96.00	50	38	8.91	<0.001
	83.23	rs13481127	96.00	44	44	2.91	>0.01
	98.55	rs27041242	99.00	46	45	3.18	>0.01
	114.33	rs27000576	96.00	43	45	2.23	>0.01
12	13.15	rs13481307	96.00	48	40	1.64	>0.01
	25.78	rs13481351	96.00	48	40	1.64	>0.01
	40.56	rs13481405	93.00	47	39	5.63	>0.01
	55.74	rs13481462	100.00	51	41	5.26	>0.01
	75.04	rs8259450	96.00	46	42	4.55	>0.01
	83.44	rs6194112	96.00	45	43	3.68	>0.01
	99.32	rs13481604	99.00	45	46	2.47	>0.01
	114.06	rs13459138	96.00	43	45	2.23	>0.01
13	6.30	rs13481676	96.00	45	43	0.05	>0.01
	19.49	rs6345767	96.00	45	43	0.05	>0.01
	54.50	rs13481815	96.00	49	39	0.41	>0.01
	69.35	rs13481863	96.00	47	41	1.14	>0.01
	83.16	rs13481910	96.00	50	38	0.73	>0.01
	97.25	rs29566800	96.00	52	36	0.18	>0.01
	111.21	rs30511458	96.00	50	38	0.18	>0.01
	14	22.92	rs30406796	96.00	50	37	6.08
46.68		rs13482161	96.00	44	44	2.91	>0.01
59.60		rs30895903	98.00	44	46	1.60	>0.01
88.56		rs13482292	93.00	42	44	0.74	>0.01
105.71		rs30482696	90.00	43	39	1.22	>0.01
118.16		rs30947935	100.00	49	40	1.90	>0.01
15	25.20	rs13482484	95.00	40	47	0.29	>0.01
	38.82	rs13482528	96.00	42	46	0.73	>0.01
	50.42	rs13482574	96.00	42	46	0.73	>0.01
	67.56	rs13482627	93.00	42	44	0.74	>0.01
	97.72	rs16804751	97.00	48	40	2.91	>0.01
16	10.87	rs4161352	96.00	36	52	1.64	>0.01
	27.44	rs4165602	95.00	40	47	0.56	>0.01
	32.19	rs4170048	93.00	45	41	0.05	>0.01
	69.80	rs4199268	96.00	50	38	0.18	>0.01
	84.14	rs4211770	97.00	49	38	0.29	>0.01
	93.53	rs4220159	95.00	49	38	0.29	>0.01

17	11.59	rs33418817	95.00	51	36	0.56	>0.01
	40.94	rs33428427	95.00	51	35	0.05	>0.01
	55.31	rs29504995	96.00	50	38	1.64	>0.01
	72.72	rs13483097	96.00	47	41	2.23	>0.01
	85.46	rs13483140	98.00	49	40	1.36	>0.01
18	25.51	rs29827614	96.00	40	48	0.18	>0.01
	38.24	rs29823686	96.00	37	51	1.14	>0.01
	57.83	rs13483379	93.00	38	48	1.67	>0.01
	70.63	rs13483427	96.00	34	54	2.91	>0.01
	86.75	rs13483484	97.00	35	53	3.68	>0.01
19	13.93	rs6247194	96.00	45	43	0.41	>0.01
	26.00	rs13483576	96.00	46	42	0.73	>0.01
	43.57	rs4232188	96.00	36	51	0.10	>0.01
	56.34	rs6339594	96.00	38	50	0.73	>0.01

SNPs refer to the NCBI database (<http://www.ncbi.nlm.nih.gov/>)

9.3 Abbreviations of chemical compounds and solutions

AgNO ₃	silver nitrate
APS	ammonium persulfate
ATP	adenosine 5'-triphosphate
BSA	bovine serum albumine
CaCl ₂	calcium chloride
DAB	3,3'-diaminobenzidine tetrahydrochloride dehydrate
DEPC	diethylpyrocarbonate
dNTPs	deoxynucleoside triphosphate mixture
DTT	dithiotreitol
EDTA	ethylene diamine tetraacetic acid
EGTA	ethylene glycol tetraacetic acid
H ₂ O ₂	hydrogen peroxide
HEPES	N-(2-hydroxyethyl)piperazine-N'-(2-ethanesulfonic acid)
KCl	potassium chloride
KH ₂ PO ₄	monopotassium phosphate
K ₂ HPO ₄	dipotassium phosphate
NaCl	sodium chloride
MgCl ₂	magnesium chloride
MgSO ₄	magnesium sulphate
NaCl/Tris	sodium chloride/tris(hydroxymethyl)aminomethane
NADP ⁺	nicotinamide adenine dinucleotide phosphate
NADPH	reduced form of nicotinamide adenine dinucleotide phosphate

Na ₂ CO ₃	sodium bicarbonate
NaHCO ₃	sodium hydrogen carbonate
Na ₂ HPO ₄	disodium phosphate
Na ₂ S ₂ O ₃	sodium thiosulphate
NaOV	sodium orthovanadate
PMSF	phenylmethylsulfonyl fluoride
SDS	sodium dodecyl sulphate
TBE buffer	Tris borate EDTA buffer
TBS	Tris buffered saline
TBS-T	Tris buffered saline with Tween
TE buffer	Tris EDTA buffer
TEMED	tetraethylethylenediamine
Tris/HCl	tris(hydroxymethyl)aminomethane/hydrochloric acid

9.4 Evaluation of DNA concentrations via gel electrophoresis

In addition to spectrophotometrical quantification (chapter 3.2.2.2 and 3.2.2.5), DNA amounts in purified PCR products were estimated by gel electrophoresis using *EcoRI* digested Lambda DNA as reference quantity (Fig. 9.2). In each gel electrophoresis 0.5 and 1 µg of the concentration marker Lambda DNA/*EcoRI* + *HindIII*-Marker, 3 (MBI Fermentas, Germany) was applied. Electrophoresis was run on a 1.5% TBE agarose gel with a total sample volume of 12 µl (2 µl PCR product, 8 µl H₂O and 2 µl 6x DNA Loading Dye (MBI Fermentas)).

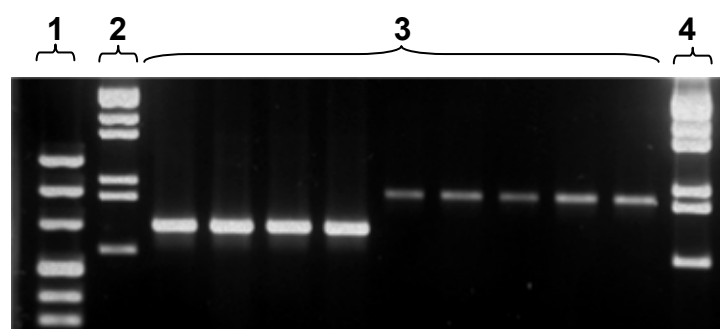


Figure 9.2: Gel electrophoresis of purified PCR products for determination of DNA concentration. 1: fragment size marker (pUC mix 8; MBI Fermentas, Germany); marker bands represents fragment sizes of 1118, 881, 692, 501/489, 404 and 331 bp (from top to bottom). 2 and 4: concentration standard (Lambda DNA/*EcoRI* + *HindIII*-Marker, 3). 2: 0.5 µg concentration standard/lane: marker bands correspond to a concentration of 19.6, 16.3, 14.2, 9.8, 8.6, and 5.8 ng (from top to bottom). 4: 1 µg concentration standard/lane: visible marker

bands represent concentrations of 39.2, 32.6, 28.4, 19.6, 17.2, and 11.6 ng. **3**: purified PCR products (2 µl/lane). DNA concentrations in the amplicates were estimated by comparison of the respective band intensity with the intensity of the concentration standard bands.

9.5 Principle of evaluation of real-time PCR primer efficiencies

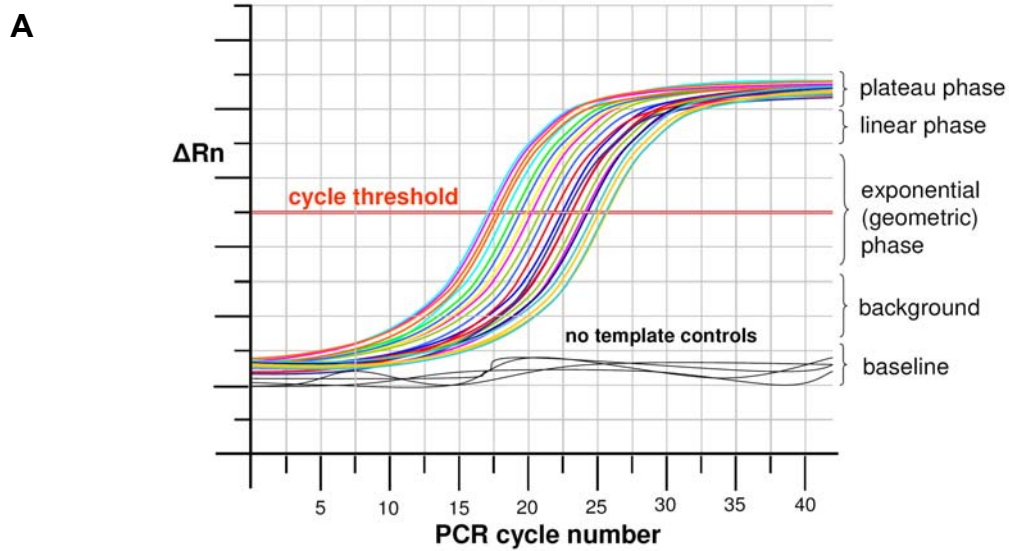
Amplification efficiencies of target and reference gene specific primers were evaluated by implementation of real-time PCR with serial diluted (range 10^{-3} - 10^{-9}) PCR products. With regard to preamplification, PCR was conducted as described in chapter 3.2.1.2 with 1 µl cDNA (20 ng), synthesised from hepatic RNA of an adult C3H wild-type control animal as described in chapters 3.2.2.2 and 3.2.2.3, and the respective primer pairs in a total reaction volume of 20 µl. PCR Master Mix composition and PCR cycling conditions are described below

Table 9.3: Master Mix and PCR conditions for evaluation primer efficiencies

PCR Master Mix		Cycling conditions		
Aqua bidest	5.25 µl	1. Initial denaturation	hot start	40 cycles
Q-solution	4.00 µl	2. Denaturation	30 sec 95°C	
10x buffer	2.00 µl	3. Annealing	60 sec 45°C	
MgCl ₂	1.25 µl	4. Extension	30 sec 72°C	
dNTPs (1 mM)	4.00 µl	5. Final extension	10 min 72°C	
Primer sense (5 µM)	1.20 µl	6. Hold	∞ 4°C	
Primer antisense (5 µM)	1.20 µl			
Taq Polymerase	0.10 µl			

PCR product dilutions were prepared by 10 serial 1:10 dilutions (1 µl PCR product + 45 µl RNase-free H₂O (Invitrogen, Germany)), resulting in dilutions from the range of 10^{-1} - 10^{-10} of the initial concentration. Quantitative real-time PCR was performed with PCR products, diluted in the range of 10^{-3} - 10^{-9} , as described in chapter 4.3.2. Real-time PCR was performed each, for quantification of the target-, as well as for the distinct reference transcripts, and all dilutions were investigated in duplicates. After manual threshold setting in the exponential phase of amplification, the intercross of the respective amplification curves with the threshold line were determined and plotted against the corresponding logarithmised dilution range. Primer efficiencies were calculated from the slope of the resulting linear regression curves as described below (Figure 9.3).

Exemplary illustration of amplification phases during real-time PCR and principle of manual threshold setting



Principle of primer efficiency calculation from real-time PCR results

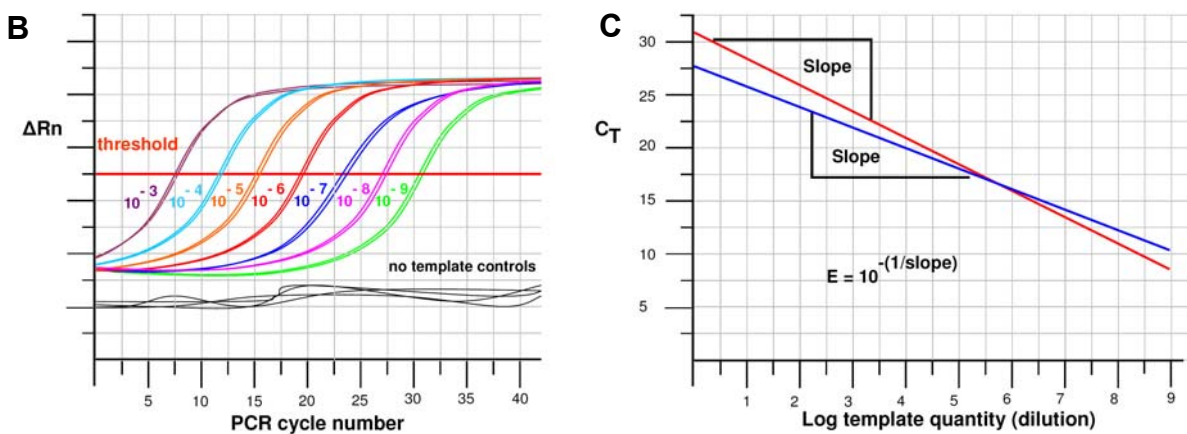


Figure 9.3: Principle of manual threshold setting for real-time PCR data from typical amplification curves (A) and evaluation of primer efficiency after real-time PCR implementation (B, C). A: Software generated amplification plot of ΔR_n (difference between the normalised reporter fluorescence in the sample and in the no template control (NTC)) as a function of the cycle number. The threshold line represents the level of detection at which a reaction reaches a fluorescent intensity above the background, and is set manually. B: typical distribution of real-time PCR amplification curves from serial 1:10 diluted (dilution range 10^{-3} - 10^{-9}), preamplified PCR products. C: C_{T} s, determined from B, were plotted against the respective logarithmised dilution range (3-9) and primer efficiencies (E) were calculated from the resulting linear regression curve, using the following equation: $E = 10^{-(1/\text{slope})}$.

9.6 Evaluation of real-time PCR results, using the $2^{-\Delta C_T}$ method

Since the applied primers for amplification of the reference and target transcripts displayed comparable amplification efficiencies of about 0.75 ± 0.02 , relative expression levels of the target transcripts were compared between the respective groups, using the $2^{-\Delta C_T}$ method (Cohen and Kretzler 2003) (Fig. 9.4).

Principle of calculating relative target transcript abundance from quantitative real-time PCR results, using the $2^{-\Delta C_T}$ method

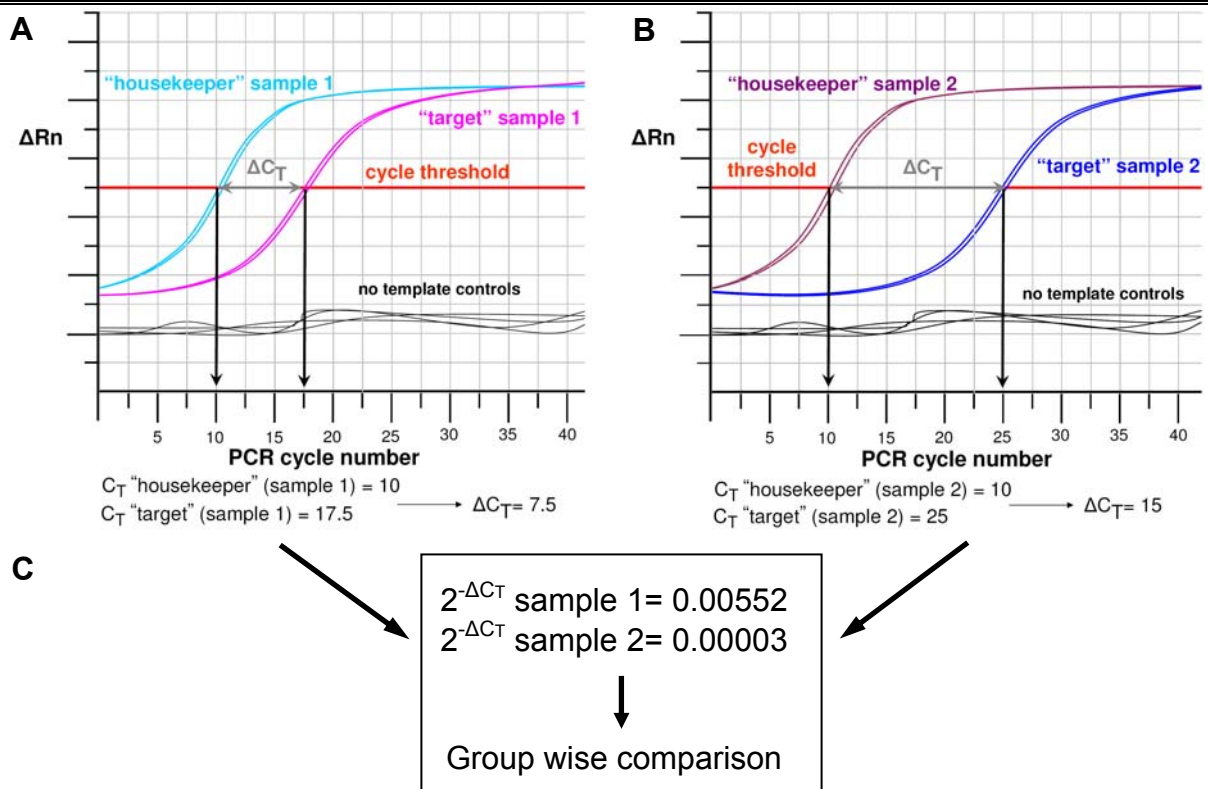


Figure 9.4: Hypothetical outline of relative quantification of real-time PCR results using the $2^{-\Delta C_T}$ method. The target transcript abundance relative to the expression of a reference transcript (housekeeping gene) was compared between sample duplicate 1 (wild-type) (A) and sample duplicate 2 (mutant) (B). The mean C_T from each of the duplicate measurements of each sample for housekeeping- and target-sequences was calculated, as demonstrated for sample 1 and sample 2. Relative target gene expression levels of the respective RNA samples were presented as $2^{-\Delta C_T}$ values and were compared group wise (C). Representing a crucial prerequisite for the reproducibility of the results, real-time PCR reactions of all samples, belonging to the respective groups to be compared, were run on identical plates, using identical Master Mixes.

9.7 Histological staining methods

Histological sections were prepared as described above (refer to chapter 3.6.2), transferred into glass cuvettes and incubated for 1 hour in a heating cabinet (90°C, Memmert GmbH&Co. KG, Germany) to enable paraffin removal from the sections. Thereafter, tissue sections were incubated for 10 minutes in xylene (SAV, Germany) for final paraffin clearance, subsequently rehydrated via a descending alcohol series (2 x 100%, 2 x 96%, 1 x 70% ethanol), and rinsed in distilled water. Further staining steps depended on the respective protocols, described below:

9.7.1 Haematoxylin and eosin (HE) staining

1. Mayer's haemalaun (AppliChem, Germany) 5 minutes
2. Rinse in running tap water 5 minutes
3. Dip in 1% eosin solution 2-7 times
4. Rinse in aqua bidest.
5. Dehydrate via ascending alcohol series
6. Xylene

Mount under glass coverslips, using Roti[®] Histokitt II (Roth, Germany)

1% eosin solution

Eosin G (Roth, Germany)	10 g
Dissolve in hot aqua bidest., then cool down	1000 ml
Glacial acetic acid (Merck, Germany)	1.5 ml

Filtrated and stored at room temperature

9.7.2 Perjodic acid-Schiff (PAS) staining

1. 1% perjodic acid 10 minutes
2. Rinse in running tap water 10 minutes
3. Schiff's reagent (Roth, Germany) 30 minutes
4. Rinse in running tap water 5 minutes
5. Mayer's haemalaun 2 minutes
6. Rinse in running tap water 5 minutes
7. Differentiate in 0.5% HCl alcohol
8. Rinse in running tap water 5 minutes
9. Ascending alcohol series
10. Xylene

Mount under glass coverslips, using Roti[®] Histokitt II (Roth, Germany)

1% periodic acid

Solution A:

Periodic acid (Sigma, Germany)	10 g
Aqua bidest.	1000 ml

Solution B:

Sodium acetate (Merck, Germany)	1.6 g
Aqua bidest.	1000 ml

Prepare both solutions separately, mix and store at 4°C

1% HCl stock solution

96% ethanol	7000 ml
Aqua bidest.	2500 ml
25% HCl (Merck, Germany)	100 ml

0.5 % HCl, ready-to-use

1% HCl stock solution	100 ml
70% ethanol	100ml

9.7.3 Masson's trichrome staining (modified according to Goldner and Weigert)

1. Weigert's iron haematoxylin 5 minutes
2. Rinse in running tap water 5 minutes
3. Differentiate in 0.5% HCl alcohol
4. Rinse in running tap water 15 minutes
5. Red colour solution 5-7 minutes
6. Rinse in 0.5% acetic acid
7. Phosphotungstic acid-orange G solution 3 minutes
8. Rinse in 0.5% acetic acid
9. Aniline blue 5 minutes
10. Rinse in 0.5% acetic acid
11. Ascending alcohol series
12. Xylene

Mount under glass coverslips, using Roti[®] Histokitt II (Roth, Germany)

Weigert's iron haematoxylin

Solution A:	
Haematoxylin cryst. (Merck, Germany)	10 g
96% ethanol	1000 ml
Maturation for 1 week	
Solution B:	
Iron (III) chloride (Honeywell Riedel-de Haën [®] , Germany)	11.6 g
Aqua bidest.	980 ml
Glacial acetic acid	10 ml
Stored separately, prepared as 1:1 mixture	

Azophloxine solution

Azophloxine (CHROMA Gesellschaft Schmid GmbH&Co., Germany)	1.25 g
Aqua bidest.	250 ml
Glacial acetic acid	0.5 ml

Red colour stock solutions

Solution A:	
Boiling aqua dest.	1000ml
Acid fuchsine (Rubin S) (Merck, Germany)	10 g
Glacial acetic acid	10 ml
Cool down in closed glass bottle	
Solution B:	
Boiling aqua bidest.	1000 ml
Xylidine Ponceau (Waldeck, Germany)	10 g
Glacial acetic acid	10 ml

Red colour solution

Solution A	20 ml
Solution B	80 ml
Azophloxine solution	20 ml

Phosphotungstic acid-orange G solution

Tungstophosphoric acid (Merck, Germany)	15 g
Orange G (Merck, Germany)	10 g
Aqua bidest.	

Aniline blue

Aniline blue (SERVA Feinbiochemica, Germany)	10 g
Aqua bidest.	1000 ml
Glacial acetic acid (Roth, Germany)	10 ml
Prepare cold (4°C)	

1% Acetic acid

Aqua bidest.	1000 ml
Glacial acetic acid	10 ml
Ready-to-use solution prepared 1:1 with aqua bidest.	

9.7.4 Fat red staining

1. Transfer cut sections into distilled water
2. 50% Ethanol 30 seconds
3. Fat red solution 5 minutes
4. 50% Ethanol 2 seconds
5. Rinse in distilled water
6. Mayer's haemalaun (AppliChem, Germany) 2 seconds
7. Rinse in distilled water
8. Rinse in tap water
9. Mount on glass slides
10. Dry
11. Mount under glass cover slips using Faramount Aquaeous Mounting Medium Ready-to-use (DAKO, Germany)

Fat red solution

96% ethanol	140 ml
Aqua bidest.	52 ml
Boil shortly	
Fat red 7B (Sigma, Germany)	0.5 g
Boil shortly and stir for 30 minutes	
Filtrate before use	

Acknowledgements

This study was implemented within the framework of the DFG- (Deutsche Forschungsgemeinschaft) supported research training group “Functional Genome Research in Veterinary Medicine” (GRK 1029), in the period of April 2007 until October 2009.

I wish to thank Prof. Dr. Rüdiger Wanke, Prof. Dr. Bernhard Aigner, and Dr. Nadja Herbach for giving me the opportunity to perform this study. My deepest gratitude is expressed for the immense time and courtesy they spent to support this doctorate. In particular, I would like to express my gratitude for teaching me the molecular genetic and pathogenetic fundamentals of diabetes mellitus and the principles of quantitative stereological investigations, and for critically discussing all the particular features of this doctorate. I feel infinite gratitude for their incredible support and encouragement.

I also would like to express my gratitude to Prof. Dr. Eckhard Wolf for kindly giving me the opportunity to work in his laboratories, for his commitment, the detailed discussions, and numerous helpful comments. Thanks to all co-workers at the Institute of Molecular Animal Breeding/Gene Center, especially to Dr. Elisabeth Kemter for providing not only primers but also helpful advices. Many thanks also to Dr. Marlon Schneider and the team of Dr. Helmut Blum.

Of particular importance were the extremely helpful lessons about quantitative real-time PCR implementation. Thus, I would like to gratefully thank Dr. Andreas Blutke (Institute of Veterinary Pathology, Ludwig Maximilian University of Munich) and Dr. Susanne Schwarz (Institute for Animal Physiology, Ludwig Maximilian University of Munich) for their generous ongoing help and endless patience.

I show my gratitude to Prof. Dr. Martin Hrabé de Angelis for generously providing both mouse strains. Particular thanks to the co-workers at the Institute of Experimental Genetics, Helmholtz Zentrum München, especially to Dr. Matthias Klaften, Dr. Sybille Wagner, Dr. Birgit Rathkolb, Dr. Corinna Moerth and Mr. T. Fuchs for performing SNP genotyping and preliminary backcross breeding of the ENU strain GLS001. I am very grateful for the data and background information, they shared with me and would like to emphasise the protruding collaboration.

Another acknowledgement goes to Prof. Dr. Bernd Kaspers for providing his laboratory equipment, especially for ELISA and quantitative real-time PCR experiments. I also wish to show my gratitude to Dr. Michaela Lohr from the Institute of Physiological Chemistry, Ludwig Maximilian University of Munich, for her helpful and dedicated tutoring in enzyme kinetics.

I would like to thank Sabine Kautz and Marion Schuster for their great collaboration and assistance, for joining a memorable time and for brightening some gloomy days. Deepest thanks also to Lisa Pichl, not only for sedulous excellent technical assistance but also for teaching me all intricacies of laboratory work. Further thanks to all members of the GRK.

I would like to show my special gratitude to all employees at the Institute of Veterinary Pathology for their help, especially to Mrs. B. Schmidt, and Mrs. M. O’Gorman for their support and company, and to Mrs. S. Zwirz and Mr. A. Ciolovan for their excellent animal management.

The last acknowledgement is dedicated to my whole family-thank you for everything!